Missouri S&T Library and Learning Resources

Scholars' Mine

Doctoral Dissertations | Student Theses and Dissertations

Fall 2014

Dissolution behavior of phosphate glasses

Li Na Ma

Follow this and additional works at: https://scholarsmine.mst.edu/doctoral_dissertations

 Part of the Materials Science and Engineering Commons

Department: Materials Science and Engineering

Recommended Citation

Ma, Li Na, "Dissolution behavior of phosphate glasses" (2014). *Doctoral Dissertations*. 2349.
https://scholarsmine.mst.edu/doctoral_dissertations/2349

This thesis is brought to you by Scholars' Mine, a service of the Missouri S&T Library and Learning Resources. This work is protected by U. S. Copyright Law. Unauthorized use including reproduction for redistribution requires the permission of the copyright holder. For more information, please contact scholarsmine@mst.edu.

DISSOLUTION BEHAVIOR OF PHOSPHATE GLASSES

by

LI NA MA

A DISSERTATION

Presented to the Faculty of the Graduate School of the

MISSOURI UNIVERSITY OF SCIENCE AND TECHNOLOGY

In Partial Fulfillment of the Requirements for the Degree

DOCTOR OF PHILOSOPHY

in

CERAMIC ENGINEERING

2014

Approved by

Richard K. Brow, Advisor

Mark E. Schlesinger, Co-advisor

Delbert E. Day

William G. Fahrenholtz

Klaus Woelk

PUBLICATION DISSERTATION OPTION

The Introduction section of this dissertation provides background information about the research topic and objectives. The body of this dissertation has been compiled in the format for publication in peer-reviewed journals. Four papers have been included in the following order. The first paper, "Structural study of Na_2O–FeO–Fe_2O_3–P_2O_5 glasses by high-pressure liquid chromatography" was published in the *Journal of Non-Crystalline Solids*, in volume 387, pages 16-20, 2014. The second paper, "Structural study of Na_2O–FeO–Fe_2O_3–P_2O_5 glasses by Raman and Mössbauer spectroscopy," was published in the *Journal of Non-Crystalline Solids,* in volume 402, pages 64-73, 2014. The third paper, "Thermal stability of Na_2O–FeO–Fe_2O_3–P_2O_5 glasses," will be submitted to the *Journal of Non-Crystalline Solids* in Aug 2014. The fourth paper, "Dissolution behavior of Na_2O–FeO–Fe_2O_3–P_2O_5 glasses," will be submitted to the *Journal of Non-Crystalline Solids* in Sep 2014.

The appendices include one paper in the form of manuscript for the *Journal of Non-Crystalline Solids* and experimental results not covered in the main body of this dissertation. The paper, "Dissolution behavior of Na_2O–CaO–P_2O_5 glasses," will be submitted to the *Journal of Non-Crystalline Solids* in Sep 2014. The second manuscript, "Dissolution behavior of Na_2O–FeO–Fe_2O_3–P_2O_5 glasses in alkali aqueous solutions," will be modified and expanded before submitting for publication.

ABSTRACT

The solubility of phosphate glasses in aqueous solutions can be tailored through compositional control to obtain a wide range of ion release rates required for a variety of applications. The principal objective of this dissertation is to advance the understanding of the dissolution behavior of phosphate glasses in aqueous environments.

Two families of glasses, sodium-iron phosphate (NFP) glasses and sodium-calcium phosphate (NCP) glasses, were evaluated. The dissolution behavior depends on the phosphate anions that constitute the glass structure and the associated metal (Me) cations. The phosphate glass structure, defined by the distribution and average size of phosphate anions and depending on the O/P and Me/P ratios, was determined by high-pressure liquid chromatography and Raman spectroscopy; Mössbauer spectrometry provided information about the coordination environment of iron. This structural information is used to explain the compositional dependence of the thermal properties and crystallization tendency of NFP glasses and melts, and the aqueous corrosion behavior of NFP and NCP glasses.

Phosphate glass dissolution data are fit to different kinetic models which describe the glass dissolution mechanisms. Information about the glass composition and structure is used to predict changes in the pH of leachate solutions, and a model based on the Gibbs free energy of hydration used to explain the compositional dependence of the glass dissolution rates.

ACKNOWLEDGMENTS

I am very grateful to my advisor, Dr. Richard K. Brow. Without his support, encouragement and patience, this study would not have been completed. His excellent guidance, numerous valuable suggestions and discussions not only made this dissertation possible, but also taught me a proper, meticulous academic approach towards research, for which I would like to express my deepest gratitude to him.

I also would like to extend my sincere appreciation to my co-advisor- Dr. Mark E. Schlesinger, who always offered his support and guidance. I also sincerely appreciate my committee members- Dr. Delbert E. Day, Dr. William G. Fahrenholtz and Dr. Klaus Woelk for their constructive suggestions. In addition, I would like to give my thanks to Dr. Mary Reidmeyer for her interesting glass blowing class and help with my research, and Dr. Wenhai Huang and Dr. Jian Lin (Tongji University, China) for introducing me to my studies at Missouri S&T.

All of my colleagues in Dr. Brow's group and my friends deserve many thanks as well. I greatly appreciate their help, helpful discussions and friendship during my Ph.D studies. Many thanks also go to the technicians and staff in MSE department and in the MRC. I thank them all for the great assistance they provided during my studies in Rolla.

Last but not least, I would like to thank my family members who made this possible: my parents– Tiesheng Ma and Huiling Liu, and my husband– Yinan Lin for their continual encouragement, support, and love that keeps me moving forward in my studies and my life as well.

TABLE OF CONTETS

Page

LIST OF ILLUSTRATIONS

PAPER IV

LIST OF TABLES

SECTION

1. PURPOSE OF THIS DISSERTATION

The dissolution behavior of phosphate glasses has been studied for many applications, nuclear waste remediation and bio-medical implants. For example, iron phosphate glasses with remarkably good chemical durability have been developed as a promising alternative for vitrifying nuclear waste. Bioactive glasses from the Na_2O–CaO–P_2O_5 system, on the other hand, are readily degradable in aqueous environments, a desirable characteristic for many biomedical applications. However, debate remains about the phosphate glass dissolution mechanisms, and much less information is available in the literature on the effects of composition and structure on the dissolution behavior of phosphate glasses. Therefore, the principal objective of this PhD research is to advance the understanding of the dissolution behavior of phosphate glasses in aqueous environments by relating dissolution processes to the structural information on the phosphate chain length distribution and the nature of the modifying metal cations.

Glasses from the Na_2O–FeO–Fe_2O_3–P_2O_5 (NFP) and Na_2O–CaO–P_2O_5 (NCP) systems in the polyphosphate range (O/P ratios 3.0 ~ 3.5) were prepared by conventional melting and quenching techniques. High-pressure liquid chromatography (HPLC) and Raman spectroscopy were used to characterize the phosphate anions that constitute the structures of these glasses, including the distributions of phosphate chain lengths and phosphate tetrahedral sites. Mössbauer spectroscopy was used to determine the coordination environments of iron cations. Disproportionation reactions of the phosphate anions in glass melts produced wider distributions of phosphate anions for glasses

containing greater amounts of high field strength cations, and this in turn affected the crystallization tendency of the glasses and melts.

The corrosion behavior of phosphate glasses in aqueous solutions was evaluated. Dissolution rates determined from weight loss measurements and ion release measurements were fit to different kinetic models, which define the glass dissolution mechanisms. Information about the glass composition and phosphate tetrahedral distributions is used to predict changes in the pH of the leachate solutions. A model based on the Gibbs free energy of hydration is used to explain the compositional dependence of the glass dissolution rates.

2. INTRODUCTION

2.1. APPLICATIONS OF PHOSPHATE GLASSES

Phosphate glasses have been studied and commercialized for a variety of applications because of their useful physical properties, including controllable chemical durability in aqueous environment, high thermal expansion coefficient, low melting and processing temperatures [1,2]. Properties and applications of phosphate glasses vary dramatically with different compositions.

For hard and soft tissue repair, biodegradable phosphate glasses can be fabricated as scaffolds for bone regeneration, glass fibers for antibacterial or trace element delivery systems and for muscle regeneration [3,4,5]. Phosphate glass fibers are also suitable for reinforcement of biodegradable implants [6]. As bioactive glasses, $Na_2O–CaO–P_2O_5$ glasses are degradable in aqueous environments and show good biocompatibility and low toxicity with a minimal inflammatory response [7,8,9]. The addition of copper and silver to phosphate glasses is known to have positive effects on the local treatment of infections [10,11]. Phosphate glass fibers incorporating Al_2O_3 and Fe_2O_3 can be used as cell guides and as reinforcing materials for regeneration of skeletal muscle, and have been observed to form myotubes, from which muscle fibers can form [12,13].

Iron phosphate glasses have been developed as potential hosts for nuclear waste disposal applications. Iron phosphate glasses with Fe/P ratios between 1:3 and 2:3 can be used for the vitrification of high level nuclear waste (HLW) because of their excellent chemical durability, which can be equivalent to or superior to silicate and borosilicate glasses [14,15,16]. In addition, fairly high alkali oxide contents (up to 20 wt%) can be tolerated in the iron phosphate glasses without deterioration of their good chemical

durability [16,17]. The addition of PbO improves shielding properties against high-energy radiation, including gamma-radiation [18,19,20]. The chemical durability of several iron phosphate glasses vitrified with simulated sodium bearing waste (SBW) and HLW meet all the current US Department of Energy (DOE) requirements [14,21]. In addition, amorphous metal phosphate coatings are sometimes used to improve the corrosion resistance of steel [22].

Chemically-durable phosphate glasses can also be used for the following applications. Alkali aluminophosphate glasses with glass transition temperatures under 400 °C have been developed for specialty hermetic seals because of their high thermal expansion coefficients (greater than 150 $\times 10^{-7}$ /°C) [23]. The introduction of alkali ions (e.g., Li^+ and Na^+) in phosphate glass is of interest for ion conduction applications. The structural features of lithium iron phosphate compounds (e.g., Li_xFePO_4) and lithium iron phosphate glasses with nano-crystalline phases make them attractive as cathode materials for rechargeable batteries [24,25]. Low optical dispersion and relatively high refractive indices (compared with silicate-based optical glasses) make phosphate glasses with good chemical durability as host matrices of rare-earth ions and transition metal ions for optical devices [23,26,27]. Phosphate glasses with transition metals or rare-earth ions also exhibit interesting semiconducting properties, magneto-optical properties and magnetic transition properties, which can be used to design and apply as spin glasses or optical isolators and optical switches [28,29,30,31]. Phosphate glasses containing divalent iron cations not only have a high transmittance in the visible range (400~700 nm), but also exhibit a large Faraday effect because of charge transfer transitions from O^{2-} to Fe^{2+} in the near-ultraviolet to blue range appropriate for emission from blue laser diodes [30].

Hydrolysis of polyphosphate anions from condensed inorganic polyphosphates in aqueous solutions has led to various applications, such as inorganic multivalent electrolytes, as chelators of metals, fertilizer, or a buffer against alkali [32]. In the biological field, phosphate esters and anhydrides play important role in bio-phosphate chemistry that involves the formation or cleavage of P–O–P bonds or P–O–C bonds, for example, phosphoryl (PO^{3-}) transfer reactions in the formation and hydrolysis of adenosine-triphosphate (ATP); structural stability of phosphate and pyrophosphate diesters in the backbones and links of complementary strands of DNA [33]. Extensive investigations of phosphate ester hydrolysis and the dominant mechanism for these reactions in aqueous solutions have been conducted [34]. In addition, hydrolysis of polyphosphate in aqueous solution can be used to detoxify and sequester heavy metals for the bioremediation of organics in metal-polluted environments [35].

2.2. STRUCTURAL FEATURES OF PHOSPHATE GLASSES

2.2.1. Structural Units in Phosphate Glasses. The properties of phosphate glasses depend on their structures, which in turn are determined by the chemistry, concentration and coordination environments of metal oxides added to the glasses and their effects on the resulting phosphate anion (chain length) distributions [23,36,37].

The building blocks for phosphate glasses are phosphate tetrahedra which can link to form P_n units, which are phosphate anions with 'n' tetrahedra that form polymer-like chains or rings, and that are cross-linked by metal cations through non-bridging oxygens. The general formula for phosphate anions can be described as $(P_nO_{3n+1})^{-(n+2)}$ with (n+2) negative charges [37,38]. Cyclic phosphate rings, such as the trimetaphosphate ($P_3O_9^{3-}$)

or the tetrametaphosphate ($P_4O_{12}^{4-}$) can also be found in glasses with compositions close to the metaphosphate (O/P = 3) [39,40]. The polymeric nature of phosphate glasses allows for their easy formation into fibers from the melt [12,13]. The axes of long phosphate chains will align in the drawing direction of metaphosphate glass fibers [41].

The oxygen-to-phosphorus (O/P) ratio in a phosphate glass composition determines the average phosphate anion length ($\bar{n}$) [23]. For a phosphate glass, $\bar{n}$ can be calculated from glass composition by Equation (1) [39],

$$\bar{n} = \frac{2}{\sum_j [M_j] Z_j / [P] - 1} \quad (1)$$

where $[M_j]$ is the molar concentration of metal cation j, Z_j is the valence of metal cation j and [P] is the molar concentration of phosphorus. This relationship is shown in Figure 2.1.

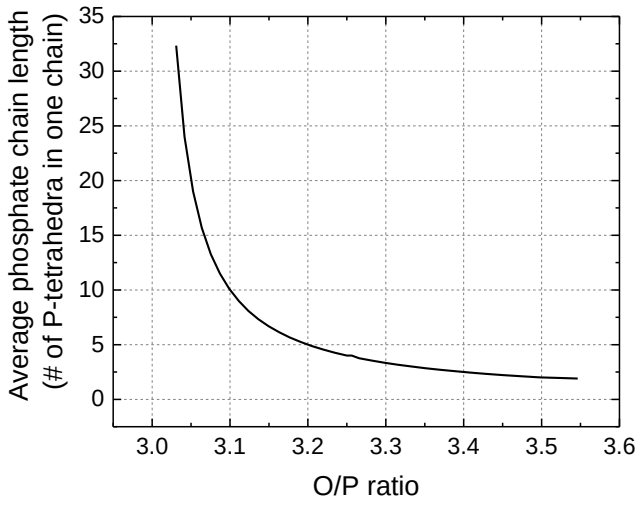

Figure 2.1. Theoretical average phosphate chain length as function of O/P ratio.

Phosphate networks are built by the phosphate tetrahedra with different numbers of bridging oxygens, including cross-linked networks (Q^3), polymer-like chains (Q^2+Q^1) or small pyro-(Q^1) and orthophosphate groups (Q^0) [23]. In the Q^i terminology, 'i' represents the number of bridging oxygens that link one phosphate tetrahedron to another. The average P–O bond length in the phosphate tetrahedra is about 1.54–1.57 Å [23,36]. For bridging oxygen (BO), the P–O bond lengths are about 1.61–1.64 Å; for nonbridging oxygen (NBO), the P–O bond lengths decrease systematically for Q^3, Q^2, Q^1 and Q^0 tetrahedra [36]. Phosphate anions with n P-tetrahedra (n>2) have two Q^1 sites and (n–2) Q^2 sites. The addition of metal oxides to a phosphate glass increases the average number of non-bridging oxygens per phosphate tetrahedron, and so breaks phosphate chains and rings, turning Q^i sites into Q^{i-1} sites. The connectivity and medium range structure characterized by two-dimensional MAS NMR for different Q^i sites in binary phosphate glasses is consistent with a model of random depolymerization [42,43,44,45].

Metal cations (M) exist in polyhedral sites in phosphate glasses and form metal chelating structures with ionic M–O_{nb} bonds to the non-bridging oxygens of the associated phosphate anions [2,32]. The M–O_{nb} bond length in phosphate glasses is longer than the average P–O bond length in phosphate tetrahedra. Commonly, the smaller average bond length for M–O_{nb}, the stronger M–O_{nb} bond strength, and the smaller oxygen coordination number for cations [23]. For high field strength cations with greater electronegativity (e.g., Mg^{2+}, Al^{3+}, Fe^{2+} and Fe^{3+}), covalent M–O_{nb} bonds form, which thus reduce the average covalency of the P–O_{nb} bond [46,47]. The formation of stronger M–O_{nb} bonds is in accordance with increasing glass transition temperature (T_g) and better chemical durability [48]. In polyphosphate glasses (O/P = 3.0–3.5), sodium polyhedra

form with coordination numbers from 4 to 6 and average Na–O bond lengths of 2.38–2.43 Å [23,49,50]. For iron phosphate glasses in the O/P range of 3.0 (metaphosphate) to 4.0 (orthophosphate), ferric ions are found in tetrahedral and octahedral sites, and ferrous ions are found in octahedral and perhaps pentahedral sites [51]. Fe–O bond lengths are about ~ 1.85 Å in $[Fe^{3+}O_4]$, ~ 2.00 Å in $[Fe^{3+}O_6]$ and ~ 2.16 Å in $[Fe^{2+}O_6]$ [51].

For glasses with mixed glass formers (e.g., SiO_2, B_2O_3, P_2O_5, Al_2O_3), desirable combinations of properties could be obtained compared to glasses with simpler structural networks [1]. Six coordinated Si^{4+}, $[SiO_6]$, is found in phosphate-rich glasses [52,53,54]. For aluminophosphate networks, a decrease in the average Al-coordination number, from six to four, is observed with increasing O/P ratios [1].

Residual water in phosphate glasses also affects the glass structure and properties, with effects similar to the ionic modifying oxides (e.g., Na_2O) [32]. Water contents can be calculated from measured hydrogen contents using an inert gas fusion method [43]. For binary sodium phosphate glasses, water contents decrease from 23 mol% to 0.5 mol% with increasing O/P ratio (2.7–3.1) [43]. In the ultraphosphate glass range (O/P < 3.0), significant amounts of water are present as terminal (–OH) groups and affects the phosphate site distributions by increasing the number of Q^2 tetrahedra and reducing the number of Q^3 tetrahedra. Polyphosphate glasses have relatively low water contents [43].

2.2.2. Disproportionation Reactions. Disproportionation reactions in glass melts, which have been related to the glass formation energy, broaden the distributions of phosphate anions in glasses [55,56]. The nature of the metal cations added to a glass

composition affects the distribution of phosphate anions. Cations with greater field strengths are associated with glasses with broader distributions of phosphate anions (Figure 2.2) and these cations are also associated with lower free energies of formation for their respective crystalline orthophosphates [56].

The Flory distribution model can be used to describe the distribution of chains in phosphate melts [38]:

$$2(\mathrm{P_nO_{3n+1}})^{-(n+2)} \leftrightarrow (\mathrm{P_{n+1}O_{3n+4}})^{-(n+3)} + (\mathrm{P_{n-1}O_{3n-2}})^{-(n+1)} \quad (2)$$

and this reaction is described with the equilibrium constant $K(P_n)$,

$$K(P_n) = \frac{[P_{n+1}][P_{n-1}]}{[P_n]^2} \quad (3)$$

Wider distributions of phosphate anions result from shifting the disproportionation reactions towards the right sides. The extent of these reactions determines the phosphate chain length distributions in a melt and affect the properties of the glasses.

For an ideal Flory distribution of phosphate chain lengths in a glass melt, the equilibrium constant $K(P_n)$ of reaction (2) equals 1, and the mole fraction of P_n units, $N(P_nO_{3n+1})$, is given by equation (6), in which $\bar{n}$ is the average phosphate chain length,

$$\mathrm{N(P_nO_{3n+1})} = \frac{1}{\bar{n}}\left(\frac{\bar{n}-1}{\bar{n}}\right)^{n-1} \quad (4)$$

The actual distributions of phosphate anions in a glass network are narrower than the ideal Flory distribution, meaning that $K(P_n)$ is less than 1 for shorter phosphate anions (n=2, 3 or 4) and approaches to 1 when n increases (Figure 2.2) [55,56,57].

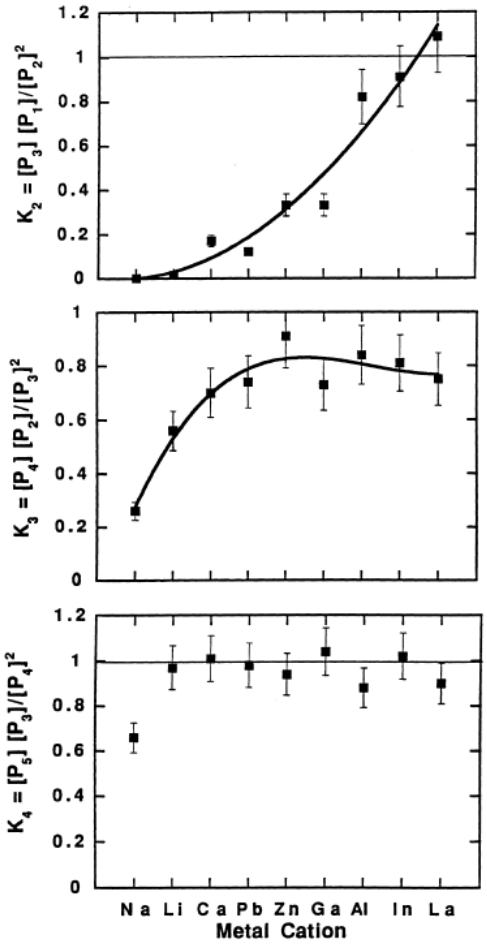

Figure 2.2. Equilibrium constants K(P_n) calculated for disproportionation reactions (2) determined from the chromatographic analyses. The ordering of the cations on the x-axis is in accordance with the free energies of formation for their respective crystalline orthophosphates [37].

The Flory distribution can also be described with the reformulated form based on the Q^i site distributions [32]:

$$2Q^i \leftrightarrow Q^{i+1} + Q^{i-1} \tag{5}$$

and the equilibrium constant $K(Q^i)$,

$$K(Q^i) = \frac{[Q^{i+1}][Q^{i-1}]}{[Q^i]^2} \tag{6}$$

In the polyphosphate range (3.0 < O/P < 3.5), the relevant site disproportionation reaction is,

$$2Q^1 \leftrightarrow Q^2 + Q^0 \quad (7)$$

If the distribution of phosphate chain lengths follows an ideal Flory distribution, $K(Q^1)$ for reaction (7) equals 0.25 and the mole fraction of P_n units is described by equation (4) [38,55]. Each phosphate chain, P_n (n > 2), has two Q^1 and (n–2) Q^2 sites, so the distribution of Q^i sites in polyphosphate glasses can be calculated from the distribution of P_n units (equation (4)). Figure 2.3 shows the distribution of Q^i sites in phosphate glasses for O/P 3.0–4.0. The disproportionation reaction produces the Q^0 sites in polyphosphate range (O/P 3.0–3.5).

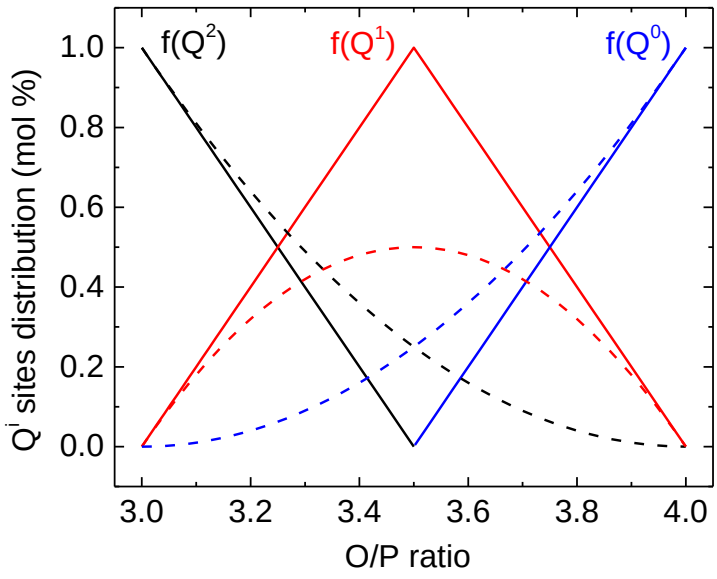

Figure 2.3. Distribution of Q^i sites in phosphate glasses for O/P 3.0–4.0. The solid lines are the predicted $f(Q^i)$ without site disproportionation. The dashed lines are the $f(Q^i)$ following ideal Flory distribution.

Liquid chromatographic techniques have been widely used to characterize the phosphate anion distributions in a glass network because the phosphate anions released to solution are the same structural units present in the original phosphate glass. In an aqueous solution under normal conditions, phosphate chains can be dissolved intact from glass surface and show slow hydrolysis reactions (activation energy 83~167 kJ/mol), and never repolymerize [2,32,37]. With the addition of a chelating agent (e.g., Na_4EDTA), the reactivity of metal cations (e.g., Ca^{2+}, Fe^{3+}) with phosphate anions is reduced, which further improves the long term stability of phosphate chains and rings in solution [58]. Improved performance and efficiency of liquid chromatography columns used in high-pressure liquid chromatography (HPLC) systems led to better separations for phosphate anions and greatly facilitated studies of the structure of amorphous polyphosphate solids [37]. However, the limitations of liquid chromatographic techniques are apparent for ultraphosphate compositions, because Q^3 species hydrolyze to form Q^2 species when the glasses are dissolved prior to analysis [43,59]. For the iron containing glasses with compositions near the metaphosphate stoichiometry ($3.0 \leq O/P \leq 3.2$) in this study, the chromatographs were not consistent with the glass compositions, in part because of the inability to resolve the longer phosphate anions [60].

2.3. PROPERTIES OF PHOSPHATE GLASSES

2.3.1. Chemical Durability. Dissolution rates and ion release rates, as well as predictable dissolution behavior, are very important characteristics for phosphate glasses used in biomedical applications and for nuclear waste disposal. For example, it is desirable that the *in vivo* degradation rates of scaffolds match the rate at which new bone

is formed [3]. Through compositional modifications, the solubility of phosphate glasses in aqueous solution can be tailored to obtain a wide range of ion release rates [2].

The dissolution behavior of glass is controlled by the reaction of the glass network with water and the extraction of ions out of the glass matrix [61]. Often, the initial stage of corrosion is controlled by an ion exchange process or the diffusion of water into the glass network, followed then by the dissolution of the glass matrix with increasing depth of alkali depletion in the outer glass surface [2,61]. The hydration reaction between glass and water is based on the hydrolytic cleavage of bonds in the glass network with different energies of hydration. The weakest bonds between metal ions and non-bridging oxygens, $M–O_{nb}$, break first during the dissolution process. The rate of ion exchange across the hydration layer as well as the H_2O penetration into the bulk glass, is determined by the surface concentration of the interdiffusing ions, the multi-component interdiffusion coefficient and the exchange potential of the interdiffusing species at the exchange site [62]. The fraction of NBO and the concentration of mobile ions (e.g., Na^+) determine the initial glass hydration rates [62].

There are debates over the dissolution mechanism that involve the two main reaction stages during the glass corrosion process. For $Na_2O–CaO–P_2O_5$ metaphosphate glasses, Bunker et al. [2] observed a square root of time dependence ($t^{1/2}$) for weight loss and proposed that this first stage of corrosion was controlled by surface hydration. In the second stage of corrosion, weight losses follow a linear time dependence controlled by the hydration of intact polyphosphate chains from glass surface (Figure 2.4). In both stages, the dissolution rate depends on the solution pH and the concentrations of other ions in the solution. Congruent dissolution indicates that all glass constituents are

released from the glass at the same rate, and the solubility limits of cations leached out of the glass matrix are not exceeded so that the sorption and coprecipitation of species is negligible. Thus, according to Bunker's model, the thickness of the hydrated layer should be constant with time and controlled by the average chain length of the phosphate anions.

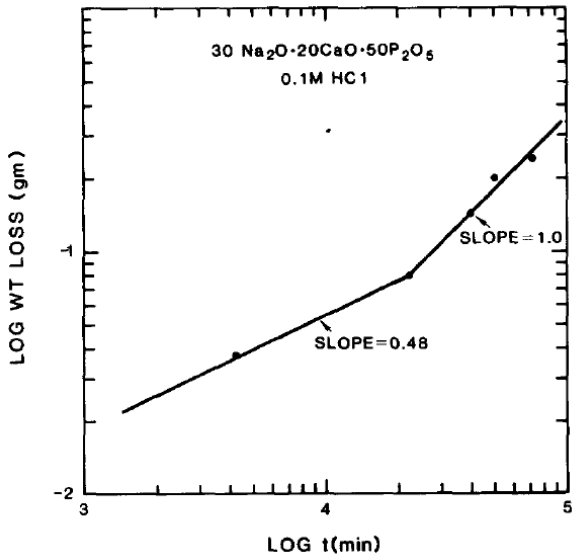

Figure 2.4. Log(weight loss) versus Log(t) for glass $30Na_2O–20CaO–50P_2O_5$ at 20 °C and pH = 3 [2].

However, the initial non-linear dissolution kinetics interpreted with the $t^{1/2}$ time law in Bunker's model was not observed in some other studies [5,63,64], where it appears that other important factors affect the dissolution kinetics of phosphate glasses in aqueous solutions. These other factors include the surface configurations and layer formation, saturation effects, solution chemistry, and the ratio of glass surface area-to-solution volume.

Delahaye et al. [63] suggested that the $t^{1/2}$ time law in Bunker's model was actually due to a decrease in the dissolution rate with an increase in the ionic strength of the leaching solution, which results in a modification of the hydrated layer with an increase in the electrostatic interactions between the polyphosphate chains. Delahaye et al. also showed that the developed hydrated layer of metaphosphate glass in an acidic solution has the same composition and structure as the surface of a pristine glass. In addition, the metal chelating structure of the phosphate anions has an effect on the dissolution reactions of the hydrated layer [65]. According to Gao et al. [66], this metal chelating structure impedes the penetration of water into the depth of the bulk glasses.

The glass surface energy could also contribute to the chemical durability of phosphate glasses. Fresh glass surfaces with higher surface energy are readily wetted by water vapor and organic contaminants from the environment, and this causes a rapid reduction in the surface energy [4]. Contact angle measurements of polar liquids on $Na_2O–CaO–P_2O_5$ glasses doped with Fe_2O_3 show that the total surface energy of phosphate glasses decreases, which reflects a decrease in the polar interactions between glass surface and water [4].

For each type of phosphate anion (P_n) hydrated from a glass surface, the stability of the different pronated $(P_nO_{3n+1})^{-(n+2)}$ anions is a function of the pH value. The interaction between phosphate anions and other components in solution is predictable from their acid dissociation constant (pK_a), which is a prerequisite for a quantitative understanding of the interaction of acids, bases and metal cations in a solution. In particular, the pH value of a solution can be predicted if the analytical concentration of polyprotic acids and the pK_a values for the dissociation of protons from these polyprotic

acids are known; conversely, it is possible to calculate the equilibrium concentration of the acids and bases in solution when the pH is known [67]. Prediction of pH values for solutions of dissolved phosphate glasses has not been reported in the literature.

After phosphate anions are dissolved in solution, hydrolysis of the P–O–P linkages may occur along with protonation, and the hydrolysis reactions are accelerated in acids [2,63]. The catalytic effects of various metal ions promote the hydrolytic and reorganization reactions involving polyphosphate anions or phosphate esters in aqueous solutions [32,68,69]. The rate of hydrolytic reactions increases with increased cation charge and with decreased cation radius. The strength of bonds between cations and the polyphosphate anions is related to the catalytic effectiveness [69]. In solution, end-group clipping and random cleavage of phosphate chains happens as well as formation of phosphate rings, which is considered a reorganization reaction. The distribution of initial degradation products are pH dependent and are determined by the hydrolysis kinetics. At very low pH, random cleavage is the dominant hydrolytic reaction. At pH 3~7, the main hydrolytic reaction is end-group clipping. At pH 8~10, the rates of end-group clipping and ring formation are much faster than the rate of random cleavage [69].

Degradation of polyphosphates in solution can be characterized by potentiometric titrations for hydrogen ions, viscosity measurements, or liquid chromatography [70,71]. Rate constants for end-group clipping, phosphate ring formation and random chain cleavage can be determined from the concentration of hydrolysis reactants and products in solution [69,71].

2.3.2. Thermal Stability and Crystallization Behavior. Structural reorganization of a glass occurs as devitrification above the glass transition temperature. Thermal stability indicates the ability of glass to resist crystallization on heating and characterizing this tendency is useful when considering the thermal stability of iron phosphate glasses as nuclear waste storage hosts, or for the process of glass fiber fabrication [72,73].

Glass forming ability is related to the ease of vitrification of a melt on cooling from above the liquidus, T_L, to the glass transition temperature, T_g [74]. Structural and kinetic approaches are used to understand the concepts of thermal stability and glass forming ability, and efforts have been made to relate these two concepts [74,75,76]. An increase in thermal stability parameters indicates a greater resistance (better stability) to crystallization on heating a glass or quenching a melt [76].

Dominant crystallization for a particular glass depends strongly on glass composition, surface quality and the surrounding environment [77,78]. DTA methods are used to identify and distinguish crystallization mechanisms [77], as well as to determine the activation energy for crystal growth [79]. For most glasses, internal and surface crystallization proceeds simultaneously and competitively [77]. For the thermal properties and crystallization behavior of sodium iron phosphate glasses, literature [72,80,81] provides insufficient information on the compositional dependence, stable crystallization phases and iron redox effects; these processes are discussed in this dissertation.

REFERENCES

[1] R.K. Brow, and D.R. Tallant. "Structural design of sealing glasses." Journal of non-crystalline solids 222 (1997): 396-406.

[2] B.C. Bunker, G.W. Arnold, and J.A. Wilder. "Phosphate glass dissolution in aqueous solutions." Journal of non-crystalline solids 64, no. 3 (1984): 291-316.

[3] M.N. Rahaman, D.E. Day, B. Sonny Bal, Q. Fu, S.B. Jung, L.F. Bonewald, and A.P. Tomsia. "Bioactive glass in tissue engineering." Acta biomaterialia 7, no. 6 (2011): 2355-2373.

[4] E.A. Abou Neel, I. Ahmed, J.J. Blaker, A. Bismarck, A.R. Boccaccini, M.P. Lewis, S.N. Nazhat, and J.C. Knowles. "Effect of iron on the surface, degradation and ion release properties of phosphate-based glass fibres." Acta Biomaterialia 1, no. 5 (2005): 553-563.

[5] E.A. Abou Neel, I. Ahmed, J. Pratten, S.N. Nazhat, and J.C. Knowles. "Characterisation of antibacterial copper releasing degradable phosphate glass fibres." Biomaterials 26, no. 15 (2005): 2247-2254.

[6] J. Choueka, J.L. Charvet, H. Alexander, Y.H. Oh, G. Joseph, N.C. Blumenthal, and W.C. LaCourse. "Effect of annealing temperature on the degradation of reinforcing fibers for absorbable implants." Journal of biomedical materials research 29, no. 11 (1995): 1309-1315.

[7] I. Ahmed, M. Lewis, I. Olsen, and J.C. Knowles. "Phosphate glasses for tissue engineering: Part 2. Processing and characterisation of a ternary-based P_2O_5-CaO-Na_2O glass fibre system." Biomaterials 25, no. 3 (2004): 501-507.

[8] J.E. Gough, P. Christian, C.A. Scotchford, C.D. Rudd, and I.A. Jones. "Synthesis, degradation, and in vitro cell responses of sodium phosphate glasses for craniofacial bone repair." Journal of biomedical materials research 59, no. 3 (2002): 481-489.

[9] J.E. Gough, P. Christian, C.A. Scotchford, and I.A. Jones. "Long-term craniofacial osteoblast culture on a sodium phosphate and a calcium/sodium phosphate glass." Journal of Biomedical Materials Research Part A 66, no. 2 (2003): 233-240.

[10] A.M. Mulligan, M. Wilson, and J.C. Knowles. "Effect of increasing silver content in phosphate-based glasses on biofilms of Streptococcus sanguis." Journal of Biomedical Materials Research Part A 67, no. 2 (2003): 401-412.

[11] A.M. Mulligan, M. Wilson, and J.C. Knowles. "The effect of increasing copper content in phosphate-based glasses on biofilms of Streptococcus sanguis." Biomaterials 24, no. 10 (2003): 1797-1807.

[12] R. Shah, A.C.M. Sinanan, J.C. Knowles, N.P. Hunt, and M.P. Lewis. "Craniofacial muscle engineering using a 3-dimensional phosphate glass fibre construct." Biomaterials 26, no. 13 (2005): 1497-1505.

[13] I. Ahmed, C.A. Collins, M.P. Lewis, I. Olsen, and J.C. Knowles. "Processing, characterisation and biocompatibility of iron-phosphate glass fibres for tissue engineering." Biomaterials 25, no. 16 (2004): 3223-3232.

[14] D.E. Day, Z. Wu, C.S. Ray, and P. Hrma. "Chemically durable iron phosphate glass wasteforms." Journal of non-crystalline solids 241, no. 1 (1998): 1-12.

[15] C.W. Kim, and D.E. Day. "Immobilization of Hanford LAW in iron phosphate glasses." Journal of non-crystalline solids 331, no. 1 (2003): 20-31.

[16] W. Huang, D.E. Day, C.S. Ray, C.W. Kim, and A. Mogus-Milankovic. "Vitrification of high chrome oxide nuclear waste in iron phosphate glasses." Journal of nuclear materials 327, no. 1 (2004): 46-57.

[17] X. Yu, D.E. Day, G.J. Long, and R.K. Brow. "Properties and structure of sodium-iron phosphate glasses." Journal of non-crystalline solids 215, no. 1 (1997): 21-31.

[18] B.C. Sales, and L.A. Boatner. "Lead-iron phosphate glass: a stable storage medium for high-level nuclear waste." Science 226, no. 4670 (1984): 45-48.

[19] B.C. Sales, and L.A. Boatner. "Lead phosphate glass as a stable medium for the immobilization and disposal of high-level nuclear waste." Materials Letters 2, no. 4 (1984): 301-304.

[20] N. Singh, K.J. Singh, K. Singh, and H. Singh. "Comparative study of lead borate and bismuth lead borate glass systems as gamma-radiation shielding materials." Nuclear Instruments and Methods in Physics Research Section B: Beam Interactions with Materials and Atoms 225, no. 3 (2004): 305-309.

[21] C.W. Kim, C.S. Ray, D. Zhu, D.E. Day, D. Gombert, A. Aloy, A. Moguš-Milanković, and M. Karabulut. "Chemically durable iron phosphate glasses for vitrifying sodium bearing waste (SBW) using conventional and cold crucible induction melting (CCIM) techniques." Journal of nuclear materials 322, no. 2 (2003): 152-164.

[22] G. Górecki. "Iron phosphate coatings-composition and corrosion resistance." Corrosion 48, no. 7 (1992): 613-616.

[23] R.K. Brow. "Review: the structure of simple phosphate glasses." Journal of Non-Crystalline Solids 263 (2000): 1-28.

[24] P. Jóźwiak, J.E. Garbarczyk, M. Wasiucionek, I. Gorzkowska, F. Gendron, A. Mauger, and C. Julien. "The thermal stability, local structure and electrical properties of lithium-iron phosphate glasses." Materials Science-Poland 27, no. 1 (2009).

[25] S. Yang, P.Y. Zavalij, and M. Stanley Whittingham. "Hydrothermal synthesis of lithium iron phosphate cathodes." Electrochemistry Communications 3, no. 9 (2001): 505-508.

[26] A.E. Marino, S.R. Arrasmith, L.L. Gregg, S.D. Jacobs, G. Chen, and Y. Duc. "Durable phosphate glasses with lower transition temperatures." Journal of non-crystalline solids 289, no. 1 (2001): 37-41.

[27] N. Peyghambarian, and A. Schülzgen. "Fiber Lasers: High-Power Devices in Compact Packages." Optics and photonics news 16, no. 6 (2005): 36-41.

[28] F.A. Wedgwood, A.C. Wright. "Short range antiferromagnetic ordering in vitreous Fe_2O_3-P_2O_5." Journal of Non-Crystalline Solids 21, no. 1 (1976): 95-105.

[29] J.L. Shaw, A.C. Wright, R.N. Sinclair, G.K. Marasinghe, D. Holland, M.R. Lees, and C.R. Scales. "Spin glass-like antiferromagnetic interactions in iron phosphate glasses." Journal of non-crystalline solids 345 (2004): 245-250.

[30] H. Akamatsu, K. Fujita, S. Murai, and K. Tanaka. "Magneto-optical properties of transparent divalent iron phosphate glasses." Applied Physics Letters 92, no. 25 (2008): 251908.

[31] L. Abbas, L. Bih, A. Nadiri, Y. El Amraoui, D. Mezzane, and B. Elouadi. "Properties of mixed Li_2O and Na_2O molybdenum phosphate glasses." Journal of Molecular Structure 876, no. 1 (2008): 194-198.

[32] J.R. Van Wazer. "Phosphorus and its compounds, volume 1: chemistry." Interscience Publishers (1958): 717-800.

[33] G.P. Haight. "Hydrolysis of phosphate esters and anhydrides: role of metal ions." Coordination Chemistry Reviews 79, no. 3 (1987): 293-319.

[34] J. Florián, and A. Warshel. "Phosphate ester hydrolysis in aqueous solution: associative versus dissociative mechanisms." The Journal of Physical Chemistry B 102, no. 4 (1998): 719-734.

[35] J.D. Keasling. "Regulation of intracellular toxic metals and other cations by hydrolysis of polyphosphate." Annals of the New York Academy of Sciences 829, no. 1 (1997): 242-249.

[36] L. Zhang, and R.K. Brow. "A Raman study of iron–phosphate crystalline compounds and glasses." Journal of the American Ceramic Society 94, no. 9 (2011): 3123-3130.

[37] B.C. Sales, L.A. Boatner, and J.O. Ramey. "Chromatographic studies of the structures of amorphous phosphates: a review." Journal of Non-Crystalline Solids 263 (2000): 155-166.

[38] P.J. Flory. "Random reorganization of molecular weight distribution in linear condensation polymers." Journal of the American Chemical Society 64, no. 9 (1942): 2205-2212.

[39] B.C. Sales, R.S. Ramsey, J.B. Bates, and L.A. Boatner. "Investigation of the structural properties of lead-iron phosphate glasses using liquid chromatography and Raman scattering spectroscopy." Journal of non-crystalline solids 87, no. 1 (1986): 137-158.

[40] A.E.R. Westman, and P.A. Gartaganis. "Constitution of sodium, potassium, and lithium phosphate glasses." Journal of the American Ceramic Society 40, no. 9 (1957): 293-299.

[41] M.E. Milberg, and M.C. Daly. "Structure of Oriented Sodium Metaphosphate Glass Fibers." The Journal of Chemical Physics 39, no. 11 (1963): 2966-2973.

[42] T.M. Alam, and R.K. Brow. "Local structure and connectivity in lithium phosphate glasses: a solid-state ^{31}P MAS NMR and 2D exchange investigation." Journal of non-crystalline solids 223, no. 1 (1998): 1-20.

[43] R.K. Brow, R.J. Kirkpatrick, and G.L. Turner. "The short range structure of sodium phosphate glasses I. MAS NMR studies." Journal of non-crystalline solids 116, no. 1 (1990): 39-45.

[44] R.K. Brow, D.R. Tallant, J.J. Hudgens, S.W. Martin, and A.D. Irwin. "The short-range structure of sodium ultraphosphate glasses." Journal of non-crystalline solids 177 (1994): 221-228.

[45] P. Losso, B. Schnabel, C. Jäger, U. Sternberg, D. Stachel, and D.O. Smith. "^{31}P NMR investigations of binary alkaline earth phosphate glasses of ultraphosphate composition." Journal of non-crystalline solids 143 (1992): 265-273.

[46] G.B. Rouse Jr, P.J. Miller, and W.M. Risen Jr. "Mixed alkali glass spectra and structure." Journal of Non-Crystalline Solids 28, no. 2 (1978): 193-207.

[47] B.N. Nelson, and G.J. Exarhos. "Vibrational spectroscopy of cation-site interactions in phosphate glasses." Journal of Chemical Physics 71, no. 7 (1979): 2739-2747.

[48] P.Y. Shih, S.W. Yung, and T.S. Chin. "Thermal and corrosion behavior of P_2O_5-Na_2O-CuO glasses." Journal of non-crystalline solids 224, no. 2 (1998): 143-152.

[49] U. Hoppe. "Short-range order of phosphate glasses studied by a difference approach using X-ray diffraction results." Journal of non-crystalline solids 183, no. 1 (1995): 85-91.

[50] S. Bruni, F. Cariati, A. Corrias, P.H. Gaskell, A. Lai, A. Musinu, and G. Piccaluga. "Short range order of sodium-zinc, sodium-copper, and sodium-nickel pyrophosphate glasses by diffractometric and spectroscopic techniques." The Journal of Physical Chemistry 99, no. 41 (1995): 15229-15235.

[51] A.C. Wright, R.N. Sinclair, J.L. Shaw, R. Haworth, G.K. Marasinghe, and D.E. Day. "A neutron diffraction study of the structure of iron phosphate glasses." Physics and Chemistry of Glasses-European Journal of Glass Science and Technology Part B 49, no. 1 (2008): 1-7.

[52] R. Dupree, D. Holland, and M.G. Mortuza. "Six-coordinated silicon in glasses." (1987): 416-417.

[53] R. Dupree, D. Holland, M.G. Mortuza, J.A. Collins, and M.W.G. Lockyer. "An MAS NMR study of network-cation coordination in phosphosilicate glasses." Journal of Non-Crystalline Solids 106, no. 1 (1988): 403-407.

[54] S. Prabakar, K.J. Rao, and C.N.R. Rao. "A MAS NMR investigation of lead phosphosilicate glasses: the nature of the highly deshielded six-coordinated silicon." Materials research bulletin 26, no. 4 (1991): 285-294.

[55] T.R. Meadowcroft, and F.D. Richardson. "Structural and thermodynamic aspects of phosphate glasses." Transactions of the Faraday Society 61 (1965): 54-70.

[56] B.C. Sales, L.A. Boatner, and J.O. Ramey. "Intermediate-range order in simple metal-phosphate glasses: The effect of metal cations on the phosphate-anion distribution." Journal of non-crystalline solids 232 (1998): 107-112.

[57] T.R. Meadowcroft, and F.D. Richardson. "Heats of formation of some crystalline and glassy phosphates." Transactions of the Faraday Society 59 (1963): 1564-1571.

[58] H. Yamaguchi, T. Nakamura, Y. Hirai, and S. Ohashi. "High-performance liquid chromatographic separation of linear and cyclic condensed phosphates." Journal of Chromatography A 172, no. 1 (1979): 131-140.

[59] J.W. Wiench, M. Pruski, B. Tischendorf, J.U. Otaigbe, and B.C. Sales. "Structural studies of zinc polyphosphate glasses by nuclear magnetic resonance." Journal of Non-Crystalline Solids 263 (2000): 101-110.

[60] L. Ma, R.K. Brow. "Structural study of Na_2O-FeO-Fe_2O_3-P_2O_5 glasses by high-pressure liquid chromatography." Journal of Non-Crystalline Solids 387 (2014): 16-20.

[61] D.E. Clark, and B.K. Zoitos. "Corrosion of glass, ceramics and ceramic superconductors: Principles, testing, characterization and applications." Noyes Publications, Park Ridge, NJ (1992).

[62] T.A. Abrajano, J.K. Bates, and C.D. Byers. "Aqueous corrosion of natural and nuclear waste glasses I. Comparative rates of hydration in liquid and vapor environments at elevated temperatures." Journal of Non-Crystalline Solids 84, no. 1 (1986): 251-257.

[63] F. Delahaye, L. Montagne, G. Palavit, J.C. Touray, and P. Baillif. "Acid dissolution of sodium–calcium metaphosphate glasses." Journal of non-crystalline solids 242, no. 1 (1998): 25-32.

[64] K. Franks, I. Abrahams, and J.C. Knowles. "Development of soluble glasses for biomedical use Part I: In vitro solubility measurement." Journal of Materials Science: Materials in Medicine 11, no. 10 (2000): 609-614.

[65] I. Ahmed, A.J. Parsons, C.D. Rudd, S.N. Nazhat, J.C. Knowles, P. Guerry, and M.E. Smith. "Comparison of phosphate-based glasses in the range $50P_2O_5$-(50– x)CaO-xNa_2O prepared using different precursors." Glass Technology-European Journal of Glass Science and Technology Part A 49, no. 2 (2008): 63-72.

[66] H. Gao, T. Tan, and D. Wang. "Dissolution mechanism and release kinetics of phosphate controlled release glasses in aqueous medium." Journal of controlled release 96, no. 1 (2004): 29-36.

[67] B. Averill, and P. Eldredge. "Chemistry: Principles, patterns, and applications." Pearson Education, Inc. (2007): 721-774.

[68] R.J. Geue, A.M. Sargeson, and R. Wijesekera. "Metal ion promoted hydrolysis of polyphosphates." Australian Journal of Chemistry 46, no. 7 (1993): 1021-1040.

[69] R.K. Osterheld. "Nonenzymic hydrolysis at phosphate tetrahedra." in E.J. Griffith, and M. Grayson, eds., "Topics in phosphorus chemistry, volume 7." Interscience Publishers (1972): 103-242.

[70] U.P. Strauss, and T.L. Treitler. "Degradation of polyphosphates in solution. I. Kinetics and mechanism of the hydrolysis at branching points in polyphosphate chains." Journal of the American Chemical Society 78, no. 15 (1956): 3553-3557.

[71] G. Kura. "Liquid chromatographic study of the hydrolysis reactions of cyclic and linear polyphosphates in aqueous solution." Journal of Chromatography A 447 (1988): 91-101.

[72] L. Zhang, L. Ghussn, M.L. Schmitt, E.D. Zanotto, R.K. Brow, and M.E. Schlesinger. "Thermal stability of glasses from the $Fe_4(P_2O_7)_3$–$Fe(PO_3)_3$ system." Journal of Non-Crystalline Solids 356, no. 52 (2010): 2965-2968.

[73] H. Arstila, M. Tukiainen, S. Taipale, M. Kellomäki, and L. Hupa. "Liquidus temperatures of bioactive glasses." Advanced Materials Research 39 (2008): 287-292.

[74] I. Avramov, E.D. Zanotto, and M.O. Prado. "Glass-forming ability versus stability of silicate glasses. II. Theoretical demonstration." Journal of non-crystalline solids 320, no. 1 (2003): 9-20.

[75] A.A. Cabral, A.A.D. Cardoso, and E.D. Zanotto. "Glass-forming ability versus stability of silicate glasses. I. Experimental test." Journal of non-crystalline solids 320, no. 1 (2003): 1-8.

[76] M.L.F. Nascimento, L.A. Souza, E.B. Ferreira, and E.D. Zanotto. "Can glass stability parameters infer glass forming ability?." Journal of non-crystalline solids 351, no. 40 (2005): 3296-3308.

[77] C.S. Ray, and D.E. Day. "Identifying internal and surface crystallization by differential thermal analysis for the glass-to-crystal transformations." Thermochimica acta 280 (1996): 163-174.

[78] E.D. Zanotto, and V.M. Fokin. "Recent studies of internal and surface nucleation in silicate glasses." Philosophical Transactions of the Royal Society of London. Series A: Mathematical, Physical and Engineering Sciences 361, no. 1804 (2003): 591-613.

[79] K. Matusita, T. Komatsu, and R. Yokota. "Kinetics of non-isothermal crystallization process and activation energy for crystal growth in amorphous materials." Journal of Materials Science 19, no. 1 (1984): 291-296.

[80] A.J. Parsons, and C.D. Rudd. "Glass forming region and physical properties in the system P_2O_5-Na_2O-Fe_2O_3." Journal of Non-Crystalline Solids 354, no. 40 (2008): 4661-4667.

[81] G.K. Marasinghe, M. Karabulut, C.S. Ray, D.E. Day, M.G. Shumsky, W.B. Yelon, C.H. Booth, P.G. Allen, and D.K. Shuh. "Structural features of iron phosphate glasses." Journal of non-crystalline solids 222 (1997): 144-152.

PAPER

I. STRUCTURAL STUDY OF $Na_2O–FeO–Fe_2O_3–P_2O_5$ GLASSES BY HIGH-PRESSURE LIQUID CHROMATOGRAPHY

Lina Ma, Richard K. Brow*

Department of Materials Science & Engineering, Missouri University of Science & Technology, Straumanis-James Hall, 1400 N. Bishop Ave, Rolla, MO, USA

ABSTRACT

Three series of $Na_2O–FeO–Fe_2O_3–P_2O_5$ glasses with compositional ranges of 3.25 < O/P < 3.5 and 0 < Fe/P < 0.67 were prepared. Glass structure was studied using high-pressure liquid chromatography (HPLC). The average chain-length of phosphate anions decreases with increasing O/P ratios and glasses with similar O/P ratios and greater Fe/P ratios have wider distributions of phosphate anion lengths due to disproportionation reactions in the glass melts.

Keywords: HPLC; iron-phosphate glass; disproportionation reaction

* Corresponding author, brow@mst.edu

1. Introduction

Iron phosphate compounds and glasses have been studied and commercialized for a variety of applications. Up to 40 wt% of a simulated high level nuclear waste can be accommodated into iron pyrophosphate (FeP) glasses with a chemical durability equivalent to that of borosilicate glass wasteforms and but in a smaller volume because of the greater density of the FeP glasses [1]. Metal phosphate coatings are sometimes used to improve the corrosion resistance of steel [2]. The structural features of lithium iron phosphate compounds (e.g., Li_xFePO_4) and lithium iron phosphate glasses with nanocrystalline phases make them attractive as cathode materials for rechargeable batteries [3,4]. Iron phosphate glasses have also been developed as biomaterials with tailored rates of degradation in aqueous environments [5].

In iron phosphate glasses, chain-like phosphate anions are linked through iron sites in a distorted iron chelate structure [6]. The phosphate chain length distributions in glass melts are affected by the chemistry and concentration of the metal cations that constitute a phosphate glass composition [7]. Studies have shown that glasses with greater field strength cations have broader distributions of phosphate anions and that these cations are also associated with lower free energies of formation for their respective crystalline orthophosphates [8].

High-pressure liquid chromatography (HPLC) is a useful technique to obtain quantitative information about the chain length distributions in a phosphate glass network because the relative area under each HPLC peak represents the relative concentrations of PO_4 units in each corresponding phosphate anion (P_n). From the relative peak areas obtained by HPLC, the overall O/P ratio, the average phosphate chain length ($\bar{n}$), average

bridging oxygen to non-bridging oxygen ratio (BO/NBO), and the fraction of phosphate tetrahedra with different bridging oxygens (Q^i sites), can be determined [9,10].

In the present work, the phosphate chain length distributions for several series of sodium-iron phosphate glasses were studied using high-pressure liquid chromatography (HPLC). These glasses serve as models for those under study for encapsulating high alkaline nuclear waste streams [11,12]. The phosphate anion distributions depend on both the O/P ratio and the Fe/P ratio. Disproportionation reactions in the glass melts produce wider distributions of phosphate chains when iron replaces sodium in glasses with constant O/P ratios.

2. Experimental Procedures

2.1. Glass melting and compositional analysis

Iron phosphate glasses with the batched compositions given in Table 1were prepared from raw materials including Na_2CO_3 (Alfa Aesar, ≥ 98%), Fe_2O_3 (Alfa Aesar, ≥ 99%) and $NH_4H_2PO_4$ (Alfa Aesar, ≥ 98%). Batches that produce 100g of glass were thoroughly mixed and melted in fused SiO_2 crucibles (Leco #728-701) between 1000 °C and 1250 °C in air for two hours; greater temperatures were generally required for melts with greater iron contents and lower O/P ratio [13]. The melts were poured onto a copper plate and quenched to room temperature by pressing with another cold copper plate. Compositional series described in Table 1 have batched O/P ratios between 3.25 and 3.5. For example, glass labeled as 3.5-0.67 is a sample with a batched O/P ratio of 3.5 and a batched Fe/P ratio of 0.67.

The compositions of the quenched glasses were determined by inductively-coupled plasma optical emission spectroscopy (ICP-OES, PerkinElmer Optima 2000 DV, Norwalk, USA). Iron phosphate glasses were digested in 3–7 M H_2SO_4 aqueous solution for 7 to 14 days at 80–90 °C in closed Teflon containers. The digestion time and temperature depended on the chemical durability of the glasses. Generally, glasses with high iron contents and low O/P ratios showed better chemical durability in the H_2SO_4 solution. Solutions for ICP were diluted with deionized H_2O, with dilution factors of 1:9 or 1:99, depending on the expected ion concentration of the solution. The ICP solution samples were tested in triplicate for every glass composition, and several glasses were three times. On average, the relative standard deviation of these analysis was less than 4% and this is taken as the uncertainty associated with the reported compositions. The Fe^{2+}/Fe_{tot} contents of the glasses were determined by a titration technique using $KMnO_4$ (2 mM), with an absolute uncertainty of 2% [14]. These glasses contain up to 5 mol% SiO_2, transferred from the crucible during melting, and the measured O/P ratios discussed in this paper take the SiO_2 content into consideration.

2.2. HPLC experiments

High-pressure liquid chromatography (HPLC, Dionex ion chromatography system) experiments were done to study the chain length distribution of phosphate anions in the glasses. Glass powders (75–150 μm, 200 mg) were partially dissolved for different times (from 10 minutes to 24 hours) in an aqueous solution (50 ml) with 0.22 M NaCl + 5 mM Na_4EDTA and a pH of 10. Phosphate chains are stable against hydrolysis under these conditions [8]. The chelating agent was added to prevent the hydrolysis of phosphate

chains by iron cations in solution [15]. In this study, the concentration of Na_4EDTA is about 2~8 times the total concentration of iron leached from glasses at the time of experiments. Phosphate chain solutions with Na_4EDTA and spiked with different concentrations of $FeCl_3$ or $FeCl_2$ showed no evidence for chain hydrolysis over 24 hours.

The carrier solution in the HPLC system is supplied by a GP-50 Gradient Pump. The sample solution is injected into the system and passes immediately through an anion exchange column. The NaCl solution concentration is then progressively ramped from 0.05 to 0.53 molar over the course of 30 min. This change in NaCl concentration causes the phosphate anions to be released from the column (IonPac® AS7 Analytical Column, 4-mm) in the order from shortest to longest. After release from the column, the sample stream is mixed with a 1.8 M H_2SO_4 solution containing ammonium molybdate. The sample then passes through a Teflon reaction coil at 140 °C, where the phosphate anions are hydrolyzed to form orthophosphate units that then react with the molybdate species to form a heteropoly blue complex. The solution then passes through a photodetector cell where the absorption of the solution is measured versus the retention time. The area under each absorption peak (P_n) is proportional to the concentration of phosphorus associated with phosphate anions with n PO_4 tetrahedra, $(P_nO_{3n+1})^{-(n+2)}$. Chain lengths up to ~16 PO_4 units are resolvable in this system, as are cyclic phosphates [8,16].

The chromatographs from iron-containing glasses with compositions near the metaphosphate stoichiometry ($3.0 \leq O/P \leq 3.2$) were not consistent with the glass compositions, in part because of the inability to resolve the longer anions. For this reason, the HPLC analyses are limited to glasses with $O/P \geq 3.25$. HPLC experiments were run in

triplicate and the average chain-lengths from these experiments, reproducible to ± 5%, are reported.

3. Results

3.1. Glass compositions

The analyzed compositions of the sodium iron phosphate glasses in this study are given in Table 1. Some ferric ions have reduced to ferrous ions so that the average Fe^{2+}/Fe_{tot} ratio for these glasses is about 0.18 ± 0.04, consistent with previous studies [17,18,19]. Some silica was transferred from the crucible to the melt so that the average Si/P in the glasses is about 0.03 ± 0.01; Bingham *et al.* [20] report that similar silica contents had little effect on the properties of their iron phosphate glasses. The calculations of O/P ratios for these glasses include the effects of the silica contamination and the iron reduction.

3.2. HPLC results

Fig. 1 shows the HPLC chromatographs for a series of glasses with similar Fe/P ratios (0.23 ± 0.01) and increasing O/P ratios. Each peak in the chromatograph, from short times to longer times, represents a phosphate anion with an increasing number of tetrahedra. The first peak, near a retention time of three minutes, is due to orthophosphate (P_1) anions, the second peak, near eight minutes, is due to pyrophosphate (P_2) anions, the third to triphosphates (P_3), etc. As the O/P ratio increases, the relative concentration of short phosphate chains ($P_n < 6$) increases. When the O/P ratio reaches 3.51, the main

phosphate anions in the glass structure are the pyrophosphate (P_2, 71%), orthophosphate (P_1, 20%), triphosphate (P_3, 9%) and tetraphosphate (P_4, 1%).

Within a compositional series with similar O/P ratios, the replacement of Na^+ ions by Fe^{3+} or Fe^{2+} ions affects the distribution of phosphate anions. Fig. 2 (a) show the HPLC chromatographs collected from glasses with similar O/P ratios of 3.49±0.01. With an increasing Fe/P ratio (as sodium replaces iron), there is an increase in the relative concentrations of both P_1 and longer phosphate chains ($P_n > 2$), compared to the concentration of P_2 units (Fig. 2 (b)). Similar data were collected from other glass series with O/P ratios > 3.25.

4. Discussion

4.1. Quantitative analysis of HPLC data

A comparison of the O/P ratios calculated from the HPLC results with values determined from the analyzed glass compositions is shown in Fig. 3. Eq. (1) is used to determine the overall O/P ratios of the glasses from the HPLC data.

$$\frac{O}{P} = \frac{\sum(\frac{3n+1}{n} * A(P_n))}{\sum(A(P_n))} \quad (1)$$

where $A(P_n)$ is the relative area of a peak assigned to a phosphate anion with n tetrahedra. There is a good agreement between the ratios expected from the ICP compositions and the ratios measured by HPLC for glasses with O/P > 3.25, where the smaller phosphate anions (orthophosphate, PO_4^{3-}, pyrophosphate, $P_2O_7^{4-}$ and triphosphate, $P_3O_{10}^{5-}$) are dominant. Fig. 3 also shows a comparison of the calculated average phosphate chain length ($\bar{n}$) from the HPLC experiments with the predicted $\bar{n}$ from glass composition. The

predicted $\bar{n}$ is calculated from glass composition by Eq. (2) based on a simple structural model for phosphate glasses [21],

$$\bar{n} = \frac{2}{\sum_j [M_j] Z_j / [P] - 1} \quad (2)$$

where $[M_j]$ is the molar concentration of metal cation j, Z_j is the valence of metal cation j and [P] is the molar concentration of phosphorus. The good agreement of the O/P ratios and $\bar{n}$ calculated from the HPLC data with values determined from the analyzed compositions for glasses with O/P > 3.25 indicates that the structural information obtained by HPLC is representative for glasses with shorter phosphate chains.

4.2. Distribution of phosphate anions and Q^i sites by disproportionation reactions

As the O/P ratio increases in the polyphosphate glass range, the relative concentration of pyrophosphate anions (P_2, $P_2O_7^{4-}$) increases. When O/P = 3.5, the pyrophosphate stoichiometry is reached and the main anionic unit in the glass network is P_2. HPLC indicates that other anions, besides the pyrophosphate anions, exist in these glasses (Fig. 2). Disproportionation reactions in glass melts, which have been related to the glass formation energy, explain the presence of P_1 and other P_n anions in glasses with nominal pyrophosphate compositions [7,8,22]. The Flory distribution model can be used to describe the distribution of chains in phosphate melts [23]:

$$2(P_nO_{3n+1})^{-(n+2)} \leftrightharpoons (P_{n+1}O_{3n+4})^{-(n+3)} + (P_{n-1}O_{3n-2})^{-(n+1)} \quad (3)$$

This reaction can be also reformulated in terms of the Q^i site distributions [7]:

$$2Q^i \leftrightharpoons Q^{i+1} + Q^{i-1} \quad (4)$$

Fig. 4 shows the fractions of P_n in each chain of glasses with similar O/P ~3.49. As Fe/P ratio increases from 0.23 to 0.66, the pyrophosphate disproportionation reaction

shifts to the right, and the anion distributions approach the Flory distribution, which is indicated by the solid curve and calculated from Eq. (5) [22],

$$N(P_nO_{3n+1}) = \frac{1}{\bar{n}}\left(\frac{\bar{n}-1}{\bar{n}}\right)^{n-1} \quad (5)$$

where N is the concentration of an anion and $\bar{n}$ is the average phosphate chain length.

Wider distributions of phosphate anions result from shifting the disproportionation reactions (3) and (4) to the right and the extent of these reactions determines the overall phosphate chain length distributions. For an ideal Flory distribution, the equilibrium constant K_n of reaction (3) equals 1. The actual distributions of phosphate anions in a glass network are narrower than the ideal Flory distribution; K_n is less than 1 for shorter phosphate anions (n = 2, 3 or 4) and approaches to 1 when n increases [8,22].

Reaction (3) can be simplified to consider the pyrophosphate anions:

$$2P_2 \leftrightharpoons P_1 + P_3 \quad (6)$$

By assuming that reaction (6) is an equilibrium chemical reaction, the equilibrium constant for the reaction, K_2, can be determined from the relative areas of the appropriate peaks in the chromatographs according to:

$$K_2 = \frac{[A(P_1)/1][A(P_3)/3]}{[A(P_2)/2]^2} \quad (7)$$

Fig. 5 shows the values of K_2 calculated for the Na-Fe-phosphate glasses with O/P > 3.25, as a function of the relative fraction of iron cations, calculated from Eq. (8),

$$Fe/(Na + Fe) = \frac{N(Fe^{2+})+N(Fe^{3+})}{N(Na^{+})+N(Fe^{2+})+N(Fe^{3+})} \quad (8)$$

where N(M) is the molar fraction of each metal cation. From Fig. 5, replacing sodium with iron promotes pyrophosphate disproportionation; viz., K_2 increases. Cations with

greater field strengths, as well as glasses with a greater $\bar{n}$, produce wider distributions of phosphate anions.

A similar disproportionation reaction analysis can be made for the Q^i site distributions:

$$2Q^1 \leftrightharpoons Q^2 + Q^0 \tag{9}$$

$$K(Q^1) = \frac{[Q^2][Q^0]}{[Q^1]^2} \tag{10}$$

Fig. 6 (a) shows the fraction of Q^i-tetrahedra, which are determined from the relative concentrations of P_n anions from the HPLC chromatographs. The corresponding equilibrium constant $K(Q^1)$ is shown in Fig. 6 (b). If the phosphate chain lengths are described by an ideal Flory distribution, then $K(Q^1) = 0.25$ [22,23]. The compositional dependence of $K(Q^1)$ is similar to the dependence of K_2 (Fig. 5 and Fig. 6 (b)). The actual distribution of phosphate chains or Q^i sites falls between an ideal Flory distribution and zero site disproportionation. As Fe/P increases, the disproportionation reactions of P_2 (reaction (6)) or Q^1 (reaction (9)) shifts to the right and the distribution of phosphate anions and Q^i sites broaden.

In their study of mixed cation phosphate glasses, Meadowcroft *et al.* [22] found that glasses with two cations with the greatest difference between their ionic field strengths have the most negative exothermic enthalpy of mixing in glass melts, and this was related to differences in the polarization of non-bridging oxygens associated with the different cations. Meadowcroft *et al.* also proposed that the extent to which the values of K_n differ from unity may be attributed to endothermic enthalpy changes associated with the disproportionation reaction (3). Heat formation measurements have shown that glasses containing cations with lower field strengths lead to a greater enthalpy ΔH_n for

each disproportionation reaction, and to narrower distributions of phosphate anions [24]. Sales *et al.* [8] have shown that greater field strength cations are also associated with lower free energies of formation for their respective crystalline orthophosphates. In the present study, as Na^+ is replaced by Fe^{2+} and/or Fe^{3+} in glass melts with a constant O/P ratio, the distribution of phosphate chains becomes broader (K_2 increases), thus indicating that the ΔH_n for the endothermic disproportionation reaction should decrease.

5. Summary

HPLC is a useful technique to obtain quantitative analysis of the phosphate anions that constitute the structures of sodium-iron phosphate glasses; quantitative analyses of the P-anion distributions are possible for glasses with O/P > 3.25. Equilibrium constants (K_2 and $K(Q^1)$) related to disproportionation reactions in the glass melts can be obtained from the chromatographs, and when iron replaces sodium, these disproportionation reactions produce wider distributions of phosphate anions.

Acknowledgements

The authors are very grateful to Charmayne E. Smith (Missouri University of Science and Technology) for her help with the HPLC experiments, Xiaoming Cheng (Missouri University of Science and Technology) for her help with the ICP analysis. This work was supported by the Nuclear Energy University Program (US Department of Energy) under grant NEUP 09-144.

Table 1 Batched and analyzed compositions of the sodium iron phosphate glasses

O/P	Fe/P	Batched composition/mol%			Analyzed mol% of glasses (RSD < 4 %)					Ion ratios in glasses			
		Na_2O	Fe_2O_3	P_2O_5	Na_2O	P_2O_5	Fe_2O_3	FeO	SiO_2	Fe^{2+}/Fe_{tot}	O/P	Fe/P	Si/P
3.25	0.50	0.00	33.33	66.67	0.00	60.75	25.19	9.01	5.05	0.15	3.28	0.49	0.04
	0.40	17.00	23.89	59.11	14.33	55.10	16.47	9.47	4.63	0.22	3.25	0.38	0.04
	0.33	28.00	17.78	54.22	25.57	51.86	12.95	7.17	2.45	0.22	3.24	0.32	0.02
	0.23	40.00	11.11	48.89	36.49	46.76	7.69	5.81	3.25	0.27	3.27	0.23	0.03
	0.13	50.00	5.56	44.44	48.31	43.28	5.63	1.52	1.26	0.12	3.30	0.15	0.01
	0.00	60.00	-	40.00	59.86	40.14	-	-	-	-	3.25	0.00	-
3.4	0.60	0.00	37.50	62.50	0.00	60.07	31.03	7.96	0.95	0.11	3.36	0.58	0.01
	0.50	16.00	28.17	55.83	14.17	52.96	21.72	8.55	2.60	0.16	3.38	0.49	0.02
	0.40	30.00	20.00	50.00	29.08	47.03	14.88	6.69	2.32	0.18	3.40	0.39	0.02
	0.33	38.00	15.33	46.67	36.21	44.05	11.14	5.76	2.84	0.21	3.42	0.32	0.03
	0.23	47.00	10.08	42.92	45.36	41.15	7.75	3.68	2.06	0.19	3.43	0.23	0.03
	0.13	55.50	5.13	39.38	55.16	38.21	4.40	1.15	1.08	0.12	3.44	0.13	0.01
	0.00	64.30	-	35.71	Cannot form glass by conventional melting and quenching techniques.								
3.5	0.67	0.00	40.00	60.00	0.00	54.88	29.94	12.34	2.84	0.17	3.48	0.66	0.03
	0.60	11.00	33.40	55.60	10.06	50.92	23.63	11.74	3.64	0.20	3.48	0.58	0.04
	0.50	25.00	25.00	50.00	23.56	47.22	18.67	8.27	2.29	0.18	3.48	0.48	0.02
	0.40	36.00	18.40	45.60	34.06	43.26	13.66	6.80	2.23	0.20	3.50	0.39	0.03
	0.33	43.00	14.20	42.80	39.45	41.72	11.43	5.33	2.07	0.19	3.50	0.34	0.02
	0.23	51.50	9.10	39.40	49.36	38.70	7.67	2.52	1.75	0.14	3.51	0.23	0.02
	0.13	59.00	4.60	36.40	Cannot form glass by conventional melting and quenching techniques.								

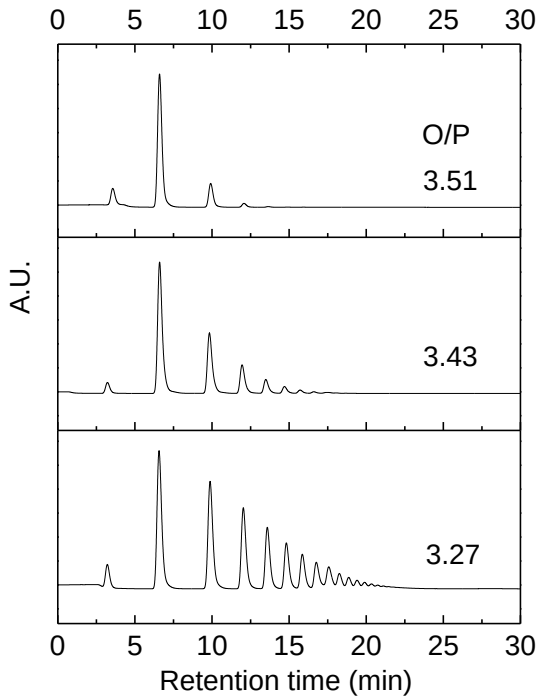

Fig. 1. HPLC chromatographs of sodium-iron phosphate glasses with similar Fe/P ratios (0.23 ± 0.01).

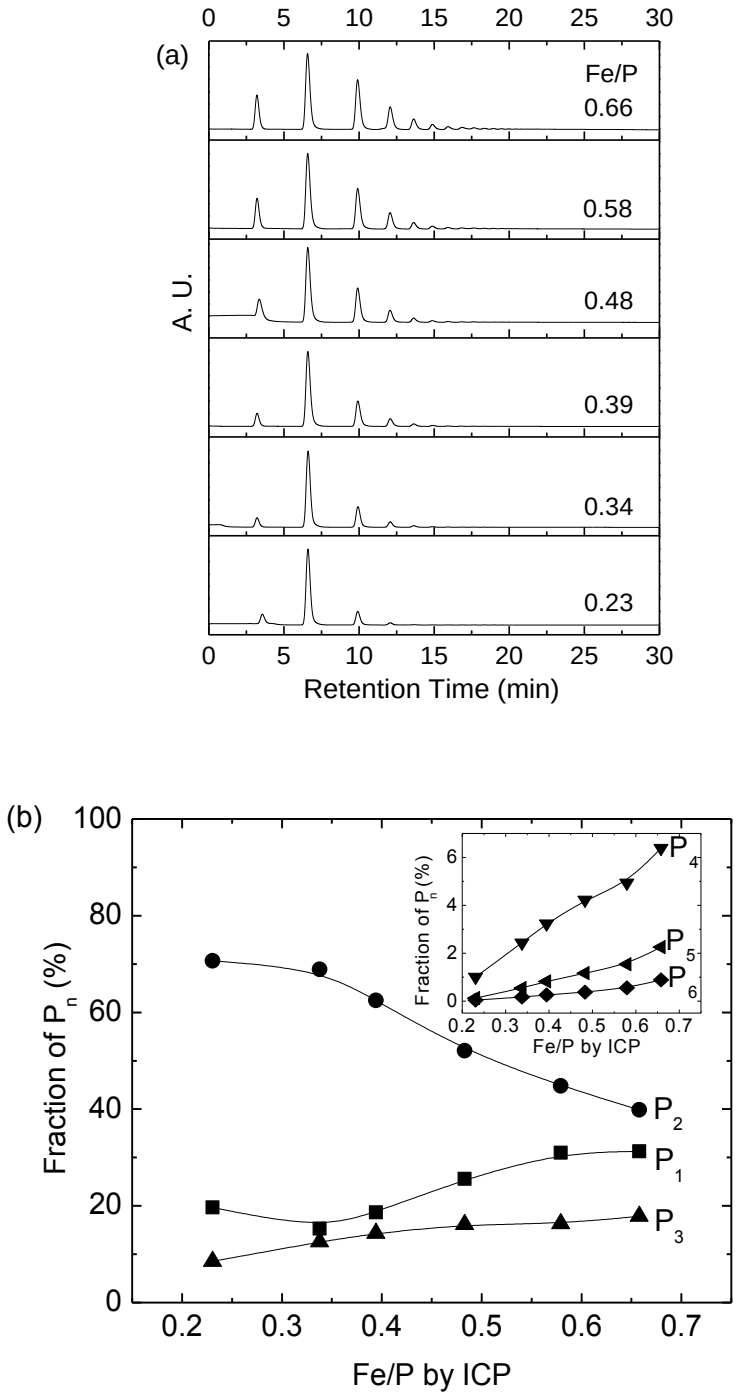

Fig. 2. (a) HPLC chromatographs of sodium-iron phosphate glasses with similar O/P ratios (3.49 ± 0.01); (b) Fraction of P_n anions determined from these chromatographs. The solid lines are guides for the eye.

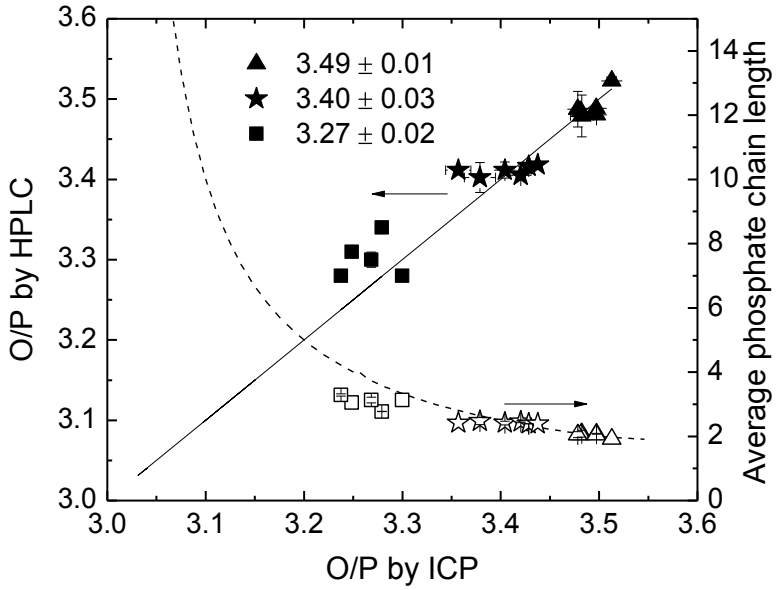

Fig. 3. A comparison of O/P ratios (left axis) and average phosphate chain-lengths ($\bar{n}$) (right axis) determined from the HPLC chromatographs with those predicted from the glass compositions (solid lines). The dashed curve is $\bar{n}$ predicted from analyzed compositions.

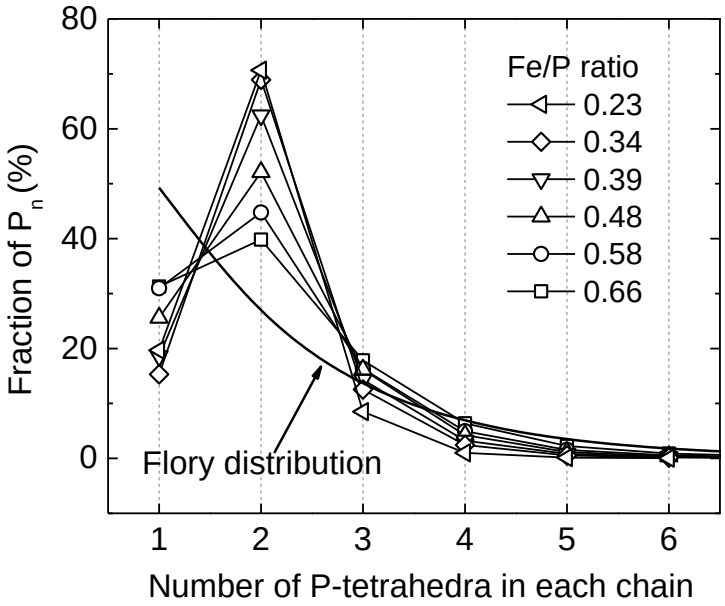

Fig. 4. P_n anion distributions for the sodium iron phosphate glasses with similar O/P ratios (3.49 ± 0.01) obtained from the chromatographs (symbols) and compared to an ideal Flory distribution (solid line).

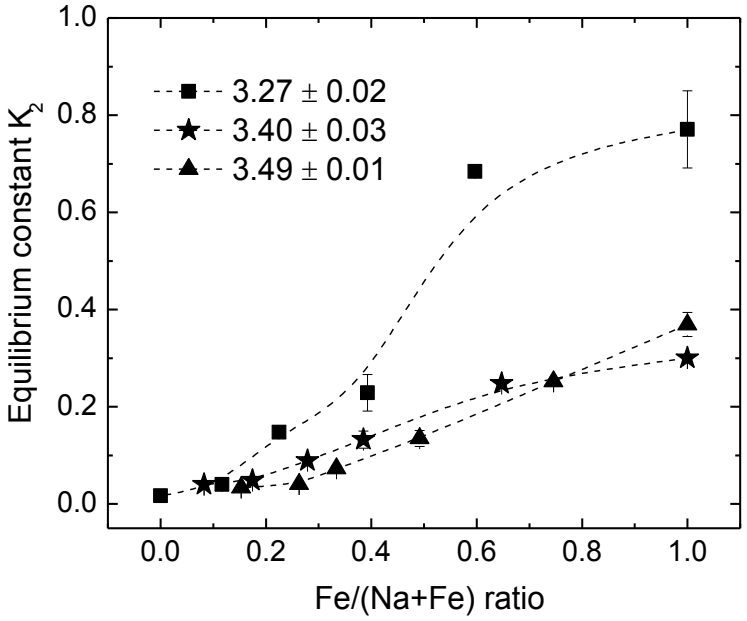

Fig. 5. Equilibrium constant (K_2, Eq. (7)) for the pyrophosphate disproportionation reaction for three series of glasses as a function of the fraction of iron cations. The dashed lines are guides for the eye.

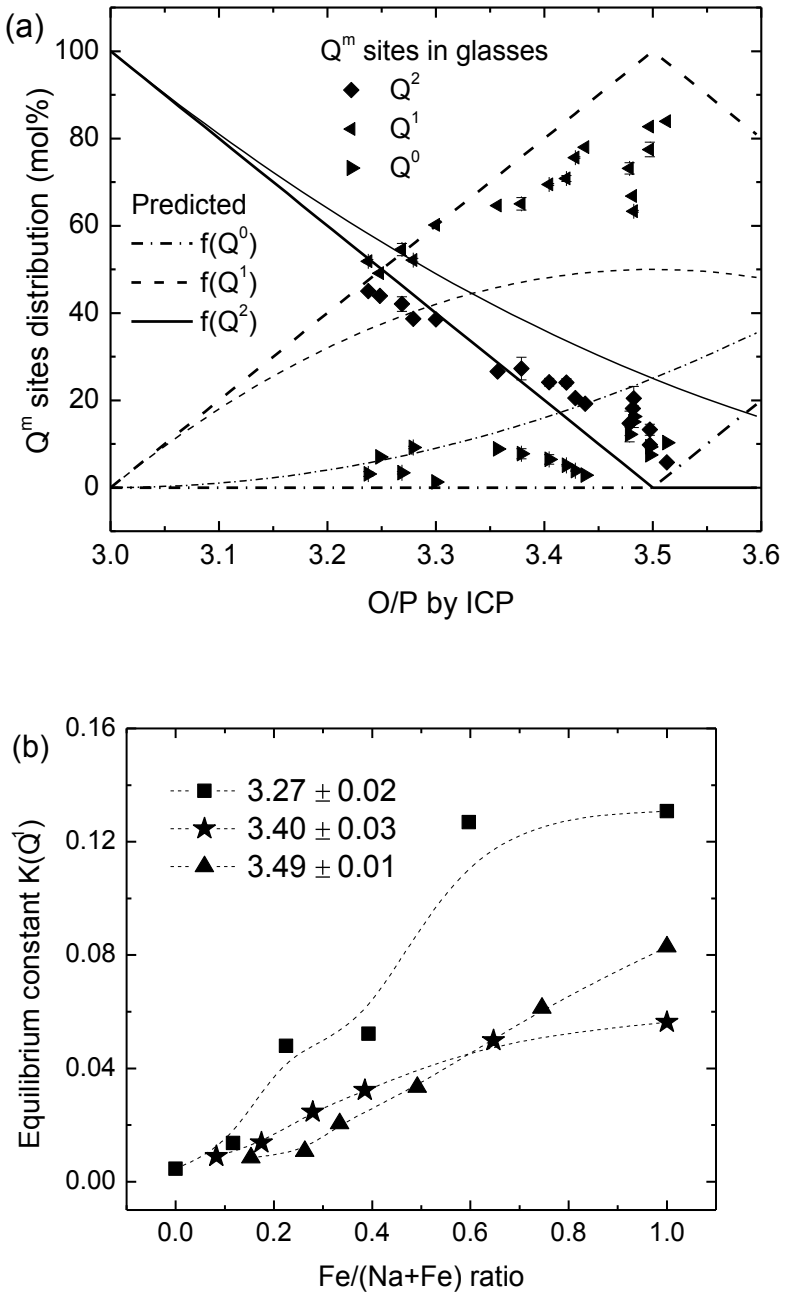

Fig. 6. (a) Distribution of Q^i sites for the sodium iron phosphate glasses calculated from the respective chromatographs. The heavy line is the predicted $f(Q^i)$ without site disproportionation. Fine lines are $f(Q^i)$ following ideal Flory distribution; (b) Equilibrium constant $K(Q^1)$ for reaction (10) determined by HPLC with compositions determined by ICP. The lines are guides for the eye.

References

[1] D.E. Day, Z. Wu, C.S. Ray, and P. Hrma. "Chemically durable iron phosphate glass wasteforms." Journal of non-crystalline solids 241, no. 1 (1998): 1-12.

[2] G. Górecki. "Iron phosphate coatings-composition and corrosion resistance." Corrosion 48, no. 7 (1992): 613-616.

[3] P. Jóźwiak, J.E. Garbarczyk, M. Wasiucionek, I. Gorzkowska, F. Gendron, A. Mauger, and C. Julien. "The thermal stability, local structure and electrical properties of lithium-iron phosphate glasses." Materials Science-Poland 27, no. 1 (2009).

[4] S. Yang, P.Y. Zavalij, and M. Stanley Whittingham. "Hydrothermal synthesis of lithium iron phosphate cathodes." Electrochemistry Communications 3, no. 9 (2001): 505-508.

[5] I. Ahmed, C.A. Collins, M.P. Lewis, I. Olsen, and J.C. Knowles. "Processing, characterisation and biocompatibility of iron-phosphate glass fibres for tissue engineering." Biomaterials 25, no. 16 (2004): 3223-3232.

[6] A.C. Wright, R.N. Sinclair, J.L. Shaw, R. Haworth, G.K. Marasinghe, and D.E. Day. "A neutron diffraction study of the structure of iron phosphate glasses." Physics and Chemistry of Glasses-European Journal of Glass Science and Technology Part B 49, no. 1 (2008): 1-7.

[7] J.R. Van Wazer. "Phosphorus and its compounds, volume 1: chemistry." Interscience Publishers (1958): 717-800.

[8] B.C. Sales, L.A. Boatner, and J.O. Ramey. "Intermediate-range order in simple metal-phosphate glasses: The effect of metal cations on the phosphate-anion distribution." Journal of non-crystalline solids 232 (1998): 107-112.

[9] B.C. Sales, L.A. Boatner, and J.O. Ramey. "Chromatographic studies of the structures of amorphous phosphates: a review." Journal of Non-Crystalline Solids 263 (2000): 155-166.

[10] B.C. Sales, J.U. Otaigbe, G.H. Beall, L.A. Boatner, and J.O. Ramey. "Structure of zinc polyphosphate glasses." Journal of non-crystalline solids 226, no. 3 (1998): 287-293.

[11] P.A. Bingham, R.J. Hand, O.M. Hannant, S.D. Forder, and S.H. Kilcoyne. "Effects of modifier additions on the thermal properties, chemical durability, oxidation state and structure of iron phosphate glasses." Journal of Non-Crystalline Solids 355, no. 28 (2009): 1526-1538.

[12] C.W. Kim, C.S. Ray, D. Zhu, D.E. Day, D. Gombert, A. Aloy, A. Moguš-Milanković, and M. Karabulut. "Chemically durable iron phosphate glasses for vitrifying sodium bearing waste (SBW) using conventional and cold crucible induction melting (CCIM) techniques." Journal of nuclear materials 322, no. 2 (2003): 152-164.

[13] L. Zhang, M.E. Schlesinger, and R.K. Brow. "Phase equilibria in the Fe_2O_3–P_2O_5 system." Journal of the American Ceramic Society 94, no. 5 (2011): 1605-1610.

[14] S.I. Grishin, J.M. Bigham, and O.H. Tuovinen. "Characterization of jarosite formed upon bacterial oxidation of ferrous sulfate in a packed-bed reactor." Applied and environmental microbiology 54, no. 12 (1988): 3101-3106.

[15] J.W. Wiench, M. Pruski, B. Tischendorf, J.U. Otaigbe, and B.C. Sales. "Structural studies of zinc polyphosphate glasses by nuclear magnetic resonance." Journal of Non-Crystalline Solids 263 (2000): 101-110.

[16] B.C. Tischendorf. Interactions between water and phosphate glasses. University of Missouri-Rolla, Rolla, MO (2005).

[17] G.K. Marasinghe, M. Karabulut, C.S. Ray, D.E. Day, M.G. Shumsky, W.B. Yelon, C.H. Booth, P.G. Allen, and D.K. Shuh. "Structural features of iron phosphate glasses." Journal of non-crystalline solids 222 (1997): 144-152.

[18] H. Akamatsu, S. Oku, K. Fujita, S. Murai, and K. Tanaka. "Magnetic properties of mixed-valence iron phosphate glasses." Physical Review B 80, no. 13 (2009): 134408.

[19] C.R. Kurkjian, and D.N.E. Buchanan. "Mössbauer absorption of Fe^{2+} in inorganic glasses." Phys. Chem. Glasses 5 (1964): 63-70.

[20] P.A. Bingham, R.J. Hand, and S.D. Forder. "Doping of iron phosphate glasses with Al_2O_3, SiO_2 or B_2O_3 for improved thermal stability." Materials research bulletin 41, no. 9 (2006): 1622-1630.

[21] B.C. Sales, R.S. Ramsey, J.B. Bates, and L.A. Boatner. "Investigation of the structural properties of lead-iron phosphate glasses using liquid chromatography and Raman scattering spectroscopy." Journal of non-crystalline solids 87, no. 1 (1986): 137-158.

[22] T.R. Meadowcroft, and F.D. Richardson. "Structural and thermodynamic aspects of phosphate glasses." Transactions of the Faraday Society 61 (1965): 54-70.

[23] P.J. Flory. "Random reorganization of molecular weight distribution in linear condensation polymers." Journal of the American Chemical Society 64, no. 9 (1942): 2205-2212.

[24] T.R. Meadowcroft, and F.D. Richardson. "Heats of formation of some crystalline and glassy phosphates." Transactions of the Faraday Society 59 (1963): 1564-1571.

II. STRUCTURAL STUDY OF Na_2O–FeO–Fe_2O_3–P_2O_5 GLASSES BY RAMAN AND MÖSSBAUER SPECTROSCOPY

Lina Ma[a], Richard K. Brow[a,*], Amitava Choudhury[b]

[a] Department of Materials Science & Engineering, Missouri University of Science & Technology, Straumanis-James Hall, 1400 N. Bishop Ave, Rolla, MO, USA

[b] Department of Chemistry, Missouri University of Science & Technology, Schrenk Hall, 400 W. 11th ST, Rolla, MO, USA

ABSTRACT

Five series of Na_2O–FeO–Fe_2O_3–P_2O_5 glasses with compositional ranges of $3.0 < O/P < 3.5$ and $0 < Fe/P < 0.67$ were prepared. Glass structure was studied using Raman spectroscopy and Mössbauer spectroscopy. For glasses with similar O/P ratios, an increase in the Fe/P ratio produced broader distributions of phosphate anions, as indicated in the Raman spectra, and the average coordination number (CN_{Fe}) of the Fe ions decreased, as indicated by the Mössbauer data. The interaction between phosphate anions and iron polyhedra causes systematic changes in the Raman frequencies as well as peak intensities.

Keywords: Raman; Mössbauer; iron-phosphate glass; disproportionation reaction

* Corresponding author, brow@mst.edu

1. Introduction

Iron phosphate glasses have been studied for a variety of applications. Their excellent chemical durability, often equivalent to or better than borosilicate glasses, makes iron phosphate glasses potential hosts to vitrify radioactive wastes [1,2,3]. Iron phosphate glasses have also been developed as biomaterials with tailored rates of degradation in aqueous environments [4]. The coexistence of two valence states of iron, Fe^{2+} and Fe^{3+}, leads to interesting semiconducting and magnetic properties for iron phosphate glasses [5,6,7,8,9].

The properties of iron phosphate glasses depend on their structures, which in turn are determined by the chemistry and concentration of metal oxides added to the glasses and their effects on the resulting phosphate anion (chain length) distributions. Structural models of iron phosphate glasses have been developed from the structures of corresponding iron phosphate crystals and tested using many techniques, including Raman spectroscopy, Mössbauer spectroscopy, X-ray and neutron diffraction, X-ray photoelectron spectroscopy, X-ray absorption fine-structure (XAFS) measurements and molecular dynamics simulation [2,10,11,12,13,14].

Compared to iron phosphate crystals, the structural complexity of iron phosphate glasses is increased by the distortion of Fe-polyhedra and by disproportionation reactions of phosphate anions in the melts [10,11]. The fraction of Fe^{2+} ions in glasses varies with preparation conditions and glass composition. The relative fraction of Fe^{2+}/Fe_{tot} is typically about 20% for glasses obtained by conventional melting (in air) and quenching techniques, although that fraction increases with increasing melt temperature [2,15,16]. For iron phosphate glasses in the O/P range from 3.0 (metaphosphate) to 4.0

(orthophosphate), ferric ions are found in tetrahedral and octahedral sites, and ferrous ions are found in octahedral and perhaps pentahedral sites [11]. Chain-like phosphate anions are linked through these iron sites in a distorted iron chelate structure. The average bond lengths and angles associated with various metal polyhedra also vary with glass composition [17,18,19,20].

Disproportionation reactions in melts broaden the distributions of phosphate anions in the glasses [21,22]. The nature of the metal cations added to a glass composition affects the distribution of phosphate anions. Cations with greater field strengths are associated with glasses with broader distributions of phosphate anions and these cations are also associated with lower free energies of formation for their respective crystalline orthophosphates [22].

In the present work, five series of Na_2O–FeO–Fe_2O_3–P_2O_5 glasses with constant O/P ratios (3.0~3.5) and different Fe/P (0~0.67) ratios were prepared by conventional melting (in air) and quenching techniques. These compositions are simpler versions of the iron phosphate glasses used to encapsulate high alkaline nuclear waste streams [13]. A chromatographic study of the phosphate anion distributions in some of these glasses is presented elsewhere [23].

2. Experimental Procedures

Iron phosphate glasses, with the batched compositions given in Table 1, were prepared from raw materials including Na_2CO_3 (Alfa Aesar, ≥ 98%), Fe_2O_3 (Alfa Aesar, ≥ 99%) and $NH_4H_2PO_4$ (Alfa Aesar, ≥ 98%). Batches that produced 100g of glass were thoroughly mixed and melted in fused SiO_2 crucibles (Leco #728-701) between 1000 °C

and 1250 °C in air for two hours; greater temperatures were generally required for melts with greater iron contents. The melts were poured onto a copper plate and quenched to room temperature by pressing with another copper plate. Compositional series, labeled from A to E, have batched O/P ratios between 3.0 and 3.5, as described in Table 1. For example, glass E-0.67 is a sample in the E-series with batched O/P ratio of 3.5 and a batched Fe/P ratio of 0.67. Binary Na_2O–P_2O_5 glasses with batched O/P ratios in the range 3.0–3.25 (50–60 mol% Na_2O) were also melted in air and quenched to room temperature.

The compositions of the quenched glasses were determined by inductively-coupled plasma optical emission spectroscopy (ICP-OES, PerkinElmer Optima 2000 DV, Norwalk, USA). Iron phosphate glasses were digested in 3–7 M H_2SO_4 aqueous solution for 7 to 14 days at 80–90 °C in closed Teflon containers. The digestion time and temperature depended on the chemical durability of the glasses. Generally, glasses with high iron contents and low O/P ratios dissolved more slowly in the H_2SO_4 solution. Binary sodium phosphate glasses were dissolved in deionized H_2O. Solutions for ICP were diluted with deionized H_2O, with dilution factors of 1:9 or 1:99, depending on the expected ion concentration of the solution. The Fe^{2+}/Fe_{tot} contents of the glasses were determined by a titration technique using $KMnO_4$ (2 mM), with an absolute uncertainty of 2% [24].

Raman spectra were collected from the top melt surface of each quenched glass using a Horiba Jobin Yvon LabRAM Aramis μ-Raman spectrometer (Horiba-Jobin Yvon, Inc., Edison, NJ). A 632.8 nm He-Ne laser with initial power of 17 mW was used as the excitation source with a 10× objective. All spectra reported here have been normalized to

a constant maximum peak intensity, and there was no evidence for laser-induced changes in the Raman spectra collected.

^{57}Fe Mössbauer spectra were collected to characterize the valence states of iron as well as the coordination environment of iron polyhedra (FeO_n) in the glass network. The spectra were collected in transmission geometry at room temperature using a conventional constant acceleration spectrometer with a 50mCi ^{57}Co gamma-ray source embedded in rhodium matrix. The velocity scale of the spectrometer was calibrated using a spectrum of α-Fe foil at room temperature. All Mössbauer spectra were analyzed by Lorentzian line fitting into three doublet sites using the Recoil software [25,26]. Peak positions and areas were allowed to vary until a best-fit solution was achieved. To minimize the effect of sample preparation on spectral line width and line shape, Mössbauer absorber parameters were calculated based on the stoichiometry of the glass sample to optimize sample thickness, according to the Recoil software. Uniformly spread 60–80 mg/cm^2 sample powder (200–250 micron thickness) were loaded on the 1 cm diameter sample holder, corresponding to approximately 2×10^{18} Fe-57 atoms/cm^2.

3. Results

3.1. Glass compositions

Table 1 lists the compositions of sodium iron phosphate glasses prepared for this study. Because Fe (III) was reduced to Fe (II) in the melt, and because some SiO_2 from the crucible was incorporated into the melts, the analyzed compositions from the ICP analyses are slightly different from the batched compositions. The average Si/P ratio in

the glasses is about 0.03 ± 0.01; Bingham et al. [27] report that similar silica contents had little effect on the properties of their iron phosphate glasses.

Titration analyses indicate that the average Fe^{2+}/Fe_{tot} ratio for all glasses is about 0.19 ± 0.05, consistent with previous studies [15,16,28]. Greater concentrations of ferrous ions (up to 31%) were found in glasses with lower O/P ratios, which were melted at higher temperatures. The fraction of Fe^{2+} species determined by the titration technique is systematically lower, by about 15%, than what was determined by Mössbauer spectroscopy (Table 2). Since there is no evidence for oxidation of Fe^{2+} in sulfuric acid during glass digestion, and there is some uncertainty in fitting the Mössbauer spectra, related to accurately knowing the recoil-free fraction for each Fe valence state [29], the Fe^{2+}/Fe_{tot} ratios determined by the titration method are used in the quantitative analyses of glass structures discussed below. However, as will be seen, the small differences in Fe^{2+}/Fe_{tot} determined by the two techniques have no significant effects on the structural analyses and the systematic study presented here.

Fig. 1 shows the compositional diagram of the Na_2O–FeO–Fe_2O_3–P_2O_5 glasses with the analyzed compositions (Table 1) indicated by the black symbols. A glass series with a constant O/P ratio (3.0, 3.1, 3.25, 3.4 and 3.5) is indicated by the respective lines. The calculated O/P ratios account for both the presence of the ferrous ions and the incorporation of the silica in glasses. Each line assumes that the Fe^{2+}/Fe_{tot} ratio is the average analyzed Fe^{2+}/Fe_{tot} ratio for that glass series.

3.2. Raman spectroscopic results

Fig. 2 shows the Raman spectra from glasses with similar Fe/P ratios (0.23 ± 0.01) and different O/P ratios. Fig. 3 (a) and Fig. 3 (b) show the spectra from glasses with similar O/P ratios, the B-series (3.12 ± 0.02) and E-series (3.49 ± 0.01), respectively, but different Fe/P ratios. Raman band assignments listed in Table 3 are from the literature [10,30,31]. Peaks in the range from about 970 cm^{-1} to about 1320 cm^{-1} are assigned to symmetric and asymmetric stretching modes of non-bridging oxygens on different P-tetrahedra, with a systematic decrease in peak frequency for $P–O_{nb}$ bonds on Q^2, Q^1, and Q^0 tetrahedra. The Q^i terminology is used to describe a phosphate tetrahedron with 'i' bridging oxygens [32].

Peaks in the 680–770 cm^{-1} range are assigned to the P–O–P symmetric stretching modes associated with bridging oxygens that link two neighboring tetrahedra, with greater frequencies associated with bridging oxygens linked to one or two Q^1 tetrahedra. Asymmetric P–O–P stretching modes produce peaks in the range 890–1000 cm^{-1}, e.g., peaks near 894 cm^{-1} in the spectra of the E-series of glasses (O/P ~3.49) in Fig. 3 (b) [10].

For the series of glasses with similar Fe/P ratios, the Raman spectra in Fig. 2 are consistent with the formation of progressively shorter phosphate anions with increasing O/P ratios. The intensities of the peaks in the range 1130–1220 cm^{-1}, assigned to the PO_2 symmetric stretching modes of non-bridging oxygens on Q^2-tetrahedra, decrease with increasing O/P ratio relative to the broader peaks in the 1030–1100 cm^{-1} range, assigned to the PO_3 symmetric stretching modes of non-bridging oxygens on Q^1-tetrahedra. With increasing O/P ratio, the P–O–P symmetric stretching mode shifts from ~700 cm^{-1} to ~745 cm^{-1}, consistent with the replacement of Q^2 tetrahedra by Q^1 tetrahedra as the

average P-anion becomes shorter, and perhaps as the average P–O–P bond angle increases. Peaks associated with the P–O–P asymmetric stretching mode (centered ~890 cm^{-1}) are evident in the Raman spectra for glasses with O/P ≥ 3.27. In the low frequency range (200–600 cm^{-1}) in Fig. 2, the intensities of the bending modes associated with smaller anions grow in spectra from glasses with greater O/P ratios.

Systematic structural changes in glasses with similar O/P ratios and different Fe/P ratios were also observed in the Raman spectra. For example, as the Fe/P ratio increases from 0 to 0.42 for glasses with O/P ~3.12 (Fig. 3 (a)), the frequency of the PO_2 peak increases, from 1142 cm^{-1} to 1200 cm^{-1}, and the peak broadens. The increase in peak frequency as Fe replaces Na is consistent with the reported effects of increasing cation field strengths on the Raman spectra of metaphosphate glasses [33,34], and the broader peaks indicate a more complex average coordination environment for these Q^2 tetrahedra. In addition, the relative intensity of the peak assigned to the PO_3-stretching modes associated with the Q^1-tetrahedra (centered near 1068 cm^{-1}) increases, indicating that more chain-terminating tetrahedra, and so shorter phosphate anions, are associated with the greater Fe/P glasses. Similar observations can be made of the Raman spectra for glasses with O/P~3.49 (Fig. 3 (b)). With increasing Fe/P ratio, the Raman peak assigned to the PO_3 stretching modes of non-bridging oxygens on Q^1-tetrahedra also increases in frequency (from 1044 to 1077 cm^{-1}) and becomes broader. For every glass series with similar O/P ratios, the frequency of the peaks associated with symmetric P–O–P-stretching mode (680–770 cm^{-1}) increases and the relative intensity decreases with increasing Fe/P ratio.

The Raman spectrum for each glass in this study was decomposed into seven Gaussian peaks in the range of 650–1400 cm^{-1} and the relative intensity of each of these peaks was determined. Peak position and FWHM (full width at half maximum) were allowed to vary until a best-fit solution was achieved [10]. An example of a spectral decomposition is shown for the E-0.33 glass in Fig. 4.

3.3. Mössbauer spectroscopic results

Mössbauer spectra for glasses in the E-series (O/P ~3.49) are shown in Fig. 5 (a). These spectra are similar to those reported for iron phosphate glasses with similar O/P ratios [11,15,19,20,35], and so are analyzed in a similar manner. Each Mössbauer spectrum was decomposed into three sets of doublets using Lorentzian line shapes (e.g., Fig. 5 (b)). These doublets represent Fe^{2+} (less intense absorption) in an octahedral site, and Fe^{3+} (more intense absorption) in both tetrahedral and octahedral sites; two doublets are used to decompose the markedly asymmetric Fe^{3+} contributions to each spectrum. These fits are consistent with earlier Mössbauer studies of iron phosphate glasses [9,11,15,19,35].

The corresponding parameters, isomer shift (IS in mm/s), quadrupole splitting (QS in mm/s), FWHM (full width at half maximum) of the Lorentzian contribution to the peak (w in mm/s), and the relative fractions of the three doublet sites to total iron contents ($[FeO_n]/Fe$), as well as the fitting uncertainties (χ^2), are listed in Table 2. The IS values obtained are in the range typical of the isomer shift for iron phosphate glasses and compounds [19,20,35,36]. For the two Fe^{3+} sites, the octahedral site corresponds to the larger IS value. With increasing Fe/P ratios for glasses with similar O/P (e.g., E-series

with O/P ~3.49), the fraction of ferrous ions in tetrahedral sites, $f[Fe^{3+}O_4]$, generally increases; this leads to a decrease in the average Fe coordination number (CN_{Fe}) (Table 2).

4. Discussion

4.1. Iron coordination sites

The isomer shift (IS) of ^{57}Fe provides information about the iron oxidation states, iron coordination sites and the covalency of the iron-ligand bonds [36,37]. An increase of iron oxidation state leads to a decrease of the isomer shift, and for a given oxidation state, a smaller coordination number relates to a lower isomer shift [36]. The isomer shifts of the iron coordination sites in the Na–Fe–phosphate glasses are consistent with these observations (Fig. 6). From the room temperature IS for different [FeO_n] polyhedra in various compounds, the existence of [FeO_5] cannot be ruled out from all possible iron coordination sites in these glasses, because the intermediate overlapping position of IS for five-coordination falls between the IS for tetrahedral and octahedral coordination (Fig. 6) [36].

The correlation between the isomer shift and electron density of the 4s orbital for Fe^{2+} and Fe^{3+} ions with at least singly occupied 3d orbitals shows that an increase in covalency of the iron-ligand bond reduces the isomer shift. This occurs because of the increased overlapping of the iron 4s-orbital with surrounding ligand orbitals, some electron transfer from the ligands to the 4s-orbital adds covalent character to the ionic iron-ligand bond, therefore modifying the electron density around the nucleus [36,37,38,39]. In Fig. 6, the isomer shift of iron sites decreases in the order of Fe^{2+}(oct) > Fe^{3+}(oct) > Fe^{3+}(tet), which is consistent with an increase in the relative covalent

character of the Fe–O bond and a decrease in the Fe–O interaction distance for these iron coordination sites [11]. However, the correlation between Fe–O bond length and isomer shift is invalid for most iron polyhedra; the compounds with greater Fe–O distances do not have particularly greater isomer shifts, and studies show that the decrease of IS with coordination number arises primarily from the covalence effects rather than the decrease of the Fe–O distances [36].

In this study, as the polymerization of the phosphate glass network decreases with increasing O/P ratio, the covalency of the Fe–O bond in the three different iron coordination sites does not change appreciably (Table 2). For a glass series with similar O/P ratios, an increase in the Fe/P ratio has a significant effect on the covalency of the Fe–O bonds for glasses near the metaphosphate composition, e.g., the degree of Fe–O bond covalency in the Fe^{2+}(oct) sites increases with increasing Fe/P ratio for the glasses with O/P ~3.04 ± 0.01, as indicated by the systematic decrease in IS as shown in Table 2.

The iron sites in crystalline compounds or glasses have a broad range of quadrupole interactions, which are related to the electric field gradient at the nucleus, spin-states and distortion geometry. Quadrupole splitting (QS) values range from zero in symmetric compounds to 3.5 mm/s for highly distorted compounds [29,37]. For all three iron coordination sites in these phosphate glasses, Fe^{2+} is in the distorted high-spin octahedral site with inequivalent electronic configuration ($3d^6(^5D_4)$); therefore, the quadrupole splitting value of Fe^{2+}(oct) in a Mössbauer spectrum is the largest (Fig. 7 (a)) [29,35].

For Fe^{3+} with a spherically symmetric electric field environment ($3d^5(^6S)$), the QS values only depend on the deformation of the charge distribution, which in turn is

affected by the surrounding ions, and so QS for Fe^{3+} is a measure of the distortion of the iron sites, with a larger QS value meaning more distortion [20,35]. Similar to the effects of different cations on the distortion of phosphate tetrahedra, as iron is incorporated into the glass structure, an increase in the number of non-bridging oxygens involved in the iron coordination site could also cause an increase in the degree of distortion of that site. For the sodium-free iron phosphate glasses, increasing the O/P ratio increases distortion of both Fe^{3+} sites, as indicated by the increase in QS (Fig. 7 (b)). In addition, as the Fe/P ratio increases for glasses with similar O/P ratio (e.g., series E, O/P ~3.49), the QS values for both Fe^{3+} sites increase (Fig. 7 (b)), again indicating an increase in the distortion of these Fe^{3+} sites. Comparing the QS values for the two Fe^{3+} sites, the local environment around the tetrahedral Fe^{3+} sites is generally more distorted than around the octahedral sites for glasses with greater O/P ratios. These compositionally-dependent trends in QS value for Fe^{3+} sites are consistent with other studies [19,20,35].

In earlier neutron diffraction and Mössbauer studies of iron polyphosphate glasses [11,19], the fraction of $[Fe^{3+}O_4]$ increased with increasing O/P ratio, decreasing the CN_{Fe} from 6.1 to 4.8, and decreasing the average Fe–O bond length from 1.958 Å to 1.931 Å. The change in Fe–O bond length is consistent with what has been reported for iron phosphate crystals, where the Fe–O bond length decreases in the order of $[Fe^{2+}O_6]$ (2.16 Å) > $[Fe^{3+}O_6]$ (2.02 Å) > $[Fe^{3+}O_4]$ (1.85 Å) [11]. The FWHM of the Lorentzian contribution to the absorption peak in the Mössbauer spectra is related to the distribution of the Fe–O bond lengths for equivalent sites in glasses, which further indicates the uniformity of sites [20,29]. The FWHM values of iron sites for glasses in Table 2 decrease in the order of Fe^{2+}(oct) > Fe^{3+}(oct) > Fe^{3+}(tet). As the glass composition

changes, the broadening of absorption peaks for each iron site (increasing FWHM) indicates an increase of distortion and local disorder at the corresponding iron site [20,40]. As the Fe/P ratio increases for glasses with similar O/P ratio (e.g., O/P ~3.49), the uniformity of Fe^{2+}(oct) and Fe^{3+}(tet) sites decreases as does the average CN_{Fe}.

4.2. Phosphate tetrahedral network

The introduction of metal oxides into metaphosphate glasses increases the O/P ratio and produces non-bridging oxygens: Fe–O–P and Na–O–P. The connectivity of the phosphate glass network through bridging P–O–P bonds is reduced and the average chain length of the phosphate anions decreases. In other words, as the O/P ratio increases, the fraction of Q^2 sites decreases and the fraction of Q^1 sites increases [32].

The effects of composition on the relative concentrations of Q^i sites are shown by the changes in the relative peak intensities of the respective Raman spectra (e.g., Fig. 2). Fig. 8 (a) shows the effects of O/P ratio for the series with similar Fe/P ratios (0.23 ± 0.01) on the relative intensities of three Gaussian peaks used to fit the spectra, those associated with Q^0 (970–1020 cm^{-1}), Q^1 (1030–1100 cm^{-1}), and Q^2 (1130–1220 cm^{-1}) tetrahedra. With increasing O/P ratio in the polyphosphate glass range, the intensities of peaks associated with the Q^0 and Q^1 sites increase and the relative intensity of the Q^2 peak decreases. The compositional dependences of the relative intensities of the appropriate Raman peaks are in qualitative agreement with the measured distributions of phosphate anions determined by high-pressure liquid chromatography (HPLC) [23]. Those data are also shown in Fig. 8 (a).

The depolymerization of the phosphate network with increasing O/P ratio leads to systematic changes in the $(POP)_{sym}$ peak near 700 cm^{-1}. As shown in Fig. 2, with increasing O/P ratio, a shoulder near 740 cm^{-1} grows in intensity relative to the intensity of the peak at 700 cm^{-1}, becoming the dominant peak when O/P = 3.51. The greater frequency peak is due to $(POP)_{sym}$ modes associated with chain-terminating Q^1 tetrahedra, which dominate the phosphate structure at the pyrophosphate stoichiometry.

As the Fe/P ratio increases for glasses with similar O/P ratios, both the $(PO_2)_{sym}$ peak (1130–1220 cm^{-1}) and $(PO_3)_{sym}$ peak (1030–1100 cm^{-1}) broaden, indicating a greater complexity of phosphate anions in these glasses. In addition, the Raman spectra for glasses with low O/P ratios (e.g., series B, O/P ~3.12) indicate a greater relative intensity for the $(PO_3)_{sym}$ peak associated with chain-terminating tetrahedra for glasses with the greater Fe/P ratios (Fig. 8 (b)). To maintain the glass stoichiometry, either the relative fractions of Q^1 and Q^2 sites must stay the same as the Fe/P ratio increases, or additional Q^1 sites must be balanced by the formation of new Q^3 sites. It is possible that the peak near 1300 cm^{-1} in the spectra of glasses with greater Fe/P ratios in Fig. 3 (a) might be assigned to the $(P{=}O)_{sym}$ stretching mode on a Q^3 tetrahedron [41], however, this assignment seems unlikely given the chemical reactivity of such sites. A more likely assignment for the 1300 cm^{-1} peak is to $(PO_2)_{asym}$ modes associated with Q^2-tetrahedra. The increase in the relative intensity of the peak at 1068 cm^{-1} may instead reflect a change in the overall distributions of phosphate chains and rings with increasing Fe/P ratio. The average chain length for a glass with an O/P ratio of ~3.12 is eight [23]. In the iron-free glass, the narrow Raman peak indicates that the distribution of chain lengths around this average is small. As the Fe/P ratio increases, the peaks broaden, indicating a

broader distribution of longer and shorter phosphate anions. It is conceivable that, because of differences in symmetry and bond lengths, the Raman scattering cross-section of a $(PO_3)_{sym}$ mode on a Q^1 tetrahedron that terminates a small phosphate anion associated with an iron ion is significantly different from that on a Q^1 tetrahedron that terminates a longer phosphate anion associated with sodium ion. Thus, changes in relative intensities of the associated Raman peaks do not necessarily indicate changes in Q-distributions. Unfortunately, the quantitative HPLC analyses for anion distributions in these sodium iron phosphate glasses were limited to glasses with O/P > 3.25 [23], and so an independent determination of the P-anion distributions in the glasses with greater phosphate contents is not available.

The interpretation of the compositional dependences of the relative intensities of the $(PO_2)_{sym}$ and $(PO_3)_{sym}$ peaks for the O/P ~3.12 glasses is supported by the behavior of the $(POP)_{sym}$ peak in Fig. 3 (a). The peak maximum shifts to greater frequency, from 663 to 710 cm^{-1}, as the Fe/P ratio increases, but the shape of the peak does not change. For compositions with increasing O/P ratios, a high frequency peak near 745 cm^{-1} emerges as the fraction of Q^1 tetrahedra increases (i.e., Fig. 2). This new peak does not emerge in the series with the constant O/P ratio, indicating that the relative fraction of Q^1 sites does not change.

When O/P = 3.5, the pyrophosphate stoichiometry is reached and the dominant phosphate tetrahedron in the glass network is Q^1. However, Raman spectra indicate that both Q^0 and Q^2 tetrahedra are also associated with these glasses (Fig. 3 (b) and Fig. 8 (c)). These compositions could be analyzed by HPLC and the site distributions from that study

[23] are also shown in Fig. 8 (c). The uncertainty associated with the decompositions of the broad Raman spectra makes the qualitative trend not as clear as the HPLC results.

Disproportionation reactions in glass melts explain the presence of Q^0 and Q^2 sites in glasses with nominal pyrophosphate compositions [21,42]:

$$2Q^1 \leftrightharpoons Q^2 + Q^0 \quad (1)$$

The extent of these reactions determines the distributions of phosphate tetrahedra and phosphate anions. For glasses with similar O/P ratios, as the Fe/P increases, the disproportionation reaction shifts to the right and the distributions of Q^i sites and phosphate anions broaden.

In the Raman spectra of glasses with similar O/P ratios (Fig. 3), the systematic variation, with Fe/P ratio, of the frequency of Raman peaks associated with the various stretching modes indicates that there is no preferential substitution of iron for sodium on any particular phosphate site [33], but does indicate that there are systematic changes in the nature of the average phosphate tetrahedron that constitutes the polyphosphate anions. This is consistent with studies of mixed cation metaphosphate glasses that indicate that the two non-bridging oxygens on a Q^2 tetrahedron are bonded to both cations instead of preferring one or the other [43,44].

The frequencies of the $(PO_2)_{sym}$ and $(POP)_{sym}$ stretching Raman modes are determined by the chemistry of the cations associated with the non-bridging oxygens on the Q^2 units and change significantly with cation field strength (cation charge/(radius)^2) for binary phosphate glasses near the metaphosphate stoichiometry [45]. Table 4 and Fig. 9 summarizes these effects from many Raman studies reported in the literature. The greater cation field strength does correlate with greater frequencies for both the $(PO_2)_{sym}$

(Fig. 9 (a)) and $(POP)_{sym}$ (Fig. 9 (b)) vibrational modes within a particular series of compositions. However, the general dependence is more complex, reflecting different distributions and configurations of phosphate anions, as well as differences in the cation coordination environment.

The Raman peak frequencies have been related to the degree of covalency of the P–O and M–O bonds, and to changes in the O–P–O bond angles in the phosphate tetrahedra [33,34,46,47]. As high field strength metal cations are introduced into a glass structure, an increase in the covalency of the M–O bond results in an increase in the rigidity of the metaphosphate network as well as an increase in phosphate chain entanglement, which is consistent with an increase in the glass transition temperature [32,48]. For the Na–Fe–phosphate glasses with similar O/P ratios (e.g., series B), the frequency of the $(PO_2)_{sym}$ stretching mode increases from 1142 to 1200 cm^{-1} with increasing Fe/P. Because iron has a greater electronegativity than sodium, the average covalency of the $P–O_{nb}$ will be reduced, leading to narrower average O–P–O bond angles and greater frequencies for the PO_2 stretching mode [33,34,49,50].

Studies have shown that the P–O–P symmetric stretching mode (680–770 cm^{-1}) is sensitive to the configuration of the chains and to the cation polyhedra to which the chains are linked; this sensitivity is related to the delocalization of π-electrons in the P–O bonds [49,51,52]. The frequency shift of the $(POP)_{sym}$ peak reflects the average cationic environment over distances greater than a single phosphate tetrahedron [57], and is affected by the field strength of the cations (Table 4, Fig. 9 (b)). In each metal cation group, the $(POP)_{sym}$ frequency for metaphosphate glasses generally increases with cation field strength. A change in the covalent character of the $P–O_{nb}$ bond also affects the

$(POP)_{sym}$ frequency, which is associated with the reduction of π bond character in phosphate tetrahedra [49,53,54]. For glasses with similar O/P ratios, the greater frequency of $(POP)_{sym}$ is associated with smaller P–O–P bond angles [33,47]. Similar to the FWHM of PO_2-stretching modes, an increase in FWHM of $(POP)_{sym}$ suggests that the P–O–P environment is becoming more inhomogeneous with increasing Fe/P ratio [55].

For glasses with greater O/P ratios (≥ 3.27), the peak near 628 cm^{-1} (e.g., Fig. 2 and Fig. 3 (b)) decreases in intensity as Fe/P ratio increases. In the Raman spectra from alkali metaphosphate glasses, this narrow peak was observed to increase in intensity as the size of alkali increased, and this was attributed to an increase in the P–O–P bond angles associated with the stretching mode of ordered phosphate chains segments [32]. This straightening of the phosphate chains due to the ion constriction effect could be expected to occur in the vicinity of a larger cation in glass network [56]. For the sodium iron phosphate glasses in this study, the straightening of phosphate chains is expected more in glasses with greater O/P ratios and greater soda contents.

There is an interesting correlation between the composition of the Na–Fe–phosphate glasses and the intensity of the $(POP)_{sym}$ stretching mode (680–770 cm^{-1}) relative to the intensity of the $P–O_{nb}$ stretching mode (1040–1200 cm^{-1}). Fig. 10 shows that for a series of glasses with similar O/P ratios, an increase in the Fe^{3+}/P ratio correlates with a decrease in the relative intensity of the $(POP)_{sym}$ stretching mode. This same intensity ratio was found to decrease as ferric ions replaced ferrous ions in a series of sodium-free iron phosphate glasses with similar O/P ratios (~3.03) [10], and that data is also shown in Fig. 10. Nelson et al. related a similar dependence of the relative peak intensities in the Raman spectra from a series of alkali metaphosphate glasses to the

covalent character of the $P–O_{nb}$ bond [34], but it is unclear what systematic changes in the nature of the bridging oxygen bonds might be responsible for trends in relative peak intensity shown in Fig. 10.

5. Summary

Raman and Mössbauer spectra collected from five series of $Na_2O–FeO–Fe_2O_3–P_2O_5$ polyphosphate glasses provide information about the distributions of phosphate tetrahedra and the iron polyhedra that constitute the glass network.

Three iron coordination sites are indicated by the isomer shifts of peaks in the Mössbauer spectroscopic results. With increasing Fe/P ratios for glasses with similar O/P ratios, the fraction of $[Fe^{3+}O_4]$ increases and the distortion of the tetrahedral and octahedral Fe^{3+} sites increases.

Systematic structural changes in the frequencies and peak intensities were observed in the Raman spectra for in-chain and out-chain stretching modes. The shifts of $P–O_{nb}$ stretching modes and $(POP)_{sym}$ to lower frequency are associated with a greater average bond angles of O–P–O bond and P–O–P bond for lower Fe/P ratio glasses with similar O/P ratio.

The replacement of sodium by iron causes wider distributions of phosphate anions resulted from the disproportionation reactions. Systematic Raman frequency shifts indicate that there is no preferential substitution of iron for sodium on any particular phosphate site.

Acknowledgements

The authors are very grateful to Xiaoming Cheng (Missouri University of Science and Technology) for her help with the ICP analysis. This work was supported by the Nuclear Energy University Program (US Department of Energy) under grant NEUP 09-144 and by the National Science Foundation (DMR-1207520).

Table 1 Batched and analyzed compositions of the Na–Fe–phosphate glasses

O/P	Fe/P	Batched composition/mol%			Analyzed mol% of glasses (RSD < 4 %)					Ion ratios in glasses			
		Na_2O	Fe_2O_3	P_2O_5	Na_2O	P_2O_5	Fe_2O_3	FeO	SiO_2	Fe^{2+}/Fe_{tot}	O/P	Fe/P	Si/P
A-Series	0.33	0.00	25.00	75.00	0.00	67.31	19.03	11.95	1.72	0.24	3.04	0.37	0.01
3.0	0.23	20.00	15.00	65.00	18.55	59.17	9.36	8.51	4.42	0.31	3.04	0.23	0.04
	0.13	35.00	7.50	57.50	34.15	55.62	6.40	1.93	1.90	0.13	3.03	0.13	0.02
	0.00	50.00	–	50.00	51.40	48.60	–	–	–	–	3.03	0.00	–
B-Series	0.40	0.00	28.57	71.43	0.00	65.26	23.20	7.77	3.77	0.14	3.15	0.42	0.03
3.1	0.33	14.00	21.24	64.76	13.33	59.74	14.28	10.09	2.56	0.26	3.10	0.32	0.02
	0.23	30.00	12.86	57.14	28.17	53.98	8.69	6.10	3.05	0.26	3.12	0.22	0.03
	0.13	42.00	6.57	51.43	39.76	49.66	4.67	2.95	2.96	0.24	3.13	0.12	0.03
	0.00	54.50	–	45.50	54.74	45.26	–	–	–	–	3.10	0.00	–
C-Series	0.50	0.00	33.33	66.67	0.00	60.75	25.19	9.01	5.05	0.15	3.28	0.49	0.04
3.25	0.40	17.00	23.89	59.11	14.33	55.10	16.47	9.47	4.63	0.22	3.25	0.38	0.04
	0.33	28.00	17.78	54.22	25.57	51.86	12.95	7.17	2.45	0.22	3.24	0.32	0.02
	0.23	40.00	11.11	48.89	36.49	46.76	7.69	5.81	3.25	0.27	3.27	0.23	0.03
	0.13	50.00	5.56	44.44	48.31	43.28	5.63	1.52	1.26	0.12	3.30	0.15	0.01
	0.00	60.00	–	40.00	59.86	40.14	–	–	–	–	3.25	0.00	–
D-Series	0.60	0.00	37.50	62.50	0.00	60.07	31.03	7.96	0.95	0.11	3.36	0.58	0.01
3.4	0.50	16.00	28.17	55.83	14.17	52.96	21.72	8.55	2.60	0.16	3.38	0.49	0.02
	0.40	30.00	20.00	50.00	29.08	47.03	14.88	6.69	2.32	0.18	3.40	0.39	0.02
	0.33	38.00	15.33	46.67	36.21	44.05	11.14	5.76	2.84	0.21	3.42	0.32	0.03
	0.23	47.00	10.08	42.92	45.36	41.15	7.75	3.68	2.06	0.19	3.43	0.23	0.03
	0.13	55.50	5.13	39.38	55.16	38.21	4.40	1.15	1.08	0.12	3.44	0.13	0.01
	0.00	64.30	–	35.71	Cannot form glass by conventional melting and quenching techniques.								

Continue table on next page

Table 2 Batched and analyzed compositions of the Na–Fe–phosphate glasses (cont.)

O/P	Fe/P	Batched composition/mol%			Analyzed mol% of glasses (RSD < 4 %)					Ion ratios in glasses			
		Na_2O	Fe_2O_3	P_2O_5	Na_2O	P_2O_5	Fe_2O_3	FeO	SiO_2	Fe^{2+}/Fe_{tot}	O/P	Fe/P	Si/P
E-Series	0.67	0.00	40.00	60.00	0.00	54.88	29.94	12.34	2.84	0.17	3.48	0.66	0.03
3.5	0.60	11.00	33.40	55.60	10.06	50.92	23.63	11.74	3.64	0.20	3.48	0.58	0.04
	0.50	25.00	25.00	50.00	23.56	47.22	18.67	8.27	2.29	0.18	3.48	0.48	0.02
	0.40	36.00	18.40	45.60	34.06	43.26	13.66	6.80	2.23	0.20	3.50	0.39	0.03
	0.33	43.00	14.20	42.80	39.45	41.72	11.43	5.33	2.07	0.19	3.50	0.34	0.02
	0.23	51.50	9.10	39.40	49.36	38.70	7.67	2.52	1.75	0.14	3.51	0.23	0.02
	0.13	59.00	4.60	36.40	Cannot form glass by conventional melting and quenching techniques.								

Table 2 Summary of Mössbauer spectra fitting results

Glasses	Fe^{2+}/Fetot	Fe^{2+}(oct)			Fe^{3+}(oct)			Fe^{3+}(tet)			Fraction of sites (%)			CN_{Fe}	χ^2
	by titration	IS	QS	w	IS	QS	w	IS	QS	w	Fe^{2+}(oct)	Fe^{3+}(oct)	Fe^{3+}(tet)		
A-0.33	0.24	1.11(1)	2.46(1)	0.52(2)	0.58(2)	0.64(1)	0.44(2)	0.37(1)	0.63(1)	0.36(2)	29.6(9)	40.8(58)	29.6(56)	5.4(4)	1.26
A-0.23	0.31	1.31(1)	2.11(2)	0.56(2)	0.49(1)	0.61(1)	0.40(2)	0.31(1)	0.66(1)	0.32(2)	34.1(9)	44.1(39)	21.8(37)	5.6(3)	1.50
A-0.13	0.13	1.30(5)	2.11(10)	0.61(7)	0.45(2)	0.57(2)	0.56(2)	0.27(3)	0.68(4)	0.26(14)	16.0(14)	79.5(58)	4.6(5)	5.9(4)	0.66
B-0.40	0.14	1.05(1)	2.54(3)	0.48(4)	0.55(2)	0.73(1)	0.46(2)	0.32(2)	0.71(1)	0.38(4)	19.1(13)	51.0(78)	29.9(75)	5.4(6)	0.77
B-0.33	0.26	1.13(1)	2.43(2)	0.52(2)	0.57(2)	0.57(1)	0.42(2)	0.38(1)	0.56(1)	0.36(2)	27.1(10)	38.4(69)	34.6(67)	5.3(5)	1.23
B-0.23	0.26	1.16(1)	2.40(1)	0.52(2)	0.54(1)	0.55(0)	0.40(2)	0.37(1)	0.56(1)	0.32(2)	30.1(9)	44.7(54)	25.2(52)	5.5(4)	1.60
B-0.13	0.24	1.15(1)	2.38(3)	0.56(3)	0.54(2)	0.55(1)	0.41(2)	0.37(2)	0.55(1)	0.36(3)	24.4(12)	41.3(93)	34.2(92)	5.3(7)	0.85
C-0.50	0.15	1.02(2)	2.54(3)	0.51(5)	0.53(2)	0.78(1)	0.50(3)	0.28(1)	0.80(1)	0.34(5)	20.1(14)	56.6(70)	23.3(64)	5.5(5)	0.82
C-0.23	0.27	1.29(1)	2.08(2)	0.56(2)	0.49(1)	0.63(1)	0.38(2)	0.30(1)	0.67(1)	0.32(2)	32.4(8)	42.1(36)	25.6(34)	5.5(3)	1.54
D-0.60	0.11	1.01(4)	2.61(9)	0.51(13)	0.55(3)	0.85(2)	0.49(5)	0.28(2)	0.86(2)	0.39(6)	13.4(26)	49.0(12)	37.0(11)	5.2(2)	0.63
D-0.23	0.19	1.27(3)	2.11(6)	0.50(4)	0.47(1)	0.58(2)	0.42(2)	0.27(1)	0.65(1)	0.28(2)	18.7(11)	64.7(35)	16.6(32)	5.7(3)	1.01
E-0.67	0.17	1.25(2)	2.09(4)	0.62(6)	0.49(2)	0.91(1)	0.44(4)	0.24(2)	0.93(1)	0.38(4)	22.3(17)	44.1(75)	33.6(70)	5.3(5)	0.85
E-0.50	0.18	1.29(1)	2.04(3)	0.58(4)	0.52(1)	0.77(1)	0.44(2)	0.28(1)	0.81(1)	0.40(2)	22.2(11)	42.3(47)	35.5(44)	5.3(3)	1.05
E-0.40	0.20	1.29(2)	2.08(4)	0.52(4)	0.49(2)	0.68(2)	0.44(2)	0.28(2)	0.75(1)	0.34(4)	22.6(17)	51.4(68)	26.0(63)	5.5(5)	0.79
E-0.33	0.19	1.29(2)	2.06(3)	0.54(4)	0.48(1)	0.65(1)	0.44(2)	0.27(1)	0.72(1)	0.32(4)	22.7(12)	57.1(44)	20.2(40)	5.6(3)	0.94
E-0.23	0.14	1.23(19)	2.09(37)	0.48(8)	0.48(3)	0.59(6)	0.42(2)	0.28(2)	0.65(1)	0.32(4)	13.1(16)	64.0(77)	22.9(72)	5.5(6)	0.63

Table 3 Summary of Raman band assignments for Na–Fe–phosphate glasses

Raman frequency ranges (cm^{-1})	Assignment
200–660	Network bending [10,30,31]
440–580	O–P–O symmetric bond bending [30,31]
540–660	O–P–O asymmetric bond bending [30,31]
680–720	P–O–P symmetric stretch (Q^2) [10]
710–770	P–O–P symmetric stretch (Q^1) [10]
890–1000	P–O–P asymmetric stretch [10]
970–1020	PO_4 symmetric stretch (Q^0) [10]
1030–1100	PO_3 symmetric stretch (Q^1) [10]
~1200	PO_3 asymmetric stretch (Q^1) [10]
1130–1220	PO_2 symmetric stretch (Q^2) [10]
1250–1320	PO_2 asymmetric stretch (Q^2) [10]

Table 4 Summary of average M–O distance, field strength and coordination number (CN) of cations, $(PO_2)_{sym}$ (1130–1230 cm^{-1}), $(POP)_{sym}$ (660–720 cm^{-1}) and intensity ratio $I(POP)/I(PO_2)$ in Raman spectra for glasses near metaphosphate composition.

Species	M	M–O (Å)	Field strength Valence/Å^2	CN	$(PO_2)_{sym}$ cm^{-1}	$(POP)_{sym}$ cm^{-1}	$\frac{I(POP)}{I(PO_2)}$	Reference
Alkali (1+)	Li	2.01	0.25	3.9(5)	1175	699	0.56	[33,34,57,58,59,60]
	Na	2.46	0.17	5.0(4)	1166	681	0.42	[33,34,59,61,62,63]
	K	2.86	0.12	3.7(7)	1156	678	0.22	[33,34,63]
	Rb	2.90	0.12	5.0(5)	1151	667	–	[33,56,57,59]
	Cs	3.09	0.10	–	1149	658	0.17	[33,34]
Transition and post-transition (1+)	Cu	1.85	0.29	–	1180	703	1.00	[47,64]
	Ag	2.49	0.16	3.4(3)	1146	680	0.37	[34,60,65]
	Tl	2.80	0.13	–	1137	–	0.12	[34]
Alkaline earth (2+)	Mg	2.05	0.48	4.0(3)	1210	708	0.50	[34,66,67,68,69]
	Ca	2.39	0.35	5.3(2)	1179	694	0.43	[34,55,66,69,70]
	Sr	2.53	0.31	6.0(2)	1172	686	0.39	[34,71,63]
	Ba	2.75	0.26	8.0(5)	1158	689	0.32	[34,62,66,63]
Transition and post-transition (2+)	Cu	1.95	0.53	–	1188	714	0.75	[47,64]
	Zn	1.98	0.51	4.1(2)	1207	703	0.48	[34,46,64,68,69,72]
	Fe	2.16	0.43	6.1(5)	1170	683	0.55	[10,11]
	Mn	2.20	0.41	5.7(4)	1181	694	0.43	[34,71,73]
	Cd	2.30	0.38	–	1173	700	0.50	[34,74]
	Hg	2.50	0.32	–	1155	–	0.48	[34]
	Pb	2.55	0.31	5.0(4)	1153	700	0.28	[34,65,68,75,76]
Rare-earth (3+)	La	2.43	0.51	6.4(6)	1179	696	0.45	[34,62,66,77]
	Ce	2.39	0.53	5.3(5)	1182	669	0.38	[34,77,78,79]
	Pr	2.37	0.53	6.4(6)	1186	696	0.43	[34,77,80,81]
	Sm	2.35	0.54	6.8(7)	1191	703	0.31	[62,77,82]
	Eu	2.32	0.56	6.1(6)	1193	708	0.37	[34,77,80,83]
	Gd	2.29	0.57	6.2(6)	1194	703	0.32	[34,53,77,84]
Transition and post-transition (3+)	Al	1.82	0.91	6.0(2)	1222	715	0.56	[34,43,67,85]
	Ga	1.93	0.81	6.0(2)	1210	715	–	[49,86]
	Fe	1.99	0.76	6.1(5)	1184	720	0.12	[10,11]
	Bi	2.34	0.55	–	1142	–	0.22	[34]

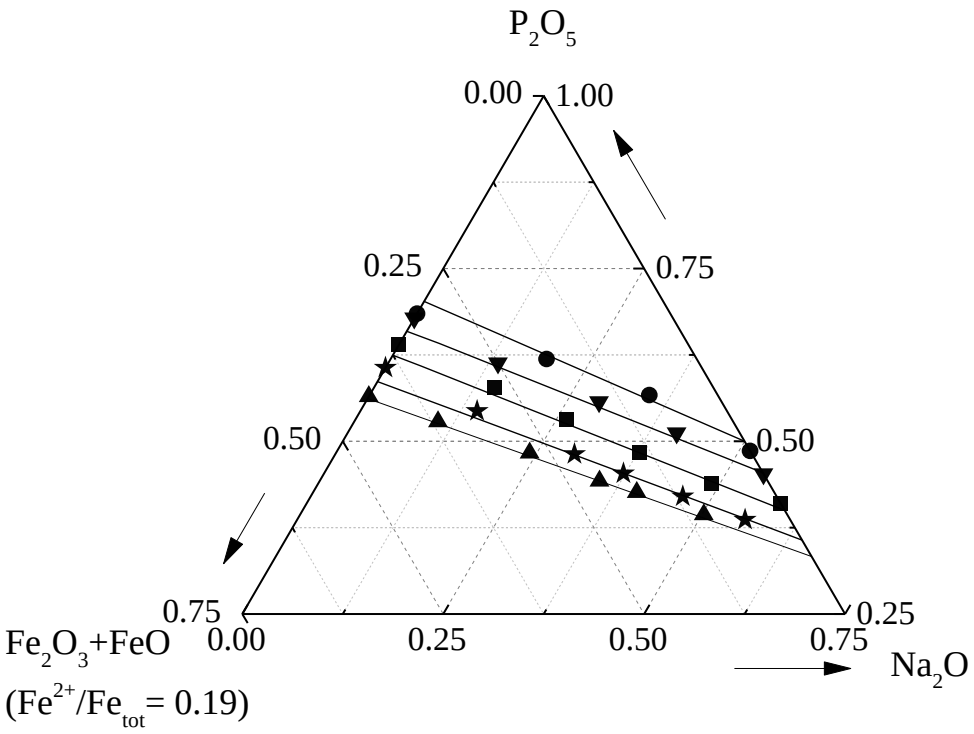

Fig. 1. Compositional diagram of the Na_2O–FeO–Fe_2O_3–P_2O_5 glasses in this study. The black symbols are associated with analyzed compositions in series with similar O/P ratios: ~3.04 (●), ~3.12 (▼), ~3.27 (■), ~3.40 (★) and ~3.49 (▲).

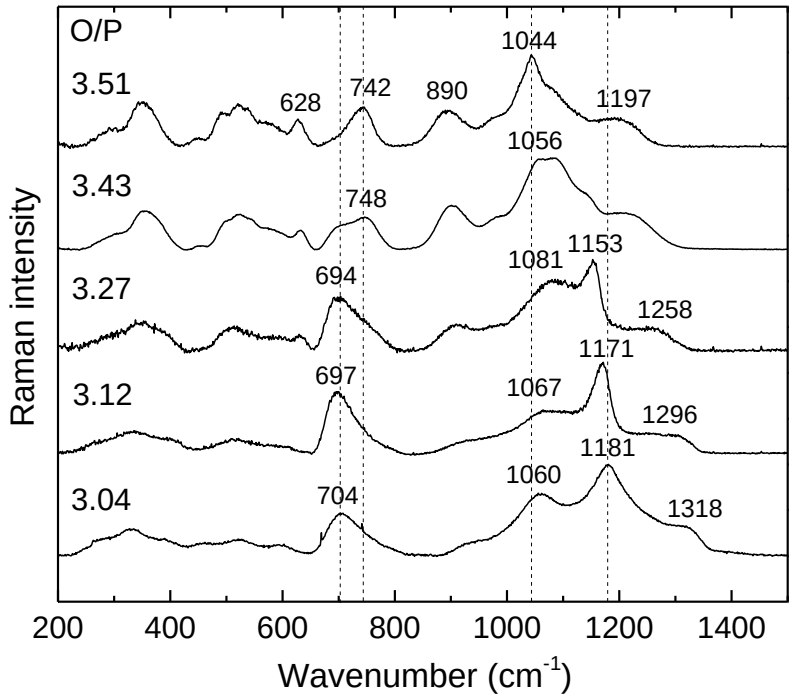

Fig. 2. Raman spectra of Na–Fe–P glasses with Fe/P = 0.23 ± 0.01

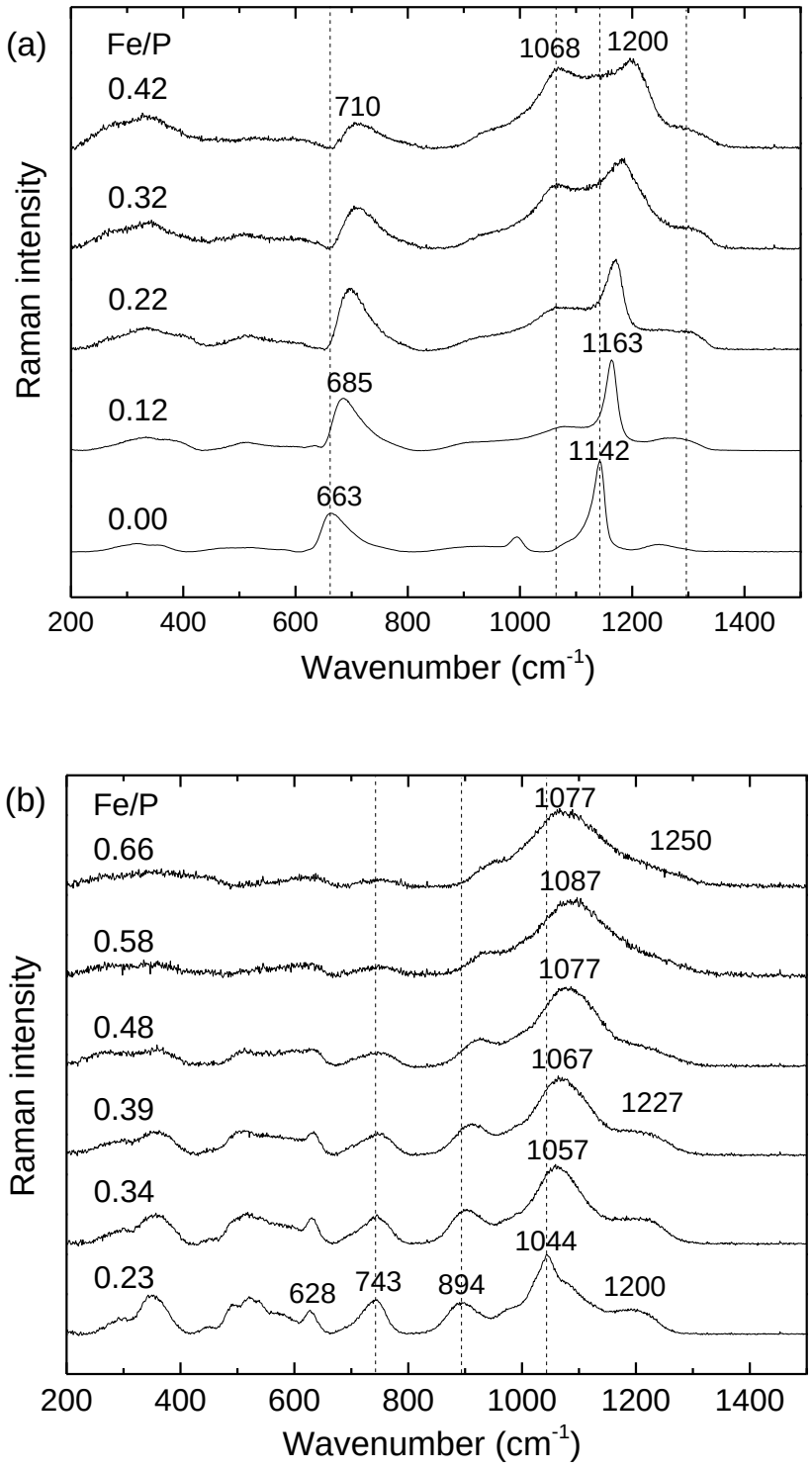

Fig. 3. Raman spectra of Na–Fe–P glasses (a) O/P = 3.12 ± 0.02; (b) O/P = 3.49 ± 0.01

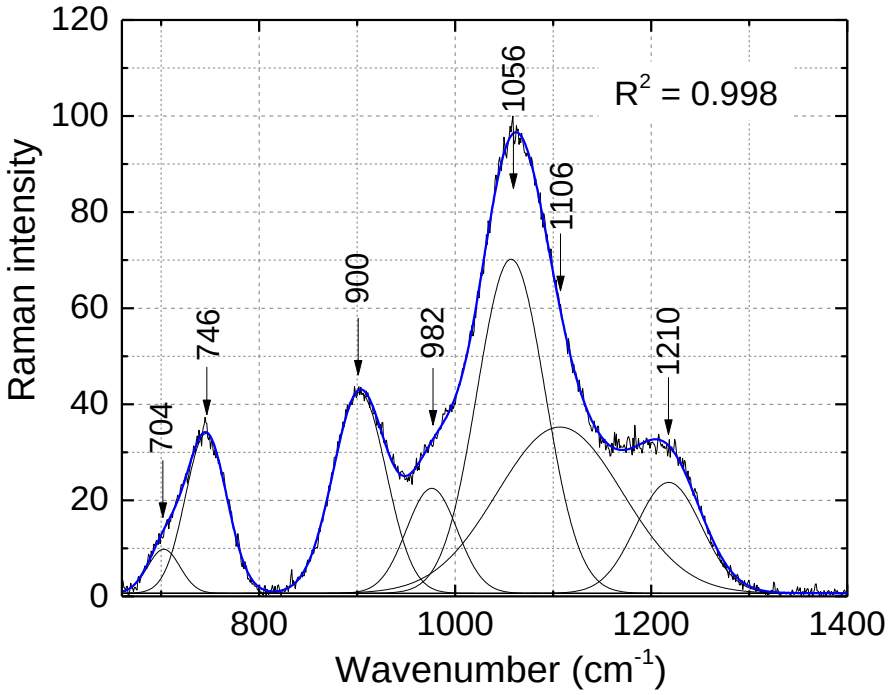

Fig. 4. Deconvolution of the Raman spectrum (black line) from the E-0.33 glass into seven Gaussian peaks in the range 650–1400 cm^{-1}. The sum of the Gaussian peaks is indicated by the blue line.

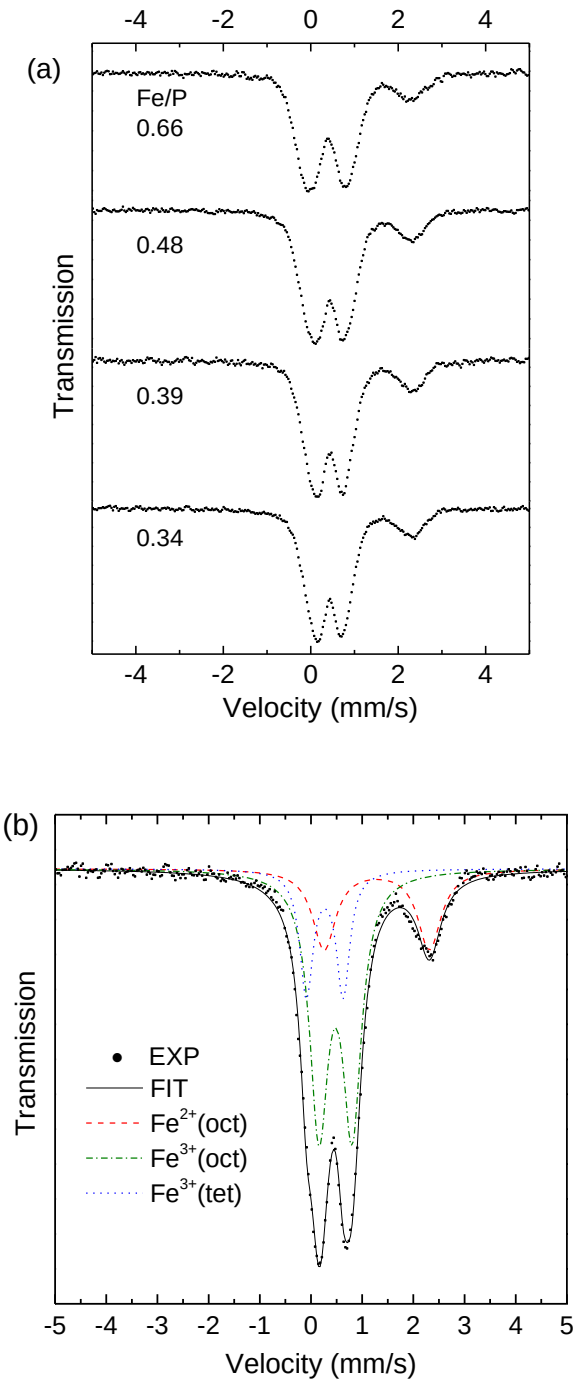

Fig. 5. (a) Mössbauer spectra of Na–Fe–P glasses with O/P = 3.49 ± 0.01; (b) Deconvolution of the Mössbauer spectrum (black dots) for the E-0.33 glass into three sets of doublets. The sum of Lorentzian sites is indicated by the black solid line.

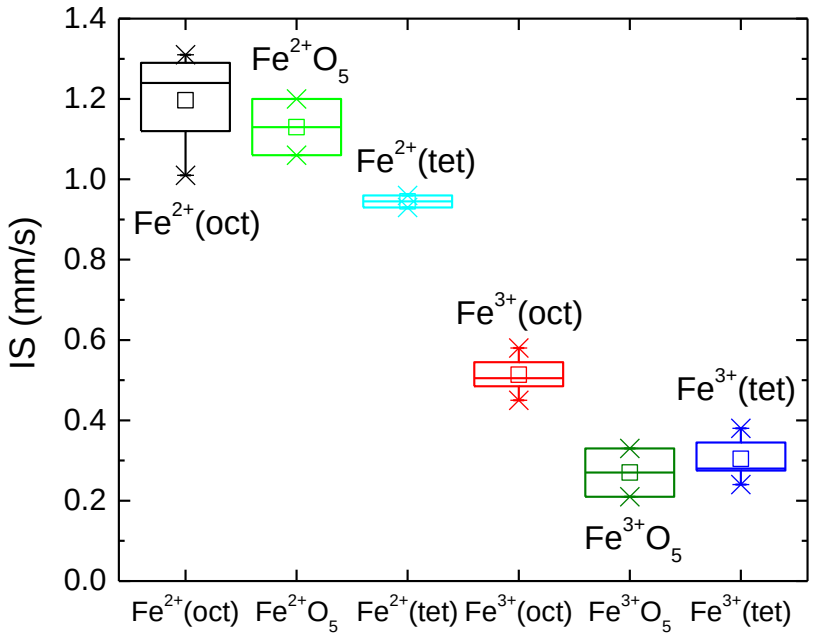

Fig. 6. Box chart of isomer shifts for sodium iron phosphate glasses. IS values for [FeO_5] from reference [36].

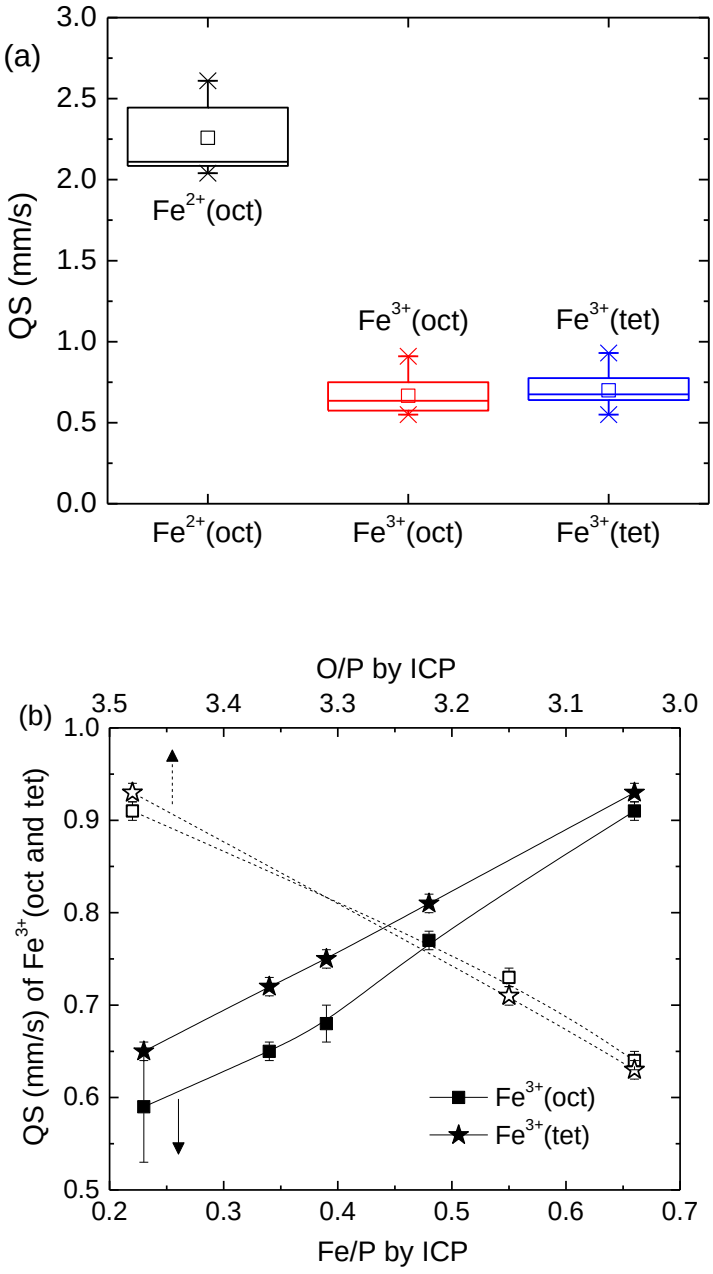

Fig. 7. (a) Box chart of QS for sodium iron phosphate glasses; (b) QS for Fe^{3+} in octahedral and tetrahedral sites. Top x-axis (open symbols and dashed lines): QS changing with O/P ratio for sodium-free iron phosphate glasses; bottom x-axis (solid symbols and solid lines): QS changing with Fe/P ratio for E-series glasses with O/P = 3.49 ± 0.01. Lines are guides for the eye.

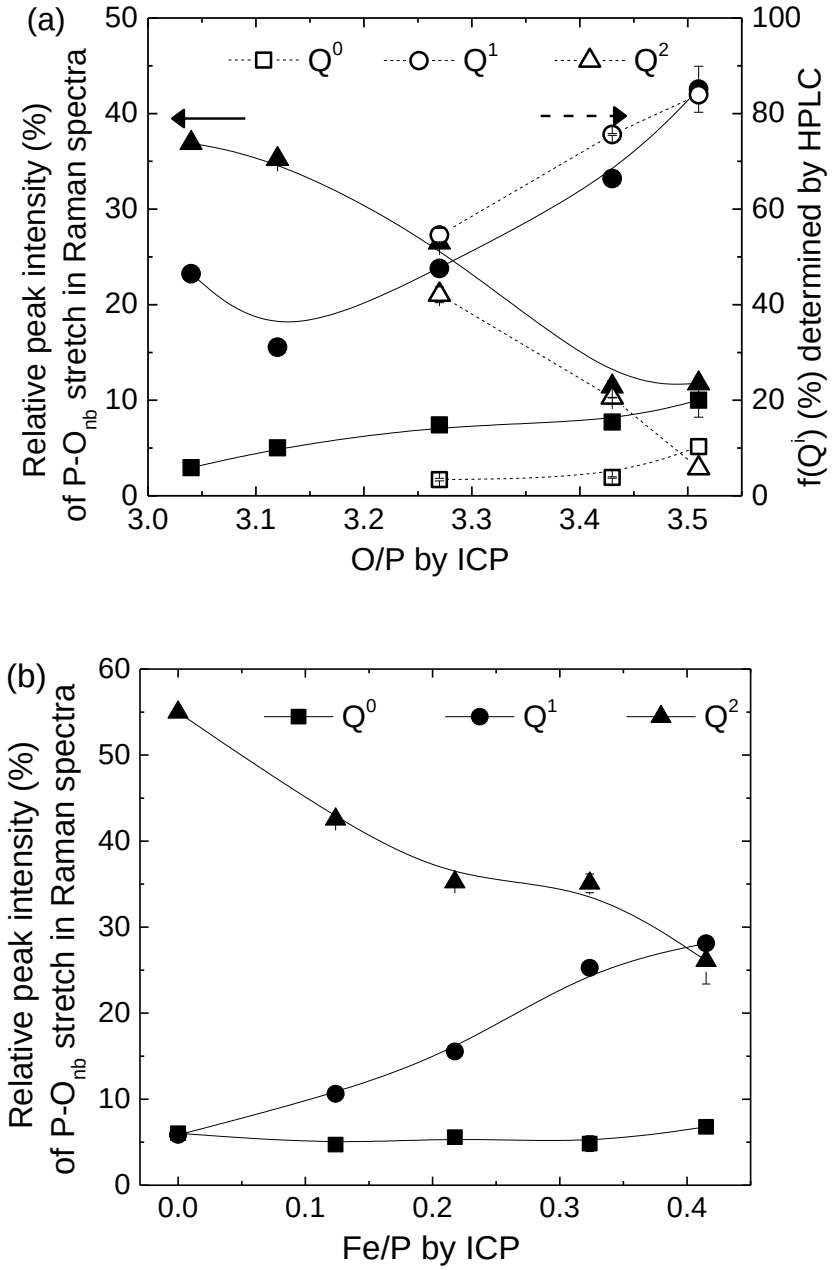

Fig. 8. Relative intensities (left y-axis) of three Gaussian peaks in the range of 950–1200 cm^{-1}. The peak positions are (□) 970–1020 cm^{-1} (○) 1040–1090 cm^{-1} (Δ) 1130–1200 cm^{-1}. Open symbols, dashed lines and right y-axis are the $f(Q^i)$ determined by HPLC [23]. (a) Glasses with Fe/P 0.23 ± 0.01; (b) Glasses with O/P = 3.12 ± 0.02; (c) Glasses with O/P = 3.49 ± 0.01. Solid and dashed lines are guides for the eye.

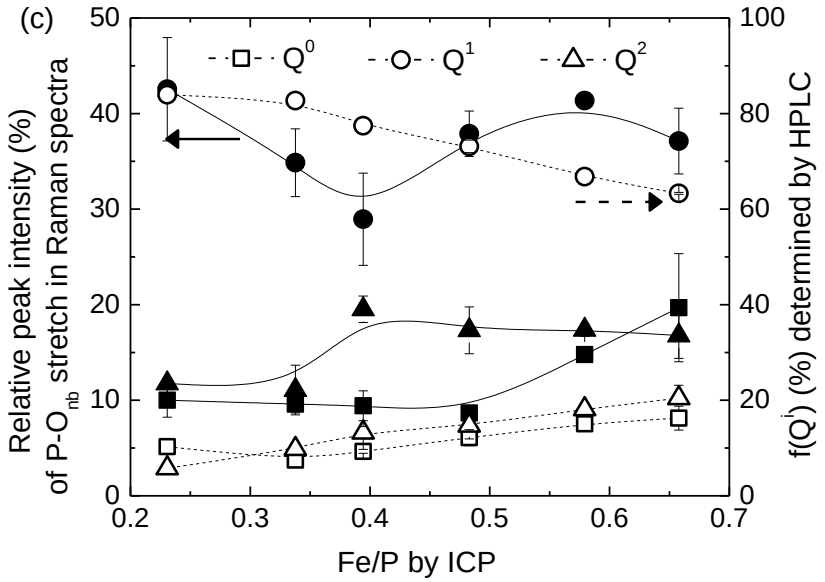

Fig. 8. Relative intensities (left y-axis) of three Gaussian peaks in the range of 950–1200 cm^{-1}. The peak positions are (□) 970–1020 cm^{-1} (○) 1040–1090 cm^{-1} (Δ) 1130–1200 cm^{-1}. Open symbols, dashed lines and right y-axis are the $f(Q^i)$ determined by HPLC [23]. (a) Glasses with Fe/P 0.23 ± 0.01; (b) Glasses with O/P = 3.12 ± 0.02; (c) Glasses with O/P = 3.49 ± 0.01. Solid and dashed lines are guides for the eye. (cont.)

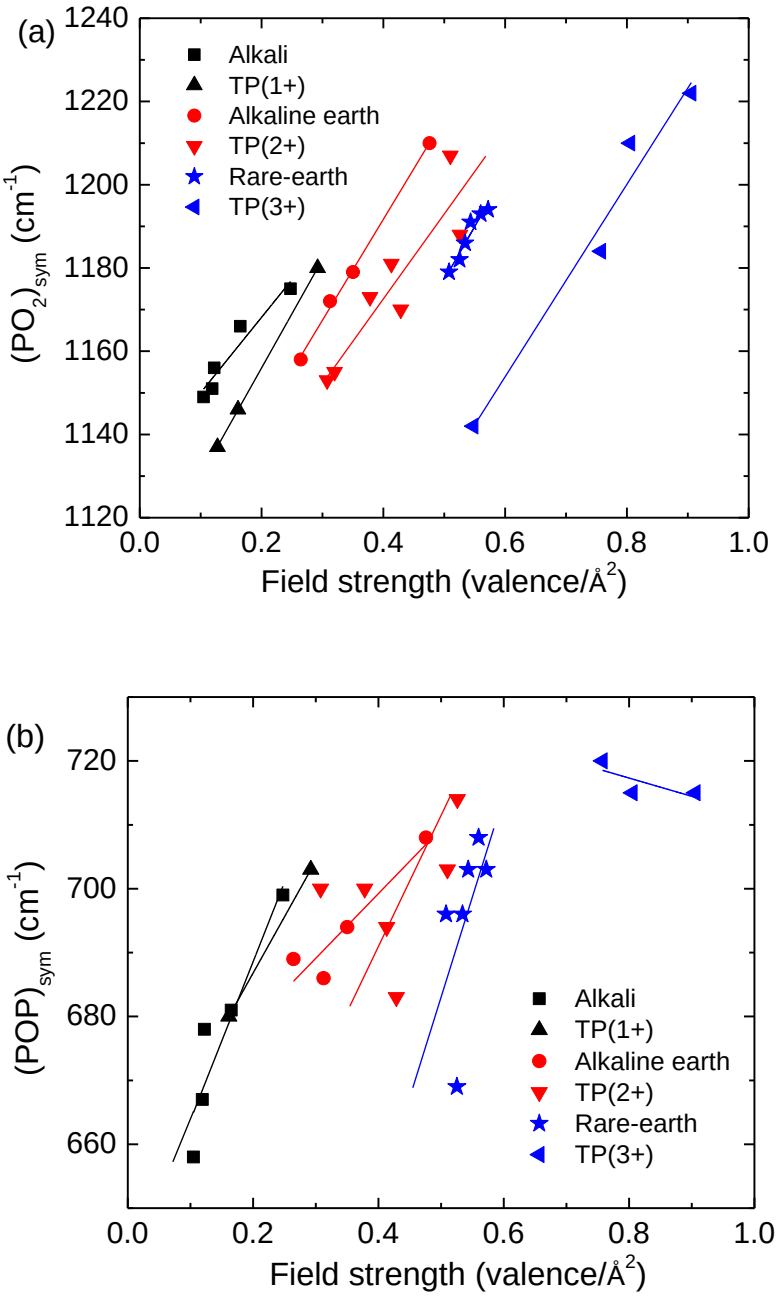

Fig. 9. Distributions of Raman peak positions (cm^{-1}) with cation field strength (valence/$Å^2$) for binary phosphate glasses near the metaphosphate composition. Data are also listed in Table 4. (a) $(PO_2)_{sym}$ stretching (1130–1220 cm^{-1}); (b) $(POP)_{sym}$ stretching (680–720 cm^{-1}). Lines are guides for the eye.

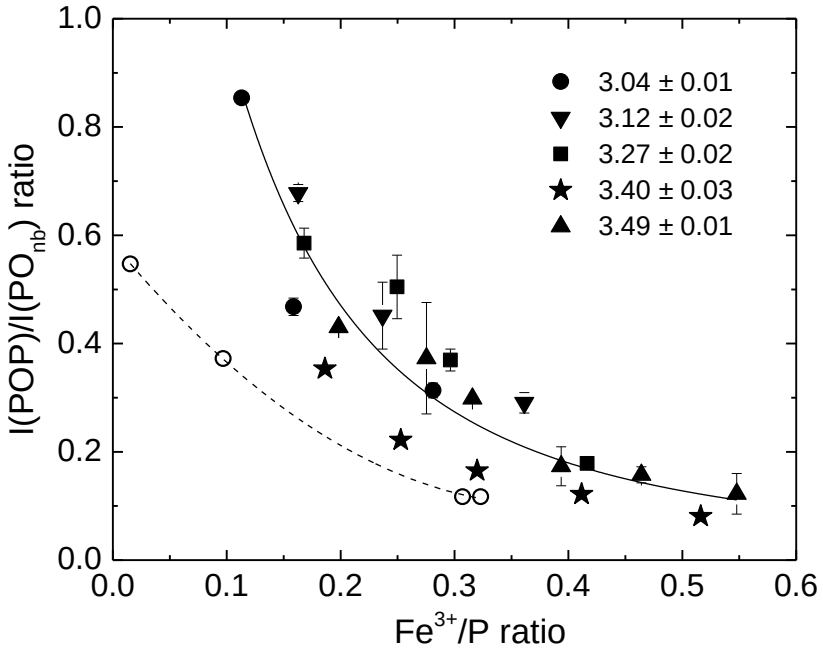

Fig. 10. Intensity ratios for $(POP)_{sym}$ (680–770 cm^{-1}) and PO_{nb}-stretching as function of Fe^{3+}/P ratios. Solid symbols for glasses in this study; open symbols (○) for soda-free iron phosphate glasses with O/P ~3.03 from reference [10]. Lines are guides for the eye.

References

[1] B. Samuneva, P. Tzvetkova, I. Gugov, and V. Dimitrov. "Structural studies of phosphate glasses." Journal of materials science letters 15, no. 24 (1996): 2180-2183.

[2] X. Yu, D.E. Day, G.J. Long, and R.K. Brow. "Properties and structure of sodium-iron phosphate glasses." Journal of non-crystalline solids 215, no. 1 (1997): 21-31.

[3] D.E. Day, Z. Wu, C.S. Ray, and P. Hrma. "Chemically durable iron phosphate glass wasteforms." Journal of non-crystalline solids 241, no. 1 (1998): 1-12.

[4] I. Ahmed, C.A. Collins, M.P. Lewis, I. Olsen, and J.C. Knowles. "Processing, characterisation and biocompatibility of iron-phosphate glass fibres for tissue engineering." Biomaterials 25, no. 16 (2004): 3223-3232.

[5] A. Al-Shahrani, A. Al-Hajry, and M.M. El-Desoky. "Electrical relaxation in mixed lithium and sodium iron phosphate glasses." Physica B: Condensed Matter 364, no. 1 (2005): 248-254.

[6] P. Bergo, S.T. Reis, W.M. Pontuschka, J.M. Prison, and C.C. Motta. "Dielectric properties and structural features of barium-iron phosphate glasses." Journal of non-crystalline solids 336, no. 3 (2004): 159-164.

[7] F.A. Wedgwood, A.C. Wright. "Short range antiferromagnetic ordering in vitreous Fe_2O_3-P_2O_5." Journal of Non-Crystalline Solids 21, no. 1 (1976): 95-105.

[8] J.L. Shaw, A.C. Wright, R.N. Sinclair, G.K. Marasinghe, D. Holland, M.R. Lees, and C.R. Scales. "Spin glass-like antiferromagnetic interactions in iron phosphate glasses." Journal of non-crystalline solids 345 (2004): 245-250.

[9] H. Akamatsu, K. Fujita, S. Murai, and K. Tanaka. "Magneto-optical properties of transparent divalent iron phosphate glasses." Applied Physics Letters 92, no. 25 (2008): 251908.

[10] L. Zhang, and R.K. Brow. "A Raman study of iron–phosphate crystalline compounds and glasses." Journal of the American Ceramic Society 94, no. 9 (2011): 3123-3130.

[11] A.C. Wright, R.N. Sinclair, J.L. Shaw, R. Haworth, G.K. Marasinghe, and D.E. Day. "A neutron diffraction study of the structure of iron phosphate glasses." Physics and Chemistry of Glasses-European Journal of Glass Science and Technology Part B 49, no. 1 (2008): 1-7.

[12] C.H. Booth, , P.G. Allen, J.J. Bucher, N.M. Edelstein, D.K. Shuh, G.K. Marasinghe, M. Karabulut, C.S. Ray, and D.E. Day. "Oxygen and phosphorus coordination around iron in crystalline ferric ferrous pyrophosphate and iron-phosphate glasses with UO_2 or Na_2O." Journal of materials research 14, no. 6 (1999): 2628-2639.

[13] P.A. Bingham, R.J. Hand, O.M. Hannant, S.D. Forder, and S.H. Kilcoyne. "Effects of modifier additions on the thermal properties, chemical durability, oxidation state and structure of iron phosphate glasses." Journal of Non-Crystalline Solids 355, no. 28 (2009): 1526-1538.

[14] B. Al-Hasni, and G. Mountjoy. "Structural investigation of iron phosphate glasses using molecular dynamics simulation." Journal of Non-Crystalline Solids 357, no. 15 (2011): 2775-2779.

[15] G.K. Marasinghe, M. Karabulut, C.S. Ray, D.E. Day, M.G. Shumsky, W.B. Yelon, C.H. Booth, P.G. Allen, and D.K. Shuh. "Structural features of iron phosphate glasses." Journal of non-crystalline solids 222 (1997): 144-152.

[16] H. Akamatsu, S. Oku, K. Fujita, S. Murai, and K. Tanaka. "Magnetic properties of mixed-valence iron phosphate glasses." Physical Review B 80, no. 13 (2009): 134408.

[17] J.R. Van Wazer, and D.A. Campanella. "Structure and properties of the condensed phosphates. IV. Complex ion formation in polyphosphate solutions." Journal of the American Chemical Society 72, no. 2 (1950): 655-663.

[18] B.C. Bunker, G.W. Arnold, and J.A. Wilder. "Phosphate glass dissolution in aqueous solutions." Journal of non-crystalline solids 64, no. 3 (1984): 291-316.

[19] Y. Lin, Y. Zhang, W. Huang, K. Lu, and Y. Zhao. "Structural study of iron in phosphate glasses." Journal of Non-Crystalline Solids 112, no. 1 (1989): 136-141.

[20] G. Concas, F. Congiu, E. Manca, C. Muntoni, and G. Pinna. "Mössbauer spectroscopic investigation of some iron-containing sodium phosphate glasses." Journal of non-crystalline solids 192 (1995): 175-178.

[21] T.R. Meadowcroft, and F.D. Richardson. "Structural and thermodynamic aspects of phosphate glasses." Transactions of the Faraday Society 61 (1965): 54-70.

[22] B.C. Sales, L.A. Boatner, and J.O. Ramey. "Intermediate-range order in simple metal-phosphate glasses: The effect of metal cations on the phosphate-anion distribution." Journal of non-crystalline solids 232 (1998): 107-112.

[23] L. Ma, R.K. Brow. "Structural study of Na_2O-FeO-Fe_2O_3-P_2O_5 glasses by high-pressure liquid chromatography." Journal of Non-Crystalline Solids 387 (2014): 16-20.

[24] S.I. Grishin, J.M. Bigham, and O.H. Tuovinen. "Characterization of jarosite formed upon bacterial oxidation of ferrous sulfate in a packed-bed reactor." Applied and environmental microbiology 54, no. 12 (1988): 3101-3106.

[25] K. Lagarec, and D.G. Rancourt. "Recoil-Mössbauer Spectral Analysis Software for Windows." University of Ottawa, Ottawa, ON (1998).

[26] K. Lagarec, and D.G. Rancourt. "Extended Voigt-based analytic lineshape method for determining *N*-dimensional correlated hyperfine parameter distributions in Mössbauer spectroscopy." Nuclear Instruments and Methods in Physics Research Section B: Beam Interactions with Materials and Atoms 129, no. 2 (1997): 266-280.

[27] P.A. Bingham, R.J. Hand, and S.D. Forder. "Doping of iron phosphate glasses with Al_2O_3, SiO_2 or B_2O_3 for improved thermal stability." Materials research bulletin 41, no. 9 (2006): 1622-1630.

[28] C.R. Kurkjian, and D.N.E. Buchanan. "Mössbauer absorption of Fe^{2+} in inorganic glasses." Phys. Chem. Glasses 5 (1964): 63-70.

[29] G.J. Long, ed. "Mössbauer spectroscopy applied to inorganic chemistry. Vol. 1." Springer, 1984.

[30] R. Baddour-Hadjean, and J.P. Pereira-Ramos. "Raman Microspectrometry Applied to the Study of Electrode Materials for Lithium Batteries." Chemical reviews 110, no. 3 (2010): 1278-1319.

[31] I. Szczygieł, L. Macalik, E. Radomińska, T. Znamierowska, M. Mączka, P. Godlewska, and J. Hanuza. "Luminescence, electronic absorption and vibrational IR and Raman studies of binary and ternary cerium ortho-, pyro-and meta-phosphates doped with Pr^{3+} ions." Optical Materials 29, no. 9 (2007): 1192-1205.

[32] R.K. Brow. "Review: the structure of simple phosphate glasses." Journal of Non-Crystalline Solids 263 (2000): 1-28.

[33] G.B. Rouse Jr, P.J. Miller, and W.M. Risen Jr. "Mixed alkali glass spectra and structure." Journal of Non-Crystalline Solids 28, no. 2 (1978): 193-207.

[34] B.N. Nelson, and G.J. Exarhos. "Vibrational spectroscopy of cation-site interactions in phosphate glasses." Journal of Chemical Physics 71, no. 7 (1979): 2739-2747.

[35] M. Karabulut, G.K. Marasinghe, C.S. Ray, D.E. Day, G.D. Waddill, C.H. Booth, P.G. Allen, J.J. Bucher, D.L. Caulder, and D.K. Shuh. "An investigation of the local iron environment in iron phosphate glasses having different Fe (II) concentrations." Journal of non-crystalline solids 306, no. 2 (2002): 182-192.

[36] F. Menil. "Systematic trends of the ^{57}Fe Mössbauer isomer shifts in (FeO_n) and (FeF_n) polyhedra. Evidence of a new correlation between the isomer shift and the inductive effect of the competing bond *T*-*X* ($\rightarrow$ Fe)(where *X* is O or F and *T* any element with a formal positive charge)." Journal of Physics and Chemistry of Solids 46, no. 7 (1985): 763-789.

[37] F. Neese. "Prediction and interpretation of the ^{57}Fe isomer shift in Mössbauer spectra by density functional theory." Inorganica Chimica Acta 337 (2002): 181-192.

[38] L.R. Walker, G.K. Wertheim, and V. Jaccarino. "Interpretation of the Fe^{57} isomer shift." Physical Review Letters 6, no. 3 (1961): 98-101.

[39] J. Danon. "Chemical applications of Mössbauer spectroscopy." V.I. Goldanskii and R.H. Herber, eds., Academic Press, New York (1968): 159-267.

[40] S.K. Banerjee, W. O'Reilly, and C.E. Johnson. "Mössbauer-effect measurements in FeTi spinels with local disorder." Journal of Applied Physics 38 (1967): 1289.

[41] J.J. Hudgens, R.K. Brow, D.R. Tallant, and S.W. Martin. "Raman spectroscopy study of the structure of lithium and sodium ultraphosphate glasses." Journal of non-crystalline solids 223, no. 1 (1998): 21-31.

[42] J.R. Van Wazer. "Phosphorus and its compounds, volume 1: chemistry." Interscience Publishers (1958): 717-800.

[43] J. Schneider, S.L. Oliveira, L.A.O. Nunes, and H. Panepucci. "Local structure of sodium aluminum metaphosphate glasses." Journal of the American Ceramic Society 86, no. 2 (2003): 317-324.

[44] U. Hoppe. "A structural model for phosphate glasses." Journal of non-crystalline solids 195, no. 1 (1996): 138-147.

[45] J. Swenson, A. Matic, A. Brodin, L. Börjesson, and W.S. Howells. "Structure of mixed alkali phosphate glasses by neutron diffraction and Raman spectroscopy." Physical Review B 58, no. 17 (1998): 11331-11337.

[46] R.K. Brow, D.R. Tallant, S.T. Myers, and C.C. Phifer. "The short-range structure of zinc polyphosphate glass." Journal of non-crystalline solids 191, no. 1 (1995): 45-55.

[47] J. Koo, B.-S. Bae, and H.-K. Na. "Raman spectroscopy of copper phosphate glasses." Journal of non-crystalline solids 212, no. 2 (1997): 173-179.

[48] J.J. Hudgens, and S.W. Martin. "Glass transition and infrared spectra of low-alkali, anhydrous lithium phosphate glasses." Journal of the American Ceramic Society 76, no. 7 (1993): 1691-1696.

[49] L.K. Elbouaanani, B. Malaman, and R. Gérardin. "Structure refinement and magnetic properties of C–$Fe(PO_3)_3$ studied by neutron diffraction and Mössbauer techniques." Journal of Solid State Chemistry 148, no. 2 (1999): 455-463.

[50] D. Ilieva, B. Jivov, G. Bogachev, C. Petkov, I. Penkov, and Y. Dimitriev. "Infrared and Raman spectra of Ga_2O_3–P_2O_5 glasses." Journal of non-crystalline solids 283, no. 1 (2001): 195-202.

[51] A.N. Lazarev. "Vibrational spectra and structure of silicates." Consultants Bureau, New York (1972).

[52] A.N. Lazarev, A.P. Mirgorodskii, and I.S. Ignatiev. "Vibrational spectra of complex oxides." Science, Leningrad (1975): 296.

[53] D. Ilieva, B. Jivov, D. Kovacheva, Ts. Tsacheva, Y. Dimitriev, G. Bogachev, and Ch. Petkov. "FT–IR and Raman spectra of Gd phosphate crystals and glasses." Journal of non-crystalline solids 293 (2001): 562-568.

[54] D.A. Skoog, F.J. Holler, and T.A. Nieman. "Principles of instrumental analysis, 5th Edition." Thomson Learning, Inc. (1998).

[55] J.E. Pemberton, L. Latifzadeh, J.P. Fletcher, and S.H. Risbud. "Raman spectroscopy of calcium phosphate glasses with varying calcium oxide modifier concentrations." Chemistry of Materials 3, no. 1 (1991): 195-200.

[56] D.L. Sidebottom. "Influence of glass structure on the ac conductivity of alkali phosphate glasses." Journal of Physics: Condensed Matter 15, no. 16 (2003): S1585-S1594.

[57] J. Swenson, A. Matic, A. Brodin, L. Börjesson, and W.S. Howells. "Structure of mixed alkali phosphate glasses by neutron diffraction and Raman spectroscopy." Physical Review B 58, no. 17 (1998): 11331-11337.

[58] J. Swenson, A. Matic, L. Börjesson, and W.S. Howells. "Experimental insight into the mixed mobile ion effect in glasses." Solid state ionics 136-137 (2000): 1055-1060.

[59] J. Swenson, A. Matic, C. Karlsson, L. Börjesson, C. Meneghini, and W.S. Howells. "Random ion distribution model: A structural approach to the mixed-alkali effect in glasses." Physical Review B 63, no. 13 (2001): 132202.

[60] M. Scagliotti, M. Villa, and G. Chiodelli. "Short range order in the network of the borophosphate glasses: Raman results." Journal of non-crystalline solids 93, no. 2 (1987): 350-360.

[61] R.K. Brow, D.R. Tallant, J.J. Hudgens, S.W. Martin, and A.D. Irwin. "The short-range structure of sodium ultraphosphate glasses." Journal of non-crystalline solids 177 (1994): 221-228.

[62] A. Mierzejewski, G.A. Saunders, H.A.A. Sidek, and B. Bridge. "Vibrational properties of samarium phosphate glasses." Journal of non-crystalline solids 104, no. 2 (1988): 323-332.

[63] U. Hoppe, G. Walter, R. Kranold, and D. Stachel. "Structural specifics of phosphate glasses probed by diffraction methods: a review." Journal of Non-Crystalline Solids 263&264 (2000): 29-47.

[64] A. Musinu, G. Piccaluga, G. Pinna, G. Vlaic, D. Narducci, and S. Pizzini. "Coordination of zinc and copper in phosphate glasses by EXAFS." Journal of non-crystalline solids 136, no. 3 (1991): 198-204.

[65] A. Musinu, G. Paschina, G. Piccaluga, and G. Pinna. "Short range order of metaphosphate glasses by X-ray diffraction." Journal of non-crystalline solids 177 (1994): 97-102.

[66] M.A. Karakassides, A. Saranti, and I. Koutselas. "Preparation and structural study of binary phosphate glasses with high calcium and/or magnesium content." Journal of non-crystalline solids 347, no. 1 (2004): 69-79.

[67] D.W. Hall, S.A. Brawer, and M.J. Weber. "Vibronic spectra of Gd^{3+} in metaphosphate glasses: Comparison with Raman and infrared spectra." Physical Review B 25, no. 4 (1982): 2828-2837.

[68] U. Hoppe, R. Kranold, A. Barz, D. Stachel, J. Neuefeind, and D.A. Keen. "Combined neutron and X-ray scattering study of phosphate glasses." Journal of non-crystalline solids 293-295 (2001): 158-168.

[69] E. Matsubara, Y. Waseda, M. Ashizuka, and E. Ishida. "Structural study of binary phosphate glasses with MgO, ZnO, and CaO by x-ray diffraction." Journal of non-crystalline solids 103, no. 1 (1988): 117-124.

[70] K.M. Wetherall, D.M. Pickup, R.J. Newport, and G. Mountjoy. "The structure of calcium metaphosphate glass obtained from x-ray and neutron diffraction and reverse Monte Carlo modelling." Journal of Physics: Condensed Matter 21, no. 3 (2009): 035109.

[71] I. Konidakis, C.P.E. Varsamis, E.I. Kamitsos, D. Möncke, and D. Ehrt. "Structure and Properties of Mixed Strontium− Manganese Metaphosphate Glasses." The Journal of Physical Chemistry C 114, no. 19 (2010): 9125-9138.

[72] K. Meyer. "Characterization of the structure of binary zinc ultraphosphate glasses by infrared and Raman spectroscopy." Journal of non-crystalline solids 209, no. 3 (1997): 227-239.

[73] B. Brendebach, F. Reinauer, N. Zotov, M. Funke, R. Glaum, J. Hormes, and H. Modrow. "X-ray absorption near edge structure (XANES) investigation of MnO_y-doped sodium metaphosphate glasses and crystalline reference materials." Journal of non-crystalline solids 351, no. 12 (2005): 1072-1076.

[74] C. Garrigou-Lagrange, M. Ouchetto, and B. Elouadi. "Infrared spectra of vitreous lithium and cadmium mixed phosphates." Canadian journal of chemistry 63, no. 7 (1985): 1436-1446.

[75] O. Cozar, D.A. Magdas, L. Nasdala, I. Ardelean, and G. Damian. "Raman spectroscopic study of some lead phosphate glasses with tungsten ions." Journal of non-crystalline solids 352, no. 28 (2006): 3121-3125.

[76] B.C. Sales, R.S. Ramsey, J.B. Bates, and L.A. Boatner. "Investigation of the structural properties of lead-iron phosphate glasses using liquid chromatography and Raman scattering spectroscopy." Journal of non-crystalline solids 87, no. 1 (1986): 137-158.

[77] R. Anderson, T. Brennan, J.M. Cole, G. Mountjoy, D.M. Pickup, R.J. Newport, and G.A. Saunders. "An extended x-ray absorption fine structure study of rare-earth phosphate glasses near the metaphosphate composition." Journal of materials research 14, no. 12 (1999): 4706-4714.

[78] S.H. Morgan, R.H. Magruder, and E. Silberman. "Raman Spectra of Rare-Earth Phosphate Glasses." Journal of the American Ceramic Society 70, no. 12 (1987): C-378.

[79] J.M. Cole, E.R.H. van Eck, G. Mountjoy, R.J. Newport, T. Brennan, and G.A. Saunders. "A neutron diffraction and ^{27}Al MQMAS NMR study of rare-earth phosphate glasses, $(R_2O_3)_x(P_2O_5)_{1-x}$, x = 0.187-0.263, R = Ce, Nd, Tb containing Al impurities." Journal of Physics: Condensed Matter 11, no. 47 (1999): 9165-9178.

[80] D.T. Bowron, G. Bushnell-Wye, R.J. Newport, B.D. Rainford, and G.A. Saunders. "X-ray diffraction studies of rare-earth metaphosphate glasses." Journal of Physics: Condensed Matter 8, no. 19 (1996): 3337-3346.

[81] K. Sun, and W.M. Risen. "Rare earth phosphate glasses." Solid state communications 60, no. 9 (1986): 697-700.

[82] J.M. Cole, A.C. Wright, R.J. Newport, R.N. Sinclair, H.E. Fischer, G.J. Cuello, and R.A. Martin. "The structure of the rare-earth phosphate glass $(Sm_2O_3)_{0.205}(P_2O_5)_{0.795}$ studied by anomalous dispersion neutron diffraction." Journal of Physics: Condensed Matter 19, no. 5 (2007): 056002.

[83] H.M. Farok, H.B. Senin, G.A. Saunders, W. Poon, and H. Vass. "Optical and ultrasonic properties of europium phosphate glasses." Journal of materials science 29, no. 11 (1994): 2847-2859.

[84] M. Karabulut, E. Metwalli, A.K. Wittenauer, R.K. Brow, G.K. Marasinghe, C.H. Booth, J.J. Bucher, and D.K. Shuh. "An EXAFS investigation of rare-earth local environment in ultraphosphate glasses." Journal of non-crystalline solids 351, no. 10 (2005): 795-801.

[85] R.K. Brow, R. James Kirkpatrick, and G.L. Turner. "Nature of Alumina in Phosphate Glass: II, Structure of Sodium Alurninophosphate Glass." Journal of the American Ceramic Society 76, no. 4 (1993): 919-928.

[86] U. Hoppe, D. Ilieva, and J. Neuefeind. "The structure of gallium phosphate glasses by high-energy X-ray diffraction." Zeitschrift fur Naturforschung A-Journal of Physical Sciences 57, no. 8 (2002): 709-715.

III. CRYSTALLIZATION BEHAVIOR OF $Na_2O–FeO–Fe_2O_3–P_2O_5$ GLASSES

Lina Ma[a], Richard K. Brow[a,*], Luciana Ghussn[b], Mark E. Schlesinger[a]

[a] Department of Materials Science & Engineering, Missouri University of Science & Technology, Straumanis-James Hall, 1400 N. Bishop Ave, Rolla, MO, USA

[b] Fundação Parque Tecnológico de Itaipu, Brazil

ABSTRACT

The crystallization tendencies of five series of $Na_2O–FeO–Fe_2O_3–P_2O_5$ (NFP) glasses with different O/P (3.0–3.5) and Fe/P (0.13–0.67) ratios were studied. Characteristic temperatures, including the glass transition temperature (T_g) and crystallization temperature (T_x^h), were obtained using differential thermal analysis (DTA), and liquidus temperatures (T_L) were determined by microscopic evaluation of heat-treated samples. The compositional dependence of glass structure and the characteristic temperatures are discussed. The glass stability (GS) against crystallization is described using parameters based on the characteristic temperatures. For the glass series with O/P ratios near the pyrophosphate composition (O/P ~3.5), the glass stability goes through a minimum value around Fe/P ~ 0.40, which corresponds to the crystalline phase $NaFeP_2O_7$.

Keywords: iron-phosphate glass; thermal stability; glass formation ability; iron redox

* Corresponding author, brow@mst.edu

1. Introduction

As potential hosts to vitrify high-level nuclear waste (HLW), some phosphate minerals and iron phosphate glasses have advantages that include their chemical stability, resistance to radiation damage, and solubility for substantial quantities of actinides [1]. The excellent chemical durability of iron phosphate glasses is often equivalent to or better than many other nuclear waste storage hosts, including borosilicate glasses [2,3,4,5]. In addition, iron phosphate glasses can tolerate high concentrations of waste components, including alkali oxides (up to 20 wt%) and chromium oxide (up to 4.5 wt%) without deterioration of their good chemical durability [5,6]. Iron phosphate glasses with PbO have been developed for radiation shielding applications, including gamma-radiation [2,7]. Iron phosphate glasses have also been developed as biomaterials with tailored rates of degradation in aqueous environments and as corrosion-resistant, reinforcing fibers for composite materials [8,9,10,11]. Phosphate glasses containing divalent iron cations also exhibit interesting semiconducting properties, magneto-optical properties and magnetic transition properties, which can be used to design and apply as spin glasses or optical isolator and optical switch [12,13,14,15,16].

The fraction of Fe^{2+} ions in an iron phosphate glass varies with the initial batch materials and preparation conditions, increasing when ferrous raw materials are used and/or if melts are processed under reducing conditions [16,17,18]. The relative amount of Fe^{2+}/Fe_{tot} is typically about 20% for the glasses made by conventional melting (in air) and quenching techniques [4,17,19].

The structural complexity of iron phosphate glasses is increased by the distortion of Fe-polyhedra and by disproportionation reactions of phosphate anions in the melts

[20,21,22,23,24]. The structural complexity further changes the ability of an iron phosphate glass to incorporate a variety of elements into its structure, and affects the thermal stability of super-cooled iron phosphate melts against crystallization. Understanding the thermal stability of a glass against crystallization on heating is useful for sintering glass powders and designing nuclear waste storage hosts that may heat as a result of radioactive decay and geological thermal cycles [9,25]. Glass forming ability indicates the likelihood of cooling a melt from above the liquidus temperature to the glass transition temperature without crystallization [26]. Structural and kinetic approaches are used to understand the concepts of thermal stability and glass forming ability, and efforts have been made to relate these two concepts [26,27,28].

Several parameters regarding glass stability on heating are obtained from differential thermal analysis (DTA) or differential scanning calorimetry (DSC) experiments, which provide characteristic temperatures, including the glass transition temperature (T_g), the crystallization onset temperature on heating (T_x^h), and the crystallization peak temperature on heating (T_c^h) [28]. The melting point (T_m), solidus temperature (T_S) and liquidus temperature (T_L) of a composition are also important characteristic temperatures. From DSC/DTA data, the T_S and T_L could be determined for some glasses by the beginning (onset) and the end (offset) of the melting endotherms, if the endotherm also corresponds the first exotherm on the cooling curve [25,29,30]. For glasses without clear melting peaks, hot stage microscopy or the gradient furnace methods are used to measure the liquidus temperature [25,31].

Several important glass stability parameters that utilize the characteristic temperatures are given in Table 1. An increase in each of these parameters, for example

the increase in the difference between crystallization temperatures and T_g, indicates a greater resistance to crystallization on heating a glass or quenching a melt (better stability). For silicate glasses, studies have shown that an increase in glass stability parameters indicates a decrease in the critical cooling rate, and so an increase in glass forming ability [26,27]. Nascimento et al.[28] compared and evaluated these and other glass stability parameters and found that the Weinberg and Hrubÿ parameters, which include three characteristic temperatures, have the best empirical correlations with glass-forming ability.

The $Na_2O–FeO–Fe_2O_3–P_2O_5$ (NFP) glass system is a model for iron phosphate compositions used to vitrify high alkaline nuclear waste streams [32]. The glass-forming region and thermal properties of sodium iron phosphate and sodium-free iron phosphate glasses have been studied and reported in the literature [18,33,34,35], but less is known about the effects of glass structure and iron redox on thermal stability or crystallization behavior of these glasses. In the present work, five series of $Na_2O–FeO–Fe_2O_3–P_2O_5$ glasses with different O/P (3.0–3.5) and Fe/P (0.13–0.67) ratios that cover the broad glass-forming range were prepared by conventional melting (in air) and quenching techniques. Glass stability against crystallization are described using the parameters in Table 1, and the effects of composition on thermal stability are discussed in terms of the network structure, stable crystalline phases and iron redox. Studies of the phosphate anion distributions and iron coordination sites in these same NFP glasses are presented elsewhere [22,23].

2. Experimental Procedures

The experimental procedures for preparing and analyzing the sodium iron phosphate glasses used in this study have been described in a previous study [22,23]. Briefly, glasses were made from batches of raw materials including Na_2CO_3 (Alfa Aesar, ≥ 98%), Fe_2O_3 (Alfa Aesar, ≥ 99%) and $NH_4H_2PO_4$ (Alfa Aesar, ≥ 98%) that were melted in fused SiO_2 crucibles (Leco #728-701) between 1000 °C and 1250 °C in air for two hours. Glass compositions, including small amounts of silica from the crucibles, were determined by inductively-coupled plasma optical emission spectroscopy (ICP-OES, PerkinElmer Optima 2000 DV, Norwalk, USA), and the fraction of iron present as Fe^{2+} was determined by a wet chemical technique [36]. Compositional series with similar O/P ratios, from 3.0 to 3.5, are labeled from A to E as defined in a previous study [23]. For example, glass E-0.66 is a sample in the E-series with a batched O/P ratio of 3.5 and an analyzed Fe/P ratio of 0.66.

Differential thermal analysis (Perkin Elmer, 7 series/UNIX DTA 7, Norwalk, Connecticut USA) was used to determine the characteristic temperatures, including T_g (onset), T_x^h and T_c^h (ºC). About 30 mg of glass powder with designated particle size ranges (75–150 μm) were heated in an alumina crucible at 15 ºC/min under a nitrogen atmosphere (flow rate 30 cm^3/min) from 25 to 1150 ºC. For most of the sodium iron phosphate glasses in this study, T_m, T_S and T_L could not be accurately determined from the DTA scans because of small and diffuse changes in heat associated with crystal melting [25]. The liquidus temperatures (T_L) were determined instead by crystallizing the glass powders (75–150 μm) in air by holding them for nine hours at the offset temperature of the DTA crystallization peaks. The crystalline phases in these samples

were identified by X-ray diffraction (XRD) with a Philips X'pert multipurpose diffractometer with PIXcel detector, using Cu Kα radiation and Ni filter, at 45 kV and 40 mA. The crystallized samples were then heated in air in a platinum boat for up to 30 minutes at increasing temperatures, and then quenched and analyzed by optical microscopy (Hirox KH-8700 digital microscopy with MXG-2500 REZ zoom lens) and Raman spectroscopy (Horiba Jobin Yvon LabRAM Aramis μ-Raman with a 632.8 nm He-Ne laser and a 10× objective). The apparent T_L was determined to be the midpoint between the highest temperature where crystals were observed and the lowest temperature where no crystals were observed [37].

3. Results

3.1. Characteristic temperatures

Fig. 1 (a) shows a DTA scan for the E-0.23 glass to indicate how the characteristic temperatures were determined. Fig. 1 (b) shows the DTA patterns for the E-series (O/P = 3.49 ± 0.01) glasses. Similar DTA data were collected for the other glasses and the characteristic temperatures, T_g, T_x^h and T_c^h (°C), are given in Table 2. These temperatures were reproducible to ± 3°C based on multiple DTA runs of selected glasses. For a glass series with similar O/P ratios, the replacement of Na^+ ions by Fe^{2+} and Fe^{3+} ions affects the T_g and the crystallization behavior of the glasses. Fig. 2 shows a systematic increase in T_g with increasing Fe/(Na+Fe) ratio, although glasses with O/P ≥ 3.4 exhibit maxima in T_g for Fe/(Na+Fe) ratios near 0.5–0.7. A decrease in T_g is observed (Table 2) for the sodium-free iron phosphate glasses with increasing O/P ratio, from 576°C for glass A-0.37 to 487°C for glass E-0.66.

The crystalline phases that form when the E-series glasses were held for nine hours at the offset temperatures of the respective DTA exotherms were determined by XRD and are shown in Fig. 3 (a). The O/P ratio of this series is near the pyrophosphate stoichiometry (O/P = 3.5), and as the Fe/P ratio increases, the dominant crystalline phases are the related pyrophosphates that appear in the order $Na_4P_2O_7$ (PDF 71-1631), $Na_7Fe_3(P_2O_7)_4$ [38], $NaFeP_2O_7$ (PDF 36-1454) and $Fe_4(P_2O_7)_3$ (PDF 36-318). For the Na-free iron phosphate glasses, the crystalline phases evolve from $Fe(PO_3)_3$ (PDF 38-109), for glasses with O/P < 3.3, to $Fe_4(P_2O_7)_3$ (PDF 36-318) with increasing O/P ratios (Fig. 3 (b)) [35].

3.2. Thermal stability

Fig. 4 shows an example of how the liquidus temperatures, T_L, were determined in this study. The E-0.23 glass was held for nine hours at 557 ºC, the offset temperature of the DTA crystallization exotherm (Fig. 1 (a)), and the crystallized sample was then heated to the higher temperatures, held for 30 min, then cooled to room temperature and analyzed by optical microscopy and Raman spectroscopy. Crystals could be detected on the surface of the glass cooled from 830 ºC (Fig. 4 (a)). Raman spectra of these crystals (Fig. 4 (b)) indicate that they are likely $Fe_4(P_2O_7)_3$ [21,23]. No crystals were detected in the sample quenched from 847 ºC and this sample has a Raman spectrum similar to that from the sample quenched from 1100ºC (Fig. 4 (b)). Therefore, for the crystalized E-0.23 samples, 830 ºC is the highest temperature where crystals were observed and 847 ºC is the lowest temperature where no crystals were observed, and so the T_L for the E-0.23

glass is taken as the midpoint, 839 ºC. The liquidus temperatures were measured by the same technique for the other glasses in this study, and are summarized in Table 2.

Glass stability parameters K_A, K_W and K_H (Table 1) were calculated from the characteristic temperatures and are given in Table 2. The compositional dependences of these three parameters are similar. Fig. 5 (a) shows a minimum in the stability parameters for the series E glasses (O/P ~3.49) for the composition Fe/(Na+Fe) = 0.33. Minima in the glass stability parameters also occur for the series of sodium-free iron phosphate glasses around O/P 3.3–3.4 (Fig. 5 (b)).

4. Discussion

4.1. Glass transition temperature

Fig. 6 (a) shows that the glass transition temperatures of the Na-free iron phosphate glasses decrease with increasing O/P ratio, consistent with literature [9]. A similar decrease in T_g with increasing O/P ratio was also noted for $ZnO–P_2O_5$ polyphosphate glasses [39]. The differences between the values of T_g measured in this study and those reported in the literature are most likely due to differences in composition, including the degree of iron reduction, Al_2O_3 contamination [9,24] or SiO_2 contamination (this study), arising from differences in melting conditions.

For phosphate glasses with O/P ratios in the range 3.0–3.5, the ratio of the bridging oxygen (BO) connecting two phosphate tetrahedra to the terminal oxygen (TO) that link one P-tetrahedron to the modifying metal ion (Me) polyhedra, BO/TO, can be calculated from [40],

$$\frac{BO}{TO} = \frac{4-\frac{O}{P}}{2(\frac{O}{P}-2)} \quad (1)$$

The predicted ratios of BO/TO for NFP glasses in this study are consistent with the BO/TO ratios determined by HPLC analyses, as described in a previous study of phosphate anion distributions [22]. With an increase in O/P ratio, the number of relative longer (P–O)–Me bonds increases, and the relative numbers of shorter (P–O)–P bonds decreases, as does the average phosphate chain length. The shorter chains and weaker P–O bonds correlate with the decrease in T_g temperature for the Na-free iron phosphate glasses.

For glasses with similar O/P ratios but different modifying oxides, the bonds between the metal polyhedra and phosphate anions determine the compositional dependence of the glass properties, like T_g. In general, cations with greater field strengths increase the structural rigidity of the network, which increases the temperature required to activate rotational motions, and so increase T_g [40,41]. For a series of NFP glasses with similar O/P ratios, the replacement of lower field strength Na ions by Fe ions generally increases the glass transition temperature, as shown in Fig. 2 and Fig. 6 (b). For the NFP glasses with compositions near the pyrophosphate stoichiometry, however, there is a maximum in T_g with increasing iron content, as seen in the present study and reported in the literature (Fig. 6 (b)). Similar observations of a maximum T_g were also made for mixed alkali $xNa_2O–(20–x)R_2O–32Fe_2O_3–48P_2O_5$ (R = K and Cs) glasses [33]. Such behavior cannot be explained by the simple modifier field strength argument outlined above.

In the previous Raman spectroscopic study of these NFP glasses [23], it was shown that the frequency of the symmetric stretching modes of non-bridging oxygens

(O_{nb}) generally increased with an increase in iron content for glasses with similar O/P ratios. Fig. 7 shows some results from that study; here, the $(PO_3)_{sym}$ modes are associated with non-bridging oxygens on Q^1 tetrahedra and the $(PO_2)_{sym}$ are associated with NBOs on Q^2 tetrahedra. The shifts to greater Raman frequencies can be associated with shorter average P–O_{nb} bond lengths [21] or narrower average O_{nb}–P–O_{nb} bond angles [23,42,43], indicating that stronger P–O_{nb} bonds may then be correlated with greater values for T_g. Supporting this correlation are the maxima in the $(PO_3)_{sym}$ Raman frequencies for the glasses with O/P = 3.40 and 3.49 in the same compositional ranges, Fe/(Na+Fe) = 0.45–0.70, where there are maxima in the values of T_g.

4.2. Glass forming ability and thermal stability

Glass forming ability describes the ease of vitrification of a melt on cooling from T_L to T_g, and so is affected by thermodynamic and structural factors as well as the kinetic process of glass formation [26,44]. Glasses that have two modifying cations with large differences in ionic field strengths will have large negative exothermic enthalpies of mixing for their melts ($\Delta H_{mix} < 0$) [45], and so will favor homogeneous melts instead of phase separated ones [46]. Compared to Na^+, iron cations are less basic and have greater electronegativity, and so the enthalpy of the formation of Fe–O bonds is more negative than that of the formation of Na–O bonds. At the same time, as the Fe content increases, the distribution of phosphate chains in a melt becomes broader, and the enthalpy for the endothermic disproportionation reactions (ΔH_n) decreases [45]. These enthalpy changes indicate that the replacement of Na by Fe should improve the glass forming ability of a phosphate melt and this is consistent with the laboratory observation that sodium-free

iron phosphate melts near the pyrophosphate composition are much better glass formers than are Na-pyrophosphate melts.

From a structural view, a greater degree of P–O–P connectivity in a glass melt could provide steric inhibition to crystallization [39]. Therefore, vitrification is easier if there are relatively greater concentrations of longer phosphate chains or wider distributions of phosphate anions in the melts. The increased structural complexity that results from disproportionation reactions leads to good glass forming ability for pyrophosphate melts with high field strength cations (e.g., Fe, Zn, Cd, and Bi), compared to melts with K, Na, or Li [39].

Even though glass formation favors the presence of complex anionic structures in a phosphate melt, the stability of the competing crystalline phases also influences glass formation and needs to be taken into consideration [44]. Studies have shown that glass-forming ability can be estimated by several thermal stability parameters (e.g., Table 1) defined by three characteristic temperatures [28]. Greater thermal stability is associated with lower critical cooling rates (q_{cr}), and thus with greater glass forming ability.

Thermal stability indicates the ability of glass to resist crystallization on heating. The compositional trends of the thermal stability parameters can be used to indicate trends in glass forming ability. A ternary contour map of the compositional dependence of the Hrubý thermal stability parameter, K_H, is shown in Fig. 8, where K_H is calculated from the measured characteristic temperatures shown in Table 2. Glasses with long phosphate chains (lower O/P ratio) or with low sodium contents generally have better thermal stability. Glass compositions with the lowest K_H are close the compositions of the stable crystalline phase $Na_7Fe_3(P_2O_7)_4$ and $NaFeP_2O_7$.

For the E-series, near the pyrophosphate stoichiometry, thermal stability does not vary systematically with the Fe content (Fig. 5 (a)), but instead, the corresponding glass composition around the minimum in thermal stability readily crystallized on heating to form $NaFeP_2O_7$ (Fig. 3 (a)). Compositions of the crystalline phases identified by XRD (Fig. 3) are indicated in Fig. 8. Melts with compositions near other stable intermediate compounds are also associated with the lower glass forming ability [34].

The glass forming region for the $Na_2O–Fe_2O_3–P_2O_5$ system determined by Parsons et al [34] shows a discontinuity around compositions near $Na_7Fe_3(P_2O_7)_4$ (crystal 2 in Fig. 8) and $NaFeP_2O_7$ (crystal 3 in Fig. 8). The crystalline phase $NaFeP_2O_7$ was observed in iron phosphate glass with 5 wt% Na_2O and 30 wt% HLW (Fe/P ~0.43) [47]. Bingham et al. [48] report a limit to glass formation in the $[(1–x)(0.6P_2O_5–0.4Fe_2O_3)] + xNa_2SO_4$ system at 30–40 mol% Na_2O with a Fe/(Na+Fe) ratio ~0.38, similar to the minimum in glass forming ability near ~43 mol% Na_2O and Fe/(Na+Fe) ~0.33 in Fig. 5 (a). Dissolution studies for iron phosphate with the same waste loading have shown that glassy wasteforms have better chemical durability than crystallized wasteforms [5,6], and thus compositions with the lowest thermal stability should be avoided when designing waste glasses with greater chemical durability.

The effect of the stability of the competing crystalline phases on glass formation cannot be ignored [44], which may mean that the best glass forming compositions in a system are not necessarily the eutectic compositions with the lowest liquidus temperatures. A study of the thermal stability of glasses from the ferric $Fe(PO_3)_3–Fe_4(P_2O_7)_3$ system shows that the K_A and K_w parameters continuously decrease with increase O/P ratio, and reaches the minimum value for iron phosphate glasses with O/P

ratio ~3.40 [9], which is very close to the eutectic point in the system of $Fe(PO_3)_3$–$Fe_4(P_2O_7)_3$ [37]. In the present study, for the sodium-free iron phosphate glasses, the thermal stability also exhibits a minimum value near O/P~3.36 (Fig. 5 (b)), with the formation of the mixed ferrous-ferric phosphate compound $Fe_4(P_2O_7)_3$.

4.3. Effects of iron redox

Phosphate melts prepared with Fe_2O_3 will partially reduce to form Fe^{2+} under most circumstances. The difference in electron density and chemistry between Fe^{3+} and Fe^{2+} affects the physical and chemical properties of glass melts, including structure, viscosity, and the behavior of volatile components [49].

Under reducing conditions [16,17], the extent of Fe^{3+} reduction is determined by the partial pressure of oxygen or oxygen fugacity during melting [49]. For glasses melted in air, the melting temperature determines the ratio of Fe^{3+}/Fe_{tot}, and the following reaction is endothermic [17,50,51],

$$2Fe^{3+}_{glass} + O^{2-}_{glass} \leftrightharpoons 2Fe^{2+}_{glass} + \tfrac{1}{2}O_2 \quad (2)$$

For iron pyrophosphate glasses melted in air, the equilibrium constant K of reaction (2) depends on the temperature according to [51,52],

$$\ln(K) = 9.40 - 1.58 \times 10^4/T \quad (3)$$

and the enthalpy (ΔH) of reaction (2) is calculated to be 131 ± 9 kJ/mol. For silicate glasses with iron less than 1 mol%, the enthalpy of reaction (2) was determined to be 144~171 kJ/mol, which is larger than that for phosphate glass [50,52]. This is consistent with the observations that the relative amount of Fe^{3+} reduced to Fe^{2+} is smaller in silicate glasses than that in phosphate glasses melted at the same temperature [49,53].

The distribution of phosphate anions will also be affected by the iron redox because the phosphate anions in the glass melts are in equilibrium with O^{2-} as shown by reaction (4) [45],

$$2PO_4^{3-} \leftrightharpoons P_2O_7^{4-} + O^{2-} \quad (4)$$

Zhang et al [9] report an increase in the Fe^{2+}/Fe_{tot} ratio with an increase in the O/P ratio for glasses melted at the same temperature, indicating that reaction (4) is favored for glasses with greater O/P ratios. The reduction of ferric ions to ferrous ions reduces the oxygen available to form smaller phosphate anions, and this in turn will affect the equilibrium between phosphate anions, as represented by [45,54],

$$2(\mathrm{P_nO_{3n+1}})^{-(n+2)} \leftrightharpoons (\mathrm{P_{n+1}O_{3n+4}})^{-(n+3)} + (\mathrm{P_{n-1}O_{3n-2}})^{-(n+1)} \quad (5)$$

As indicated by the equilibrium states of reactions (2) and (4), the reduction of Fe^{3+} to Fe^{2+} will result in greater amount of pyrophosphate anions in the glass network because of the shift of the equilibrium of reactions (2) and (4) to the right. Studies have shown that the glass forming ability of the pyrophosphate melts deteriorates as the fraction of Fe^{2+} increases [18].

The liquidus temperatures of the Na-free iron phosphate glass melts in this study are 40–260 °C greater than the corresponding liquidus surface reported by Zhang et al. in a recent study of the $Fe(PO_3)_3$–$Fe_4(P_2O_7)_3$ system [37]. This may be because the glasses in the present study are more reduced (Fe^{2+}/Fe_{tot} ~ 0.19 ± 0.05 [23]) than the ferric materials studied by Zhang et al. [37], and are consistent with the increase in melting temperatures for sodium-free iron pyrophosphate glasses with an increase in Fe^{2+}/Fe_{tot} ratio reported by Bingham et al. [55].

5. Summary

The thermal stability and crystallization behavior of several series of Na_2O–FeO–Fe_2O_3–P_2O_5 (NFP) glasses with different O/P (3.0–3.5) and Fe/P (0.13–0.67) ratios were studied. The glass transition temperatures were related to the nature of the P–O_{nb} bonds with the Na and Fe ions. The thermal stability against crystallization of sodium-free iron phosphate glasses is generally better than that of the sodium-containing iron phosphate glasses, and decreases with O/P ratio in the range 3.04~3.36. The minimum values of the thermal stability parameters correspond to the compositions of the stable crystalline compounds. The redox behavior of iron in the glass melts affects the glass thermal stability and the liquidus temperature, in part by affecting the phosphate anion distributions in the glass melts.

Acknowledgements

The authors are very grateful to Kathryn Goetschius (Missouri University of Science and Technology) for her help with the XRD experiments and for useful discussion on thermal stability, and Dr. Chandra S. Ray (Missouri S&T) for reviewing this manuscript and for useful discussions on glass crystallization. This work was supported by the Nuclear Energy University Program (US Department of Energy) under grant NEUP 09-144.

Table 1 Thermal stability parameters. Characteristic temperatures are in absolute temperature (K).

Parameters	Equations
Angell[56,57]	$K_A = T_x^h - T_g$
Weinberg[58]	$K_W = \frac{T_c^h - T_g}{T_m}$
Hrubÿ[59]	$K_H = \frac{T_x^h - T_g}{T_m - T_x^h}$

Table 2 Summary of characteristic temperatures and thermal stability parameters from the DTA data. Compositional information is from Ref. [23]. The error of T_g, T_x^h and T_c^h is ≤ 3 ºC, the error for measured T_L is listed in the table, and the errors for $K_A \leq 4$ K, for $K_W \leq 6\%$, for $K_H \leq 8\%$.

Batched		Analyzed				Characteristic temperatures (ºC)				Thermal stability parameters		
O/P	Fe/P	O/P	Fe/P	Fe^{2+}/Fe_{tot}	Fe/(Na+Fe)	T_g	T_x^h	T_c^h	T_L	K_A	K_W	K_H
A-Series	0.33	3.04	0.37	0.24	1.00	576	748	780	1210 ± 7	172	0.14	0.37
3.0	0.23	3.04	0.23	0.31	0.42	447	562	591	1142 ± 7	115	0.10	0.20
	0.13	3.03	0.13	0.13	0.18	353	451	571	880 ± 5	98	0.19	0.23
B-Series	0.40	3.15	0.42	0.14	1.00	572	730	779	1208 ± 5	158	0.14	0.33
3.1	0.33	3.10	0.32	0.26	0.59	500	605	622	1099 ± 5	105	0.09	0.21
	0.23	3.12	0.22	0.26	0.29	403	592	714	930 ± 6	189	0.26	0.56
	0.13	3.13	0.12	0.24	0.13	344	411	455	961 ± 4	67	0.09	0.12
C-Series	0.50	3.28	0.49	0.15	1.00	527	657	693	1229 ± 5	130	0.11	0.23
3.25	0.40	3.25	0.38	0.22	0.60	489	577	601	1080 ± 8	88	0.08	0.17
	0.33	3.24	0.32	0.22	0.39	443	595	618	1029 ± 6	152	0.13	0.35
	0.23	3.27	0.23	0.27	0.23	382	495	512	1004 ± 9	113	0.10	0.22
	0.13	3.30	0.15	0.12	0.12	360	427	454	865 ± 9	67	0.08	0.15
D-Series	0.60	3.36	0.58	0.11	1.00	497	620	645	1187 ± 6	123	0.10	0.22
3.4	0.50	3.38	0.49	0.16	0.65	513	645	669	1043 ± 5	132	0.12	0.33
	0.40	3.40	0.39	0.18	0.39	476	537	555	1040 ± 6	61	0.06	0.12
	0.33	3.42	0.32	0.21	0.28	433	503	515	1064 ± 9	70	0.06	0.12
	0.23	3.43	0.23	0.19	0.17	395	513	530	920 ± 6	118	0.11	0.29
	0.13	3.44	0.13	0.12	0.08	357	431	456	691 ± 8	74	0.10	0.28

Continue table on next page

Table 2 Summary of characteristic temperatures and thermal stability parameters from the DTA data. Compositional information is from Ref. [23]. The error of T_g, T_x^h and T_c^h is ≤ 3 ºC, the error for measured T_L is listed in the table, and the errors for $K_A \leq 4$ K, for $K_W \leq 6\%$, for $K_H \leq 8\%$. (cont.)

Batched		Analyzed				Characteristic temperatures (ºC)				Thermal stability parameters		
O/P	Fe/P	O/P	Fe/P	Fe^{2+}/Fe_{tot}	Fe/(Na+Fe)	T_g	T_x^h	T_c^h	T_L	K_A	K_W	K_H
E-Series	0.67	3.48	0.66	0.17	1.00	487	664	713	1138 ± 8	177	0.16	0.37
3.5	0.60	3.48	0.58	0.20	0.75	502	642	666	1167 ± 5	140	0.11	0.27
	0.50	3.48	0.48	0.18	0.49	523	603	615	1095 ± 5	80	0.07	0.16
	0.40	3.50	0.39	0.20	0.33	467	516	537	1080 ± 5	49	0.05	0.09
	0.33	3.50	0.34	0.19	0.26	438	530	544	956 ± 5	92	0.09	0.22
	0.23	3.51	0.23	0.14	0.15	403	489	510	839 ± 9	86	0.10	0.24

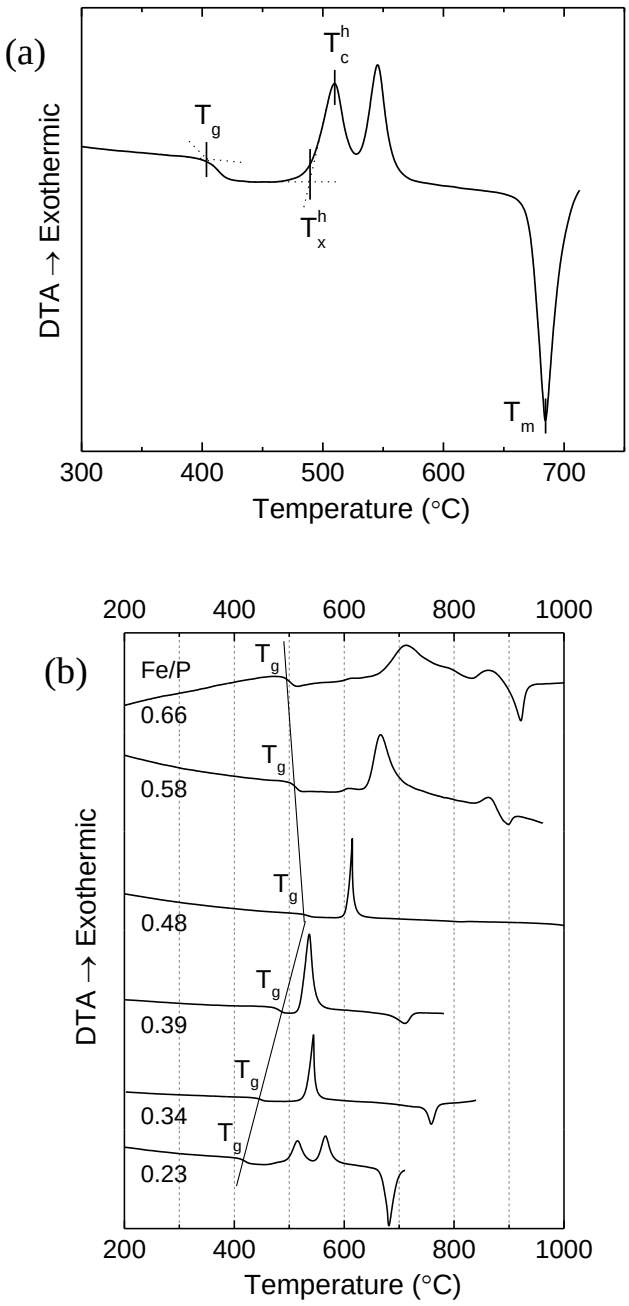

Fig. 1. DTA data for glass powders (75–150 μm) heated in air at 15 °C/min. (a) E-0.23 glass, showing the determination of the characteristic temperatures, the onset glass transition temperature (T_g), the onset crystallization temperature (T_x^h), the crystallization peak temperature on heating (T_c^h) and melting point (T_m); (b) E-series NFP glasses (O/P = 3.49 ± 0.01).

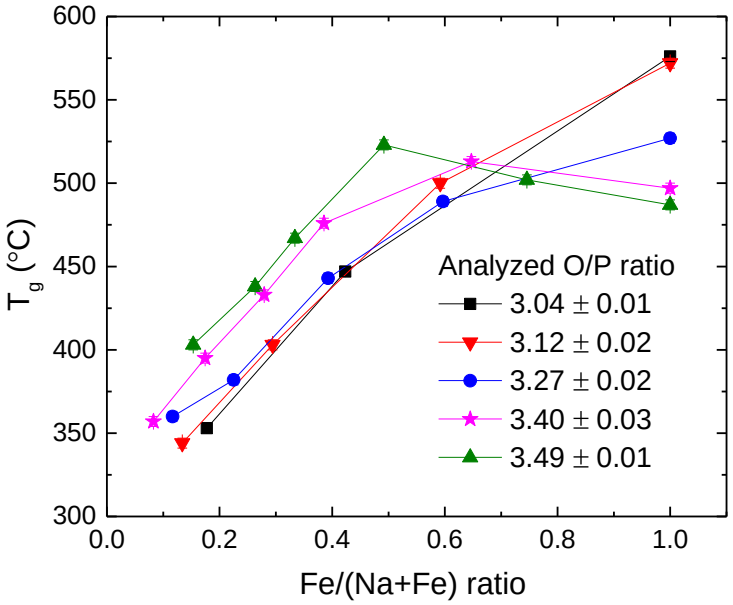

Fig. 2. The dependence of T_g on Fe/(Na+Fe) for each series of NFP glasses, determined by DTA (75–150 μm glass powder, heated at 15 °C/min).

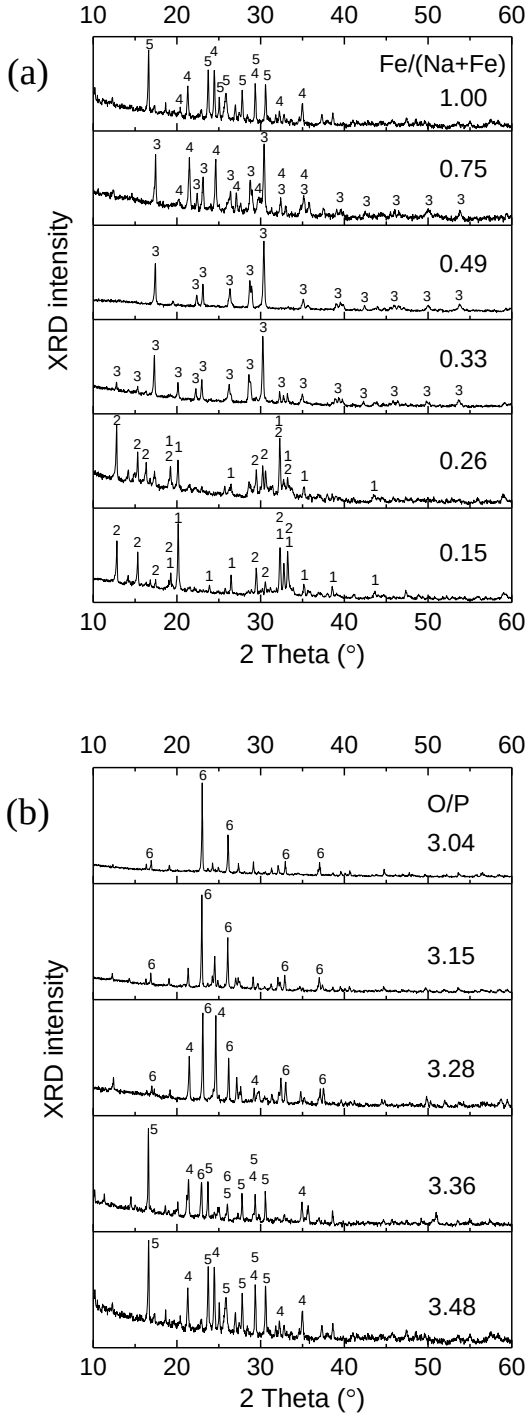

Fig. 3. X-ray diffraction patterns of glasses heat treated for nine hours above the respective exothermic crystallization peaks from DTA. (a) E-series glasses (O/P = 3.49 ± 0.01); (b) Sodium-free iron phosphate glasses with increasing O/P ratios. The identified crystalline phases are 1: $Na_4P_2O_7$ (PDF 71-1631); 2: $Na_7Fe_3(P_2O_7)_4$ [38]; 3: $NaFeP_2O_7$ (PDF 36-1454); 4: $Fe_2Fe(P_2O_7)_2$ [60]; 5: $Fe_4(P_2O_7)_3$ (PDF 36-318); 6: $Fe(PO_3)_3$ (PDF 38-109).

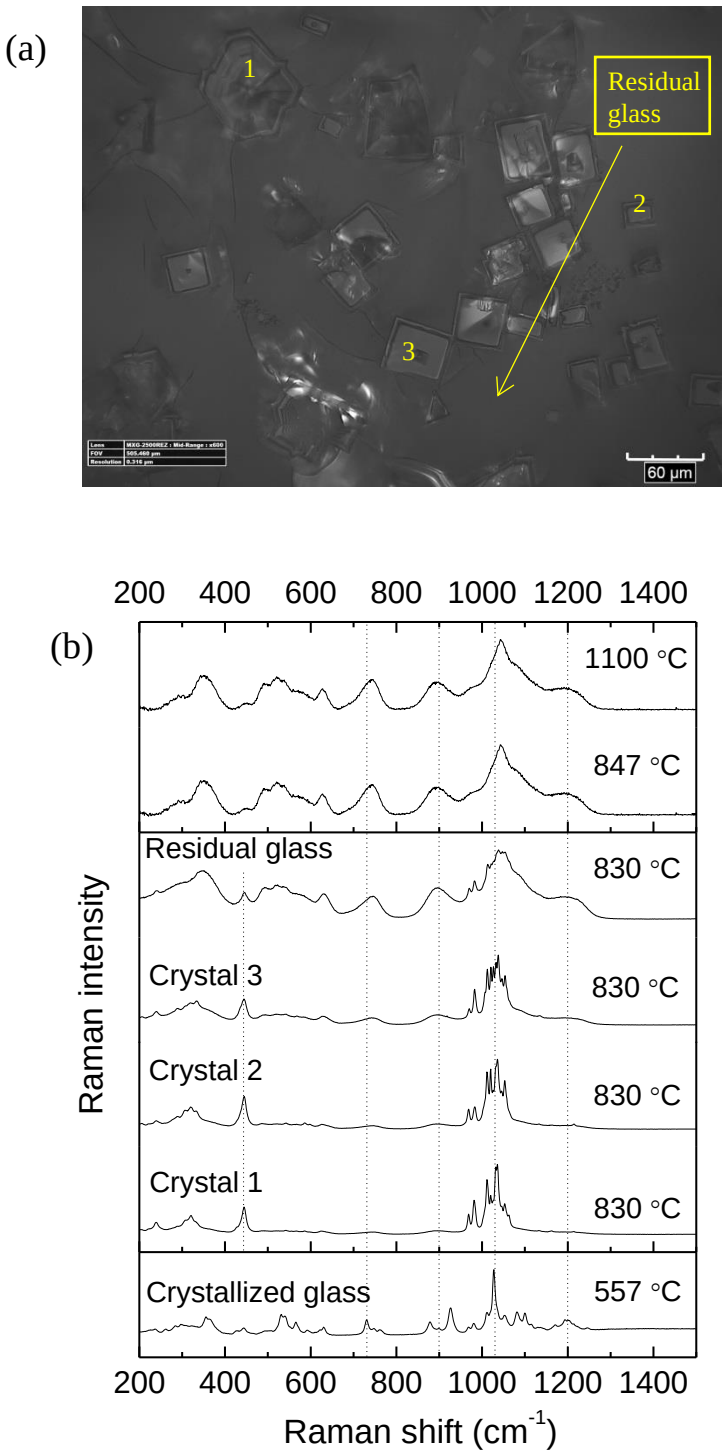

Fig. 4. (a) Optical image of crystals on the surface of E-0.23 glass, initially crystallized at 557 ºC for 9 hours, then reheated to 830 ºC for 30 minutes before quenching (×600); (b) Raman spectra of the crystallized E-0.23 glass after reheating to the temperatures indicated. The points where the spectra were collected from the 830 ºC sample are indicated on the optical image.

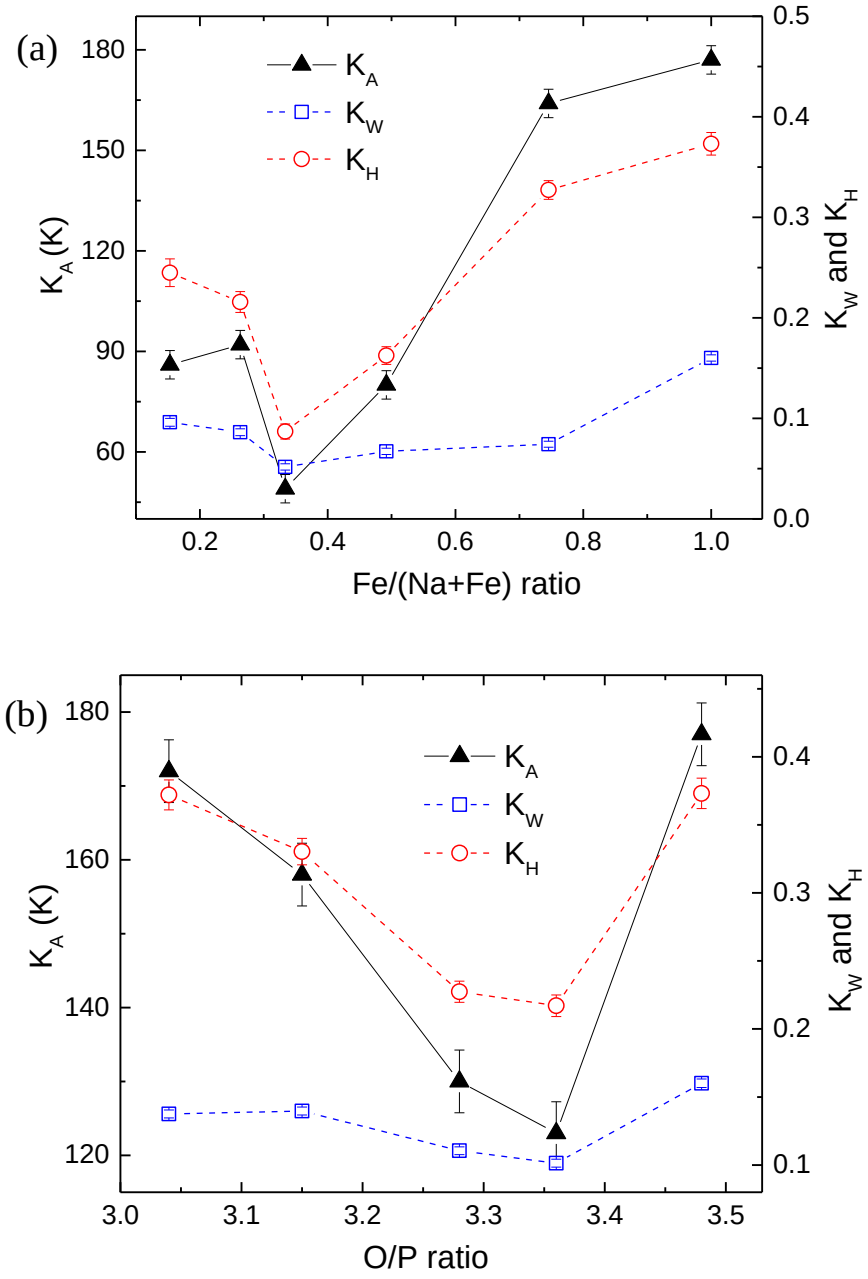

Fig. 5. Thermal stability parameters, K_A, K_W and K_H, presented (a) as a function of Fe/(Na+Fe) ratio for the E-series glasses (O/P = 3.49 ± 0.01); (b) as a function of O/P ratio for the sodium-free iron phosphate glasses.

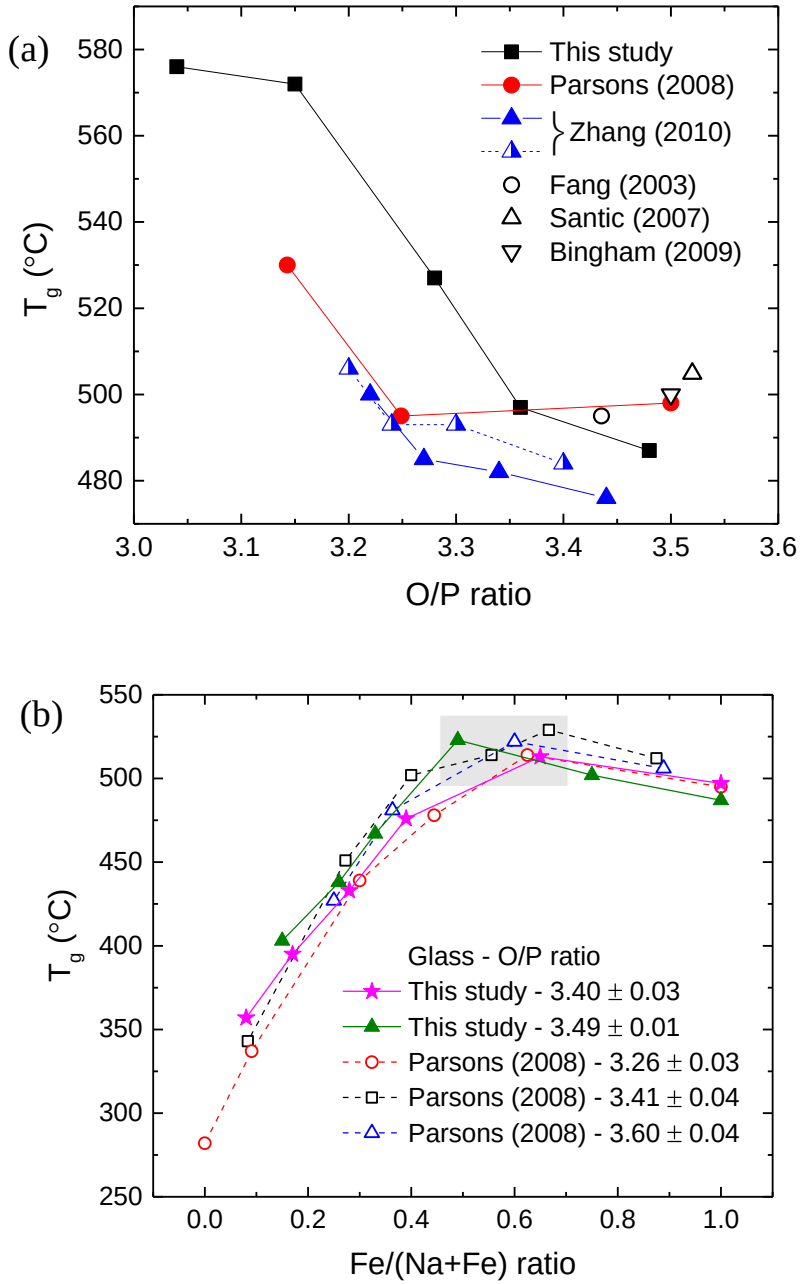

Fig. 6. T_g values (a) changing with O/P ratio for Na-free iron phosphate glasses; (b) changing with the Fe/(Na+Fe) ratio for several series sodium iron phosphate glasses with similar O/P ratios. References as follow, Parsons (2008) [34], Zhang (2010) [9], Fang (2003) [33], Santic (2007) [24], Bingham (2009) [32].

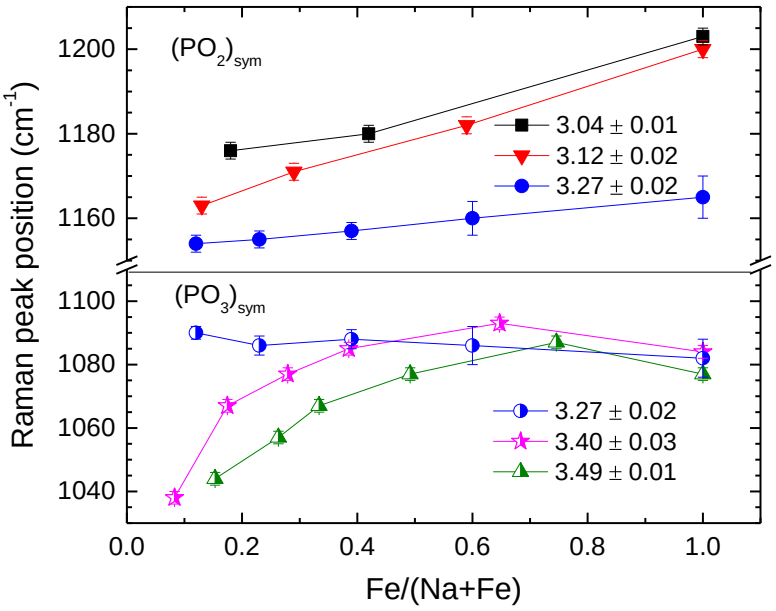

Fig. 7. Raman peak position (cm^{-1}) of PO_2 symmetric stretch and PO_3 symmetric stretch changing with Fe/(Na+Fe) ratio for five glass series in this study from reference [23].

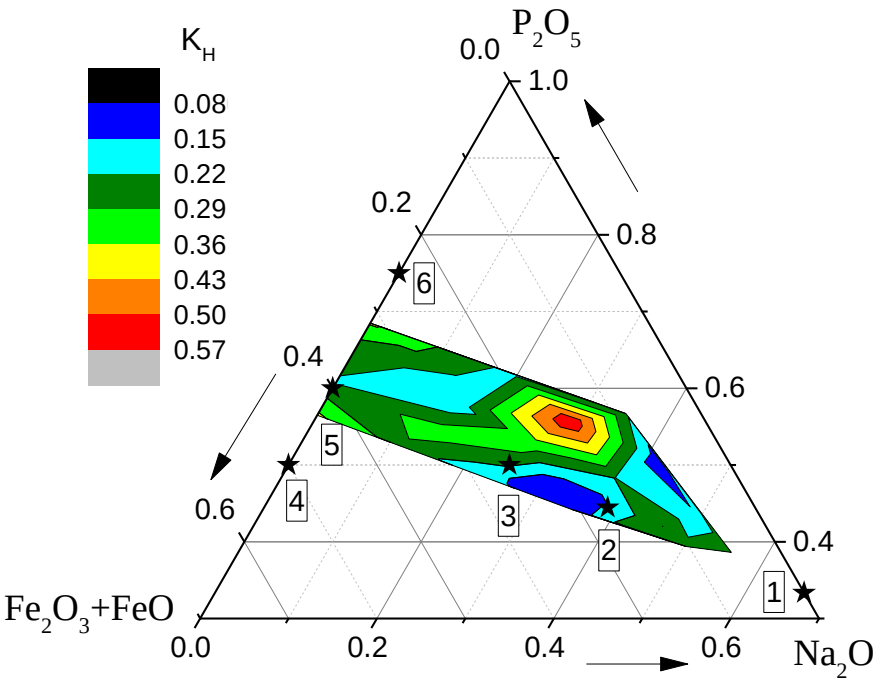

Fig. 8. Compositional dependence of the thermal stability parameter, K_H. Crystalline phases marked by numbers are, 1: $Na_4P_2O_7$; 2: $Na_7Fe_3(P_2O_7)_4$; 3: $NaFeP_2O_7$; 4: $Fe_2Fe(P_2O_7)_2$; 5: $Fe_4(P_2O_7)_3$; 6: $Fe(PO_3)_3$.

References

[1] E.H. Oelkers, and J.M. Montel. "Phosphates and nuclear waste storage." Elements 4, no. 2 (2008): 113-116.

[2] B.C. Sales, and L.A. Boatner. "Lead-iron phosphate glass: a stable storage medium for high-level nuclear waste." Science 226, no. 4670 (1984): 45-48.

[3] B. Samuneva, P. Tzvetkova, I. Gugov, and V. Dimitrov. "Structural studies of phosphate glasses." Journal of materials science letters 15, no. 24 (1996): 2180-2183.

[4] X. Yu, D.E. Day, G.J. Long, and R.K. Brow. "Properties and structure of sodium-iron phosphate glasses." Journal of non-crystalline solids 215, no. 1 (1997): 21-31.

[5] D.E. Day, Z. Wu, C.S. Ray, and P. Hrma. "Chemically durable iron phosphate glass wasteforms." Journal of non-crystalline solids 241, no. 1 (1998): 1-12.

[6] W. Huang, D.E. Day, C.S. Ray, C.W. Kim, and A. Mogus-Milankovic. "Vitrification of high chrome oxide nuclear waste in iron phosphate glasses." Journal of nuclear materials 327, no. 1 (2004): 46-57.

[7] N. Singh, K.J. Singh, K. Singh, and H. Singh. "Comparative study of lead borate and bismuth lead borate glass systems as gamma-radiation shielding materials." Nuclear Instruments and Methods in Physics Research Section B: Beam Interactions with Materials and Atoms 225, no. 3 (2004): 305-309.

[8] I. Ahmed, C.A. Collins, M.P. Lewis, I. Olsen, and J.C. Knowles. "Processing, characterisation and biocompatibility of iron-phosphate glass fibres for tissue engineering." Biomaterials 25, no. 16 (2004): 3223-3232.

[9] L. Zhang, L. Ghussn, M.L. Schmitt, E.D. Zanotto, R.K. Brow, and M.E. Schlesinger. "Thermal stability of glasses from the $Fe_4(P_2O_7)_3$–$Fe(PO_3)_3$ system." Journal of Non-Crystalline Solids 356, no. 52 (2010): 2965-2968.

[10] V. Simon, S.G. Chiuzbăian, M. Neumann, D. Eniu, E. Indrea, A. Török-Kiss, and S. Simon. "Photoelectron spectroscopy on iron-containing CaO–SiO_2–P_2O_5 glass ceramics." Modern Physics Letters B 14, no. 21 (2000): 767-772.

[11] S.T. Lin, S.L. Krebs, S. Kadiyala, K.W. Leong, W.C. LaCourse, and B. Kumar. "Development of bioabsorbable glass fibres." Biomaterials 15, no. 13 (1994): 1057-1061.

[12] A. Al-Shahrani, A. Al-Hajry, and M.M. El-Desoky. "Electrical relaxation in mixed lithium and sodium iron phosphate glasses." Physica B: Condensed Matter 364, no. 1 (2005): 248-254.

[13] P. Bergo, S.T. Reis, W.M. Pontuschka, J.M. Prison, and C.C. Motta. "Dielectric properties and structural features of barium-iron phosphate glasses." Journal of non-crystalline solids 336, no. 3 (2004): 159-164.

[14] F.A. Wedgwood, A.C. Wright. "Short range antiferromagnetic ordering in vitreous Fe_2O_3-P_2O_5." Journal of Non-Crystalline Solids 21, no. 1 (1976): 95-105.

[15] J.L. Shaw, A.C. Wright, R.N. Sinclair, G.K. Marasinghe, D. Holland, M.R. Lees, and C.R. Scales. "Spin glass-like antiferromagnetic interactions in iron phosphate glasses." Journal of non-crystalline solids 345 (2004): 245-250.

[16] H. Akamatsu, K. Fujita, S. Murai, and K. Tanaka. "Magneto-optical properties of transparent divalent iron phosphate glasses." Applied Physics Letters 92, no. 25 (2008): 251908.

[17] M. Karabulut, E. Metwalli, D.E. Day, and R.K. Brow. "Mössbauer and IR investigations of iron ultraphosphate glasses." Journal of non-crystalline solids 328, no. 1 (2003): 199-206.

[18] G.K. Marasinghe, M. Karabulut, C.S. Ray, D.E. Day, M.G. Shumsky, W.B. Yelon, C.H. Booth, P.G. Allen, and D.K. Shuh. "Structural features of iron phosphate glasses." Journal of non-crystalline solids 222 (1997): 144-152.

[19] H. Akamatsu, S. Oku, K. Fujita, S. Murai, and K. Tanaka. "Magnetic properties of mixed-valence iron phosphate glasses." Physical Review B 80, no. 13 (2009): 134408.

[20] A.C. Wright, R.N. Sinclair, J.L. Shaw, R. Haworth, G.K. Marasinghe, and D.E. Day. "A neutron diffraction study of the structure of iron phosphate glasses." Physics and Chemistry of Glasses-European Journal of Glass Science and Technology Part B 49, no. 1 (2008): 1-7.

[21] L. Zhang, and R.K. Brow. "A Raman study of iron–phosphate crystalline compounds and glasses." Journal of the American Ceramic Society 94, no. 9 (2011): 3123-3130.

[22] L. Ma, R.K. Brow. "Structural study of Na_2O-FeO-Fe_2O_3-P_2O_5 glasses by high-pressure liquid chromatography." Journal of Non-Crystalline Solids 387 (2014): 16-20.

[23] L. Ma, R.K. Brow, A. Choudhury. " Structural study of Na_2O-FeO-Fe_2O_3-P_2O_5 glasses by Raman and Mössbauer spectroscopy." Journal of Non-Crystalline Solids 402 (2014): 64-73.

[24] A. Šantić, A. Moguš-Milanković, K. Furić, V. Bermanec, C.W. Kim, and D.E. Day. "Structural properties of Cr_2O_3–Fe_2O_3–P_2O_5 glasses, Part I." Journal of Non-Crystalline Solids 353, no. 11 (2007): 1070-1077.

[25] H. Arstila, M. Tukiainen, S. Taipale, M. Kellomäki, and L. Hupa. "Liquidus temperatures of bioactive glasses." Advanced Materials Research 39 (2008): 287-292.

[26] I. Avramov, E.D. Zanotto, and M.O. Prado. "Glass-forming ability versus stability of silicate glasses. II. Theoretical demonstration." Journal of non-crystalline solids 320, no. 1 (2003): 9-20.

[27] A.A. Cabral, A.A.D. Cardoso, and E.D. Zanotto. "Glass-forming ability versus stability of silicate glasses. I. Experimental test." Journal of non-crystalline solids 320, no. 1 (2003): 1-8.

[28] M.L.F. Nascimento, L.A. Souza, E.B. Ferreira, and E.D. Zanotto. "Can glass stability parameters infer glass forming ability?." Journal of non-crystalline solids 351, no. 40 (2005): 3296-3308.

[29] E.B Ferreira, E.D. Zanotto, S. Feller, G. Lodden, J. Banerjee, T. Edwards, and M. Affatigato. "Critical Analysis of Glass Stability Parameters and Application to Lithium Borate Glasses." Journal of the American Ceramic Society 94, no. 11 (2011): 3833-3841.

[30] V.M. Fokin, R.M.C.V. Reis, A.S. Abyzov, C.R. Chinaglia, and E.D. Zanotto. "Nonstoichiometric crystallization of lithium metasilicate–calcium metasilicate glasses. Part 1-Crystal nucleation and growth rates." Journal of Non-Crystalline Solids 362 (2013): 56-64.

[31] Standard Practices for Measurement of Liquids Temperature of Glass by the Gradient Furnace Method, ASTM Standard Designation, C829-81 (2010).

[32] P.A. Bingham, R.J. Hand, O.M. Hannant, S.D. Forder, and S.H. Kilcoyne. "Effects of modifier additions on the thermal properties, chemical durability, oxidation state and structure of iron phosphate glasses." Journal of Non-Crystalline Solids 355, no. 28 (2009): 1526-1538.

[33] X. Fang, C.S. Ray, and D.E. Day. "Glass transition and fragility of iron phosphate glasses.: II. Effect of mixed-alkali." Journal of non-crystalline solids 319, no. 3 (2003): 314-321.

[34] A.J. Parsons, and C.D. Rudd. "Glass forming region and physical properties in the system P_2O_5-Na_2O-Fe_2O_3." Journal of Non-Crystalline Solids 354, no. 40 (2008): 4661-4667.

[35] A. Mogus-Milankovic, M. Rajic, A. Drasner, R. Trojko, and D.E. Day. "Crystallisation of iron phosphate glasses." Physics and chemistry of glasses 39, no. 2 (1998): 70-75.

[36] S.I. Grishin, J.M. Bigham, and O.H. Tuovinen. "Characterization of jarosite formed upon bacterial oxidation of ferrous sulfate in a packed-bed reactor." Applied and environmental microbiology 54, no. 12 (1988): 3101-3106.

[37] L. Zhang, M.E. Schlesinger, and R.K. Brow. "Phase equilibria in the Fe_2O_3–P_2O_5 system." Journal of the American Ceramic Society 94, no. 5 (2011): 1605-1610.

[38] C. Masquelier, F. d'Yvoire, E. Bretey, P. Berthet, and C. Peytour-Chansac. "A new family of sodium ion conductors: the diphosphates and diarsenates $Na_7M_3(X_2O_7)_4$; (M=Al, Ga, Cr, Fe; X=P, As)." Solid State Ionics 67, no. 3 (1994): 183-189.

[39] R.K. Brow, D.R. Tallant, S.T. Myers, and C.C. Phifer. "The short-range structure of zinc polyphosphate glass." Journal of non-crystalline solids 191, no. 1 (1995): 45-55.

[40] R.K. Brow. "Review: the structure of simple phosphate glasses." Journal of Non-Crystalline Solids 263 (2000): 1-28.

[41] J.J. Hudgens, and S.W. Martin. "Glass transition and infrared spectra of low-alkali, anhydrous lithium phosphate glasses." Journal of the American Ceramic Society 76, no. 7 (1993): 1691-1696.

[42] G.B. Rouse Jr, P.J. Miller, and W.M. Risen Jr. "Mixed alkali glass spectra and structure." Journal of Non-Crystalline Solids 28, no. 2 (1978): 193-207.

[43] B.N. Nelson, and G.J. Exarhos. "Vibrational spectroscopy of cation-site interactions in phosphate glasses." Journal of Chemical Physics 71, no. 7 (1979): 2739-2747.

[44] Z.P. Lu, and C.T. Liu. "Glass formation criterion for various glass-forming systems." Physical review letters 91, no. 11 (2003): 115505.

[45] T.R. Meadowcroft, and F.D. Richardson. "Structural and thermodynamic aspects of phosphate glasses." Transactions of the Faraday Society 61 (1965): 54-70.

[46] D.R. Gaskell. Introduction to the thermodynamics of materials, fourth edition. Taylor & Francis Group, New York, NY, 2008.

[47] T. Fukui, T. Ishinomori, Y. Endo, M. Sazarashi, S. Ono, and K. Suzuki. "Iron phosphate glass as potential waste matrix for high-level radioactive waste." WM 3 (2003): 23-27.

[48] P.A. Bingham, and R.J. Hand. "Sulphate incorporation and glass formation in phosphate systems for nuclear and toxic waste immobilization." Materials Research Bulletin 43, no. 7 (2008): 1679-1693.

[49] A.J. Berry, H.St.C. O'Neill, K.D. Jayasuriya, S.J. Campbell, and G.J. Foran. "XANES calibrations for the oxidation state of iron in a silicate glass." American Mineralogist 88, no. 7 (2003): 967-977.

[50] C.S. Ray, X. Fang, M. Karabulut, G.K. Marasinghe, and D.E. Day. "Effect of melting temperature and time on iron valence and crystallization of iron phosphate glasses." Journal of non-crystalline solids 249, no. 1 (1999): 1-16.

[51] X. Fang, C.S. Ray, A. Moguš-Milanković, and D.E. Day. "Iron redox equilibrium, structure and properties of iron phosphate glasses." Journal of non-crystalline solids 283, no. 1 (2001): 162-172.

[52] A. Paul. Chemistry of glasses. London: Chapman and Hall, 1982.

[53] D. Holland, A. Mekki, I.A. Gee, C.F. McConville, J.A. Johnson, C.E. Johnson, P. Appleyard, and M. Thomas. "The structure of sodium iron silicate glass–a multi-technique approach." Journal of non-crystalline solids 253, no. 1 (1999): 192-202.

[54] P.J. Flory. "Random reorganization of molecular weight distribution in linear condensation polymers." Journal of the American Chemical Society 64, no. 9 (1942): 2205-2212.

[55] P.A. Bingham, R.J. Hand, and S.D. Forder. "Doping of iron phosphate glasses with Al_2O_3, SiO_2 or B_2O_3 for improved thermal stability." Materials research bulletin 41, no. 9 (2006): 1622-1630.

[56] E.I. Cooper, and C.A. Angell. "Far-IR transmitting, cadmium iodide-based glasses." Journal of Non-Crystalline Solids 56, no. 1 (1983): 75-80.

[57] M.G. Drexhage, O.H. El-Bayoumi, H. Lipson, C.T. Moynihan, A.J. Bruce, J. Lucas, and G. Fonteneau. "Comparative study of BaF_2/ThF_4 glasses containing YF_3, YbF_3 and LuF_3." Journal of Non-Crystalline Solids 56, no. 1 (1983): 51-56.

[58] M.C. Weinberg. "An assessment of glass stability criteria." Physics and chemistry of glasses 35, no. 3 (1994): 119-123.

[59] A. Hrubý. "Evaluation of glass-forming tendency by means of DTA." Czechoslovak Journal of Physics B 22, no. 11 (1972): 1187-1193.

[60] M. Ijjaali, G. Venturini, R. Gerardin, B. Malaman, and C. Gleitzer. "Synthesis, structure and physical properties of a mixed-valence iron diphosphate $Fe_3(P_2O_7)_2$: first example of trigonal prismatic Fe^{2+} with O^{2-}ligands." European journal of solid state and inorganic chemistry 28, no. 5 (1991): 983-998.

IV. DISSOLUTION BEHAVIOR OF $Na_2O–FeO–Fe_2O_3–P_2O_5$ GLASSES

Lina Ma, Richard K. Brow*, Mark E. Schlesinger

Department of Materials Science & Engineering, Missouri University of Science & Technology, Straumanis-James Hall, 1400 N. Bishop Ave, Rolla, MO, USA

ABSTRACT

The dissolution behavior of five series of $Na_2O–FeO–Fe_2O_3–P_2O_5$ glasses with ranges of O/P (3.0–3.5) and Fe/P (0.13–0.67) ratios were investigated in water using static and semi-dynamic tests. Glass composition, which determines the average phosphate chain length, affects the dissolution mechanism and kinetics. Initial dissolution is described by a 3D diffusion model (DM), whereas a contracting volume model (CVM) describes later dissolution kinetics. Temperature dependent rate parameters, K_{DM} and K_{CVM}, increase by several orders of magnitude with increasing Fe/P ratio, but are less dependent on the O/P ratio. The surface morphology and composition of the corroded glasses are characterized by analytical electron microscopy, which provides information about the change from DM to CVM kinetics.

Keywords: iron-phosphate glass, dissolution behavior, kinetics

* Corresponding author, brow@mst.edu

1. Introduction

Information about the dissolution processes and ion release rates of phosphate glasses in aqueous environments is important for a wide range of engineering applications, from biomaterial design to nuclear waste remediation. Through compositional control, the solubility of phosphate glasses can be tailored to obtain ion release rates that vary by many orders of magnitude [1,2]. The chemical durability of phosphate glass has been related to the composition and structure. Studies have shown that the addition of alkali oxides to phosphate glasses increase their dissolution rates in aqueous environments, whereas the addition of alkaline earth and high field strength cations (e.g., CaO, MgO, CuO, Al_2O_3 and Fe_2O_3) generally improves the chemical durability [3,4,5].

Because they possess excellent chemical durability, often superior to silicate and borosilicate glasses, iron phosphate glasses with Fe/P ratios between 1:3 and 2:3 have been developed for the vitrification of high level nuclear waste (HLW) [6,7,8,9]. In addition, high concentrations of alkali oxides (up to 20 wt%) can be tolerated in the iron phosphate glasses without deterioration of their good chemical durability [7]. The chemical durability of iron phosphate glasses with simulated sodium bearing waste (SBW) and HLW meets all current US Department of Energy (DOE) requirements [6,10,11,12].

The degradation rates of $Na_2O–CaO–P_2O_5$ glasses used as bioactive and bioresorbable materials can also be tailored by adding Fe_2O_3 to suit various end applications [13]. The good chemical durability of iron phosphate glasses has been attributed to their chemical structure. The hydration rates of phosphate chains decreases with increasing iron oxide content because of the greater chemical stability of P–O–Fe

bonds [14]. For $Na_2O–CaO–P_2O_5$ glasses doped with increasing amounts of Fe_2O_3, the contact angle of polar liquids increases, indicating a decrease in the total surface energy of the glasses and this has also been related to improved chemical durability [15]. For phosphate glasses that contain both Fe^{2+} and Fe^{3+}, the chemical durability is independent of the relative Fe^{2+} content [14].

The dissolution behavior of glass is determined by the reactions of the glass network and the release of different ions to the solution. Surface conditions and layer formation, saturation effects and solution chemistry must also be taken into account [16]. Often, the initial stage of corrosion is controlled by an ion exchange process or the diffusion of water into the glass network, followed then by the dissolution of the glass matrix with increasing depth of alkali depletion in the outer glass surface [1,12,16]. The hydration reactions between glass and water are based on the hydrolytic cleavage of bonds in the glass network that are related to different energies of hydration. The weakest bonds between metal ions and nonbridging oxygens, $M–O_{nb}$, react first during the dissolution process. The fraction of nonbridging oxygens (NBO) and the concentration of mobile ions (e.g., Na^+) determine the initial glass hydration rates [17]. The rate of ion exchange across the hydration layer as well as the penetration of water into the bulk glass is determined by the surface concentration of the interdiffusing ions, the multi-component interdiffusion coefficient and the exchange potential of the interdiffusing species at the exchange site [17].

One treatment of the glass/water reactions is based on transition state theory in combination with reversible and irreversible thermodynamics. Two main approaches, geochemical and thermodynamic, have been used to study the glass dissolution processes.

Models derived from these two approaches have been applied successfully to many corrosion studies of nuclear waste glasses [16,18,19,20,21]. Both the geochemical and thermodynamic approach to glass corrosion depend on a quantitative determination of the equilibrium, which is described by a complex solubility product changing with the amount of glass dissolved into solution [20,22]. The hydration and hydrolysis processes associated with glasses in aqueous solutions have been related to the free energy changes for reactions that occur between the glass constituents and the absorbed water molecules, and the overall free energies of hydration for different compositions were estimated [16]. The relationships between the calculated thermodynamic stability and glass dissolution rates can then be used to estimate the relative glass durability in aqueous solutions [18].

In the present study, the dissolution behavior of sodium iron phosphate glasses is systematically investigated by two types of dissolution tests. Leachate solution analysis shows that the congruence and leaching kinetics of each constituent is compositionally dependent. The kinetics that control glass dissolution are discussed with respect to the structure and composition of the corroded glass.

2. Experimental Procedures

2.1. Glass preparation

The procedures for preparing and analyzing the structures of the sodium iron phosphate glasses used in the present study have been described in previous papers [23,24]. Briefly, glasses were made from batches of raw materials including Na_2CO_3 (Alfa Aesar, ≥ 98%), Fe_2O_3 (Alfa Aesar, ≥ 99%) and $NH_4H_2PO_4$ (Alfa Aesar, ≥ 98%) that were melted in fused SiO_2 crucibles (Leco #728-701) between 1000 °C and 1250 °C in

air for two hours. Iron phosphate glasses were digested in 3–7 M H_2SO_4 aqueous solution for 7 to 14 days at 80–90 °C in closed Teflon containers, and cation concentrations, including small amounts of silica from the crucibles, were determined by inductively-coupled plasma optical emission spectroscopy (ICP-OES, PerkinElmer Optima 2000 DV, Norwalk, USA). The fraction of iron present as Fe^{2+} was determined by a wet chemical technique [25]. Compositional series with similar O/P ratios (3.0–3.5) are labeled from A to E according to their iron contents. For example, glass E-0.66 is a sample in the E-series with a batched O/P ratio of 3.5 and an analyzed Fe/P ratio of 0.66.

2.2. Dissolution studies

Glass powders were ultrasonically prewashed in absolute ethanol to remove dust particles, and two types of corrosion tests with different experimental conditions were conducted:

Test A (static): Glass powders (~200 mg, 300–425 μm, triplicates) were placed into polypropylene tubes (Evergreen Scientific, 50 ml centrifuge tubes) with 50 ml of deionized H_2O. The initial SA/V ratio (ratio of powder surface area to leachate volume) was held constant at ~24 ± 1 m^{-1}. These experiments were done at different temperatures (21, 40, 60 and 80 ºC ± 2 ºC).

Test B (semi-dynamic): Glass powders (~450 mg, 150–355 μm, triplicates) were sealed into small bags (~2 cm × 2 cm) made from Nylon mesh (Blick Art Materials, 284 TPI mesh, opening size of 51 microns). Samples were put into 50 ml deionized H_2O at 60 ± 2 ºC with SA/V ratio ~77 ± 2 m^{-1}, and solutions were replenished with 50 ml deionized H_2O for every indicated time interval.

For both tests, weight losses were measured, and ion concentrations (ppm levels) in leachate solutions were analyzed for specific time intervals using ICP-OES. Solutions for ICP were filtered to remove solid particles and diluted with 1wt% HNO_3. Dilution factors were 1:9 or 1:99, depending on the predicted ion concentrations of the solution. The pH values of leachate solutions were measured using a pH electrode (Fisher Scientific accumet Research AR25).

The surface morphologies and compositions corroded glasses were characterized by scanning electron microscopy (SEM) (FEI Helios NanoLab 600 DualBeam FIB/SEM) with energy-dispersive X-ray spectrometry (EDS). Samples were coated with carbon prior to these analyses.

3. Results

3.1. Static Dissolution

The concentrations of ions released into solution were normalized to the initial glass composition. The normalized elemental mass release, NL(i) (mg/cm^2), was calculated by Eq. (1),

$$\mathrm{NL(i)} = \frac{C_i}{(f_i)\cdot(\mathrm{SA(t)/V})} \quad (1)$$

where C_i is the measured concentration (ppm) of element i in solution, f_i is the mass fraction (wt%) of element i in the initial glass, SA(t)/V is the time-dependent ratio of glass surface area (cm^2) to leachate volume (L) [6]. Instantaneous release rates for each element can be determined from the slope, $\partial[\mathrm{NL(i)}]/\partial \mathrm{t}$, at any given time in the plot of NL(i) versus time [16]. If all glass constituents are released into solution in the same proportion as they are present in the solid, congruent dissolution is observed and

∂[NL(i)]/ ∂t is the same for all elements. The average release rate is equal to the instantaneous release rates only if NL(i) is linear with time.

Fig. 1 (a) shows that for the static dissolution Test A, the amount of P released into water from the D-series glasses (O/P = 3.40 ± 0.03) decreases by nearly four orders of magnitude with an increase in the Fe/P ratio from 0.23 to 0.58. Fig. 1 (b) shows the normalized mass release (mg/cm^2) data for sodium, phosphorus and iron from the same series of experiments. Congruent dissolution is observed for glasses with low iron contents (Fe/P = 0.23 and 0.32), and preferential release of sodium is observed from glasses with greater iron content (Fe/P = 0.39 and 0.49); the glass with Fe/P = 0.58 is Na-free. Fig. 1 (c) shows how the pH of the leachate solutions changes with time for the D-series glasses. In general, glasses with greater Na-contents (lower Fe/P ratios) create more basic leachate solutions. Static dissolution tests on the E-series glasses (O/P = 3.49 ± 0.01) showed similar results for the ion release data and leachate solution pH, with the latter increasing to 8.3–8.7 for glass E-0.23.

Fig. 2 shows some results from static dissolution (Test A) experiments for the B-series of glasses. These glasses have lower O/P ratios (3.12 ± 0.02) than the D-series, and so have longer average phosphate chains. Fig. 2 (a) shows the normalized mass release (mg/cm^2) data for sodium, phosphorus and iron. Once again, glasses with lower Fe/P ratios dissolve congruently, especially initially, whereas glasses with greater Fe/P ratios preferentially release elements in the order Na > P > Fe. In contrast to the glasses with greater O/P ratios, the pH values of the leachate solutions of the B-series glasses decrease with time, with the more acidic solutions associated with glasses with the lowest iron content, and so the greatest P_2O_5 contents (Fig. 2 (b)). Static dissolution tests on A-

series glasses (O/P = 3.04 ± 0.01) showed similar compositional dependences of leach rates and leachate solution pH, with the latter decreasing to 2.9–3.1 for glass A-0.13.

About 3 mole% SiO_2 was incorporated into the Na–Fe–phosphate melts from the crucible [23,24]. Fig. 3 shows the Si/P ratios in leachate solutions for the A-series glasses (O/P = 3.04 ± 0.01). The glasses with greater iron contents (Fe/P = 0.23 and 0.37) released substantially more Si than did the glass with Fe/P = 0.13. The latter glass dissolved congruently. Similar results were observed for other glass series; glasses with greater iron contents released Si into DI H_2O at relatively greater rates than other constituents.

3.2. Semi-dynamic dissolution

Fig. 4 (a) compares the normalized mass release (mg/cm^2) data for sodium, phosphorus and iron from the C-series of glasses, (O/P = 3.27 ± 0.02), obtained in the static dissolution Test A, with that obtained from the semi-dynamic dissolution Test B. The glass with Fe/P = 0.23 dissolves congruently at a much greater rate when the solution is refreshed (Test B) than in static conditions (Test A). For the more durable glasses with greater Fe/P ratios, there is less difference in the release rates for the two tests. Similar compositionally-dependent results were observed for other glass series tested by these two techniques.

Fig. 4 (b) compares the effects of the testing protocol for two glasses with similar normalized mass release rates, but much different compositions. Glass A-0.23 has an O/P of 3.04 and glass E-0.33 has an O/P of 3.50. Glass A-0.23 exhibits congruent dissolution behavior in the semi-dynamic Test B for the entire 130 hours of the test, whereas

preferential release of ions (Na > P > Fe) is evident after about 24 hours in static Test A. For glass E-0.33, both tests reveal congruent dissolution behavior for the entire 130 hours. Changes in solution pH and the Si release behavior were similar for the two tests.

4. Discussion

4.1. Dissolution kinetics

Two shrinking-core models [26] are applied to the glass dissolution data. Glass particles are assumed to have spherical geometries and reactions between the aqueous solution and the glass particles are three dimensional (3D), occurring at the outer surface of the particles. The reaction interface moves into the particle and the unreacted glass core shrinks uniformly so that the reacting area decreases with reaction time.

If a diffusion process controls the rate of reaction for spherical particles, a 3D diffusion model (DM) could be used to describe that reaction [27,28]:

$$1 - (1 - \alpha)^{1/3} = k_{DM} t^{1/2} \quad (2)$$

where α is the mass fraction of a particle that has reacted in time t, and k_{DM} is the temperature-dependent reaction rate parameter.

A contracting volume model (CVM) would describe linear reaction kinetics, with a reaction rate parameter of k_{CVM}, for spherical particles [27,28,29]:

$$1 - (1 - \alpha)^{1/3} = k_{CVM} t \quad (3)$$

The P-release data for all static dissolution (Test A) experiments were analyzed to determine the time-dependence of α(P) and then were fit by the DM and CVM rate equations. An example of the model-fitting is shown for glass B-0.12 in Fig. 5. Initially, there is a rapid release of phosphorus to solution and the release kinetics are consistent

with the Diffusion Model (Eq. 2). After about fifteen hours, the release kinetics slow down compared to the original DM predictions, and are instead well-fit by the Contracting Volume Model (Eq. 3).

Fig. 6 shows the two-model fit applied to glasses from the B-series (O/P = 3.12 ± 0.02) and the D-series (O/P = 3.40 ± 0.03). In every case, the initial P-release data fit the Diffusion Model and later data fit the Contracting Volume Model, although the reaction time where the transition from one model to the other differed for different glasses (Table 1). For glasses with longer phosphate chains (e.g., series B, O/P ~3.12), the transition time from DM to CVM does not change significantly with Fe/P ratio, whereas for glass series with shorter phosphate chains (e.g., series D, O/P ~3.40), the first stage controlled by the 3D diffusion mechanism is generally prolonged as Fe/P ratio increases.

Fig. 7 (a) shows the dependence of k_{DM} on the Fe/P ratio and Fig. 8 (a) shows a similar dependence of k_{CVM}. Clearly, glasses with greater iron contents react more slowly in both reaction regimes. Fig. 7 (b) and Fig. 8 (b) summarize the compositional dependences of k_{DM} and k_{CVM}, respectively, for all glasses reacted in DI water using Test A. Here, it is apparent that the Fe/P ratio has a greater effect on the dissolution kinetics of the Na–Fe–phosphate glasses than the O/P ratio. The slowest reacting glasses studied here are Na-free and have O/P ratios near 3.4. The superior chemical durability of this glass composition is attributed to the low rate of glass surface hydration. Bunker et al. [1] related surface hydration to inter-chain hydrogen bonding in the hydrated glass surface; two phosphate chain ends are linked by hydrogen bonds leading to longer effective chain lengths and slower dissolution rates.

The dissolution kinetics of Series D (O/P = 3.40 ± 0.03) glasses were determined at different temperatures using the static dissolution Test A, and activation energies (Q) were calculated assuming an Arrhenius dependence of the reaction rate constants on absolute temperature (T):

$$k_{DM} = k_0 \exp(-Q/RT) \quad (4)$$

where k_0 is a pre-exponential factor and R is the gas constant.

Fig. 9 (a) shows the Arrhenius analyses of the different ion release data sets for glass D-0.23, which exhibits congruent dissolution behavior. Also shown is an analysis of the reacted volume (α) based on the total ion release concentrations and on the weight loss data. Fig. 9 (b) shows that minima in the activation energies for the glasses from series D (O/P ~3.40) occurs at Fe/(Na+Fe) ~0.39.

4.2. Dissolution mechanism

Bunker et al. [1] developed the general description for the dissolution reactions between phosphate glasses and water. The first stage of dissolution is controlled by diffusion, including penetration of H_2O into the glass network and diffusion of ions through the developing hydrated layer back into solution. Water hydrates the phosphate anions by reacting with the metal (Na,Fe) –O–P bonds that link neighboring P-anions:

$$-P-O-(Na,Fe)-O-P + 2H_2O \rightarrow$$
$$-P-OH\ HO-P- + (Na,Fe)(OH)_2 \quad (5)$$

At longer times, according to Bunker, linear reaction kinetics dominate as the hydrated metals and phosphate anions are released into solution. Under neutral pH conditions, the P-anions released from the glass hydrolyze slowly and so are (initially)

representative of the P-anions in the original glass structure, making it possible to use solution techniques like chromatography to characterize phosphate glass structures [23,30].

The reaction rate constants for both the diffusion (Fig. 8) and the contracting volume (Fig. 8) models clearly show that increasing the relative iron concentration of a Na–Fe–phosphate glass reduces the dissolution rates of the glasses. From Bunker's model, smaller values of k_{DM} might be interpreted as slower diffusion of water into a Fe-rich glass and/or slower diffusion of reaction products through the hydrated layer, and the smaller values of k_{CVM} may indicate slower hydration rates for Fe–O–P bonds compared to Na–O–P bonds.

Fig. 10 (a) compares α(P) obtained in the static dissolution Test A with those from the semi-dynamic dissolution Test B for the C-series of glasses (O/P ratio ~3.27). The pH values of the respective leachate solutions are shown in Fig. 10 (b). The pH reaches a constant value because the species released from the glasses form buffered solutions [1]. Replenishing the solution shortens the time duration of the first dissolution stage with greater rate parameter k_{DM}, and the dissolution kinetics quickly enter the second stage with smaller rate parameter k_{CVM}, which causes the initial α(P) to be smaller in semi-dynamic Test B than in static Test A. However, because replenishing the solution increases the k_{CVM} for the second stage, the α(P) in Test B becomes greater than in Test A. Glasses with high iron contents (e.g., C-0.49) have longer first stages (DM controlled) than glasses with low iron contents (e.g., C-0.23).

4.3. Dissolution and glass composition

For sodium iron phosphate glasses in the present study, the dissolution behavior can be categorized into three types based on congruent dissolution or selective dissolution shown in compositional map of Fig. 11.

Type I: glasses show selective dissolution for both stages. For example, for Na-free iron phosphate glasses, the mass release rates of glass constituents level off after entering the second stage of dissolution, and an increasing the O/P ratio decreases k_{DM} and k_{CVM} (Fig. 7 (b) and Fig. 8 (b)). For this kind of dissolution process, ion concentrations in the leachate are far below the solubility limits, and saturation is not involved in the decrease in the mass release rates. No precipitation phases or alteration layers are observed on glass surfaces by SEM. EDS analysis (Table 2) indicate that the surface composition of these corroded glasses are similar to the initial, unreacted glass. This is inconsistent with the selective dissolution observation, which indicates that the surface alteration caused by selective leaching are below the detection limits of EDS analysis. A more exquisite characterization for glass surface is needed.

Type II: glass show congruent dissolution for both stages. The first stage controlled by diffusion is usually too short to be observed, and glass dissolution quickly enters the second stage, where phosphate anions are released from the glass network, along with the metal ions, by hydration reactions at the glass surface [1]. An example of the surface morphology that develops for this kind of glass is shown in Fig. 12. The glass surface is covered by layers of etch pits that increase in size with corrosion time. Similar observations were made in a corrosion study of Na–Ca–phosphate glasses and were explained by a surface reaction-limited corrosion mechanism [31]. EDS analysis (Table 2)

show the surface composition of the Type II corroded glasses are also similar to those of the original glasses.

Type III: Glasses show congruent dissolution at the first stage, then show selective leaching at the second stage. For example, glass A-0.13, evenly distributed pits (0.3–0.8 μm) form on glass surfaces during the first stage (DM) of dissolution (Fig. 13 (a)). During the second stage (CVM), the mass release of glass constituents continuous and linear with the leachate becoming acidic (2.9–3.1). Electron microscopy reveals that precipitates are present (Fig. 13 (b1)), and EDS indicates that these phases are Na-deficient (Na/P ~0.03 and Fe/P ~0.57) (Table 2). More extensive surface precipitates, associated with etch pits, are shown in Fig. 13 (b2).

Ion concentration analysis by ICP shows that the iron contents in leachate (ppm) for glass E-0.23 in Fig. 12 are about seven times greater than for glass A-0.13 in Fig. 13 (b) and that the phosphorus concentration is about two times greater. This indicates that the pH value of the leachate influences the dissolution kinetics and the formation of precipitates. Acid environment in Type III promotes the sorption and co-precipitation processes, even though the ion concentration is much smaller than that in weakly basic leachate for Type II corrosion.

4.4. pH prediction

There are three types of sites on phosphate anions, each with a different acid dissociation constant (pK_a), that can be protonated in a leachate at an appropriate pH value: middle site 1, terminal site 2 and terminal site 3 [1,32],

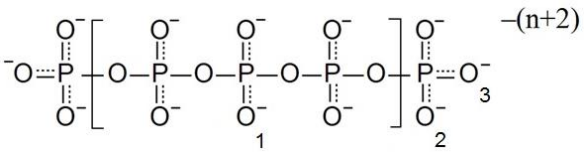

(6)

Middle site 1 has a pK_a value between pH 1–2. Terminal site 3 has a pK_a value around pH 12. The pK_a values for terminal site 2 are sensitive to the presence of cations in solutions and vary between pH 3–11 [1,32]. Therefore, for phosphate anions in the leachate solutions for this study, with final pH values from 3 to 9 (Fig. 1 (c) and Fig. 2 (b)), the middle sites 1 are all in anionic form and should be associated with Na^{+}, Fe^{2+} or Fe^{3+} and the terminal sites 3 are all protonated. Terminal sites 2 are likely partially protonated and so can have a buffering effect on the solution pH. The greater the number of middle sites 1, the more negative the surface charge of the anion will be. However, according to Bunker et al. [1], there seems to be no correlation between the surface charge and the rate of glass dissolution.

To predict the pH value of a leachate, the following assumptions are made: (1) There is no hydrolysis of phosphate chains released to solution over the course of the dissolution experiments; this is consistent with reports of hydrolysis rates in the literature [33]; (2) The phosphate anion distributions in solution are the same as those in the original glasses, as were determined by high-performance liquid chromatography (HPLC) and reported in a previous study [23]; (3) In a leachate solution , phosphate anions with chain lengths n > 2 have both anionic terminal site 2 and protonated terminal site 3 and can be described by the formula $(H_2P_nO_{3n+1})^{-n}$; (4) The iron redox in solution is the same as that in the original glass.

The pH value of leachates in the static dissolution Test A reached a constant value in the first 24 hours of glass dissolution (e.g., Fig. 2 (b)). Since the phosphate anions are

the major anions in solution, the total number of terminal phosphates in chains released to the leachate solution can be determined from the total phosphorus released and the phosphate chain length distributions [23], and these can then be related to the solution pH value. Fig. 14 shows a correlation between the pH value and the concentration (mol) of terminal phosphates in the leachates from the static Test A experiments after 24 hours of dissolution of the two glass series near the pyrophosphate stoichiometry (series D, O/P ~3.40).

For a better prediction of solution pH, the charged species in a leachate, especially for phosphate anions PO_4^{3-} and $P_2O_7^{4-}$, need to be determined for different pH ranges according to their pK_a values. Table 3 lists the pK_a values of all the possible species in an aqueous solution containing Na, P, Fe, and Si ions. From these values, the major species and buffer reactions in the leachate solutions of Na–Fe–phosphate glasses with pH range 2–7 and 7–10 can be determined, and these are listed in Table 4. Because of high field strength, hydrated iron cations in aqueous solution attract electron density between the O and the H atoms, making weaker O–H bonds and easier dissociation of the H^+ ions from coordinated H_2O [34].

According to the principle of charge balance in solution, total positive charge (A) equals the total negative charge (B), which can be expressed by the following equations,

$$A = [H^+] + [Na^+] + 2\{[Fe(H_2O)_5(OH)]^{2+}\} + 2\{[Fe(H_2O)_6]^{2+}\} + \{[Fe(H_2O)_5(OH)]^+\} = [H^+] + C \quad (7)$$

$$B = [OH^-] + [H_2PO_4^-] + [HPO_4^{2-}] + [PO_4^{3-}] + [H_2P_2O_7^{2-}] + [HP_2O_7^{3-}] + [P_2O_7^{4-}] + \sum_{i=3}^{n} n\,[(H_2P_nO_{3n+1})^{-n}] + [(H_3SiO_4)^-] + [(HCO_3)^-] + 2[(CO_3)^{2-}] = [OH^-] + D \quad (8)$$

At 25 ºC,

$$K_w = [H^+][OH^-] = 1.01 \times 10^{-14} \quad (9)$$

Combining equations leads to,

$$(C - D) = [OH^-] - [H^+] = \frac{1.01\times10^{-14}}{[H^+]} - [H^+] \quad (10)$$

The concentration (mol/L) of hydrogen ions required to balance this charge is then calculated from,

$$[H^+] = \frac{-(C-D)+\sqrt{(C-D)^2+4.04\times10^{-14}}}{2} \quad (11)$$

The starting pH value of DI H_2O used in this study is 6.11 ± 0.23 at room temperature. According to acid-base equilibria and mass balance of H_2CO_3 in DI H_2O, the amount of CO_2 in solution can be calculated as ~ 10^{-7} mol for any leachate solution [36]. The concentrations of other ions in solution were measured by ICP-OES. The major species in

a leachate are chosen for different pH ranges from Table 4, and then the pH values were calculated from equations 7–11. The justifiability of the predicted pH value is verified by checking whether the chosen major species and buffer reactions can exist in the range of predicted pH value. If not, the major species need to be revised until the predicted pH value can pass the verification step. Fig. 15 shows the comparison of measured and predicted pH values of leachate solutions. For glass series with longer phosphate chains (e.g., O/P ~3.12, Fig. 15 (a)) and glasses with greater iron contents (e.g., Na-free iron phosphate glasses, Fig. 15 (b)), the verification step can be passed easily and the predicted pH values from the ion concentrations in leachate solutions are quite close to the measured pH values. For glasses with short phosphate chains, the verification step is more difficult to pass because of greater concentrations of orthophosphate and pyrophosphate anions involved in the buffer reactions.

5. Summary

The dissolution behavior of five series of Na_2O–FeO–Fe_2O_3–P_2O_5 glasses with a range of O/P (3.0–3.5) and Fe/P (0.13–0.67) ratios were investigated by static and semi-dynamic dissolution tests in water. Selective leaching, with the preferential release of sodium and phosphorus, occurs for glasses with greater Fe/P ratios, whereas congruent dissolution is observed for glasses with lower Fe/P ratios. Two kinetic stages are observed for the dissolution processes. The first stage follows a 3D diffusion model and the second stage follows a linear contracting volume model. For glasses with greater O/P ratios (O/P > 3.3) and lower iron contents (Fe/P < 0.32), the first stage is not observed.

The rate parameter, k_{DM}, for the 3D diffusion model and the rate parameter, k_{CVM}, for the contracting volume model decrease by several orders of magnitudes with an increase in Fe/P ratio, and they are much more dependent on iron content than the O/P ratio (average phosphate chain length). pH values of solutions were predicted from the ion concentrations in leachate solutions and are matched with the measured pH values.

Acknowledgements

The authors are very grateful to Missouri S&T colleagues Xiaoming Cheng, for her help with the ICP analysis, Jenhsien Hsu, for his help with SEM and EDS analysis, and Jaime George, for helpful discussion on dissolution kinetics. This work was supported by the Nuclear Energy University Program (US Department of Energy) under grant NEUP 09-144.

Table 1 Transition time from DM to CVM kinetics in static dissolution Test A.

Glass series	Analyzed		Transition time (hour)	
	O/P	Fe/P	Average	error
A	3.04	0.37	18	2
	3.04	0.23	21	3
	3.03	0.13	18	2
B	3.15	0.42	18	2
	3.10	0.32	21	3
	3.12	0.22	21	3
	3.13	0.12	12	1
C	3.28	0.49	19	3
	3.25	0.38	18	3
	3.24	0.32	24	5
	3.27	0.23	18	2
D	3.36	0.58	27	3
	3.38	0.49	26	2
	3.40	0.39	18	1
	3.42	0.32	15	3
	3.43	0.23	6	1
E	3.48	0.66	24	5
	3.48	0.58	24	4
	3.48	0.48	36	1
	3.50	0.39	27	3
	3.50	0.34	6	1
	3.51	0.23	<6	–

Table 2 Compositional differences between as-made and corroded glass surfaces.

Dissolution	Glass examples	Unreacted ICP-OES		Corroded EDS		
		Fe/P	Na/P	Fe/P	Na/P	Surface condition
Type I	A-0.37	0.37	–	0.34 (3)	–	No precipitation phases or alteration layers are observed.
	B-0.42	0.42	–	0.40 (1)	–	
	C-0.49	0.49	–	0.49 (1)	–	
	E-0.66	0.66	–	0.64 (3)	–	
Type II	E-0.23	0.23	1.28	0.26 (1)	1.29 (3)	Fig. 12
Type III	A-0.13	0.13	0.61	0.13 (1)	0.59 (1)	Fig. 13 (a)
				0.57 (1)	0.03 (1)	Fig. 13 (b)

Table 3 Acid dissociation constants (pK_a) of possible species in an aqueous solution containing Na, P, Fe, Si ions [35,36].

Aqueous acid-base equilibria	Step	pK_a	T (°C)
$[Fe(H_2O)_6]^{3+} \leftrightarrow [Fe(H_2O)_5(OH)]^{2+} + H^+$		2.17	25
$[Fe(H_2O)_6]^{2+} \leftrightarrow [Fe(H_2O)_5(OH)]^{+} + H^+$		8.30	25
$H_4SiO_4 \leftrightarrow (H_3SiO_4)^- + H^+$	1	9.9	30
$(H_3SiO_4)^- \leftrightarrow (H_2SiO_4)^{2-} + H^+$	2	11.8	30
$(H_2SiO_4)^{2-} \leftrightarrow (HSiO_4)^{3-} + H^+$	3	12	30
$(HSiO_4)^{3-} \leftrightarrow (SiO_4)^{4-} + H^+$	4	12	30
$H_3PO_4 \leftrightarrow (H_2PO_4)^- + H^+$	1	2.15	25
$(H_2PO_4)^- \leftrightarrow (HPO_4)^{2-} + H^+$	2	7.20	25
$(HPO_4)^{2-} \leftrightarrow (PO_4)^{3-} + H^+$	3	12.35	25
$H_4P_2O_7 \leftrightarrow (H_3P_2O_7)^- + H^+$	1	0.83	25
$(H_3P_2O_7)^- \leftrightarrow (H_2P_2O_7)^{2-} + H^+$	2	2.26	25
$(H_2P_2O_7)^{2-} \leftrightarrow (HP_2O_7)^{3-} + H^+$	3	6.72	25
$(HP_2O_7)^{3-} \leftrightarrow (P_2O_7)^{4-} + H^+$	4	9.46	25
$H_3PO_3 \leftrightarrow (H_2PO_3)^- + H^+$	1	1.3	20
$(H_2PO_3)^- \leftrightarrow (HPO_3)^{2-} + H^+$	2	6.70	20
$H_2CO_3 \leftrightarrow (HCO_3)^- + H^+$	1	6.35	25
$(HCO_3)^- \leftrightarrow (CO_3)^{2-} + H^+$	2	10.33	25

Table 4 Major species and buffer reactions in leachate solutions of Na–Fe–phosphate glasses with pH ranges 2–7 and 7–10.

pH 2–7	pH 7–10
$(H_2PO_4)^- \leftrightarrow (HPO_4)^{2-} + H^+$	$(HPO_4)^{2-} \leftrightarrow (PO_4)^{3-} + H^+$
$(H_2P_2O_7)^{2-} \leftrightarrow (HP_2O_7)^{3-} + H^+$	$(HP_2O_7)^{3-} \leftrightarrow (P_2O_7)^{4-} + H^+$
$(H_2PO_3)^- \leftrightarrow (HPO_3)^{2-} + H^+$	$(HPO_3)^{2-}$
$H_2CO_3 \leftrightarrow (HCO_3)^- + H^+$	$(HCO_3)^- \leftrightarrow (CO_3)^{2-} + H^+$
$H_4SiO_4 \leftrightarrow (H_3SiO_4)^- + H^+$	
$[Fe(H_2O)_5(OH)]^{2+}$	
$[Fe(H_2O)_6]^{2+} \leftrightarrow [Fe(H_2O)_5(OH)]^+ + H^+$	

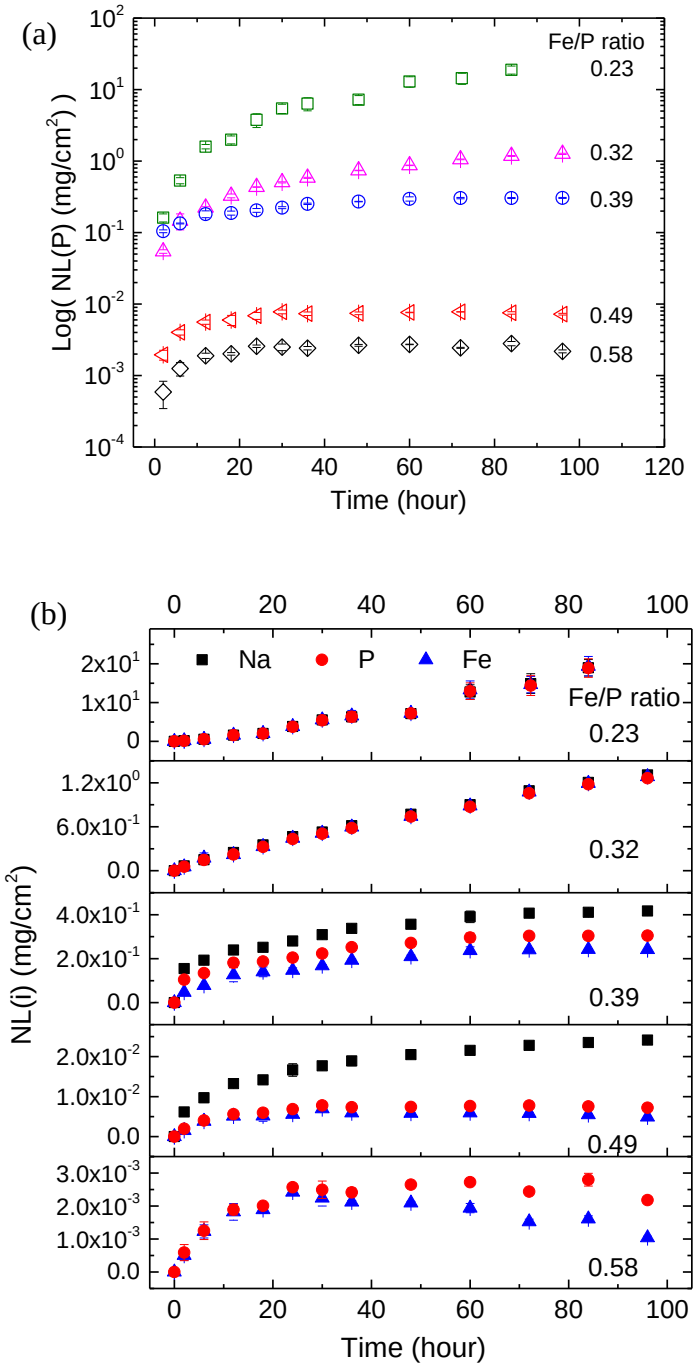

Fig. 1. Glass series D (O/P = 3.40 ± 0.03) dissolved in DI H_2O at 60 ± 2 ºC by static dissolution Test A. (a) Logarithm of normalized phosphorus mass release (mg/cm^2). (b) Normalized mass release (mg/cm^2) of sodium, phosphorus and iron. (c) pH values of leachate solutions.

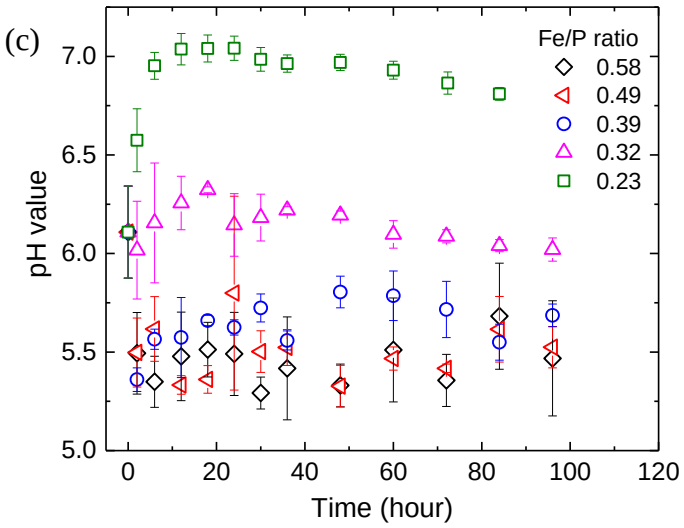

Fig. 1. Glass series D (O/P = 3.40 ± 0.03) dissolved in DI H_2O at 60 ± 2 ºC by static dissolution Test A. (a) Logarithm of normalized phosphorus mass release (mg/cm^2). (b) Normalized mass release (mg/cm^2) of sodium, phosphorus and iron. (c) pH values of leachate solutions. (cont.)

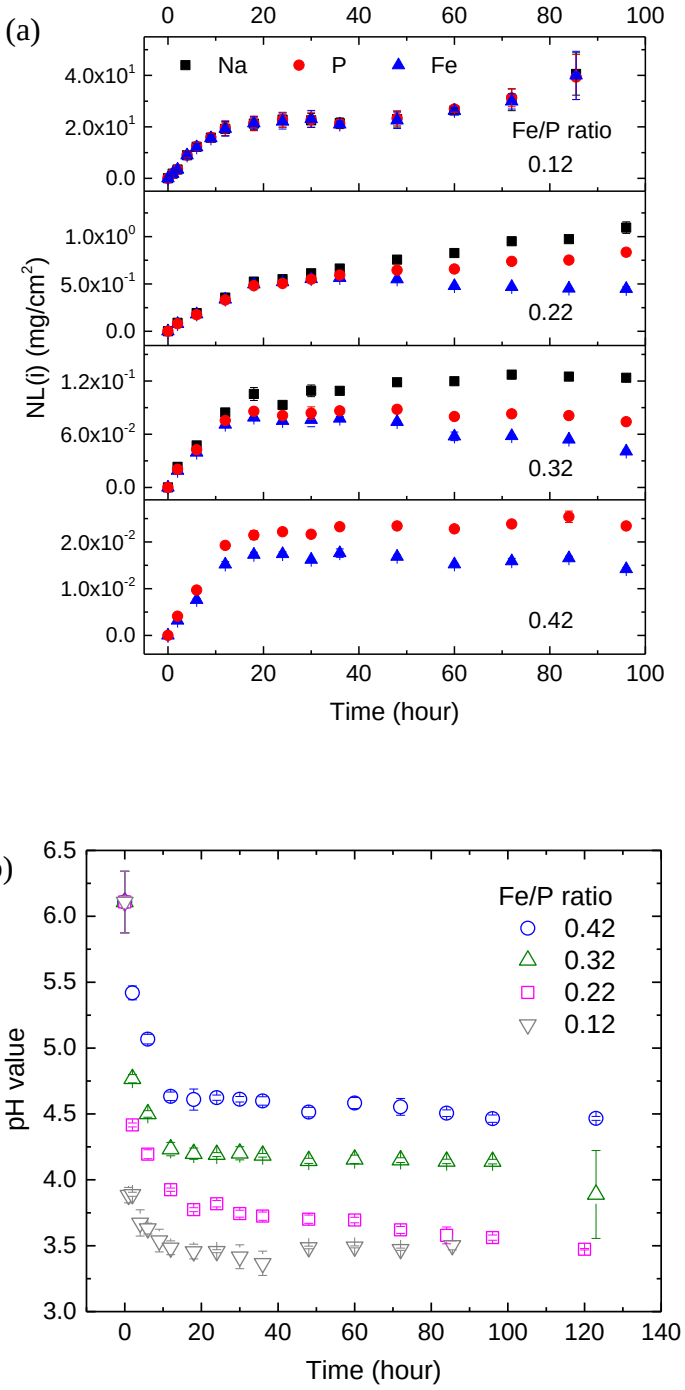

Fig. 2. Glass series B (O/P = 3.12 ± 0.02) dissolved in DI H_2O at 60 ± 2 ºC by static dissolution Test A. (a) Normalized mass release (mg/cm^2) of sodium, phosphorus and iron. (b) pH values of the leachate solutions.

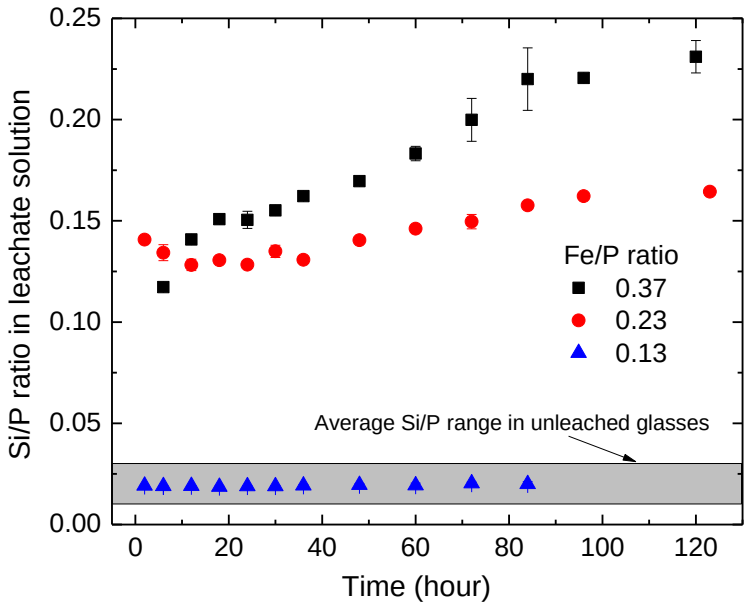

Fig. 3. Si/P ratios in leachate solutions for glass series A (O/P ratio = 3.04 ± 0.01). The average Si/P ratio in these glasses 0.02 ± 0.01, indicated by the gray band.

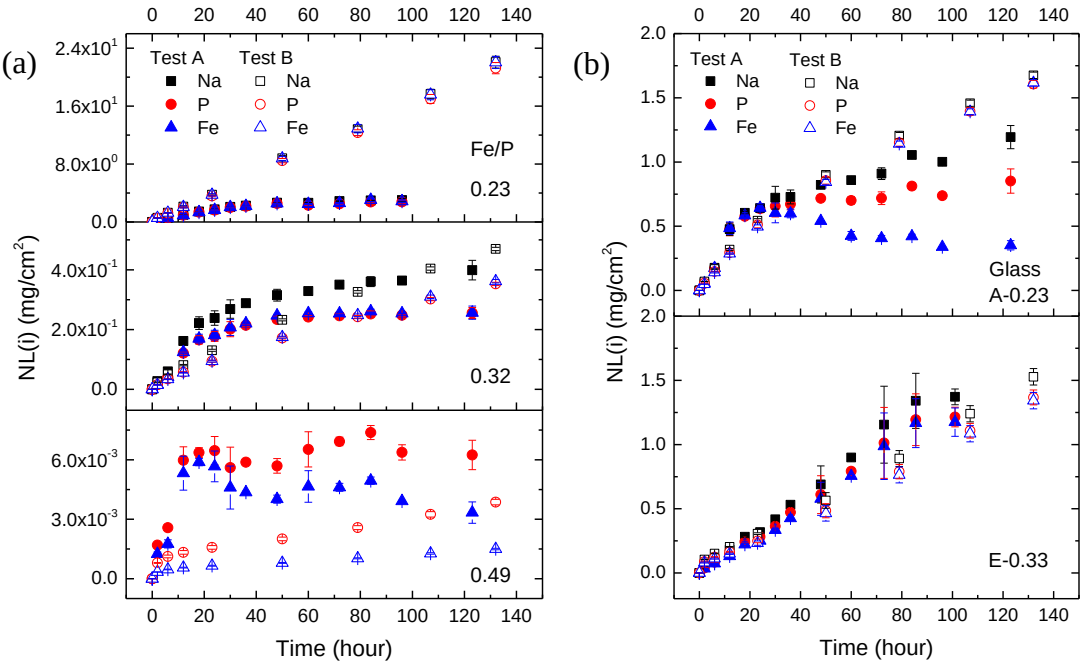

Fig. 4. Comparison of normalized mass release (mg/cm^2) of sodium, phosphorus and iron between static dissolution Test A and semi-dynamic dissolution Test B. (a) Glass series C (O/P = 3.27 ± 0.02). (b) Glasses with similar ranges of normalized mass release (mg/cm^2) rates.

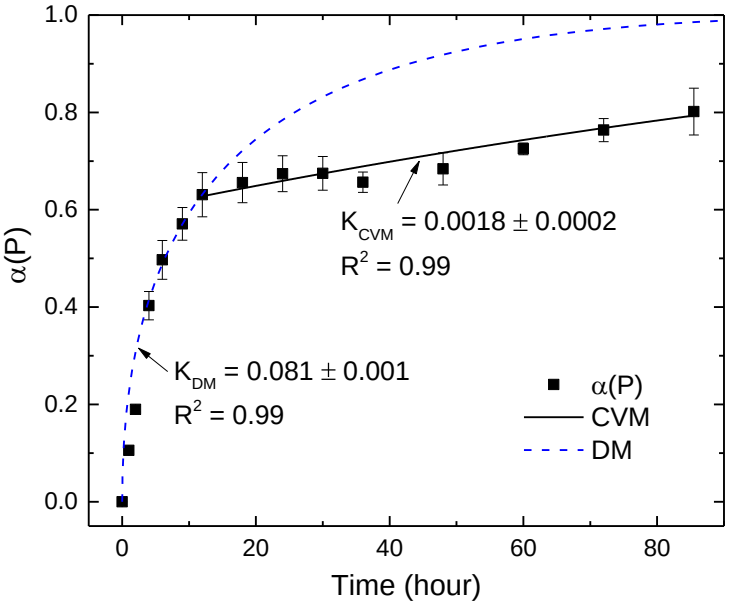

Fig. 5. Static dissolution Test A: Mass fraction of phosphorus leached from glass B-0.12, α(P), changed with dissolution time (hour), fitted by the 3D diffusion model (DM, dashed line) and contracting volume model (CVM, solid line). Temperature-dependent rate parameters are given.

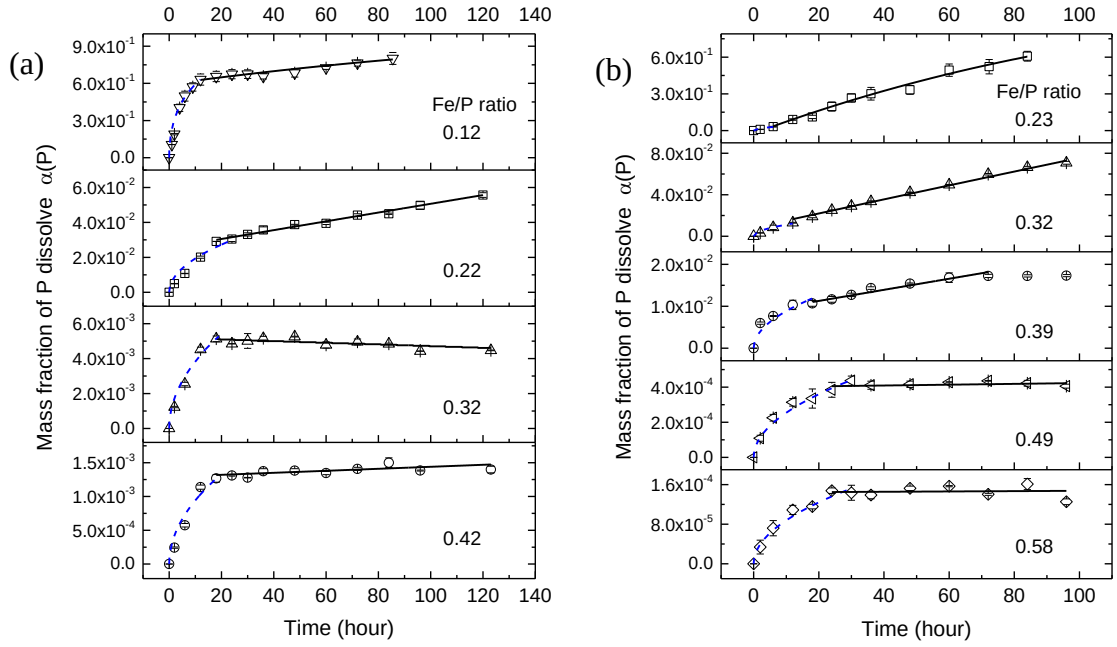

Fig. 6. Static dissolution Test A: α(P) fitted by the 3D diffusion model (DM, dashed line) and contracting volume model (CVM, solid line); (a) Glass series B (O/P = 3.12 ± 0.02). (b) Glass series D (O/P = 3.40 ± 0.03).

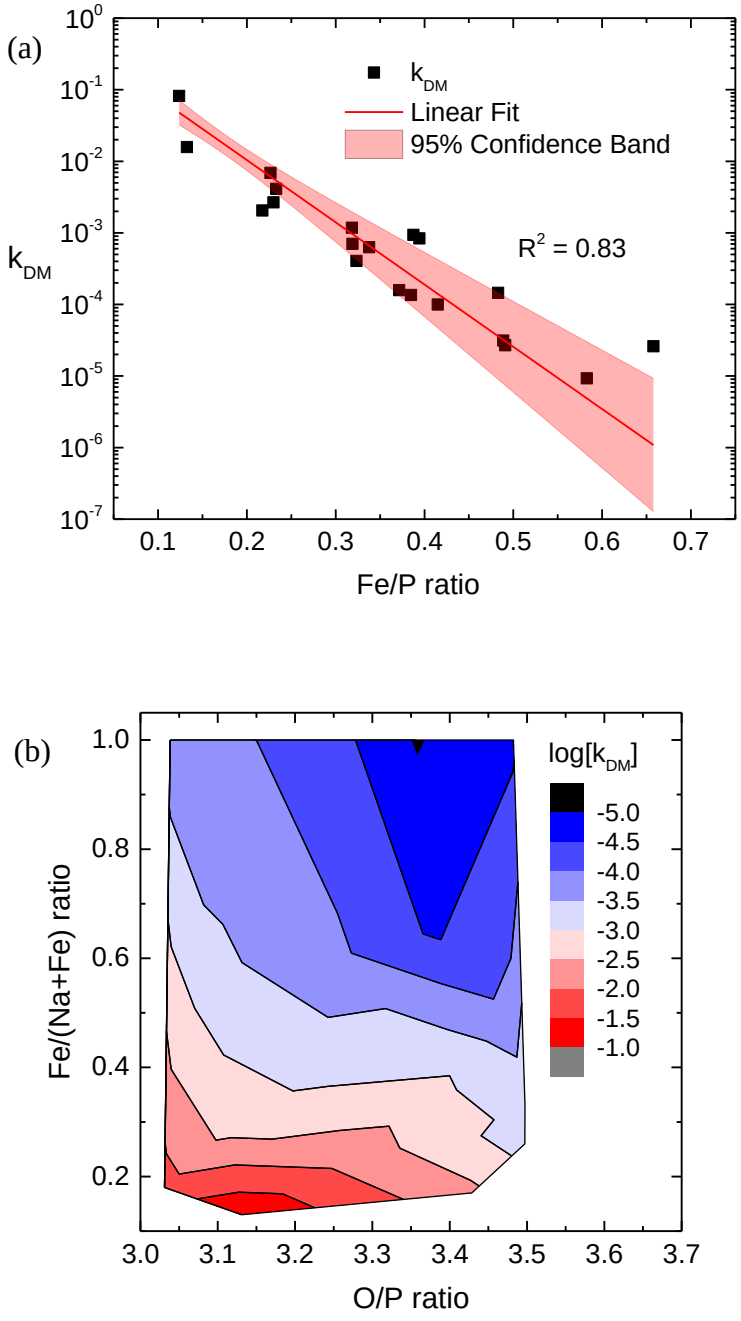

Fig. 7. Static dissolution Test A: (a) The effect of Fe/P ratio on the rate parameter for the 3D diffusion model, k_{DM}. (b) Compositional dependence of k_{DM} in room temperature DI water.

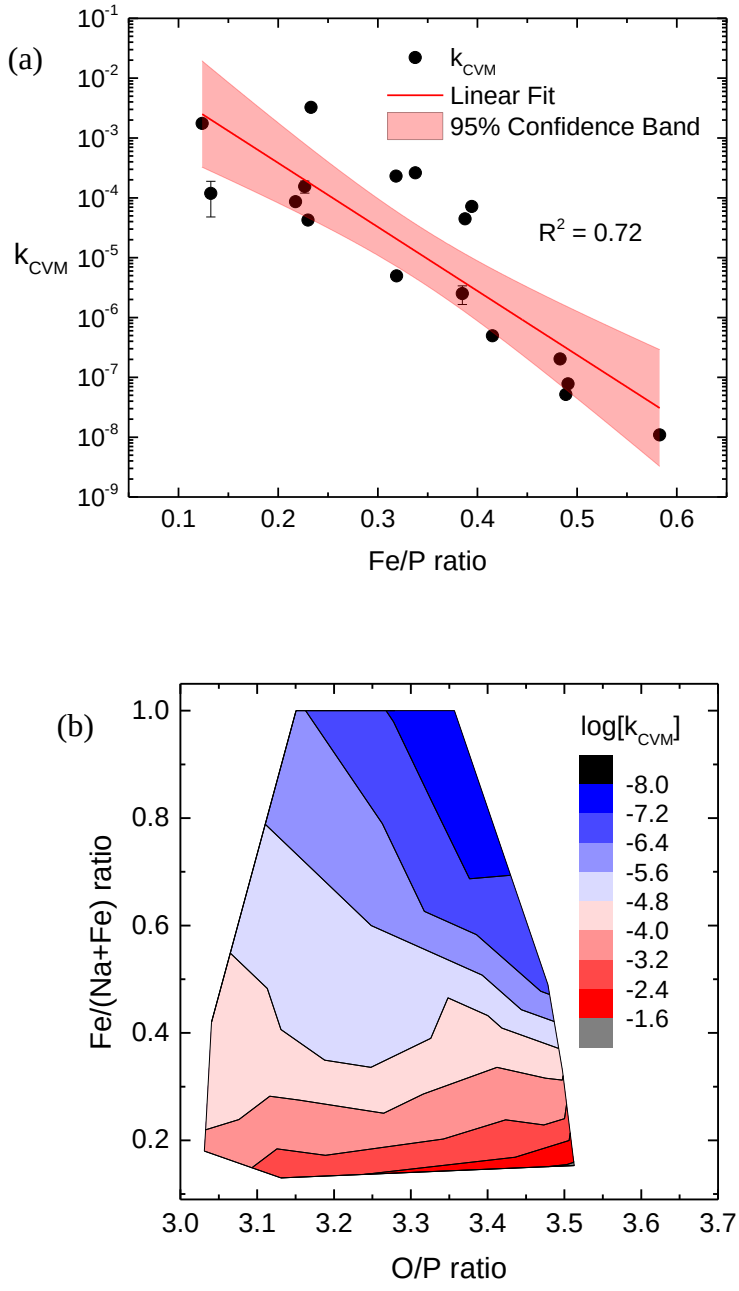

Fig. 8. Static dissolution Test A: (a) The effect of Fe/P ratio on the rate parameters for the contracting volume model, k_{CVM}. (b) Compositional dependence of k_{CVM} in room temperature DI water.

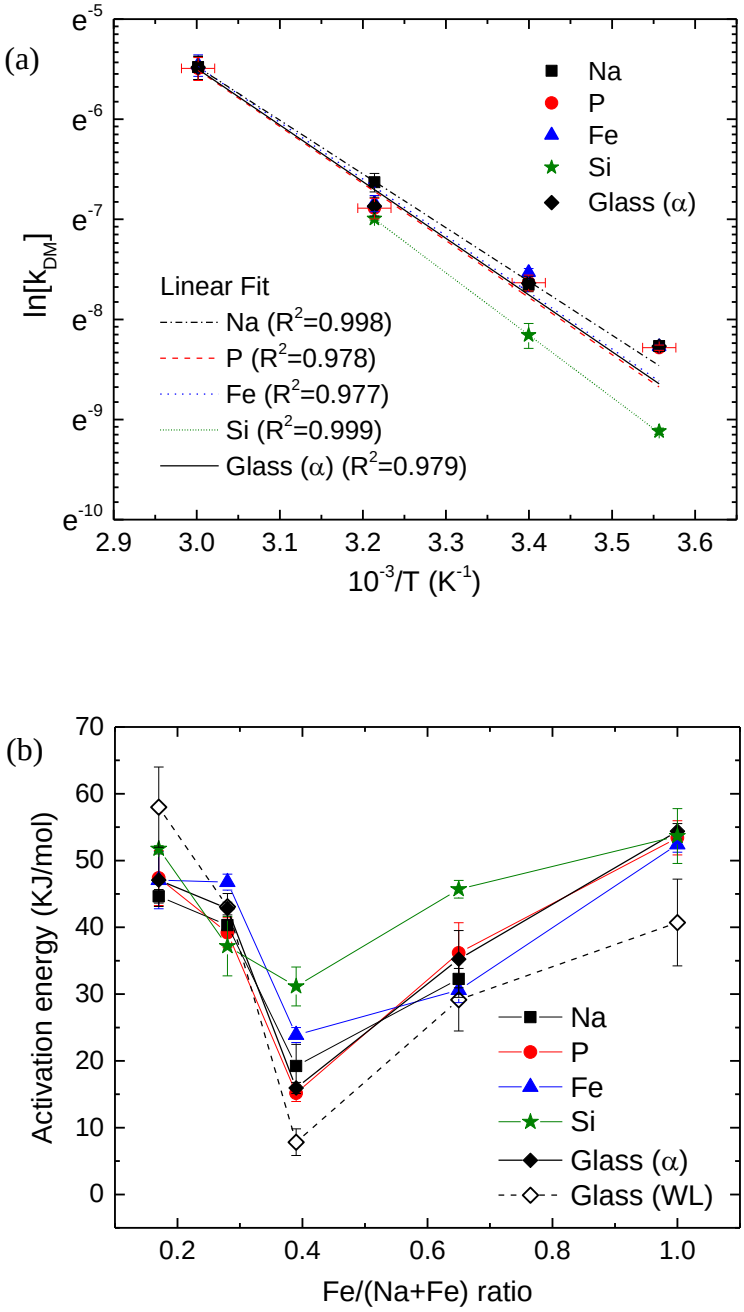

Fig. 9. Static dissolution Test A: (a) Arrhenius analyses of k_{DM} for glass D-0.23; (b) Compositional dependence of activation energies for glass series D (O/P = 3.40 ± 0.03), based on individual ion release rates, total ion concentrations (α, ◆) and weight loss measurement (WL, ◇).

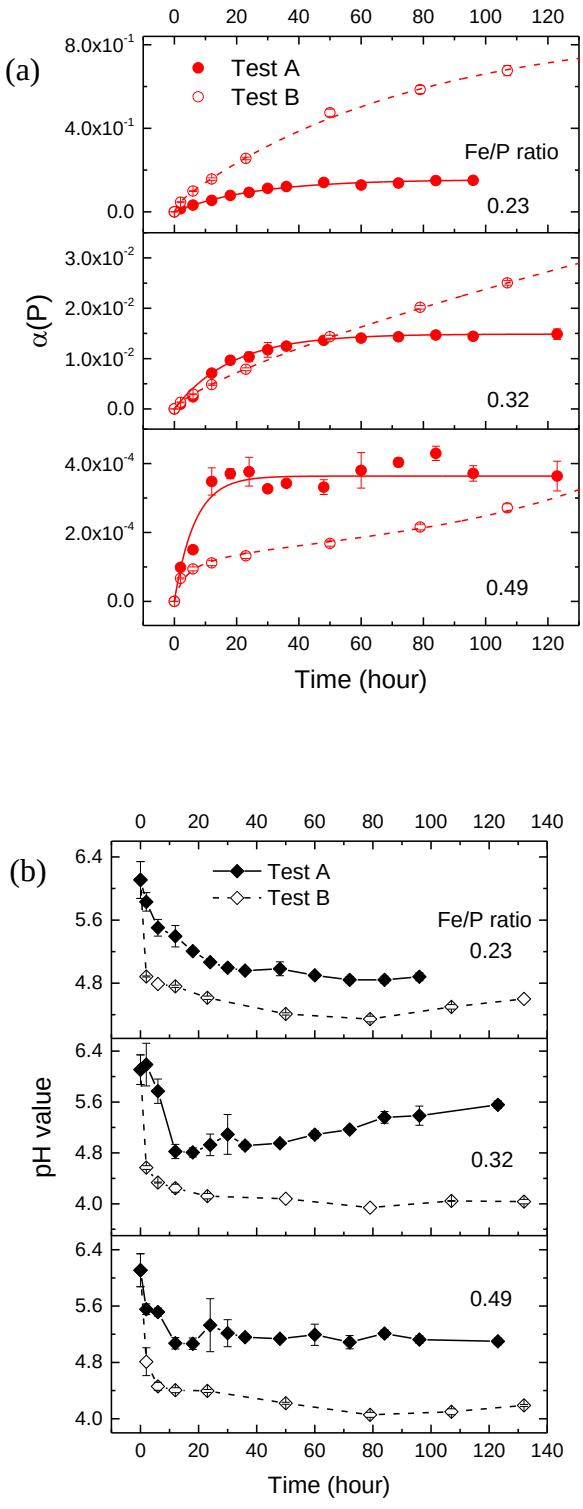

Fig. 10. Comparison of mass fraction of phosphorus, α(P), released from glasses and changes in leachate pH, for glass series C (O/P = 3.27 ± 0.02) for static dissolution Test A and semi-dynamic dissolution Test B. The lines are guides for the eyes.

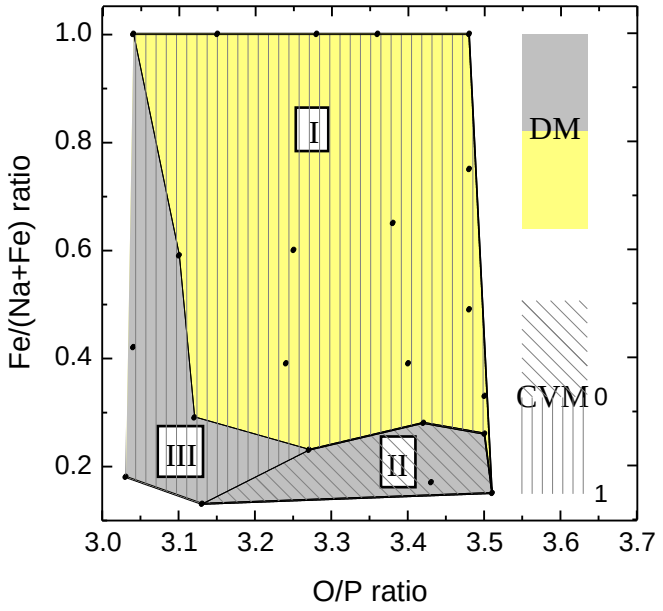

Fig. 11. Compositional map for dissolution stage 1 (Diffusion Model), congruent dissolution behavior (gray) and selective leaching behavior (yellow). Compositional map for dissolution stage 2 (Contracting Volume Model), congruent dissolution behavior (angled lines) and selective leaching behavior (vertical lines).

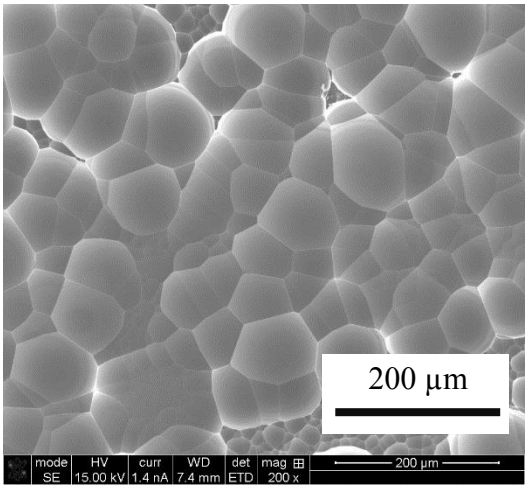

Fig. 12. Surface morphology of glass E-0.23 after a static dissolution Test A in water for 10 hours; solution pH was ~8.6.

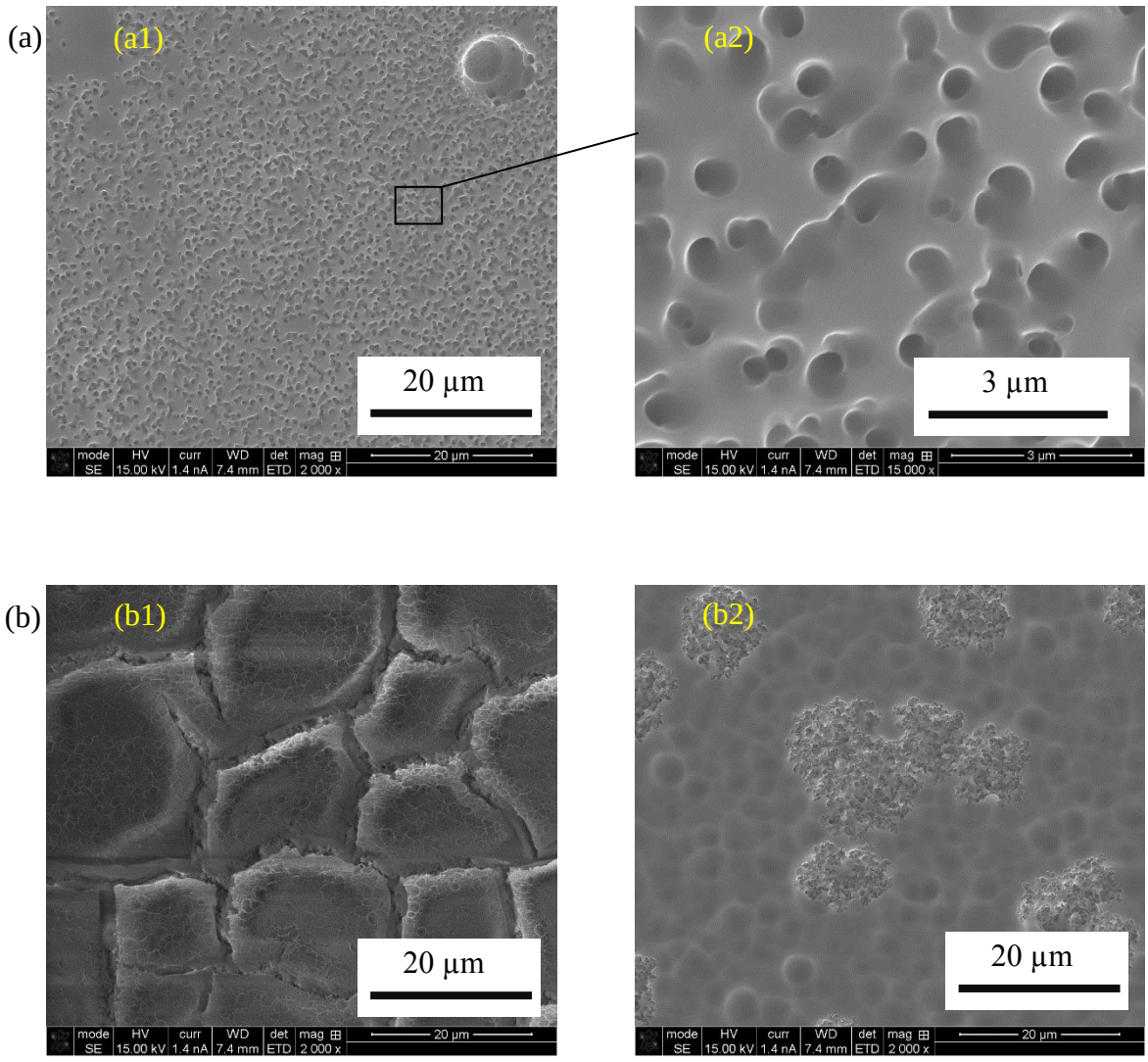

Fig. 13. Surface morphology of glass A-0.13 in static dissolution Test A. (a) 18 hours, pH value ~3.1. Greater magnification of specific area of (a1) is shown in (a2). (b) 84 hours, pH value ~3.0, two types of surface morphology are observed (b1 and b2).

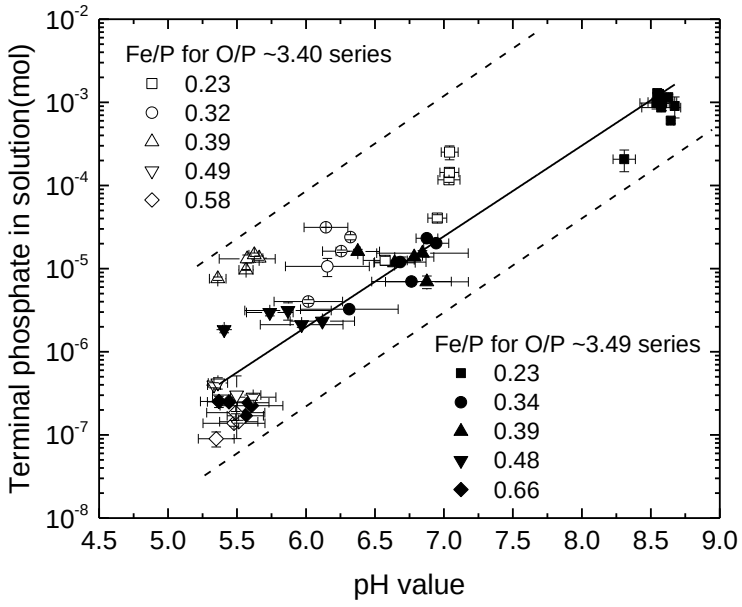

Fig. 14. Relationship between amount (mol) of terminal phosphate in solution and the pH value of leachates for glass series D (O/P ~3.40) and E (O/P~3.49). Lines are guides for the eye.

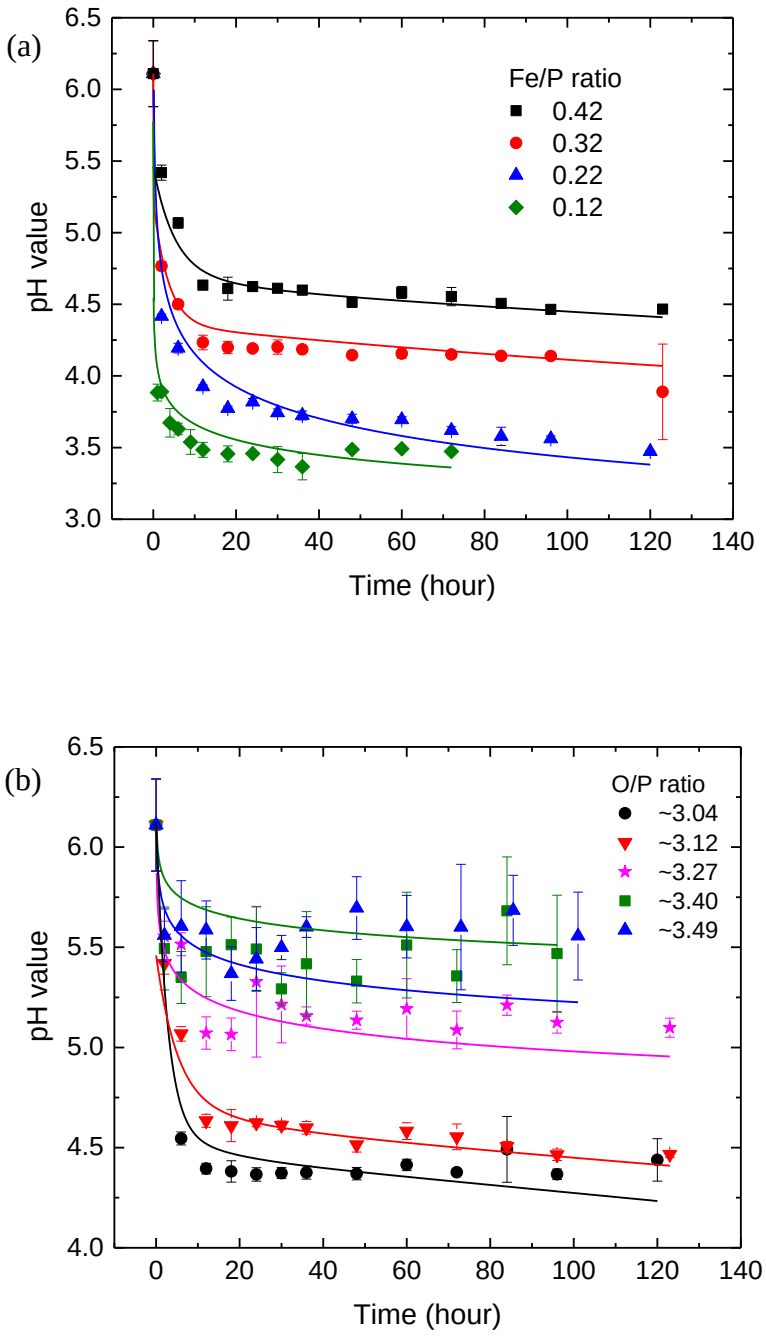

Fig. 15. Comparison of measured (symbols) and predicted (solid lines) pH values of leachate solutions. (a) Glass series B (O/P ~3.12); (b) Na-free iron phosphate glasses.

References

[1] B.C. Bunker, G.W. Arnold, and J.A. Wilder. "Phosphate glass dissolution in aqueous solutions." Journal of non-crystalline solids 64, no. 3 (1984): 291-316.

[2] B.C. Sales, and L.A. Boatner. "Lead-iron phosphate glass: a stable storage medium for high-level nuclear waste." Science 226, no. 4670 (1984): 45-48.

[3] X. Yu, D.E. Day, G.J. Long, and R.K. Brow. "Properties and structure of sodium-iron phosphate glasses." Journal of non-crystalline solids 215, no. 1 (1997): 21-31.

[4] Y.B. Peng, and D.E. Day. "High thermal expansion phosphate glasses. PT.1." Glass Technology 32, no. 5 (1991): 166-173.

[5] I. Ahmed, M. Lewis, I. Olsen, and J.C. Knowles. "Phosphate glasses for tissue engineering: Part 2. Processing and characterisation of a ternary-based P_2O_5–CaO–Na_2O glass fibre system." Biomaterials 25, no. 3 (2004): 501-507.

[6] D.E. Day, Z. Wu, C.S. Ray, and P. Hrma. "Chemically durable iron phosphate glass wasteforms." Journal of non-crystalline solids 241, no. 1 (1998): 1-12.

[7] W. Huang, D.E. Day, C.S. Ray, C.W. Kim, and A. Mogus-Milankovic. "Vitrification of high chrome oxide nuclear waste in iron phosphate glasses." Journal of nuclear materials 327, no. 1 (2004): 46-57.

[8] C.W. Kim, and D.E. Day. "Immobilization of Hanford LAW in iron phosphate glasses." Journal of non-crystalline solids 331, no. 1 (2003): 20-31.

[9] L. Zhang, L. Ghussn, M.L. Schmitt, E.D. Zanotto, R.K. Brow, and M.E. Schlesinger. "Thermal stability of glasses from the $Fe_4(P_2O_7)_3$–$Fe(PO_3)_3$ system." Journal of Non-Crystalline Solids 356, no. 52 (2010): 2965-2968.

[10] C.W. Kim, C.S. Ray, D. Zhu, D.E. Day, D. Gombert, A. Aloy, A. Moguš-Milanković, and M. Karabulut. "Chemically durable iron phosphate glasses for vitrifying sodium bearing waste (SBW) using conventional and cold crucible induction melting (CCIM) techniques." Journal of nuclear materials 322, no. 2 (2003): 152-164.

[11] American Society for Testing and Materials (ASTM), Standard Test Methods for Determining Chemical Durability of Nuclear, Hazardous, and Mixed Waste Glasses: The Product Consistency Test (PCT), C 1285-97, 1998.

[12] A. Jiřička, J.D. Vienna, P. Hrma, and D.M. Strachan. "The effect of experimental conditions and evaluation techniques on the alteration of low activity glasses by vapor hydration." Journal of non-crystalline solids 292, no. 1 (2001): 25-43.

[13] I. Ahmed, C.A. Collins, M.P. Lewis, I. Olsen, and J.C. Knowles. "Processing, characterisation and biocompatibility of iron-phosphate glass fibres for tissue engineering." Biomaterials 25, no. 16 (2004): 3223-3232.

[14] Karabulut, Mevlüt, G. K. Marasinghe, Chandra S. Ray, D. E. Day, G. D. Waddill, C. H. Booth, P. G. Allen, J. J. Bucher, D. L. Caulder, and D. K. Shuh. "An investigation of the local iron environment in iron phosphate glasses having different Fe (II) concentrations." Journal of non-crystalline solids 306, no. 2 (2002): 182-192.

[15] Abou Neel, E. A., I. Ahmed, J. J. Blaker, A. Bismarck, A. R. Boccaccini, M. P. Lewis, S. N. Nazhat, and J. C. Knowles. "Effect of iron on the surface, degradation and ion release properties of phosphate-based glass fibres." Acta Biomaterialia 1, no. 5 (2005): 553-563.

[16] D.E. Clark, and B.K. Zoitos. "Corrosion of glass, ceramics and ceramic superconductors: Principles, testing, characterization and applications." Noyes Publications, Park Ridge, NJ (1992).

[17] T.A. Abrajano, J.K. Bates, and C.D. Byers. "Aqueous corrosion of natural and nuclear waste glasses I. Comparative rates of hydration in liquid and vapor environments at elevated temperatures." Journal of Non-Crystalline Solids 84, no. 1 (1986): 251-257.

[18] D. Perret, J.L. Crovisier, P. Stille, G. Shields, U. Mäder, T. Advocat, K. Schenk, and M. Chardonnens. "Thermodynamic stability of waste glasses compared to leaching behaviour." Applied geochemistry 18, no. 8 (2003): 1165-1184.

[19] R. Conradt, and P. Geasee. "An improved thermodynamic approach to the stability of multi-component silicate glasses in aqueous solutions." Berichte der Bunsengesellschaft für physikalische Chemie 100, no. 9 (1996): 1408-1410.

[20] R. Conradt. "Chemical durability of oxide glasses in aqueous solutions: A review." Journal of the American Ceramic Society 91, no. 3 (2008): 728-735.

[21] B. Grambow. "Geochemical approach to glass dissolution." Corrosion of glass, ceramics and ceramic superconductors (1992): 124-152.

[22] R. Conradt. "A proposition for an improved theoretical treatment of the corrosion of multi-component glasses." Journal of nuclear materials 298, no. 1 (2001): 19-26.

[23] L. Ma, R.K. Brow. "Structural study of Na_2O-FeO-Fe_2O_3-P_2O_5 glasses by high-pressure liquid chromatography." Journal of Non-Crystalline Solids 387 (2014): 16-20.

[24] L. Ma, R.K. Brow, A. Choudhury. "Structural study of Na_2O-FeO-Fe_2O_3-P_2O_5 glasses by Raman and Mössbauer spectroscopy." Submitted to Journal of non-crystalline solids in Feb, 2014.

[25] S.I. Grishin, J.M. Bigham, and O.H. Tuovinen. "Characterization of jarosite formed upon bacterial oxidation of ferrous sulfate in a packed-bed reactor." Applied and environmental microbiology 54, no. 12 (1988): 3101-3106.

[26] O. Levenspiel. Chemical reaction engineering. John Wiley, New York, 1972.

[27] M.N. Rahaman. "Ceramic processing." CRC Press, 2006.

[28] Y. Gu, W. Xiao, L. Lu, W. Huang, M.N. Rahaman, and D. Wang. "Kinetics and mechanisms of converting bioactive borate glasses to hydroxyapatite in aqueous phosphate solution." Journal of Materials Science 46, no. 1 (2011): 47-54.

[29] S.B. Jung, and D.E. Day. "Conversion kinetics of silicate, borosilicate, and borate bioactive glasses to hydroxyapatite." Physics and Chemistry of Glasses-European Journal of Glass Science and Technology Part B 50, no. 2 (2009): 85-88.

[30] B.C. Sales, L.A. Boatner, and J.O. Ramey. "Chromatographic studies of the structures of amorphous phosphates: a review." Journal of Non-Crystalline Solids 263 (2000): 155-166.

[31] F. Delahaye, L. Montagne, G. Palavit, J. Claude Touray, and P. Baillif. "Acid dissolution of sodium–calcium metaphosphate glasses." Journal of non-crystalline solids 242, no. 1 (1998): 25-32.

[32] J.R. Van Wazer, and K.A. Holst. "Structure and Properties of the Condensed Phosphates. I. Some General Considerations about Phosphoric Acids." Journal of the American Chemical Society 72, no. 2 (1950): 639-644.

[33] J.R. Van Wazer. "Phosphorus and its compounds, volume 1: chemistry." Interscience Publishers (1958): 717-800.

[34] B. Averill, and P. Eldredge. "Chemistry: Principles, patterns, and applications." Pearson Education, Inc. (2007): 721-774.

[35] W.B. Jensen. "The Lewis Acid-Base Concepts: An Overview." Wiley-Interscience, New York, 1980.

[36] W.M. Haynes, ed. "CRC Handbook of Chemistry and Physics." CRC press, 2012.

SECTION

3. CONCLUSIONS AND FUTURE WORK

The research presented in this dissertation provides information and characterization techniques for the study of phosphate glass structure, dissolution behavior and thermal stability. The major research findings and their significance are summarized as follows.

Distributions of phosphate anions (P_n) and phosphate tetrahedra (Q^i) in a glass network can be quantitatively determined by HPLC techniques. This structural information can be used to explain the compositional dependence of the thermal properties, crystallization tendency, and the dissolution behavior of these glasses. The pH of aqueous leachate solutions can also be predicted from the ion concentrations in solution and the distributions of phosphate anions in the solutions. Understanding the relationships between glass structure and properties will be useful for the design of new phosphate glasses for different applications.

The effects of iron on the properties of phosphate glasses were addressed in this dissertation. Iron promotes the disproportionation of phosphate anions, and so produces wider distributions of P_n units around the average phosphate chain length, which further improves glass forming ability, possibly greater thermal stability against crystallization. With an increase in iron content for glasses with similar O/P ratio, the average coordination number (CN_{Fe}) of the Fe ions decreased, and the distortion of the tetrahedral and octahedral Fe^{3+} sites increases, indicated by Mössbauer study. The interaction between phosphate anions and iron polyhedra causes systematic changes in the bond length and bond angle of $P–O_{nb}$ bonds.

The thermal stability studies of Na-Fe-phosphate glasses in the polyphosphate range indicate that the presence of stable crystalline compounds with similar compositions have the strongest effects on the thermal stability of glasses. For the design of iron phosphate glasses used for nuclear waste verifications, the compositions around stable intermediate sodium iron phosphate compounds should be avoided.

The dissolution behavior of Na-Fe-phosphate glasses was systematically studied. The map showing the compositional dependence of dissolution rate parameters will be useful for the compositional design of glasses for applications which are based on the tailored rates of degradation of phosphate glasses. The study on dissolution behavior of Na-Ca-phosphate glasses extended the knowledge about Na-Ca-phosphate dissolution in literature, from the metaphosphates to the polyphosphates. Compositional dependence is addressed for dissolution rate parameters and time duration of each dissolution stage. With an increase in O/P ratio, the glass chemical durability is improved with a prolonged the first stage, and activation energies decrease from 83 ± 5 kJ/mol for glass with O/P 3.01 to 24 ± 4 kJ for glass with O/P 3.46. Comparing to the thermodynamic approach to the study of glass dissolution process in literature, distributions of the Q^i sites were considered for the calculation the Gibbs free energy of hydration (kJ/mol) instead of simply using glass composition. The Gibbs free energy of hydration decreases with increasing O/P ratio, which is consistent with the observations that glasses with greater O/P ratios have a lower dissolution rates.

There remain several unresolved questions and interesting possibilities that need to be addressed in the future.

Structural characterization for phosphate glasses with lower O/P ratios. Raman spectroscopy and HPLC are useful techniques to characterize distributions of phosphate anions or phosphate tetrahedral sites in glass networks, but both techniques have limitations to quantify the fraction of Q^i sites. For Raman spectroscopy, quantitative analysis of structural units in glass network is difficult because of the unknown cross-sections of fitted Gaussian peaks to the Raman spectra. For HPLC, overestimations of the O/P ratios and underestimated $\bar{n}$ for glasses with longer phosphate chains occurred. The separation efficiency of the liquid chromatography column is only one part of the reason for these problems, whereas the dissolution process of phosphate glass is probably the main cause for the inconsistent HPLC results. This can be seen from the following analysis.

For phosphate glasses with average chain length > 12, it is difficult for the separation column used in this dissertation to quantitatively distinguish these large phosphate anions. These large anions come out of the column without full separation and form the hump in HPLC chromatographs (Figure 3.1).

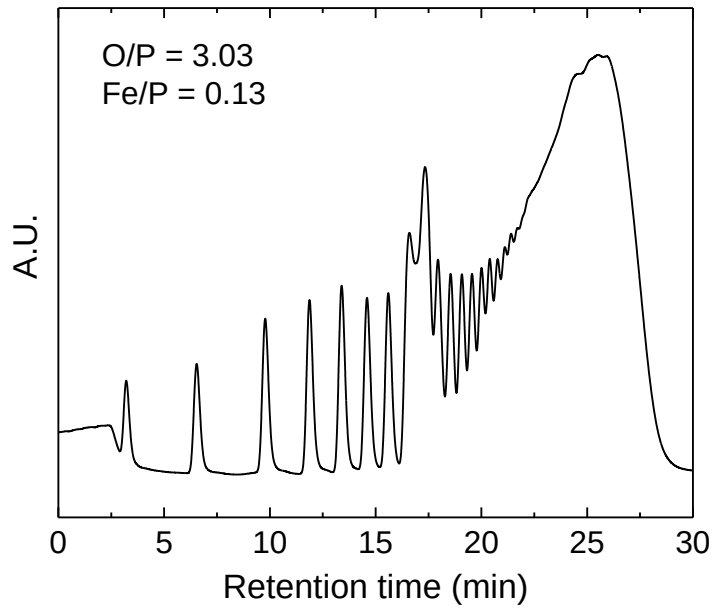

Figure 3.1 HPLC chromatographs of sodium-iron phosphate glass A-0.13

For the determination of O/P ratios, $\bar{n}$ and Q^i fractions, the hump is taken as a single phosphate chain (P_n), but actually it contains other phosphate chains longer than P_n, like P_{n+1}, P_{n+2}, etc. In the polyphosphate glass range, assuming there are no phosphate ring structures, for the determination of Q^i fractions associated with large phosphate chains, $f(Q^i)$, there are 2 Q^1 and (n–2) Q^2 tetrahedra in a single phosphate chain (P_n). Therefore, for all the large phosphate chains in the chromatographic hump, from P_n to P_m (m > n), the fraction of Q^1 tetrahedra is given by,

$$f(Q^1) = \sum_n^m [2f(P_n)] = 2[\frac{A(P_n)}{n} + \frac{A(P_{n+1})}{n+1} + \cdots + \frac{A(P_m)}{m}] \quad (1)$$

where $A(P_n)$ is the concentration of phosphorus associated with P_n. The fraction of Q^2 tetrahedra is given by,

$$f(Q^2) = \sum_n^m [(n-2)f(P_n)] = \sum_n^m [A(P_n)] - f(Q^1) \quad (2)$$

where $\sum_n^m[A(P_n)]$ is the total concentration of phosphorus associated with hump, $A(P_h)$. If one assumes that all of the phosphate chains in the hump are the same length, either the shortest possible (n) or the longest (m), then the differences of the calculated $f(Q^1)$ and $f(Q^2)$ between these two options would be,

$$\Delta[f(Q^1)] = \frac{m-n}{mn} \cdot 2A(P_h) \quad (3)$$

$$\Delta[f(Q^2)] = \frac{n-m}{mn} \cdot 2A(P_h) \quad (4)$$

From Eq. (3) and Eq. (4), it can be seen by assuming all the phosphate chains in the hump have the same shortest length n, $f(Q^1)$ is overestimated whereas $f(Q^2)$ is underestimated. If n = 20, m = 200, and there are ~ 60 mol% P in the hump (e.g., glass A-0.13 in Figure 3.1), the overestimated $f(Q^1)$ < 5.4% and the underestimated $f(Q^2)$ < 5.4%, then the overestimated O/P would be < 0.03. Table 3.1 shows the O/P ratio determined from HPLC technique for sodium iron phosphate glasses with O/P < 3.3, the overestimated O/P is > 0.05. Therefore, the inaccuracy of HPLC results for iron phosphate glasses with O/P < 3.3 cannot be ascribed just to the separation efficiency of column.

Studies have shown the catalytic effects of metal ions with high field strengths promote hydrolytic reactions of polyphosphate anions in aqueous solutions [1,2,3], so there is a possibility that long phosphate chains could be hydrolyzed to smaller segments by, for example, iron cations in a hydrated layer before or during the release of phosphate chains into solution, before the chelating $EDTA^{4-}$ anions in solution could reduce the hydrolytic activity of the Fe^{2+} and Fe^{3+} ions. Future study of the catalytic effects of metal-ions on hydrolysis of polyphosphate chains in aqueous solution or on then hydrated

surface layers may be helpful in improving the utility of the HPLC technique for characterizing phosphate glass structures.

Another issue that may contribute to inaccurate structural information by HPLC is the presence of Q^3 sites in phosphate glasses with O/P < 3.3. The covalent M–O bond, where M stands for one equivalent of any cation or organic radical in a phosphate composition, will promote the exchange between structural units in amorphous phosphates. This means that the site disproportionation reactions, $2Q^2 \leftrightarrow Q^3 + Q^1$ and $2Q^1 \leftrightarrow Q^2 + Q^0$ will be driven to the right [4]. Strauss et al. [5] studied chain branching in Na–P metaphosphate glasses and estimated that the number of branches originally present in glass is of the order of one branch for every 1000 P atoms. Wiench et al. [6] found that Q^3 sites were not stabilized by EDTA in dissolution solutions and the low concentrations (0.2~0.9%) of Q^3 sites detected by solid state NMR for zinc polyphosphate glasses with O/P 3.0~3.11 could not be detected by HPLC. In the present study, compared to Na^+, Fe^{2+} and Fe^{3+} are less basic and have greater electronegativity, which cause less bond polarity and greater bond strength with oxygen; in addition, iron cations have greater field strengths compared to Zn^{2+}. These conditions make the presence of Q^3 sites possible for iron phosphate glasses with compositions close to the metaphosphate. According to the Antibranching Rule [4], the branching points are quickly degraded to end or middle groups in aqueous solution. Future study on the distribution, connection and proportion of Q^3 sites in polyphosphate glass structure, as well as the dissolution mechanism of Q^3 in aqueous solutions, will help resolve this issue.

Table 3.1 O/P ratio, average phosphate chain length ($\bar{n}$) and Q^i fractions of sodium iron phosphate glasses with O/P < 3.3 determined from HPLC results.

ICP		HPLC				
O/P and $\bar{n}$	Fe/P	O/P	$\bar{n}$	Q^0	Q^1	Q^2
Series A	0.33	3.29	3.26	8.32	41.04	50.64
O/P = 3.04 ± 0.01	0.23	3.26	3.45	6.76	38.55	54.68
$\bar{n}$ = 19 ~ 32	0.13	3.10	7.77	1.12	18.01	80.87
Series B	0.40	3.29	3.22	7.55	43.46	48.98
3.12 ± 0.02	0.33	3.30	3.19	7.54	44.23	48.24
$\bar{n}$ = 7 ~ 10	0.23	3.17	5.28	2.70	27.93	69.37
	0.13	3.18	4.81	2.72	31.24	66.04

Dissolution behavior. In the present study, the dissolution behavior of sodium calcium phosphate glasses and sodium iron phosphate glasses were investigated in DI H_2O, but no detailed studies were done under other pH conditions. In the literature, dissolution rates of phosphate glasses have been related to the pH value of aqueous solutions [7]. For the $Li_2O/Na_2O–CaO–P_2O_5$ glasses in Bunker's study [7], dissolution rates are the lowest in the range pH 5 to pH 9. Similar results were observed when buffered solutions were used to dissolve the sodium calcium phosphate glasses in the present study (Figure 3.2). However, phthalate and phosphate anions in the buffered solutions may affect the dissolution processes involving the phosphate chains from the glass surface due to greater ionic strength of the leaching solution, compared to the earlier experimental conditions [7,8]. For the $Na_2O–FeO–Fe_2O_3–P_2O_5$ glasses in this study, H_2SO_4 solutions were used to dissolve glasses for compositional analysis.

Laboratory experience shows that the dissolution rate of iron phosphate glasses increases in H_2SO_4 solutions with an increase in O/P ratio [9], but decreased in DI H_2O; see the fourth paper in this dissertation, "Dissolution behavior of Na_2O–FeO–Fe_2O_3–P_2O_5 glasses"). A systematic study of the dissolution of phosphate glasses in solutions with different pH conditions and ionic strengths is needed to achieve a thorough understanding of the phosphate glass dissolution behavior. The relationship between the amount of H^+ or OH^- consumed and the glass dissolution rate could be determined, and will provide a more detailed picture of the glass dissolution processes.

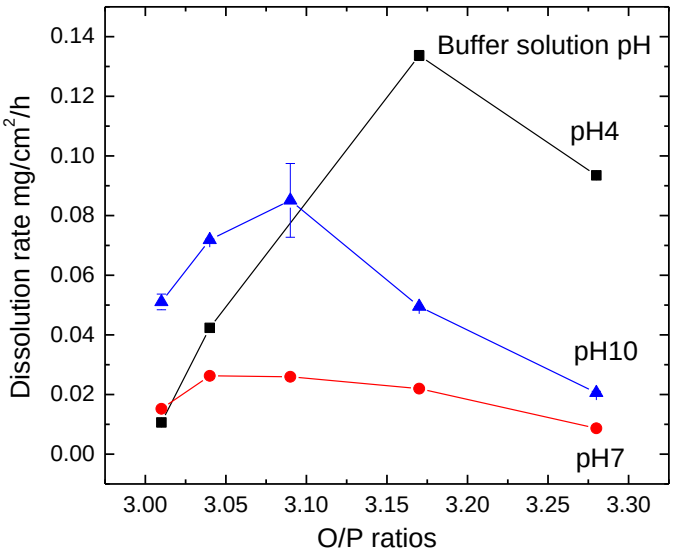

Figure 3.2 Dissolution rates of xNa_2O–xCaO–$(100–2x)P_2O_5$ glasses with different O/P ratios in buffer solutions at 25 °C for 500 hours. Buffer solution (50 ml): pH4 from potassium hydrogen phthalate (KHP), pH7 from Na_2HPO_4 and KH_2PO_4, pH 10 from Na_2CO_3, $CHNaO_3$ and KHP.

Generally, dissolution behavior of phosphate glasses includes two processes, hydration and hydrolysis, which may happen at the same time for some compositions. The glass dissolution rate is mainly controlled by the glass hydration, but also affected by the hydrolysis of phosphate chains in solution or in the hydrated layer, because the glass dissolution rate is also as a function of local pH value. In a future study, these two processes need to be clearly separated through solution analysis and the characterization of the structure and composition of hydrated layer, along with more quantitative data on glass structure and thermodynamic data, to achieve a better predictive model for long term glass dissolution for varies applications.

Phase diagram. Glass formation and phase equilibria in the Fe_2O_3–P_2O_5 system have been thoroughly investigated by Zhang et al [10,11,12]. However, the corresponding detailed information on the sodium iron phosphate system is scarce in the literature. In this dissertation, the study of crystallization behavior of sodium iron phosphate glasses focused on the effects of glass composition, stable crystalline phases, and iron redox on glass thermal stability and glass forming ability. However, the investigation of other sodium iron phosphate systems must still be done. In future studies, the determination of phase diagram for $Na_4P_2O_7$–$Fe_2(P_2O_7)$ system and $Na_4P_2O_7$–$Fe_4(P_2O_7)_3$ system will be useful and helpful for the compositional design of sodium iron phosphate glasses used for nuclear waste vitrification.

References

[1] J.R. Van Wazer. "Phosphorus and its compounds, volume 1: chemistry." Interscience Publishers (1958): 717-800.

[2] R.J. Geue, A.M. Sargeson, and R. Wijesekera. "Metal Ion Promoted Hydrolysis of Polyphosphates." Australian Journal of Chemistry 46, no. 7 (1993): 1021-1040.

[3] R.K. Osterheld. "Nonenzymic hydrolysis at phosphate tetrahedra." in E.J. Griffith, and M. Grayson, eds., "Topics in phosphorus chemistry, volume 7." Interscience Publishers (1972): 103-242.

[4] J.R. Van Wazer, Phosphorus and its Compounds. Interscience, New York, NY, 1958.

[5] U.P. Strauss and T.R. Treitler. Chain Branching in Glassy Polyphosphates: Dependence on the Na/P Ratio and Rate of Degradation at 25. J. Am. Chem. Soc., 77, 1473 (1955).

[6] J.W. Wiench, M. Pruski, B. Tischendorf, J.U. Otaigbe, B.C. Sales. Structural studies of zinc polyphosphate glasses by nuclear magnetic resonance. Journal of Non-Crystalline Solids 263&264 (2000) 101-110.

[7] B.C. Bunker, G.W. Arnold, and J.A. Wilder. "Phosphate glass dissolution in aqueous solutions." Journal of non-crystalline solids 64, no. 3 (1984): 291-316.

[8] F. Delahaye, L. Montagne, G. Palavit, J.C. Touray, and P. Baillif. "Acid dissolution of sodium–calcium metaphosphate glasses." Journal of non-crystalline solids 242, no. 1 (1998): 25-32.

[9] L. Ma, R.K. Brow. "Structural study of Na_2O-FeO-Fe_2O_3-P_2O_5 glasses by high-pressure liquid chromatography." Journal of Non-Crystalline Solids 387 (2014): 16-20.

[10] L. Zhang, L. Ghussn, M.L. Schmitt, E.D. Zanotto, R.K. Brow, and M.E. Schlesinger. "Thermal stability of glasses from the $Fe_4(P_2O_7)_3$–$Fe(PO_3)_3$ system." Journal of Non-Crystalline Solids 356, no. 52 (2010): 2965-2968.

[11] L. Zhang, R.K. Brow, M.E. Schlesinger, L. Ghussn, and E.D. Zanotto. "Glass formation from iron-rich phosphate melts." Journal of Non-Crystalline Solids 356, no. 25 (2010): 1252-1257.

[12] L. Zhang, M.E. Schlesinger, and R.K. Brow. "Phase equilibria in the Fe_2O_3–P_2O_5 system." Journal of the American Ceramic Society 94, no. 5 (2011): 1605-1610.

APPENDIX A

DISSOLUTION BEHAVIOR OF $Na_2O–CaO–P_2O_5$ GLASSES

A. DISSOLUTION BEHAVIOR OF $Na_2O–CaO–P_2O_5$ GLASSES

Lina Ma, Richard K. Brow*, Mark E. Schlesinger

Department of Materials Science & Engineering, Missouri University of Science & Technology, Straumanis-James Hall, 1400 N. Bishop Ave, Rolla, MO, USA

ABSTRACT

A series of $xNa_2O–xCaO–(100–2x)P_2O_5$ (NCP, $24 \leq x \leq 31$, $3.0 \leq (O/P) \leq 3.5$) glasses were reacted in deionized water for different times and temperatures. Dissolution rates were determined from weight loss measurements and from the concentrations of ions released to the water using inductively-coupled plasma optical emission spectroscopy (ICP-OES). These Na–Ca–phosphate glasses dissolve congruently in DI H_2O, with the relative concentrations of ions in solution the same as those in the original glasses. The dissolution rate constants decrease by an order of magnitude as the O/P ratio of the glass increases from 3.0 to 3.5. Dissolution mechanisms were studied and dissolution exhibits both linear and square-root time dependences, depending on the conditions. The activation energy of glass dissolution was found to decrease, from 83 ± 5 kJ/mol to 23 ± 5 kJ/mol, with an increase in the O/P ratio. The Gibbs free energy of hydration was calculated from the glass composition by considering the appropriate sodium and calcium phosphate compounds, and this increased with increasing O/P ratio.

Keywords: Phosphate glass; dissolution behavior; Gibbs free energy of hydration; HPLC

* Corresponding author, brow@mst.edu

1. Introduction

Bioactive and bioresorbable glasses have been studied and developed for tissue engineering applications with the goal of promoting cell functionality [1]. Silicate, borate and phosphate based bioactive glasses have been fabricated as scaffolds for bone regeneration, glass fibers for antibacterial or trace element delivery systems and muscle regeneration, and nanofiber glasses for venous stasis wounds healing in soft tissue repair [1,2,3,4].

Bioactive phosphate glasses, including those in the $Na_2O–CaO–P_2O_5$ system, are degradable in aqueous environments [5,6]. Through compositional modifications, the solubility of phosphate glasses can be tailored to obtain a wide range of ion release rates for many applications. Increasing the CaO, CuO, Al_2O_3 and Fe_2O_3 contents of phosphate glasses decreases their dissolution rates in aqueous solutions [2,3,7]. Phosphate glasses with controlled ion release rates have been developed to treat trace-element deficiencies in animals or used as agricultural fertilizers [8]. The addition of copper and silver are known to have positive effects on the local treatment of infections [9,10], and phosphate glass fibers incorporating Al_2O_3 and Fe_2O_3 have been used for regeneration of skeletal muscle [11,12]. The polymeric structure of the phosphate anions in metaphosphate glasses allows for easy fiber drawing from glass melts [11,12,13], and the metal chelating properties of the phosphate anions may enhance the growth of bone cells [14,15,16].

Debate remains about the phosphate glass dissolution mechanisms. For $Na_2O–CaO–$ metaphosphate glasses, Bunker et al. [7,17] observed an initial dissolution stage with square-root time dependence for weight loss, and linear time-dependence in a second stage. Bunker attributed the first stage to water diffusion and surface hydration,

and the second stage to the hydration of phosphate anions and their release to solution. The initial square-root time dependence was not observed in other studies [3,18,19], and it appears that there are other important factors that affect the dissolution kinetics of phosphate glasses in solution, including surface layer formation and the solution chemistry. For example, an increase in ionic strength of the leaching solution can modify the electrostatic interactions between the polyphosphate chains in the hydrated surface layer and decrease the dissolution rate [18]. Hydrated layers that develop on the surfaces of metaphosphate glasses in acidic solutions appear to have the same composition and structure as the pristine glass [18].

From a thermodynamic viewpoint, glass corrosion processes can be understood in terms of the reactions that produce complex solubility products when the glasses dissolve [20,21]. The hydration processes involved in these reactions are related to the free energy changes for reactions that occur between the glass constituents and the absorbed water molecules, and the overall free energies of hydration for different glass compositions can be estimated from the glass compositions [22]. The relationship between the calculated thermodynamic stability and glass dissolution rate can then be used to estimate the relative glass durability in an aqueous solution [23].

In the present work, the dissolution behavior of $Na_2O–CaO–P_2O_5$ (NCP) glasses with a range of O/P ratios (3.0–3.5) were studied to provide further insight into the mechanism of phosphate glass dissolution. High-pressure liquid chromatography (HPLC) was used to characterize the phosphate anion distributions in the original glasses. The dependence of dissolution behavior on glass composition and structure, defined by the average phosphate anion size and depending on the O/P ratio, will be discussed.

2. Experimental Procedure

2.1. Glass melting and compositional analysis

Sodium calcium phosphate glasses, with the batched composition (Na_2O/CaO ratio = 1) given in Table 1, were prepared from raw materials including Na_2CO_3 (Alfa Aesar, ≥ 98%), $NaPO_3$ (Fisher Scientific, ≥ 98%), $CaHPO_4$ (Fisher Scientific, ≥ 99%), and $NH_4H_2PO_4$ (Alfa Aesar, ≥ 98%). Batches that produced 50g of glass were thoroughly mixed and melted in Al_2O_3 crucibles (AdValue Technology, High Form 99.6%) between 900 °C and 1200 °C in air for one hour. The melts were poured into graphite molds (10 × 10 × 50 mm) and annealed ±5 °C around the appropriate glass transition temperature (T_g) for 4–12 hours.

Glass compositions were determined by inductively-coupled plasma optical emission spectroscopy (ICP-OES, PerkinElmer Optima 2000 DV, Norwalk, USA). Glass powders (75–150 μm) were digested in 3 wt% HNO_3 aqueous solution for 4 days at 60 °C in closed Teflon containers. Solutions for ICP were diluted with 1 wt% HNO_3 aqueous solution, with dilution factors of 1:9 or 1:99, depending on the expected ion concentration of the solution.

2.2. Dissolution test

Samples of annealed glass, approximately 12.0 × 9.0 × 1.5 mm were sliced and polished to a finish of 1200 (P-4000) grit with silicon carbide paper (ALLIED High Tech Productes, # 50-10040), then cleaned with ethanol. These pieces were suspended in 50 ml of deionized water using Zebco Omniflex Line (OMNIFLEX4LB). The initial ratio of glass surface area to leachate volume (SA/V ratio) was 0.06 ± 0.01 cm^{-1}. After specified

times, sample weight loss was measured, the ion concentrations in leachate solutions were analyzed using ICP-OES, and the pH values of the leachate solutions were measured (Fisher Scientific Accumet Research AR25).

Two types of corrosion tests were conducted and each test was done in triplicate for each glass composition:

Test A (static): Bulk glasses were suspended in deionized H_2O at different temperatures (8 °C to 90 °C ± 2 °C). At specific time intervals, glasses were removed from solution, rinsed in absolute ethanol, and then dried at 90 °C for two hours. The weight loss and pH value were measured, and the solutions collected for ICP-OES.

Test B (semi-dynamic): Bulk glasses were suspended in deionized H_2O at room temperature (22 ± 2 °C). After samples were removed, weight losses recorded and solutions analyzed as described for Test A, the leachate solutions were replaced with 50 ml deionized H_2O.

2.3. Structural analysis

Phosphate anion distributions in the starting glasses were characterized by high-pressure liquid chromatography (HPLC, Dionex ion chromatography system). Glass powders (75–150 μm, 200 mg) were partially dissolved for different times (2–12 hour) in an aqueous solution (50 ml) with 0.22 M NaCl + 5 mM Na_4EDTA and a pH of 10. Detailed procedures for these analyses are described in a previous study [24].

3. Results

3.1. Glass compositions

The analyzed glass compositions, shown in Table 1, differ in several ways from the batched compositions because of volatilization of phosphorus from the melts and the dissolution of small amounts (0.1–5.6 mol %) of Al_2O_3 into the melts during glass preparation. The O/P ratios listed account for these compositional variations. Glasses prepared at higher temperatures generally had higher amounts of Al_2O_3.

3.2. HPLC study

Fig. 1 shows HPLC chromatographs of glasses with O/P ratios between 3.01 and 3.48. The area under each absorption peak (P_n) is proportional to the concentration of phosphorus associated with specific phosphate anions with n PO_4 tetrahedra, $(P_nO_{3n+1})^{-(n+2)}$ [24]. The broad hump in the chromatographs of glasses with O/P ≤ 3.17 are unresolved anions with n greater than about 12. As the O/P ratio increases, the relative concentration of shorter phosphate anions increases. When O/P reaches 3.48, the main phosphate anions in the glass structure are the pyrophosphate (P_2, 66%), orthophosphate (P_1, 25%), triphosphate (P_3, 8%) and tetraphosphate (P_4, 1%).

A comparison of the O/P ratios and average phosphate chain lengths ($\bar{n}$) calculated from the HPLC data with values calculated from the analyzed glass compositions is shown in Fig. 2 (a). The determination of the overall O/P ratios and $\bar{n}$ is described in a previous study [24]. For glasses with O/P ≤ 3.17, the hump is taken as a single phosphate chain (P_n), even though longer phosphate chains will be present. This assumption leads to an overestimation of the O/P ratio and an underestimation of $\bar{n}$,

compared with the values calculated from the analyzed compositions (Fig. 2 (a)). For glasses with O/P > 3.1, there is a good agreement between the values expected from the ICP compositions and the values measured by HPLC; this indicates that the structural information obtained by HPLC is representative of Na–Ca–phosphate glasses with O/P > 3.1.

Fig. 2 (b) shows the fraction of phosphate tetrahedra with different bridging oxygens (Q^i, where i is the number of bridging oxygens on a P-tetrahedron) determined from the relative concentrations of phosphate anions from the HPLC chromatographs. Similar to what was found for sodium iron phosphate glasses in a previous study [24], the actual distribution of Q^i sites falls between an ideal Flory distribution and what is expected from chemical simplicity (zero site disproportionation), especially for glasses with greater O/P ratios. For an ideal Flory distribution [25], the equilibrium constant $K(Q^1)$ for a disproportionation reaction of Q^i sites (Eq. (1)) equals 0.25 [24] in polyphosphate range (O/P 3.0–3.5),

$$2Q^1 \leftrightharpoons Q^2 + Q^0 \quad (1)$$

If there is no site disproportionation in the melt, then $K(Q^1) = 0$. The information on the distribution of Q^i sites in the glass network will be used below for the estimation of overall Gibbs free energies of hydration for different glass compositions.

3.3. Dissolution behavior

Mass release data for sodium, calcium and phosphorus determined by ICP analyses were normalized to the initial glass composition and surface area by Eq. (2), in which C_i is the measured concentration (ppm) of element i in solution, f_i is the mass

fraction (wt%) of element i in the original glass, and SA/V is the ratio of glass surface area (cm^2) to leachate volume (V) [26],

$$\mathrm{NL(i)(mg/cm^2)} = \frac{C_i}{(f_i)\cdot(\mathrm{SA/V})} \quad (2)$$

If every glass constituent is released into solution in the same proportion as it is present in the original glass, then congruent dissolution is observed, and $\partial[\mathrm{NL(i)}]/\partial \mathrm{t}$ will be the same for all elements [22]. The normalized mass release (mg/cm^2) data during the semi-dynamic (Test B) experiments for several NCP glasses are shown in Fig. 3. Congruent dissolution was observed for all glasses up to ~ 500 hours of dissolution time at room temperature (22 ± 2 °C). Ion release rates decrease with increasing O/P ratio in the glass compositions.

Fig. 4 shows how the pH of the leachate solutions changes with time for the different glasses in the static dissolution Test A. Glasses with greater Na_2O/CaO contents, and so shorter phosphate chains (greater O/P ratios), produce leachates with greater pH values. Ahmed et al. [27] show a similar decrease in solution pH for the dissolution of Na-Ca-phosphate glasses near the metaphosphate stoichiometry.

4. Discussion

4.1. Dissolution kinetics

Fig. 5 shows the mass fraction of glass dissolved (α) in Test A (solid symbols) and Test B (open symbols). With an increase in O/P ratios, semi-dynamic dissolution Test B promotes faster dissolution of bulk phosphate glasses comparing to the static dissolution Test A.

Fig. 6 shows an example of how kinetic models fit the dissolution data for the glass with O/P ~3.48. Here, Bunker's two-stage model was applied [17]: the first stage is described by square-root time dependence (Eq. (3)) and the second stage is described by linear time dependence (Eq. (4)).

$$\alpha = k_1 \times t^{1/2} \quad (3)$$

$$\alpha = k_2 \times t \quad (4)$$

The dissolution rate of the pyrophosphate glass is significantly faster in Test B, where fresh DI water replaces the leachate after each weight loss measurement, and there is a clear transition from square-root time dependence (solid line) to linear time dependence (dashed line) after about 100 hours. The dissolution kinetics for static Test A are fit by the square-root time dependence to 450 hours. These results indicate that for this glass, the solution chemistry affects the dissolution kinetics [18]. Similar kinetic model fitting was done for all dissolution data.

Bunker noted that the transition time between the first and the second stage was dependent on the glass composition and the pH value of the aqueous solution [17]. In the present study, for glasses with O/P ratios in the range 3.01–3.17, the first stage ($t^{1/2}$) is not clear, and linear time dependence was observed throughout the experiment. For glasses with O/P ratios in the range 3.29–3.48, as O/P ratio increases, the first stage of square-root time dependence is prolonged and the dissolution rate parameters (k_1 and k_2) obtained from the fitting results decrease, as shown in Table 2. The replenishing of leachate solution increases the glass dissolution rate at the second stage.

4.2. Activation energy

The temperature dependence of the dissolution of the glass with O/P=3.04 is shown in Fig. 7 (a). As noted above, this glass exhibits only linear (stage 2) dissolution kinetics at each temperature between 8 and 90°C, and the rate parameter, k_2, increases with temperature. Similar experiments were done on other glasses and the second stage rate parameters were used to calculate activation energies for dissolution, using the Arrhenius relation in Eq. (5), where k_0 is the pre-exponential term, Q is the activation energy, R is the gas constant (J/K/mol), and T is the absolute temperature.

$$k_2 = k_0 \exp(-Q/RT) \quad (5)$$

Fig. 7 (b) shows that the dissolution activation energy decreases with increasing O/P ratio. The actication energies for the two glasses with compositions near the metaphosphate stoichiometry are similar to what Bunker et al. [17] reported for the dissolution of a glass with the nominal molar composition $30Na_2O–20CaO–50P_2O_5$ (~ 67 kJ/mol), and to what Gao et al. [28] reported for the dissolution of a glass with the nominal molar composition $25Na_2O–25CaO–50P_2O_5$ (~ 79 kJ/mol).

4.3. Gibbs free energy of hydration

The dissolution rates of glasses in aqueous solutions have been related to the overall Gibbs free energy of the glass-water reactions [22], and a linear relation has been observed for silicate nuclear waste glasses [23].

The Gibbs free energy of hydration for phosphate glasses was estimated by considering the glass as a mixture of phosphate compounds. When phosphate glass dissolves in an aqueous solution, phosphate anions are separated intact from their

accompanying metal cations and entire chain is released into solution [17]. HPLC results for the glasses studied here show that three types of phosphate tetrahedra are present in the phosphate anions: Q^0, Q^1 and Q^2 (Fig. 2 (b)). Since the thermodynamic data for the hydration of specific phosphate anions are unavailable, phosphate glasses in this study are assumed to be composed of mixtures of sodium, calcium and aluminum phosphate compounds, and the dissolution processes of the glasses are described by the reactions of these compounds with water or H^+ in solution. The Gibbs free energy of hydration at 298.15 K for various sodium, calcium and aluminum phosphate compounds are listed in Table III. The relative fraction for these compounds can be calculated from the distribution of Q^i sites in glass network by assuming that the Na/Ca/Al ratios for each type of phosphate (e.g., orthophosphate) is the same as the compositional ratios in the bulk glasses (~ 2). The overall Gibbs free energy of hydration for a glass is then the sum of the Gibbs free energy of hydration of each phosphate compound,

$$\Delta G_{hyd} = \sum x_i (\Delta G_{hyd})_i \quad (6)$$

where x_i is the molar fraction of each phosphate compound in one molar of phosphate glasses, and $(\Delta G_{hyd})_i$ is the Gibbs free energy change of corresponding water-compound reaction [22].

Fig. 8 (a) shows the Gibbs free energy of hydration (kJ/mol) of one molar glass dissolved in DI H_2O changes as a function of the O/P ratio of the glass. The glass dissolution rate parameter, k_2, and activation energy, Q, are also shown in Fig. 8 (a). An increase in the O/P ratio increases the Gibbs free energy of hydration, which is consistent with the observations that glasses with greater O/P ratios have a lower dissolution rates. Fig. 8 (b) shows the linear relationship between ΔG_{hyd} and k_2,

$$k_2 = -1.88 \times 10^{-6} \Delta G_{hyd} + 3.13 \times 10^{-4} \quad (7)$$

where the slope is –(1.88 ± 0.19) and the intercept is 3.13 ± 0.21. From the information on glass composition and Q^i distributions, this hydration free energy model can be used to explain the compositional dependence of the glass dissolution rates and predict the dissolution rate parameter, k_2.

5. Summary

Sodium calcium phosphate glasses with compositions in the polyphosphate range (O/P ratio 3.0–3.5) dissolve congruently in DI H_2O. The dissolution processes were characterized with a two-stage dissolution kinetic model: the first stage is described by square-root time dependence and the second stage is described by linear time dependence. With an increase in O/P ratio, the first stage is prolonged and the dissolution rate parameters decrease, the glass chemical durability is improved. The replenishing of leachate solution increases the glass dissolution rate at the second stage.

With an increase in O/P ratio, activation energies decrease from 83 ± 5 kJ/mol for glass with O/P 3.01 to 24 ± 4 kJ for glass with O/P 3.46. Distributions of the Q^i sites determined from HPLC techniques were used to calculate the Gibbs free energy of hydration (kJ/mol) for each composition by assuming glass is a mixture of sodium and calcium phosphate compounds. The Gibbs free energy of hydration decreases with increasing O/P ratio, which is consistent with the observations that glasses with greater O/P ratios have a lower dissolution rates.

Acknowledgement

The authors are very grateful to Xiaoming Cheng (Missouri University of Science and Technology) for her help with the ICP analysis. This work was supported by the Nuclear Energy University Program (US Department of Energy) under grant NEUP 09-144.

Table 1 Batched and analyzed compositions of the Na–Ca–phosphate glasses.

Batched Composition mol%				Analyzed Composition mol% (RSD < 4 %)				Analyzed
P_2O_5	Na_2O	CaO	O/P	P_2O_5	Na_2O	CaO	Al_2O_3	O/P
38	31	31	3.32	35.9	31.6	29.1	3.3	3.48
40	30	30	3.25	36.1	31.4	29.9	2.6	3.46
42	29	29	3.19	38.5	29.3	26.6	5.6	3.44
44	28	28	3.14	41.4	29.3	26.1	3.2	3.29
48	26	26	3.04	45.1	28.3	24.0	2.6	3.17
45	27.5	27.5	3.11	48.5	26.5	21.9	3.1	3.09
50	25	25	3.00	48.6	26.5	24.3	0.7	3.04
52	24	24	2.96	49.7	26.2	24.0	0.1	3.01

Table 2 Summary of dissolution rate parameters (k_1 and k_2) for Test A and Test B.

O/P ratio	Test A			Test B		
	k_1 ($\times 10^{-4}$)	k_2 ($\times 10^{-5}$)	Transition Time (hour)	k_1 ($\times 10^{-4}$)	k_2 ($\times 10^{-5}$)	Transition time (hour)
3.01	–	25.3 (7)	< 25	–	30.0 (5)	< 25
3.04	–	21.5 (2)	< 25	–	20.1 (1)	< 25
3.17	–	11.2 (2)	< 25	–	11.7 (2)	< 25
3.29	9.9 (14)	6.5 (9)	~46	–	11.0 (6)	~25
3.44	9.6 (11)	6.2 (10)	~70	9.2 (13)	10.2 (8)	~45
3.46	7.4 (13)	2.8 (2)	~140	6.4 (10)	4.9 (9)	~66
3.48	6.1 (1)	–	> 400	7.5 (5)	3.8 (2)	~100

Table 3 Gibbs free energies of hydration at 298.15 K for various sodium and calcium phosphate compounds.

Reactions	K_{eq}	Ref.
$Na_3PO_4 + 1.5H^+ \leftrightarrow 3Na^+ + 0.5{HPO_4}^{2-} + 0.5{H_2PO_4}^-$	9.67×10^{14}	FactSage 6.4
$Ca_3(PO_4)_2 + 3H^+ \leftrightarrow 3Ca^{2+} + {HPO_4}^{2-} + {H_2PO_4}^-$	2.52×10^{-8}	FactSage 6.4
$Na_4P_2O_7 + 3H_2O \leftrightarrow 4Na^+ + 2{H_2PO_4}^- + 2OH^-$	5.46×10^{-11}	[29]
$Ca_2P_2O_7 + 2H_2O \leftrightarrow 2Ca^{2+} + {HPO_4}^{2-} + {H_2PO_4}^- + OH^-$	1.79×10^{-33}	FactSage 6.4
$Na_3(PO_3)_3 + 3H_2O \leftrightarrow 3Na^+ + 3{H_2PO_4}^-$	4.58×10^{14}	[29]
$Ca(PO_3)_2 + 2H_2O \leftrightarrow Ca^{2+} + {HPO_4}^{2-} + {H_2PO_4}^- + H^+$	4.63×10^{-12}	FactSage 6.4
$AlPO_4 + 1.5H^+ \leftrightarrow Al^{3+} + 0.5{HPO_4}^{2-} + 0.5{H_2PO_4}^-$	2.98×10^{-9}	FactSage 6.4

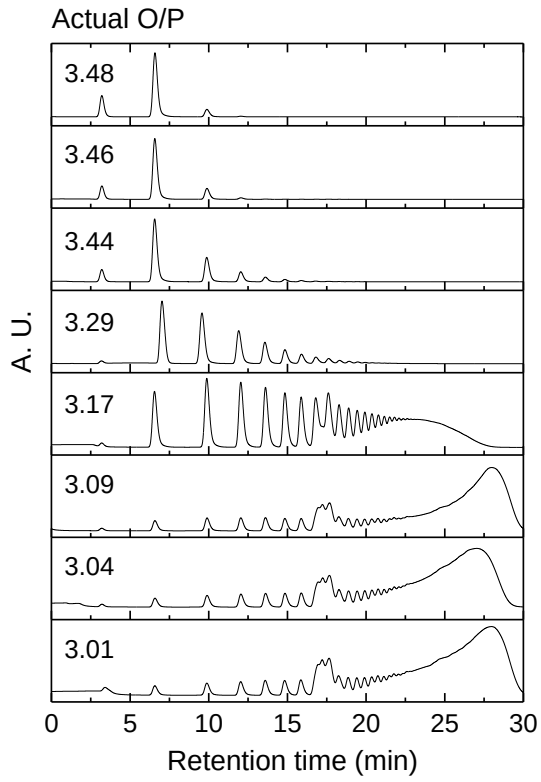

Fig. 1. HPLC chromatographs of $xNa_2O–xCaO–(100–2x)P_2O_5$ glasses.

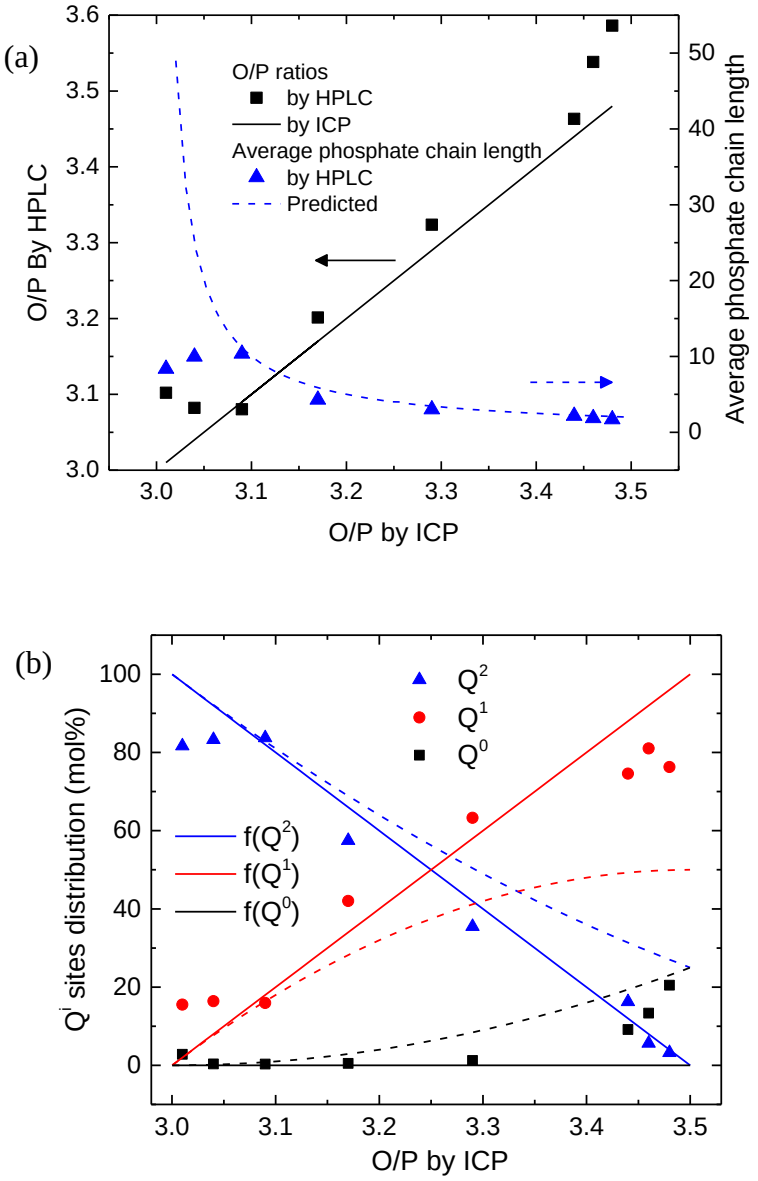

Fig. 2. (a) A comparison of O/P ratios (left axis) and average phosphate chain-length ($\bar{n}$) (right axis) determined from the HPLC chromatographs with those predicted from the glass compositions (solid line). The dashed curve is $\bar{n}$ predicted from analyzed compositions. (b) Distribution of Q^i sites for the Na–Ca–phosphate glasses calculated from the respective chromatographs. The solid lines are the predicted f(Q^i) without site disproportionation. The dashed lines are f(Q^i) following ideal Flory distribution.

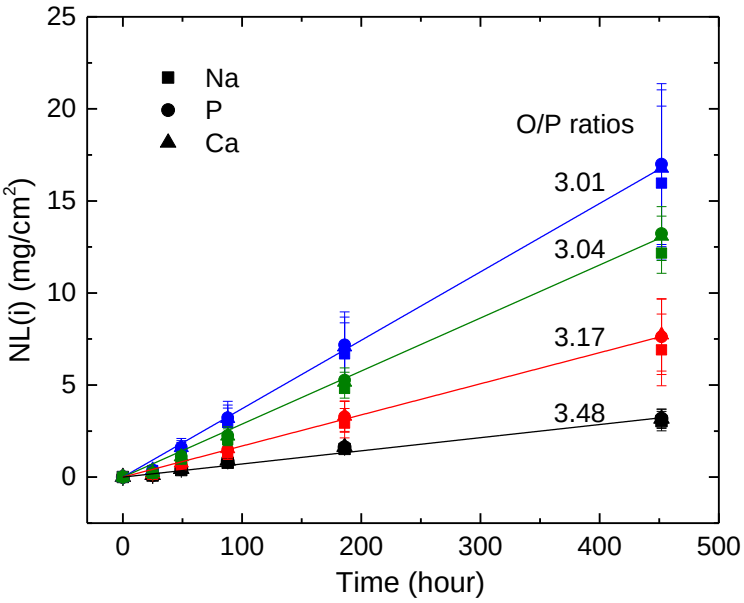

Fig. 3. Normalized mass release (mg/cm^2) of sodium, phosphorus and calcium from glasses with different O/P ratios at 22 ± 2 °C, Test B. Lines are guides for the eye.

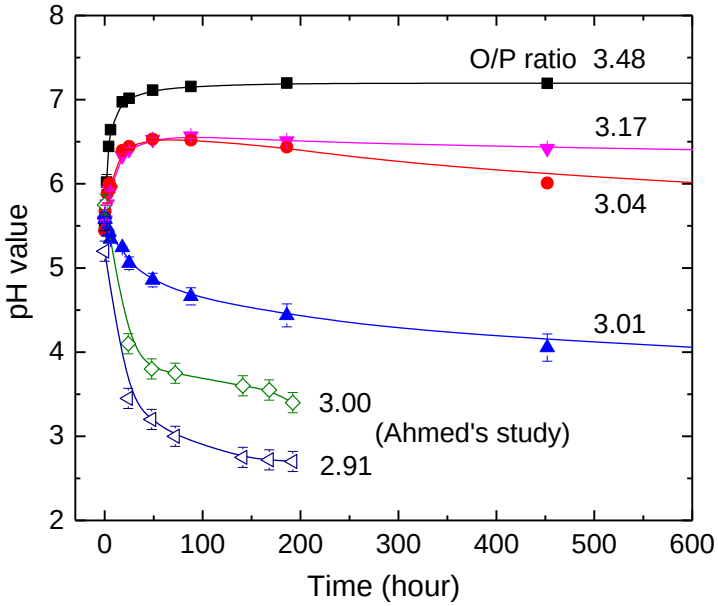

Fig. 4. pH of the leachate solutions for static dissolution Test A at room temperature (22 ± 2 °C). The open symbols are from reference [27] with SA/V ratio ~0.18 cm^{-1} and at 37 °C.

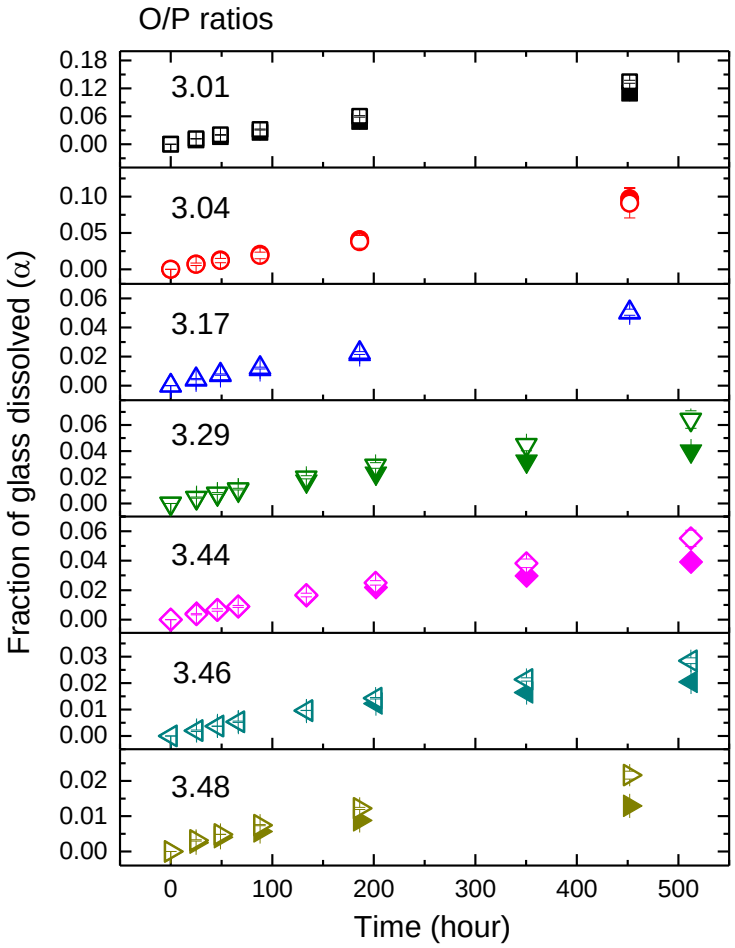

Fig. 5. Fraction of Na–Ca–phosphate glass dissolved (α) in Test A (solid symbols) and Test B (open symbols) at 22 ± 2 °C.

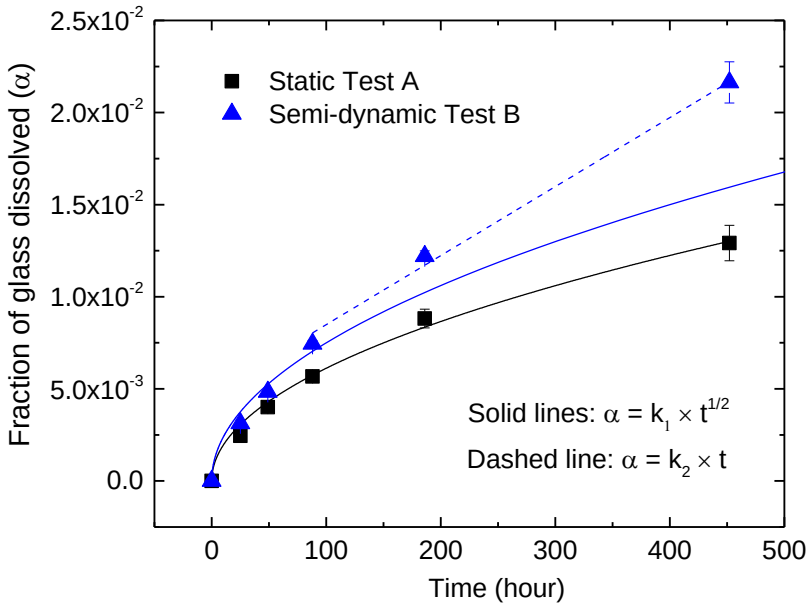

Fig. 6. Fraction of glass (O/P ~3.48) dissolved in Test A and Test B. The solid lines are the square-root time model (Eq. (3)), and the dashed line is the linear time model (Eq. (4)).

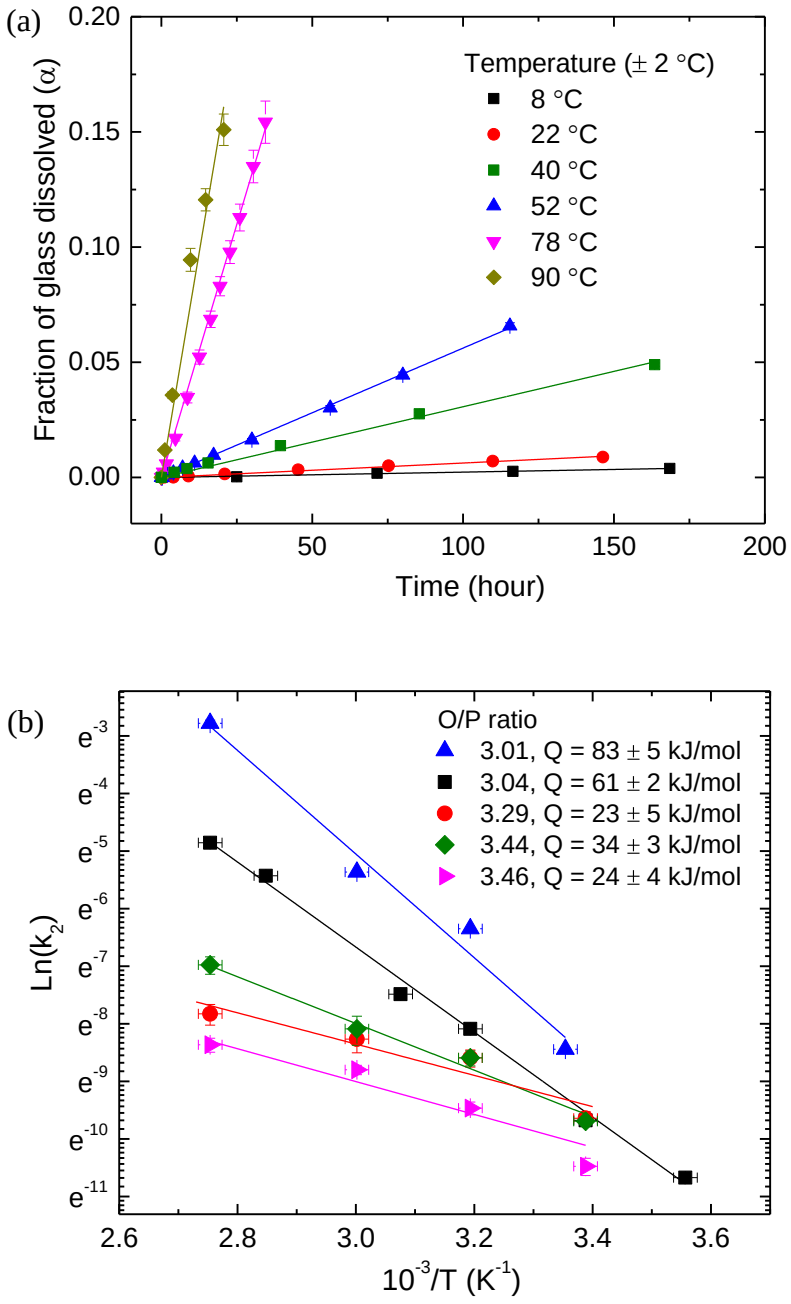

Fig. 7. (a) Temperature dependence of the P-released from the glass with O/P ratio ~3.04; lines are fit ($R^2 > 0.999$) by Eq. (4) with slopes providing values for k_2; (b) Arrhenius plots of k_2 for five different glasses. Lines are linear fits and their slopes provide the activation energies indicated on the plot.

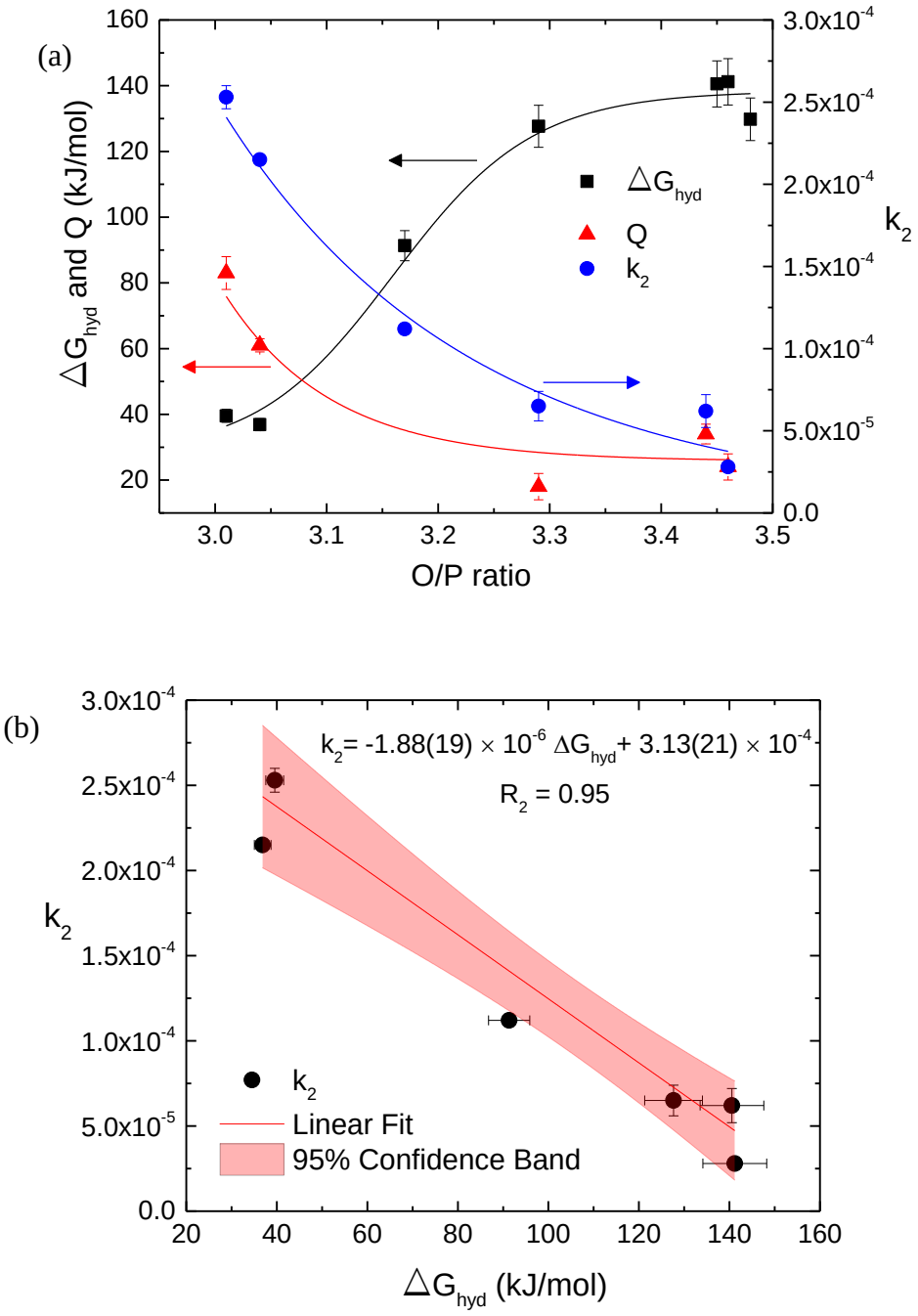

Fig. 8. (a) Left axis: Gibbs free energy (ΔG_{hyd}) of hydration and dissolution activation energies (Q) for the Na-Ca-phosphate glasses dissolved in DI H_2O. Right axis: dissolution rate parameter (k_2), from Test A change with O/P ratio. Lines are guides for the eye. (b) Linear relation between k_2 and ΔG_{hyd}, line is linear fit and equation indicated on the plot.

References

[1] M.N. Rahaman, D.E. Day, B. Sonny Bal, Q. Fu, S.B. Jung, L.F. Bonewald, and A.P. Tomsia. "Bioactive glass in tissue engineering." Acta biomaterialia 7, no. 6 (2011): 2355-2373.

[2] E.A. Abou Neel, I. Ahmed, J.J. Blaker, A. Bismarck, A.R. Boccaccini, M.P. Lewis, S.N. Nazhat, and J.C. Knowles. "Effect of iron on the surface, degradation and ion release properties of phosphate-based glass fibres." Acta Biomaterialia 1, no. 5 (2005): 553-563.

[3] E.A. Abou Neel, I. Ahmed, J. Pratten, S.N. Nazhat, and J.C. Knowles. "Characterisation of antibacterial copper releasing degradable phosphate glass fibres." Biomaterials 26, no. 15 (2005): 2247-2254.

[4] S.B. Jung. "Bioactive Borate Glasses." Bio-Glasses: An Introduction (2012): 75-95.

[5] L.L. Hench. "Bioactive materials: the potential for tissue regeneration." Journal of biomedical materials research 41, no. 4 (1998): 511-518.

[6] H.A. ElBatal, E.M.A. Khalil, and Y.M. Hamdy. "In vitro behavior of bioactive phosphate glass–ceramics from the system P_2O_5–Na_2O–CaO containing titania." Ceramics International 35, no. 3 (2009): 1195-1204.

[7] J.C. Knowles. "Phosphate based glasses for biomedical applications." Journal of Materials Chemistry 13, no. 10 (2003): 2395-2401.

[8] M. Uo, M. Mizuno, Y. Kuboki, A. Makishima, and F. Watari. "Properties and cytotoxicity of water soluble Na_2O–CaO–P_2O_5 glasses." Biomaterials 19, no. 24 (1998): 2277-2284.

[9] A.M. Mulligan, M. Wilson, and J.C. Knowles. "Effect of increasing silver content in phosphate-based glasses on biofilms of Streptococcus sanguis." Journal of Biomedical Materials Research Part A 67, no. 2 (2003): 401-412.

[10] A.M. Mulligan, M. Wilson, and J.C. Knowles. "The effect of increasing copper content in phosphate-based glasses on biofilms of *Streptococcus sanguis*." Biomaterials 24, no. 10 (2003): 1797-1807.

[11] R. Shah, A.C.M. Sinanan, J.C. Knowles, N.P. Hunt, and M.P. Lewis. "Craniofacial muscle engineering using a 3-dimensional phosphate glass fibre construct." Biomaterials 26, no. 13 (2005): 1497-1505.

[12] I. Ahmed, C.A. Collins, M.P. Lewis, I. Olsen, and J.C. Knowles. "Processing, characterisation and biocompatibility of iron-phosphate glass fibres for tissue engineering." Biomaterials 25, no. 16 (2004): 3223-3232.

[13] I. Ahmed, M. Lewis, I. Olsen, and J.C. Knowles. "Phosphate glasses for tissue engineering: Part 2. Processing and characterisation of a ternary-based P_2O_5–CaO–Na_2O glass fibre system." Biomaterials 25, no. 3 (2004): 501-507.

[14] J.R. Van Wazer, and D.A. Campanella. "Structure and properties of the condensed phosphates. IV. Complex ion formation in polyphosphate solutions." Journal of the American Chemical Society 72, no. 2 (1950): 655-663.

[15] V. Salih, K. Franks, M. James, G.W. Hastings, J.C. Knowles, and I. Olsen. "Development of soluble glasses for biomedical use Part II: The biological response of human osteoblast cell lines to phosphate-based soluble glasses." Journal of Materials Science: Materials in Medicine 11, no. 10 (2000): 615-620.

[16] M. Bitar, V. Salih, V. Mudera, J.C. Knowles, and M.P. Lewis. "Soluble phosphate glasses: in vitro studies using human cells of hard and soft tissue origin." Biomaterials 25, no. 12 (2004): 2283-2292.

[17] B.C. Bunker, G.W. Arnold, and J.A. Wilder. "Phosphate glass dissolution in aqueous solutions." Journal of non-crystalline solids 64, no. 3 (1984): 291-316.

[18] F. Delahaye, L. Montagne, G. Palavit, J. Claude Touray, and P. Baillif. "Acid dissolution of sodium–calcium metaphosphate glasses." Journal of non-crystalline solids 242, no. 1 (1998): 25-32.

[19] K. Franks, I. Abrahams, and J.C. Knowles. "Development of soluble glasses for biomedical use Part I: In vitro solubility measurement." Journal of Materials Science: Materials in Medicine 11, no. 10 (2000): 609-614.

[20] R. Conradt. "Chemical durability of oxide glasses in aqueous solutions: A review." Journal of the American Ceramic Society 91, no. 3 (2008): 728-735.

[21] R. Conradt. "A proposition for an improved theoretical treatment of the corrosion of multi-component glasses." Journal of nuclear materials 298, no. 1 (2001): 19-26.

[22] D.E. Clark, and B.K. Zoitos. "Corrosion of glass, ceramics and ceramic superconductors: Principles, testing, characterization and applications." Noyes Publications, Park Ridge, NJ (1992).

[23] D. Perret, J.L. Crovisier, P. Stille, G. Shields, U. Mäder, T. Advocat, K. Schenk, and M. Chardonnens. "Thermodynamic stability of waste glasses compared to leaching behaviour." Applied geochemistry 18, no. 8 (2003): 1165-1184.

[24] L. Ma, and R.K. Brow. "Structural study of Na_2O-FeO-Fe_2O_3-P_2O_5 glasses by high-pressure liquid chromatography." Journal of Non-Crystalline Solids 387 (2014): 16-20.

[25] P.J. Flory. "Random reorganization of molecular weight distribution in linear condensation polymers." Journal of the American Chemical Society 64, no. 9 (1942): 2205-2212.

[26] D.E. Day, Z. Wu, C.S. Ray, and P. Hrma. "Chemically durable iron phosphate glass wasteforms." Journal of non-crystalline solids 241, no. 1 (1998): 1-12.

[27] I. Ahmed, M. Lewis, I. Olsen, and J.C. Knowles. "Phosphate glasses for tissue engineering: Part 1. Processing and characterisation of a ternary-based P_2O_5–CaO–Na_2O glass system." Biomaterials 25, no. 3 (2004): 491-499.

[28] H. Gao, T. Tan, and D. Wang. "Dissolution mechanism and release kinetics of phosphate controlled release glasses in aqueous medium." Journal of controlled release 96, no. 1 (2004): 29-36.

[29] Lange’s Handbook of Chemistry; 13th ed.; J.A. Dean, ed.; McGraw Hill: New York, 1985.

APPENDIX B

DISSOLUTION BEHAVIOR OF Na_2O–FeO–Fe_2O_3–P_2O_5 GLASSES IN ALKALI AQUEOUS SOLUTIONS

B. DISSOLUTION BEHAVIOR OF Na_2O–FeO–Fe_2O_3–P_2O_5 GLASSES IN ALKALI AQUEOUS SOLUTIONS

Lina Ma, Richard K. Brow*, Mark E. Schlesinger

Department of Materials Science & Engineering, Missouri University of Science & Technology, Straumanis-James Hall, 1400 N. Bishop Ave, Rolla, MO, USA

ABSTRACT

The dissolution behavior of a series of Na_2O–FeO–Fe_2O_3–P_2O_5 glasses, with O/P ~3.40 and Fe/P ratios in the range 0.23–0.58, in alkaline solutions (pH range 10–13) was investigated. Two dissolution stages were identified: the first stage is described by a 3D diffusion model (DM), and the second stage is described by the contracting volume model (CVM). Glasses dissolve more rapidly with increasing pH and with decreasing Fe/P ratio. Iron-rich precipitates form in leachates and on corroded glass surfaces.

Keywords: iron-phosphate glass, dissolution mechanism, alkali solution

* Corresponding author, brow@mst.edu

1. Introduction

Iron phosphate glasses with Fe/P ratios between 1:3 and 2:3 show remarkably good chemical durability and so are promising alternatives for vitrifying nuclear waste. An increase in Fe_2O_3 content improves the chemical durability of phosphate glasses to an extent that it is comparable to silicate and borosilicate waste glasses [1,2,3,4]. Good chemical durability is also observed for iron phosphate glasses with fairly high alkali oxides and chrome oxide contents [2,5]. The chemical durability of iron phosphate glasses containing simulated sodium bearing waste (SBW) and high level nuclear waste (HLW) meet all the current US Department of Energy (DOE) requirements, evaluated by Product Consistency Test (PCT) and Vapor Hydration Test (VHT) [1,6,7,8].

For disposal of nuclear waste by vitrification, the radioactive waste must be incorporated into glass hosts (e.g., borosilicate), then buried in geological disposal sites with a series of barriers to prevent the hazardous radionuclides from reaching the environment [9,10]. Therefore, the safety of nuclear waste disposal must consider the breach of barriers under the temperature, pressure and geologic conditions of the repository, and requires that the vitrified nuclear wastes be resistant to corrosion by percolating geological fluids and the stability of waste form would be maintained against the leaching and transport of radionuclides in aqueous environment [10]. Significant studies have been done to investigate the dissolution behavior of iron phosphate glasses and simulated waste forms with the aim of providing an alternative to the currently methods of nuclear waste disposal [1,2,3,8,9,11].

Glass dissolution behavior is mainly controlled by the breakdown of the glass network and extraction of alkali ions out of the glass matrix. Surface conditions and layer

formation, saturation effects and solution chemistry are also taken into account [12]. The hydration reaction between glass and H_2O is based on the hydrolytic cleavage of glass network bonds. Usually, the initial stage is controlled by the ion exchange process, then followed by the matrix dissolution with increasing depth of alkali depletion in the outer glass surface [12]. Two main approaches, geochemical and thermal dynamic, have been used to study the glass dissolution process. Models derived from these two approaches have been applied successfully to many corrosion tests of nuclear waste glasses [12,13,14,15,16].

The good chemical durability of iron phosphate glasses has been related to the glass structure. Structural models were developed to explain the reduction in phosphate chain hydration rates with increasing iron oxide content, through an increase in the number of chemical stable P–O–Fe bonds and a decrease in the overall surface energy [17,18]. For iron phosphate glasses containing both Fe^{2+} and Fe^{3+}, the chemical durability is independent of the Fe^{2+} content in glass [17].

In the present study, the dissolution behavior of a series of sodium iron phosphate glasses in KOH solutions (pH = 10–13) is investigated using ion concentration measurements and weight loss measurements, and compared with dissolution processes in neutral and acidic aqueous solutions.

2. Experimental Procedures

The preparation and compositional characterization of the Na_2O–FeO–Fe_2O_3–P_2O_5 glasses used in this study are described elsewhere [19]. Briefly, glasses were made from batches of raw materials including Na_2CO_3 (Alfa Aesar, $\geqslant$ 98%), Fe_2O_3 (Alfa

Aesar, ⩾ 99%) and $NH_4H_2PO_4$ (Alfa Aesar, ⩾ 98%) that were melted in fused SiO_2 crucibles (Leco #728-701) between 1000 ºC and 1250 ºC in air for two hours. Iron phosphate glasses were digested in 3–7 M H_2SO_4 aqueous solution for 7 to 14 days at 80–90 °C in closed Teflon containers. Cation concentrations, including small amounts of silica from the crucibles, were determined by inductively-coupled plasma optical emission spectroscopy (ICP-OES, PerkinElmer Optima 2000 DV, Norwalk, USA), and the fraction of iron present as Fe^{2+} was determined by a wet chemical technique [20]. Compositional series with similar O/P ratios (3.0–3.5) are labeled from A to E. For example, glass D-0.32 is a sample in the D-series with a batched O/P ratio of 3.4 and an analyzed Fe/P ratio of 0.32.

Glass powders with particle size 75–150 μm were ultrasonically cleaned with absolute ethanol and used in static dissolution tests. About100 mg glass powder was put into 30 ml aqueous solutions at room temperature (23 ± 2 ºC) for specific time intervals and all experiments were run in triplicate. Leachate solutions include DI H_2O, KOH solutions (pH from 10 to 13) and 0.1 M HCl (pH = 1). The weight loss of glass samples was measured. Ion concentrations in leachate solutions were analyzed using inductively-coupled plasma optical emission spectroscopy (ICP-OES, PerkinElmer Optima 2000 DV, Norwalk, USA). Solutions for ICP were filtered to remove solid particle and diluted with 1wt% HNO_3. Dilution factor is 1:9 or 1:99, depending on the predicted ion concentration of the solution.

The concentrations of leached glass constituents in solution were normalized to the glass composition. The normalized elemental mass release, NL(i) (mg/cm^2), was calculated by Eq. (1), where C_i is the measured concentration (ppm) of element i in

solution, f_i is the mass fraction (wt%) of element i in unleached bulk glasses, SA(t)/V is the ratio of time-dependent glass surface area (cm^2) to leachate volume (L) [1]. Surface area at specific time SA(t) is used to account for the contraction of the glass particles as they dissolve.

$$NL(i) = \frac{C_i}{(f_i)\cdot(SA(t)/V)} \quad (1)$$

Surface morphology of corroded glasses coated by carbon was characterized by scanning electron microscopy (SEM) (FEI Helios NanoLab 600 DualBeam FIB/SEM). Na/P and Fe/P ratios on the surfaces of corroded glasses were determined using the energy-dispersive X-ray spectrometry (EDS) detector associated with the FEI Helios NanoLab 600 DualBeam.

Corroded glass surfaces were also characterized by X-ray diffraction (XRD) using a Philips X'pert multipurpose diffractometer with PIXcel detector, with Cu Kα radiation and Ni filter, at 45 kV and 40 mA.

3. Results

3.1. Glass dissolution

Figure 1 compares the weight loss (%) behavior of glass D-0.32 in different aqueous solutions. The weight loss rate in DI H_2O is the lowest, whereas the weight loss in the pH 13 KOH solution is about 50% after 24 hours with reddish brown corrosion products peeled off from glass surface. The pH value shifts from 12.8 to 12.3 after 24 hours. Scanning electron microscopy shows that precipitates formed on the glass corroded in the KOH solution (Figure 2 (a)), and EDS analysis shows that the Fe/P ratio of the corrosion products is much greater than that of the base glass (Table 1). Large

amounts of leached iron ions were precipitated in the KOH solution; however, XRD shows that the reddish brown corrosion products are amorphous (Figure 2 (b)).

3.2. Dissolution mechanism

As was done in the earlier study of the dissolution behavior of sodium iron phosphate glasses in DI H_2O, the 3D diffusion model (DM) and contracting volume model (CVM) were used to describe the time-dependence of the mass fraction of glass dissolved (α) [21,22,23]. For glass powder in spherical geometries, if a diffusion process controls the rate of reaction, a 3D diffusion model (DM) could be used to describe that reaction [21,22]:

$$1 - (1 - \alpha)^{1/3} = k_{DM} t^{1/2} \quad (2)$$

where α is the mass fraction of a particle that has reacted in time t, and k_{DM} is the temperature-dependent reaction rate parameter.

A contracting volume model (CVM) would describe linear reaction kinetics, with a reaction rate parameter of k_{CVM}, for spherical particles [21,22,23]:

$$1 - (1 - \alpha)^{1/3} = k_{CVM} t \quad (3)$$

Figure 3 is an example of mass fraction of glass leached, α(glass), from glass D-0.32 in pH 10 M KOH aqueous solutions. The first dissolution stage is described by the 3D diffusion model (DM), and the second stage is described by the contracting volume model (CVM). Similar model fits were done for the dissolution data for the glasses in the series with a constant O/P ratio. Figure 4 shows how the rate parameters, k_{DM} and k_{CVM}, change with glass compositions and with different aqueous solutions. For example, k_{DM} increases with solution pH, especially for glasses with greater iron contents. The values

of k_{CVM} show similar trends with those of K_{DM}, except for glasses with low iron contents (e.g., Fe/P ratio = 0.23 glass). Figure 4 indicates that the alkaline conditions increase the dissolution rates of iron phosphate glasses with greater iron contents by several orders of magnitudes if comparing the dissolution rates in DI H_2O.

4. Discussion

An increase in dissolution rate parameters with KOH concentrations (Figure 4) could be attributed to the reaction of iron ions with OH^- to form the precipitation products shown in Figure 2. These reactions breaks the network on the glass surface and expose fresh surface to the aqueous solutions. Figure 5 shows the Fe/P ratios of ions released after two hours to solutions with different concentrations of KOH from the glasses with O/P ratios ~3.40. The Fe/P ratios in the original glasses are represented by the horizontal lines. Fe/P ratios in solutions are all below those in bulk glasses for all glass compositions. An increase in the concentrations of KOH increases the Fe/P ratios in solution, especially for glasses with greater iron contents, but not obviously for glasses with lower iron contents, which is consistent with the observations that the dissolution rate parameters for phosphate glasses with greater iron content increases with an increase in KOH concentration.

5. Summary

The dissolution behavior in alkaline solutions (KOH) of Na-Fe-phosphate glasses with O/P ratios ~3.40 was studied. Two dissolution stages were identified: the first stage is described by the 3D diffusion model (DM), and the second stage is described by the

contracting volume model (CVM). The OH^- concentration (pH) has significant effects on the dissolution rates of these glasses, especially for glasses with greater iron contents, for which the rate parameters increase with an increase in the concentrations of KOH. Formation of a precipitating phase in solution may promote the dissolution of glasses with great iron contents by continually exposing fresh surfaces to the solutions.

Acknowledgements

The authors are very grateful to Xiaoming Cheng (Missouri University of Science and Technology) for her help with the ICP analysis. This work was supported by the Nuclear Energy University Program (US Department of Energy) under grant NEUP 09-144.

Table 1 Composition of surface products of glass D-0.32 in 0.1M KOH solution for 22 days.

mol%	Na	Si	P	K	Fe	Fe/P	Na/P
Corrosion Products (EDS)	8.2 (16)	6.4 (8)	22.8 (29)	20.6 (31)	42.0 (57)	2.0 (9)	0.4 (2)
Base Glass (ICP-OES)	37.8	1.5	46.0	0	14.7	0.32	0.82

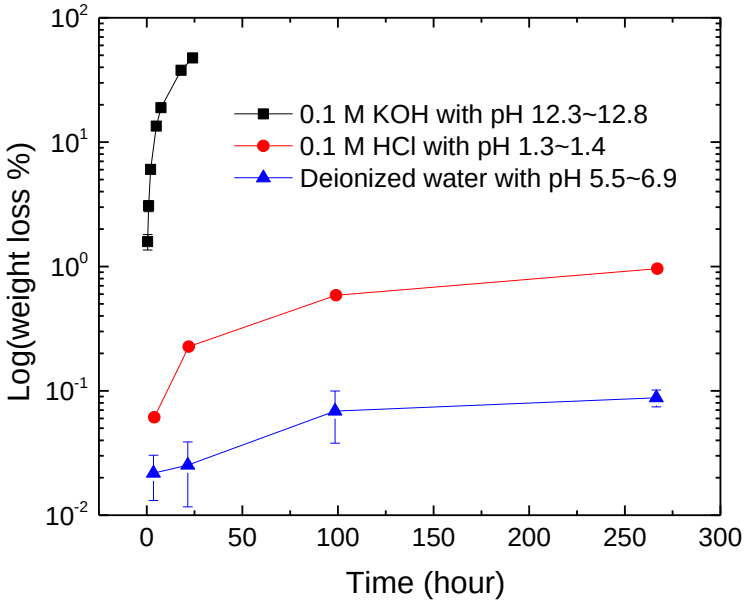

Figure 1 Weight loss (%) of glass D-0.32 in different aqueous solutions at 22 ºC.

(a)

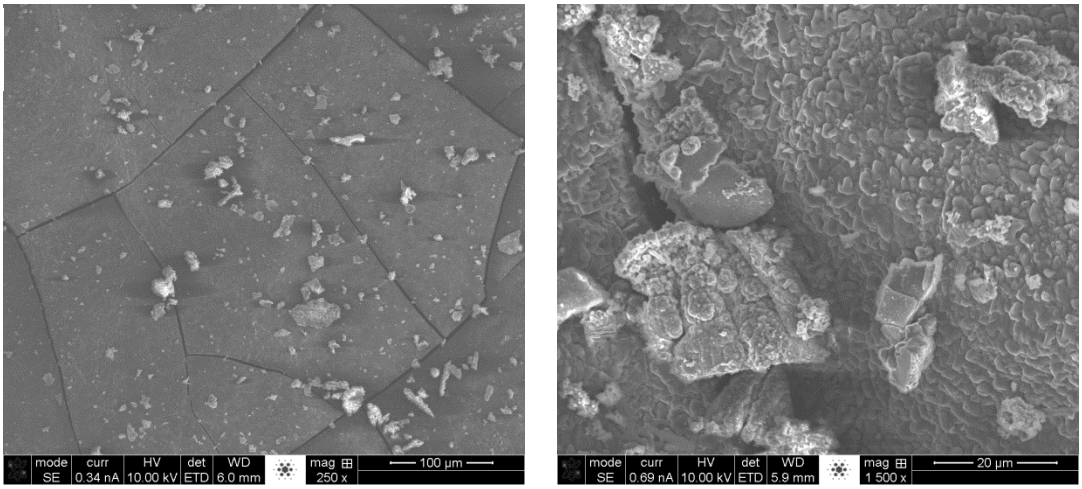

(b)

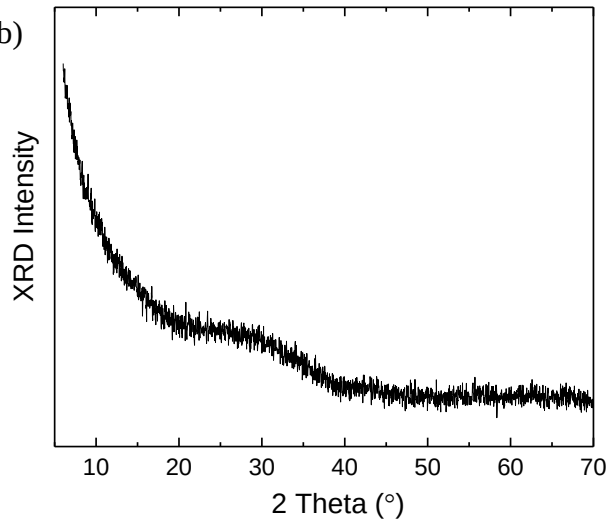

Figure 2 Glass D-0.32 in 0.1M KOH solution for 22 days. (a) Surface morphology by SEM; (b) X-ray diffraction pattern of precipitates.

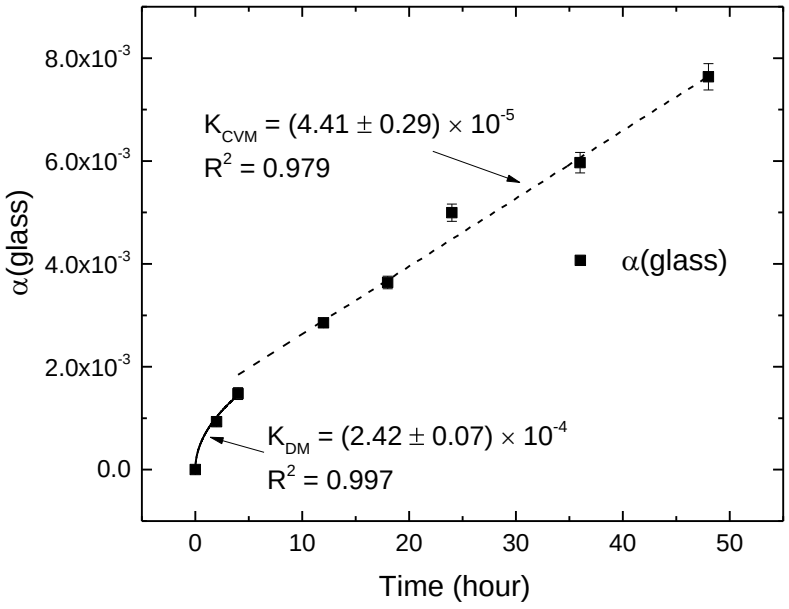

Figure 3 Mass fraction of glass leached, α(glass), from glass D-0.32 in 0.0001 M KOH aqueous solutions (pH = 10). The solid line is fitted by 3D diffusion model (DM), and the dashed line is fitted by contracting volume model (CVM). Rate parameters for these two models are marked.

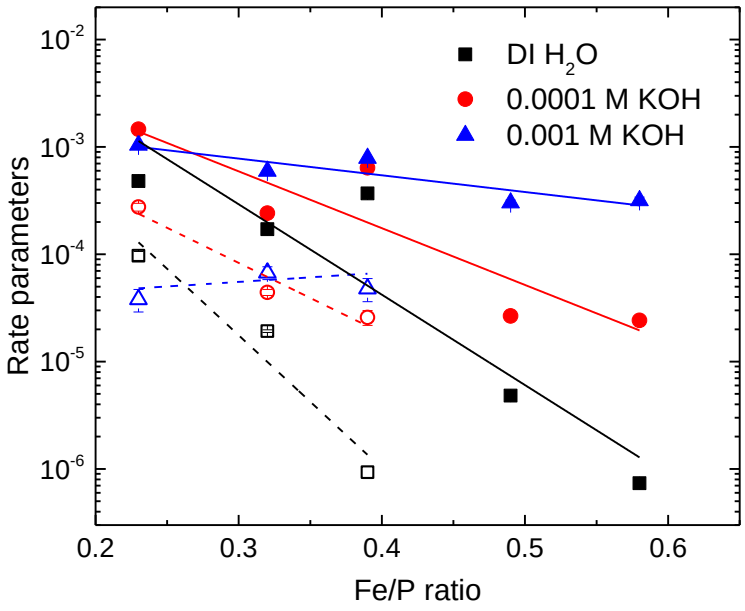

Figure 4 Changes in rate parameters with Fe/P ratio for glass series with similar O/P ratio ~3.40 in aqueous solutions. The solid symbols are the rate parameters for diffusion model, k_{DM}. The open symbols are the rate parameters for contracting volume model, k_{CVM}. The lines are guides for the eye.

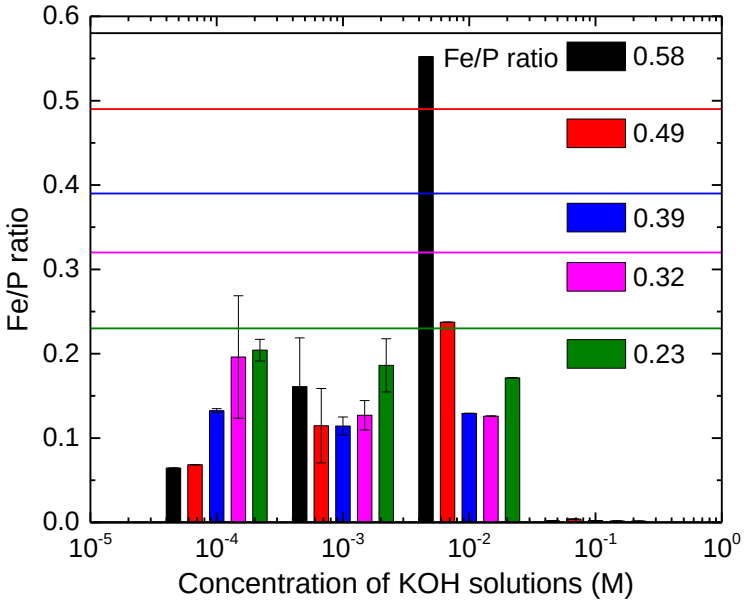

Figure 5 Fe/P ratios of ions released after two hours to KOH solutions from glasses in the series with similar O/P ratio ~3.40. The horizontal lines represent the Fe/P ratios in the original glasses.

References

[1] D.E. Day, Z. Wu, C.S. Ray, and P. Hrma. "Chemically durable iron phosphate glass wasteforms." Journal of non-crystalline solids 241, no. 1 (1998): 1-12.

[2] W. Huang, D.E. Day, C.S. Ray, C.W. Kim, and A. Mogus-Milankovic. "Vitrification of high chrome oxide nuclear waste in iron phosphate glasses." Journal of nuclear materials 327, no. 1 (2004): 46-57.

[3] C.W. Kim, and D.E. Day. "Immobilization of Hanford LAW in iron phosphate glasses." Journal of non-crystalline solids 331, no. 1 (2003): 20-31.

[4] L. Zhang, L. Ghussn, M.L. Schmitt, E.D. Zanotto, R.K. Brow, and M.E. Schlesinger. "Thermal stability of glasses from the $Fe_4(P_2O_7)_3$–$Fe(PO_3)_3$ system." Journal of Non-Crystalline Solids 356, no. 52 (2010): 2965-2968.

[5] X. Yu, D.E. Day, G.J. Long, and R.K. Brow. "Properties and structure of sodium-iron phosphate glasses." Journal of non-crystalline solids 215, no. 1 (1997): 21-31.

[6] American Society for Testing and Materials (ASTM), Standard Test Methods for Determining Chemical Durability of Nuclear, Hazardous, and Mixed Waste Glasses: The Product Consistency Test (PCT), C 1285-97, 1998.

[7] A. Jiřička, J.D. Vienna, P. Hrma, and D.M. Strachan. "The effect of experimental conditions and evaluation techniques on the alteration of low activity glasses by vapor hydration." Journal of non-crystalline solids 292, no. 1 (2001): 25-43.

[8] C.W. Kim, C.S. Ray, D. Zhu, D.E. Day, D. Gombert, A. Aloy, A. Moguš-Milanković, and M. Karabulut. "Chemically durable iron phosphate glasses for vitrifying sodium bearing waste (SBW) using conventional and cold crucible induction melting (CCIM) techniques." Journal of nuclear materials 322, no. 2 (2003): 152-164.

[9] Oelkers, Eric H., and Jean-Marc Montel. "Phosphates and nuclear waste storage." Elements 4, no. 2 (2008): 113-116.

[10] McCarthy, Gregory J., William B. White, and Diane E. Pfoertsch. "Synthesis of nuclear waste monazites, ideal actinide hosts for geologic disposal." Materials Research Bulletin 13, no. 11 (1978): 1239-1245.

[11] B.C. Sales, and L.A. Boatner. "Lead-iron phosphate glass: a stable storage medium for high-level nuclear waste." Science 226, no. 4670 (1984): 45-48.

[12] D.E. Clark, and B.K. Zoitos. "Corrosion of glass, ceramics and ceramic superconductors: Principles, testing, characterization and applications." Noyes Publications, Park Ridge, NJ (1992).

[13] D. Perret, J.L. Crovisier, P. Stille, G. Shields, U. Mäder, T. Advocat, K. Schenk, and M. Chardonnens. "Thermodynamic stability of waste glasses compared to leaching behaviour." Applied geochemistry 18, no. 8 (2003): 1165-1184.

[14] R. Conradt, and P. Geasee. "An improved thermodynamic approach to the stability of multi-component silicate glasses in aqueous solutions." Berichte der Bunsengesellschaft für physikalische Chemie 100, no. 9 (1996): 1408-1410.

[15] R. Conradt. "Chemical durability of oxide glasses in aqueous solutions: A review." Journal of the American Ceramic Society 91, no. 3 (2008): 728-735.

[16] B. Grambow. "Geochemical approach to glass dissolution." Corrosion of glass, ceramics and ceramic superconductors (1992): 124-152.

[17] Karabulut, Mevlüt, G. K. Marasinghe, Chandra S. Ray, D. E. Day, G. D. Waddill, C. H. Booth, P. G. Allen, J. J. Bucher, D. L. Caulder, and D. K. Shuh. "An investigation of the local iron environment in iron phosphate glasses having different Fe (II) concentrations." Journal of non-crystalline solids 306, no. 2 (2002): 182-192.

[18] Abou Neel, E. A., I. Ahmed, J. J. Blaker, A. Bismarck, A. R. Boccaccini, M. P. Lewis, S. N. Nazhat, and J. C. Knowles. "Effect of iron on the surface, degradation and ion release properties of phosphate-based glass fibres." Acta Biomaterialia 1, no. 5 (2005): 553-563.

[19] L. Ma, R.K. Brow, A. Choudhury. "Structural study of Na_2O-FeO-Fe_2O_3-P_2O_5 glasses by Raman and Mössbauer spectroscopy." Submitted to Journal of non-crystalline solids in Feb, 2014.

[20] S.I. Grishin, J.M. Bigham, and O.H. Tuovinen. "Characterization of jarosite formed upon bacterial oxidation of ferrous sulfate in a packed-bed reactor." Applied and environmental microbiology 54, no. 12 (1988): 3101-3106.

[21] M.N. Rahaman. "Ceramic processing." CRC Press, 2006.

[22] Y. Gu, W. Xiao, L. Lu, W. Huang, M.N. Rahaman, and D. Wang. "Kinetics and mechanisms of converting bioactive borate glasses to hydroxyapatite in aqueous phosphate solution." Journal of Materials Science 46, no. 1 (2011): 47-54.

[23] S.B. Jung, and D.E. Day. "Conversion kinetics of silicate, borosilicate, and borate bioactive glasses to hydroxyapatite." Physics and Chemistry of Glasses-European Journal of Glass Science and Technology Part B 50, no. 2 (2009): 85-88.

VITA

Li Na Ma is the daughter of Tiesheng Ma and Huiling Liu and was born in March of 1984 in Yumen, Gansu Province, China. She graduated from Railway High School of Jiayuguan, China in 2002. She then attended Tongji University in Shanghai, China and graduated in June of 2006 with a B.S. degree in Materials Science and Engineering. During her four years of college, she received five scholarships to support her undergraduate studies. She also received a Minor degree in International Finance in June of 2005 from Fudan University, Shanghai, China. In August of 2006, she began her graduate study on the optical properties of tellurite glasses embedded with metal and rare-earth nanocrystals and received an M.S. degree from Tongji University in Material Science in March of 2009. In August of 2009, she joined the research group of Dr. Richard K. Brow at Missouri University of Science and Technology in Rolla, MO, USA to pursue her Ph.D degree in Ceramic Engineering.

During her Ph.D studies, Li Na worked on the structure and dissolution behavior of phosphate glasses. Her doctoral work led to two peer-reviewed journal papers (published) and three more submitted, two posters and one oral presentation at international conferences. Li Na was awarded Third Place in the Graduate Student Poster competition at the annual meeting of the Glass & Optical Materials Division (GOMD, American Ceramic Society) in Savannah, GA, in May of 2011, and was awarded the Norbert J. Kreidl Award for Young Scholars at the GOMD meeting in San Diego, CA in June of 2013, in recognition for parts of her Ph.D research.